

Syracuse University

**SURFACE**

---

Dissertations - ALL

SURFACE

---

December 2017

## Vitamin B12 Bioconjugates In Pharmaceutical Design

Jayme Leigh Workinger  
*Syracuse University*

Follow this and additional works at: <https://surface.syr.edu/etd>



Part of the [Physical Sciences and Mathematics Commons](#)

---

### Recommended Citation

Workinger, Jayme Leigh, "Vitamin B12 Bioconjugates In Pharmaceutical Design" (2017). *Dissertations - ALL*. 804.

<https://surface.syr.edu/etd/804>

This Dissertation is brought to you for free and open access by the SURFACE at SURFACE. It has been accepted for inclusion in Dissertations - ALL by an authorized administrator of SURFACE. For more information, please contact [surface@syr.edu](mailto:surface@syr.edu).

## Abstract

This thesis addresses several questions focused on the vitamin B12 (B12) dietary uptake pathway, in particular that of the enteric B12 transport protein intrinsic factor (IF) and its receptor cubilin, and the expression and exploitation of IF/cubilin in pharmaceutical development.

**Q1:** (Chapter 2) Does an  $^{89}\text{Zr}$ -B12 conjugate allow for improved background/noise ratio, relative to  $^{99\text{m}}\text{Tc}$  and  $^{64}\text{Cu}$  B12 conjugates, in in vivo tumor uptake?

Goal: Conduct positron emission tomography (PET) imaging and biodistribution studies in mice bearing MDA-MB-453 breast cancer tumors using a new  $^{89}\text{Zr}$ -B12 conjugate.

**Q2:** (Chapter 3) What is the uptake of systemically administered holo-intrinsic factor bound to  $^{89}\text{Zr}$ -B12 in vivo?

Goal: Conduct PET imaging and biodistribution studies in healthy mouse models using IF- $^{89}\text{Zr}$ -B12 and assign organ distribution to target receptors.

**Q3:** (Chapter 4) Are functional cubilin and megalin receptors expressed in human fetal small intestinal cells?

Goal: Design a fluorescent assay to establish functional cubilin and megalin expression and conduct western blotting to complement observations.

**Q4:** (Chapter 4) Does B12-Exendin-4, a conjugate of B12 and the diabetes drug exendin-4 (Ex-4; a peptide agonist of the glucagon like peptide receptor 1) show reduced central nervous system (CNS) penetrance, thus reducing the common side effect of nausea that is observed in patients taking Ex-4?

Goal: Systemically administer fluorescently labeled Ex-4, B12, and B12-Ex4 and observe CNS uptake in rats through immunohistochemistry and confocal microscopy.

**Q5:** (Chapter 5) Does systemically administered holo-IF prevent aminoglycoside antibiotic induced hearing loss in guinea pigs?

Goal: Induce hearing loss in guinea pigs with the aminoglycoside kanamycin and prevent such loss with co-administration of holo-IF.

# **Vitamin B<sub>12</sub> Bioconjugates In Pharmaceutical Design**

By

Jayme L. Workinger

B.S. Muskingum University 2012

DISSERTATION

Submitted in partial fulfillment for the degree of

Doctor of Philosophy in Chemistry

Syracuse University

December 2017

Copyright 2017 © Jayme L. Workinger

All rights reserved

To my mother.

# Table of Contents

<b>Chapter 1: Introduction</b>	<b>Page #</b>
1.1 Vitamin B12	1
1.1.1 History of B12	2
1.1.2 Structure of B12	2
1.1.3 Metabolism of B12	4
1.1.4 Dietary Uptake of B12	5
1.1.4.1 Transport Proteins of B12	7
1.1.5 B12 Modification	9
1.1.6 B12 in Drug Delivery	11
1.2 Intrinsic Factor Protein	13
1.2.1 History of IF	13
1.2.2 The Receptor Cubilin	13
1.2.2.1 Structure of Cubilin	14
1.2.2.2 Amnionless	14
1.2.2.3 Megalin	14
1.2.2.4 The Crystal Structures of Holo-IF and Cubilin Bound to Holo-IF	15
1.3 Radioimaging Utilizing the B12 Dietary Pathway	16
1.3.1 Single Photon Emission Computed Tomography and Positron Emission Tomography Imaging	16
1.3.1.1 Radioisotope <sup>99m</sup> Techetium	17
1.3.1.2 Radioisotope <sup>64</sup> Copper	17
1.3.1.3 Radioisotope <sup>89</sup> Zirconium	17

1.3.2 Specific Targeting Using Radio-B12 Conjugates	18
1.3.2.1 A History of SPECT B12 Conjugates	19
1.3.2.2 A History of PET B12 Conjugates	20
1.4 Human and Plant N-Glycosylation	21
1.4.1 Human N- Glycosylation	22
1.4.2 Plant N- Glycosylation	22
1.4.3 Asialoglycoprotein receptor	22
1.4.4 Mannose Receptor Family	23
1.4.4.1 CD205 Receptor	23
1.4.4.2 CD206 Receptor	23
1.5 Glucagon-like-peptide Receptor Peptide Agonists	24
1.5.1 Glucagon-like Peptide-1	24
1.5.2 Exendin-4	24
1.5.3 Glucagon Receptor Family	25
1.5.2 B12-Exendin-4	26
1.5.3 H188 FRET Assay to Detect cAMP Levels	27
1.6 Cubilin and Aminoglycosides	28
1.6.1 Aminoglycoside Antibiotics	28
1.6.2 Kanamycin	29
1.7 Summary	30
1.8 References	30
<b>Chapter 2: A Vitamin B12 Conjugate of Desferrioxamine-<sup>89</sup>Zirconium as a PET 32</b>	
<b>Imaging Agent to Detect CD320 Positive Tumors</b>	<b>46</b>

2.1 Introduction	47
2.2 Design, Synthesis, and Characterization of $^{89}\text{Zr}$ -B12	47
2.2.1 Labeling and Stability of $^{89}\text{Zr}$ -B12	49
2.2.2 Confirmation of Mouse TCII Binding to Zr-B12	51
2.3 In Vitro Uptake of $^{89}\text{Zr}$ -B12 in MDA-MD-453 Human Breast Cancer Cells	51
2.3.1 CD320 Immunohistochemistry on MDA-MD-453 Human Breast Cancer Cells and Tumors	52
2.4 In Vivo Uptake of $^{89}\text{Zr}$ -B12 in a Nude Athymic Female Murine Model	53
2.4.1 PET Imaging of $^{89}\text{Zr}$ -B12 Uptake in Nude Athymic Female Mice	53
2.4.2 Biodistribution of $^{89}\text{Zr}$ -B12 Uptake in Nude Athymic Female Mice	54
2.4.3 PET Imaging of $^{89}\text{Zr}$ -B12 in Nude Athymic Female Mice Bearing MDA-MD-453 Human Breast Tumors	55
2.4.4 Biodistribution of $^{89}\text{Zr}$ -B12 in Nude Athymic Female Mice Bearing MDA-MD-453 Human Breast Cancer Tumors	56
2.4.5 CD320 Immunohistochemistry on Ex Vivo MDA-MD-453 Human Breast Cancer Tumors	59
2.5 Comparing $^{89}\text{Zr}$ -B12 to Previous Radio-B12 Experiments	60
2.6 Conclusions	60
2.7 References	61
<b>Chapter 3: The Use of Systemically Administered Intrinsic Factor in Radio-Imaging</b>	63
3.1 Introduction	63
3.2 In vivo Analysis of $^{99\text{m}}\text{Tc}$ -B12 and IF- $^{99\text{m}}\text{Tc}$ -B12	64



3.2.1 Synthesis and Characterization of B12-propargylglycine (B12-PG)	64
3.2.1.1 Labeling and Stability of $^{99m}\text{Tc}$ -B12 and IF- $^{99m}\text{Tc}$ -B12	66
3.2.2. Biodistribution of IF- $^{99m}\text{Tc}$ -B12 in Male CD-1 Mice	67
3.3 In vivo Uptake of IF- $^{64}\text{Cu}$ -B12 in Nude Athymic Female Mice	69
3.3.1 PET Imaging of IF- $^{64}\text{Cu}$ -B12 in Nude Athymic Female Mice	69
3.3.2 Biodistribution of IF- $^{64}\text{Cu}$ -B12 in Nude Athymic Female Mice	70
3.4 In vivo Uptake of IF- $^{89}\text{Zr}$ -B12 in Nude Athymic Female Mice	71
3.4.1 Human Gastric IF Binding to $^{91}\text{Zr}$ -B12	72
3.4.2 PET Imaging of IF- $^{89}\text{Zr}$ -B12 in Nude Athymic Female Mice on B12 Replete Chow	73
3.4.3 Biodistribution of IF- $^{89}\text{Zr}$ -B12 in Nude Athymic Female Mice on Normal Chow	73
3.4.4 PET Imaging of IF- $^{89}\text{Zr}$ -B12 in Nude Athymic Female Mice on B12 Deficient Chow	75
3.4.5 Biodistribution of IF- $^{89}\text{Zr}$ -B12 in Nude Athymic Female Mice on B12 Deficient Chow	76
3.5 Utilizing IF to Step Outside of the B12 Pathway	79
3.5.1 IF- $^{89}\text{Zr}$ -B12 and $^{89}\text{Zr}$ -B12 Biodistribution in Nude Athymic Female Mice on B12 Deplete and Replete Chow	79
3.6 Investigating the Glycosylation Profile of Human IF Expressed in the Plant <i>Arabidopsis thaliana</i>	83
3.6.1 GC-MS Analyses of the Glycosylation on Recombinant Human IF Expressed in Plants	84

3.6.2 IF-B12-Cy5 Uptake in Human Liver HEPG2 cells	85
3.6.3 IF-B12-Cy5 Uptake Murine Dendritic JAWSII Cells	86
3.6.4 IF-B12-Cy5 Uptake in Murine Macrophage J774A.1 Cells	87
3.7 Conclusions	88
3.8 References	89
<b>Chapter 4: Development and Validation of B12-Based Fluorescent Probes for B12 Dependent Receptor Function</b>	<b>95</b>
4.1 Introduction	95
<u>Part I:</u> Use of a New Fluorescent Vitamin B12 (B12-Cy5) Probe in the Screening of FHs 74 Int. Cells for Cubilin and Megalin	96
4.2. Design, Synthesis, and Characterization of B12-Cy5	96
4.2.1 IF-B12-Cy5 Uptake in the Cubilin Positive control cell line BN16	98
4.2.2 IF-B12-Cy5 Uptake in the Cubilin Negative control cell line CHO-K1	100
4.3 Using B12-Cy5 to Explore the Expression of Cubilin and Megalin in Human Fetal Intestinal Cells (FHs 74 Int. Cells)	101
4.3.1 Investigating Cubilin Expression in FHs 74 Int. Cells	101
4.3.1.1 Western Blot of Cubilin in FHs 74 Int. Cells	101
4.3.1.2 Flow Cytometry Uptake of IF-B12-Cy5 in FHs 74 Int. Cells	102
4.3.2 Investigating Megalin Expression in FH-74 Int. Cells	103
4.3.2.1 Western Blot of Megalin in FHs 74 Int. Cells	103
4.3.2.2 Flow Cytometry Uptake of TCII-B12-Cy5 in FHs 74 Int. Cells	104
<u>Part II:</u> Use of a New Fluorescent B12-Ex4 (B12-Ex4-Cy5) in the Screening of Rat CNS Penetration	106

4.4 Introduction	106
4.4.1 Synthesis and Characterization of B12-Ex4-Cy5	106
4.4.2 Agonism of B12-Ex4-Cy5 at the GLP-1R using H188 FRET Reporter Assay	109
4.4.3 Sprague Dawley Rat Brain Uptake of B12-Cy5 and B12-Ex4-Cy5	110
4.5. Conclusions	115
4.6 References	115
<b>Chapter 5: Mitigation of Aminoglycoside Toxicity in Pigmented Guinea</b>	
<b>Pigs Using Intrinsic Factor Expressed in <i>Arabidopsis thaliana</i></b>	120
5.1 Introduction	120
5.1.1 Mitigating Hearing Loss from Aminoglycosides using Human Gastric Intrinsic Factor	120
5.2 Inducing Hearing Loss in Pigmented Guinea Pigs using Kanamycin	121
5.2.1 Pigmented Guinea Pigs	121
5.2.2 A Discussion on Anesthesia in Pigmented Guinea Pigs	121
5.2.3 Experimental Design	123
5.2.3.1 Administering Kanamycin for 23 days	123
5.2.4 Auditory Brainstem Response Hearing Tests on Guinea Pigs Using Kanamycin	123
5.2.4.1 Auditory Brainstem Response Test	123
5.2.4.2 Auditory Brainstem Response Hearing Baseline for Pigmented Guinea Pigs	118
5.2.4.3 Kanamycin Induced Hearing Loss in Pigmented Guinea Pigs	124
5.3 Using IF to Mitigate Hearing Loss from Aminoglycoside Toxicity	127
5.3.1 Experimental Design	127

5.3.1.1 Kanamycin with IF Induced Hearing loss in Pigmented Guinea Pigs	127
5.3.2 Auditory Brainstem Response Hearing Tests in Guinea Pigs on Kanamycin and IF for 23 days	127
5.4 Antigenicity of IF expressed in <i>Arabidopsis thaliana</i> in Guinea Pigs	129
5.4.1 Effect of IF on Guinea Pig Weight	129
5.4.2 ELISA of Guinea Pig Blood to Detect for IF Antibodies Raised by Guinea Pigs	130
5.5 Summary and Conclusion	131
5.6 References	132
<b>Chapter 6: Experimental</b>	134
6.1 General Materials and Methods	134
6.1.1 HPLC Method	135
6.1.2 Synthesis of B12-Mesylate (B12-MsCl)	135
6.1.3 Synthesis and Purification of B12-Azide (B12-N <sub>3</sub> )	136
6.1.4 Synthesis and Purification of B12-Azide-Linker (B12-azide-linker)	136
6.1.5 Synthesis and purification of B12-azide-linker with Fmoc-propargylglycine (B12-FPG)	137
6.1.6 Deprotection of B12-FPG (B12-PG)	137
6.1.7 Synthesis of B12-ethylenediamine (B12-en)	138
6.1.8 Synthesis of B12-ethylenediamine-NOTA (B12-NOTA)	138
6.1.9 Synthesis of Tris[(1-benzyl-1 <i>H</i> -1,2,3-triazole-4-yl)methyl]amine (TBTA)	139
6.1.10 Synthesis of 1, 6-diazidohexane	139
6.1.11 Synthesis of 1-amine-6-azidohexane	140

6.1.12 Synthesis of B12-desferoxamine (B12-DFO)	140
6.1.13 B12-Exendin-4-Cyanine-5 (B12-Ex4-Cy5) synthesis	141
6.1.14 B12-Cyanine-5 (B12-Cy5) synthesis	141
6.1.15 B12-carboxylic acid (B12-CA) Synthesis	142
6.1.16 Synthesis of B12-aminobutyne (B12-AB)	142
6.1.17 Synthesis of B12-Exendin-4 (B12-Ex4)	143
6.2 General Radio-Chemistry Materials and Methods	143
6.2.1 Binding of radio-B12 to IF	144
6.2.2 Intrinsic Factor and $^{99m}\text{Tc}$ -B12 Binding Study	144
6.2.3 Radiolabeling of B12-PG with $^{99m}\text{Tc(I)}$ ( $^{99m}\text{TC}$ -B12)	144
6.2.4 Radiolabeled $^{99m}\text{Tc}$ -B12 Stability/Challenge Study	144
6.2.5 Radiolabeling of B12-NOTA	145
6.2.6 Mouse TCII and human gastric IF Binding to Zr-B12	145
6.2.7 $^{89}\text{Zr}$ -radiochemistry with B12-DFO	145
6.2.8 Synthesis of Zr-B12	146
6.2.9 In vitro stability of $^{89}\text{Zr}$ -B12 and IF- $^{89}\text{Zr}$ -B12	146
6.2.10 Cell lines and small animal xenografts	146
6.2.11 PET imaging experiments	147
6.2.12 Ex-vivo distribution and competitive saturation	147
6.2.13 Immunohistochemistry of MDA-MB-453 Tumor	147
6.3 General Cell Methods and Materials	148
6.3.1 IF Binding to B12-Cy5	149
6.3.2 Flow Cytometry Analysis Using B12-Cy5	149

6.3.3 GLP-1 assay for Cy5-B12-Ex4, Cbi-Ex4 and HC-Cbi-Ex4	150
6.3.4 Immunohistochemical procedures for the mouse brain	150
6.3.5 Confocal imaging of mouse brain slices	151
6.3.6 Western Blot Conditions for Cubilin and Megalin	152
6.3.7 Western Blot Conditions for HC and TCII in Shrew Blood	152
6.4 General Guinea Pig Materials and Methods	152
6.4.1 Kanamycin and IF Injections	153
6.4.3 Anesthesia Protocol for Pigmented Guinea Pigs	153
6.4.4 Auditory Brainstem Response Hearing Tests	154
6.4.5 Guinea Pig IF Antibody ELISA Kit	154
6.5 References	155
<b>Chapter 7: Future and Ongoing Work</b>	157
7.1 Using IF-B12 to Detect Cubilin Positive Tumors	157
7.2 Using Haptocorrin Binding Substrates to Increase Peptide Half-life	157
7.2.1 Design, synthesis and characterization of Cobinamide Peptide Conjugates	158
7.2.2 Agonism of Cbi-Ex4 at the GLP-1 receptor	161
7.2.3 Agonism of HC-Cbi-Ex4 at the GLP-1 receptor	163
7.2.4 Future in vivo Work Using HC-Cbi-Ex4 as a Platform Technology to Increase Peptide half-life	166
7.2.4.1 Tree Shrews as in vivo Models for HC-Cbi-Ex4	166
7.2.4.2 Analysis of Asian Shrew Blood for HC and TCII	166
7.3 Mitigate Hearing Loss in Pigmented Guinea Pigs from Aminoglycoside Toxicity	167

7.3.1 In vitro Validation of IF Interference with AG Toxicity	168
7.3.2 In Vivo Mitigation of Aminoglycoside Toxicity Using IF	168
7.4 References	169

## Appendix A: Publications

1. Kelly E. Henry, Deborah J. Kerwood, Damian G. Allis, **Jayme L. Workinger**, Ron L. Bonaccorso, George G. Holtz, Christian L. Roth, Jon Zubieta, and Robert P. Doyle. Solution Structure and Constrained Molecular Dynamics Study of Vitamin B12 Conjugates of the Anorectic Peptide PYY(3-36). *ChemMedChem*. **2016**, DOI: 10.1002/cmdc.201600073.
2. **Jayme L. Workinger** and Robert P. Doyle. The Role of Vitamin B12 in Drug Discovery. In *Vitamin B12: Advances and Insights*. Science Publishers, Boca Raton, FL. **2017**. ISBN: 9781498706995.
3. **Jayme L. Workinger**, Akhila N. Wedagedara, Ebba Nexo Robert P. Doyle, Nerissa T. Viola-Villegas. <sup>89</sup>Zr-Cobalamin PET Tracer: Synthesis, Cellular Uptake, and Use for Tumor Imaging. *ACS Omega* **2017**, 2 (10), 6314–6320.
4. Elizabeth G. Mietlicki-Baase, Claudia G. Liberini, **Jayme L. Workinger**, Ron L. Bonaccorso, David J. Reiner, Kieran Koch-Laskowski, Lauren E. McGrath, Rinzin Lhamo, Lauren M. Stein, Bart C. De Jonghe, George G. Holz, Christian L. Roth, Robert P. Doyle, and Matthew R. Hayes. A Vitamin B12 conjugate of Exendin-4 Produces

Hypoglycemia Without Associated Hypophagia or Nausea in Male Rats. **2017.** *In revision to Diabetes, Obesity and Metabolism*

**Appendix B: Curriculum Vitae**



## Abbreviations

%ID/g	Percent Injected dose per gram of tissue
%recovered/organ	Percent activity injected that has been recovered by the organ
<sup>111</sup> In	<sup>111</sup> Indium
<sup>131</sup> I	<sup>131</sup> Iodine
<sup>57</sup> Co	<sup>57</sup> Cobalt
<sup>58</sup> Co	<sup>58</sup> Cobalt
<sup>60</sup> Co	<sup>60</sup> Cobalt
<sup>64</sup> Cu	<sup>64</sup> Copper
<sup>89</sup> Zr	<sup>89</sup> Zirconium
<sup>99m</sup> Tc	<sup>99m</sup> Technetium
ABR	auditory brainstem response
AGA	Aminoglycoside antibiotics
AP	area postrema
apo-IF	Intrinsic factor not bound to B12
ASGPR	asialoglycoprotein receptor
B12	Vitamin B12, cyanocobalamin
B12-AB	B12-aminobutyne
B12-Cy5	B12-cyanine5
B12-DFO	B12-desferrioxamine
B12-Ex4	B12-Exendin-4
B12-FPG	B12-fmoc-propargylglycine
B12-PG	B12-propargylglycine

B12-PYY <sub>3-36</sub>	B12-Peptide Y Y 3-36
B16-F10	murine melanoma
BN16	Brown Norway rat yolk sac cells
cAMP	cyclic adenosine monophosphate
CC	central canal
CD205	Cluster of differentiation 205
CD206	Cluster of differentiation 206
CD320	Cluster of differentiation 320
CDT	1,1'-carbonyl-di-(1,2,4-triazole)
CFP	Cyan fluorescent protein
CHO-K1	Chinese hamster ovary cells
CNS	Central Nervous System
CPM	counts per million
CuAAC	Copper-azide-alkyne 'click'
CUBAM	Cubilin-amnionless
CUBN	Cubilin
Cy5	cyanine5
DEP	disheveled, Egl-10, and pleckstrin
DFO	desferrioxamine
DIPEA	Diisopropylamine
DMF	Dimethyl formamide
DMSO	Dimethyl sulfoxide
DPP-IV	Dipeptidyl peptidase IV

DTPA	diethylenetriamine-N,N;N',N'', N'''-pentaacetic acid
DVC	dorsal vagal complex
EC <sub>50</sub>	Effective concentration 50
EDC	1-Ethyl-3-(3-dimethylaminopropyl)carbodiimide
ELISA	Enzyme linked immunosorbent assay
EPAC	exchange protein directly activated by cAMP
Ex-4	Exendin-4
F-Ex-4	fluorescent Ex-4
FHs 74 Int.	Fetal Human Small Intestinal cell line
FPG	fmoc-propargylglycine
FRET	Fluorescence resonance energy transfer
Fuc	Fucose
Gal	galactose
GC-MS	Gas chromatography- mass specrometry
GEF	guanine nucleotide exchange factor
Glc	glucoseamine
GlcNAc	<i>n</i> -actylglucoseamine
GLP-1	glucagon-like peptide 1
GLP-1R	GLP-1 receptor
GPCR	G protein-coupled receptors
HBSS	Hank's balanced salt solution
HC	Haptocorrin/transcobalamin I/R-binder
HCT116	Human colorectal carcinoma

HEK-293	Human embryonic kidney cells
HEPG2	Human liver cells
HMPA	hexamethylphosphoramide
HObt	hydroxybenzotriazole
holo-IF	Intrinsic factor bound to B12
IBX	2-iodoxybenzoic acid
IF	Intrinsic Factor
IHC	Immunohistochemistry
IM	intramuscular injections
IP	intraperitoneal injection
iTLC	instant thin layer chromatography
J774A.1	Murine macrophage cells
JAWSII	Murine dendritic cells
K <sub>d</sub>	Dissociation constant
LC-MS	Liquid chromatography-mass spectrometry
Man	mannose
MIA PaCa2	Human pancreatic carcinoma
MRF	Mannose receptor family
MRSA	methicillin-resistant <i>Staphylococcus aureus</i>
MSCl	mesyl chloride
Ni	Nickle
NMP	<i>n</i> -methyl-2-pyrrolidone
NTS	nucleus tractus solitaries

OGTT	oral glucose tolerance test
p.i.	post injection
PAMA	[pyridine-2-ylmethyl-amino]-acetic acid
PET	Positron emission tomography
PVN	paraventricular hypothalamic nucleus
REM	ras exchange motif
ROI	Regions of interest
RP-HPLC	Reverse Phase- High Pressure Liquid Chromatography
R <sub>t</sub>	Retention time
SA	sialic acid
SC	subcutaneous injections
SCN-Bn-NOTA	isothiocyanatobenzyl-1,4,7- triazacyclononane-N,N',N''-triacetic acid
SKOV-3	Human ovarian adenocarcinoma
SPECT	Single-photon emission computed tomography
TBTA	Tris[(1-benzyl-1 <i>H</i> -1,2,3-triazole-4-yl)methyl]amine
TCII	Transcobalamin II
Xyl	xylose
YFP	Yellow fluorescent protein

## List of Figures Schemes and Tables

Chapter 1	Page
<b>Table 1.</b> A list of all thirteen essential vitamins, molecular weight, solubility, and main biological function.	1
<b>Figure 1.</b> Structure of B12. Highlighted (blue) are the major modifiable sites on B12 for conjugation to small molecules or peptides/proteins, whereby binding by the dietary uptake proteins can be minimally affected, or selected for.	3
<b>Figure 2.</b> B12 function in the cell as a co-factor with methionine synthase and methylmalonyl-CoA Mutase.	4
<b>Figure 3.</b> Dietary uptake pathway for B12 in humans. Abbreviations used: R-protein/TCI: Haptocorrin (HC); IF: Intrinsic factor; TCII: Transcobalamin II; Cbl: cobalamin/B12. Image produced and used with permission of Xeragenx LLC (St. Louis, MO, USA).	5
<b>Figure 4.</b> Transport Proteins Bound to B12. A) TCII, B) HC, and C) IF. PDB code 2BB5, 4KKI, 2PMV, respectively.	9
<b>Figure 5.</b> Megalin and cubilin's binding substrates, substrates in the center are recognized by both receptors.	15
<b>Table 2.</b> All B12-radioimaing agents reported to date. DTPA: diethylenetriamine-N,N;N',N'', N'''-pentaacetic acid; PAMA: [pyridine-2-ylmethyl-amino]-acetic acid; SCN-Bn-NOTA; isothiocyanatobenzyl-1,4,7- triazacyclononane-N,N',N''-triacetic acid. *Conjugate was selected	20

for human studies targeting tumors.

**Figure 6.** Comparing typical N-glycosylation of Human and Plants. 21

GlcNAc: *n*-acetylglucosamine, Man: mannose, Fuc: fucose, SA: sialic acid, Xyl: xylose, Gal: galactose.

**Figure 7.** Structure of Ex-4. Note significant helical content (46%) and a C-terminal hair-pin (1JRJ). 25

**Figure 8.** Conformational change of EPAC after cAMP binding. DEP: disheveled, Egl-10, and pleckstrin, GEF: guanine nucleotide exchange factor, REM: ras exchange motif, C: cyanine fluorescent protein, Y: yellow fluorescent protein. 28

**Figure 9.** Chemical structure of the AGA kanamycin. 29

## Chapter 2

**Figure 1.** The synthesis and radiolabeling of B12-DFO. Reaction 48

conditions: I) CDT (7.2 eq.) was added to B12 (1 eq.) in anhydrous DMSO at 40°C for 2 h, then DFO (7.4 eq.) was added to the reaction mixture and allowed to stir overnight at RT, and II) Radiolabeling was achieved by incubating  $^{89}\text{Zr}(\text{C}_2\text{O}_4)_2$  (1  $\mu\text{Ci}$ ) with B12-DFO (0.004  $\mu\text{mol}$ ) for 20 min at pH 7–7.5.

**Figure 2.** Characterization of B12-DFO. A) RP-HPLC:  $R_t = 9.4$  min. 49

Detection at 360 nm. Integrated purity is 97%. B) LC-MS

showed  $942[M+2H]^{2+}$  and  $648[M+3H]^{3+}$ , expected m/z 1942.

**Figure 3.** iTLC of  $^{89}\text{Zr}$ -B12 binding. The peak around 60 mm shows completely labeled B12-DFO. 50

**Figure 4.**  $^{89}\text{Zr}$ -B12 stability in A) saline and B) human serum at  $37^\circ\text{C}$  at 4, 24, and 48 h. Analysis shows the  $^{89}\text{Zr}$ -B12 tracer was stable to demetallation up to 48 h, using iTLC. 50

**Figure 5.** Mouse TCII binding of  $^{91}\text{Zr}$ -B12 (metalated with cold  $^{91}\text{ZrCl}_4$ ) and B12. TCII binding of  $^{91}\text{Zr}$ -B12 (1.6 nM) was maintained in comparison with unmodified B12 (1.3 nM). 51

**Figure 6.** Internalization of  $^{89}\text{Zr}$ -B12 (1  $\mu\text{Ci}$ , 4 pmol/well) at 1, 4, 24 h time points incubated at 4 and  $37^\circ\text{C}$  in MDA-MB-453 cells. A competition assay was also performed at each time point using unlabeled B12 (40 pmol/well). The fraction of  $^{89}\text{Zr}$ -Cbl internalized in MDA-MB-453 cells is expressed as counts per minute in  $10^5$  cells (CPM/ $10^5$ ). 52

**Figure 7.** IHC staining of MDA-MB-453 tumor sections showing (a) DAPI, (b) CD320-AF488, and (c) overlay. 53

**Figure 8.** PET imaging of  $^{89}\text{Zr}$ -B12 at 4, 24, and 48 h in nude athymic female mice.  $^{89}\text{Zr}$ -B12 (200-250  $\mu\text{Ci}$ /mouse) showed high uptake in the kidneys that did not change over 48 h. All other tissues assayed had relatively low uptake (see also Table 1, section 2.4.4). 54

**Figure 9.** Ex vivo tissue distribution of  $^{89}\text{Zr}$ -B12 at 24 h in nude athymic female mice at 24 h.  $^{89}\text{Zr}$ -B12 showed high uptake in the kidney ( $130.26 \pm 14.05$  %ID/g) and moderate uptake in the liver ( $21.5 \pm 3.91$  %ID/g). n = 4. 55



- Figure 10.** PET images of representative mice bearing MDA-MB-453 tumors imaged with  $^{89}\text{Zr}$ -B12 (1 nmol/mouse) at 4, 24, and 48 h p.i. time points, and co-injected  $^{89}\text{Zr}$ -B12 and cold B12 (~200 nmol/mouse) at 4 and 24 h p.i. time points. Mice were on a B12 deplete diet for 21 days pre-injection. The tumor location is indicated by a red circle. 56
- Figure 11.** Ex vivo tissue distribution of  $^{89}\text{Zr}$ -B12 (0.1 nmol/mouse), in nude athymic female mice bearing MDA-MD-453 tumors, at 4, 24, and 48 h. A blocking study with 100-fold (20 nmol/mouse, co-injected with tracer) of unmodified B12 displayed a significant decrease in uptake in all tissues. Mice were on a B12 deplete diet for 21 days pre-injection. n = 4. 57
- Table 1.** Biodistribution of  $^{89}\text{Zr}$ -B12 at 4, 24, and 48 h p.i. in MDA-MD-453 mouse models. 59
- Figure 12.** IHC staining of MDA-MD-453 tumor slices (a) with DAPI and (b) CD320-AF488, showing the tumors express CD320. 59

### Chapter 3

- Scheme 1.** Synthesis of B12-PG. I: B12 was activated with CDT and reacted forward with 1-amine-6-azidohexane. II: B12-azide-linker ‘clicked’ to FPG with Cu(I)/TBTA in DMF/H<sub>2</sub>O. III: B12-FPG was deprotected with 30% piperidine mixture. Overall yield based on B12 starting material was 95%. 65

**Figure 1.** RP-HPLC and LC-MS of B12-PG. A) HPLC shows > 95%,  $R_t = 9.9$  min and B) LC-MS:  $m/z$  observed  $m/z$  1637  $[M]^+$ , expected  $m/z$  1636. 65

**Figure 2.** Labeling of B12-PG with  $^{99m}\text{Tc}$  showing full metalation. A) ultraviolet detection at 360 nm, and B) gamma detection. 66

**Figure 3.** Size exclusion chromatograph of IF- $^{99m}\text{Tc}$ -B12 (1 nM) confirms IF binding to  $^{99m}\text{Tc}$ -B12. A) detection of apo-IF,  $R_t$ : 4 min, B) detection of IF- $^{99m}\text{Tc}$ -B12 through gamma, C) detection of IF- $^{99m}\text{Tc}$ -B12 at 280 nm, D) detection of IF- $^{99m}\text{Tc}$ -B12 at 360 nm. Column: Zorbax GF-250, 4  $\mu\text{m}$ , 4.6 x 250 mm, Elution Buffer: 20 mM sodium phosphate and 300 mM sodium chloride at pH 7. 67

**Figure 4.** Ex vivo tissue distribution of A)  $^{99m}\text{Tc}$ -B12 at 1, 3, and 6 h in CD-1 mice. Highest uptake observed is within the kidney with low tracer uptake in all other tissues.  $n = 3$  68

**Figure 5.** Ex vivo tissue distribution of IF- $^{99m}\text{Tc}$ -B12 (500 nM) at 1, 3, and 6 h in CD-1 mice. Highest uptake is in the kidney and liver. Kidney:  $13.15 \pm 1.58$ ,  $19.28 \pm 3.01$ , and  $28.64 \pm 1.67$  at 1, 3, and 6 h respectively. Liver:  $27.46 \pm 3.18$ ,  $32.82 \pm 6.11$ , and  $30.8 \pm 1.55$  at 1, 3, and 6 h, respectively.  $n = 3$  for each time point. 69

**Figure 6.** PET imaging of IF- $^{64}\text{Cu}$ -B12 ( $\sim 200$   $\mu\text{Ci}/\text{mouse}$ ) at 1 and 20 h p.i. High uptake in the liver and kidney is observed with little uptake in all other tissues. 70

- Figure 7.** Ex vivo tissue distribution of IF-<sup>64</sup>Cu-B12 at 24 h in nude athymic female mice. n = 2 71
- Figure 8.** Binding Affinities of Zr-B12 and B12 to human gastric IF with a  $K_d$ : 1.57 nM and 1.36 nM, respectively. 72
- Figure 9.** PET imaging of IF-<sup>89</sup>Zr-B12 and <sup>89</sup>Zr-B12 at 1 and 24 h in nude athymic mice on a B12 replete diet. In comparison to the control (<sup>89</sup>Zr-B12) IF-<sup>89</sup>Zr-B12 showed rapid and significant uptake in the liver, which did not change over 24 h. 73
- Figure 10.** Ex vivo tissue distribution of IF-<sup>89</sup>Zr-B12 and <sup>89</sup>Zr-B12 at 24 h in nude athymic female mice on a B12 replete diet. In compared to the control (<sup>89</sup>Zr-B12) IF-<sup>89</sup>Zr-B12 showed high uptake in the liver and a decrease in uptake in the kidney. n ≥ 3. 75
- Figure 11.** PET imaging of IF-<sup>89</sup>Zr-B12 and <sup>89</sup>Zr-B12 at 24 h in nude athymic female mice on a B12 deplete diet for 21 days. IF-<sup>89</sup>Zr-B12 in mice on normal chow (Figure 8) showed similar uptake at 24 h. A higher uptake in the liver was observed for <sup>89</sup>Zr-B12 than in mice on a replete diet. 76
- Figure 12.** Ex vivo tissue distribution of IF-<sup>89</sup>Zr-B12 and <sup>89</sup>Zr-B12 at 24 h in nude athymic female mice on a B12 deplete diet for 21 days. Comparison to the control (<sup>89</sup>Zr-B12) IF-<sup>89</sup>Zr-B12 showa high uptake in liver and decrease uptake in the kidney. n ≥ 3. 77

<b>Figure 13.</b> Comparing the effects of mice on a B12 deplete and replete diet 24 h p.i of IF- <sup>89</sup> Zr-B12. A 3-fold increase in uptake is seen in both the liver, kidney, and spleen in deplete mice.	78
<b>Table 1.</b> Biodistribution of <sup>89</sup> Zr-B12 and IF- <sup>89</sup> Zr-B12 on B12 replete and deplete diets. Data reported in %ID/g.	78
<b>Figure 14.</b> Ex vivo tissue distribution of <sup>89</sup> Zr-B12 in mice on a deplete or replete diet at 24 h plotted as %recovered/organ. Changes in uptake occurred in the liver, kidneys, and blood. n ≥ 3.	80
<b>Figure 15.</b> Ex vivo tissue distribution of IF- <sup>89</sup> Zr-B12 in mice on a B12 deplete or replete diet at 24 h plotted as %recovered/organ. The significant changes occurred in the blood, stomach, and large intestine, while the liver, kidneys, spleen and pancreas stayed the same. n ≥ 3.	81
<b>Figure 16.</b> Ex vivo tissue distribution of IF- <sup>89</sup> Zr-B12 and <sup>89</sup> Zr-B12 in mice on a B12 deplete or replete diet at 24 h plotted as %recovered/organ. The significant changes occurred with <sup>89</sup> Zr-B12 in the liver and kidney, while they were not significantly changed in the IF- <sup>89</sup> Zr-B12. n ≥ 3, *p = 0.05.	82
<b>Table 2.</b> Ex vivo tissue distribution of IF- <sup>89</sup> Zr-B12 and <sup>89</sup> Zr-B12 in mice on a B12 deplete or replete diet at 24 h plotted as %recovered/organ.	83
<b>Table 3.</b> GC-MS analysis of hrIF showing that fucose, xylose, mannose and <i>n</i> -acetylglycosamine are present.	85

**Figure 17.** Flow cytometry analyses of HEPG2 cells treated with IF-B12-Cy5 (100 nM) in HBSS for 1 h at 37°C. There was no shift in fluorescence with the treated cells compared to non-treated cells indicating no uptake of the complex. Ex: 640 nm Em: 660/20 nm. P2 defines a positive result. 86

**Figure 18.** Flow cytometry analyses of JAWSII cells treated with IF-B12-Cy5 or B12-Cy5 (100 nM each) in HBSS for 1 h at 37°C. A broadening in fluorescence was seen using IF-B12-Cy5 and B12-Cy5 treated cells compared to non-treated cells indicating a non-IF specific uptake/association of the complex. Ex: 640 nm Em: 660/20 nm. P2 defines a positive result. 87

**Figure 19.** Flow cytometry analysis of J774A.1 cells treated with IF-B12-Cy5 or B12-Cy5 (100 nM each) in HBSS for 1 h at 37°C. A shift in fluorescence was seen in the IF-B12-Cy5 indicating IF specific uptake/association of the complex. Ex: 640 nm Em: 660/20 nm. P2 defines a positive result. 88

#### **Chapter 4**

**Figure 1.** Synthesis of B12-Cy5. B12 was activated by replacing the terminal ribose 5'OH with an azide for 'Click' chemistry as previously reported. I: B12 was dissolved in NMP. A solution of MsCl in NMP and DIPEA were added in separately, at the same time, in three intervals 1 h apart then stirred for 1 hour at RT. II: B12-MsCl was dissolved in HMPA and NaN<sub>3</sub> was added and stirred overnight at 40°C. III: Huisgen/Sharpless CuAAC chemistry was implemented using Sulfo-Cy5 Alkyne and 96

Cu(I)/TBTA in DMF/H<sub>2</sub>O (4:1) overnight. Final yield: 98%, based on B12 starting material.

**Figure 2.** Excitation and Emission for B12-Cy5. The excitation and emission are similar to Cy5 without conjugation (646 and 662 nm, respectfully) indicating B12-Cy5 was made and B12 did not quench Cy5 fluorescence. Excitation in green and emission in red. Solvent: H<sub>2</sub>O, excitation: 645 nm, emission: 682 nm. 97

**Figure 3.** A) RP-HPLC of purified B12-Cy5. R<sub>t</sub>: 8.41 min. Purity: 99%. Detection at 371 and 640 nm. B) LC-MS Analysis of B12-Cy5 showing the compound was made. Expected m/z = 2059, observed m/z = 688 [M+3H]<sup>+3</sup>, 2031 [M+2H]<sup>+2</sup>, 695 [M+Na]<sup>+3</sup>, 700 [M+K]<sup>+3</sup>, 1042 [M+Na]<sup>+2</sup>. 98

**Figure 4.** Flow cytometry analyses of BN16 cells treated with IF-B12-Cy5 (100 nM) in HBSS for 1 h at 37°C. A three-log shift in fluorescence was seen using IF-B12-Cy5 treated cells compared to non-treated cells indicating an IF specific uptake/association of the complex, namely CUBN. The decrease in uptake at 4°C supports a receptor mediated mechanism. Ex: 640 nm Em: 660/20 nm. P2 defines a positive result. 99

**Figure 5.** Flow cytometry analyses of CHO-K1 cells treated with IF-B12-Cy5 or B12-Cy5 (100 nM) in HBSS for 1 h at 37°C. A no fluorescence change was seen in IF-B12-Cy5 or B12-Cy5 treated cells compared to non-treated cells indicating a IF was not internalized. Ex: 640 nm Em: 660/20 nm. P2 defines a positive result. 100

**Figure 6.** Western blot for CUBN. Lane 1: Thermo Fisher Scientific HiMark Pre-Stained HMW Protein Standard, Lane 2: CHO-K1 lysate (negative control), Lane 3: BN16 lysate (positive control), Lane 4: BN16 (membrane), Lane 5: FHs 74 Int., Lane 6: FHs 74 Int. (membrane). 102

**Figure 7.** Flow cytometry analysis of FHs 74 Int. cells treated with IF-B12-Cy5 or B12-Cy5 (100 nM, and 1  $\mu$ M) in HBSS for 2 h at 37°C. A fluorescence change was seen in IF-B12-Cy5 (1  $\mu$ M) treated cells compared to non-treated or IF-B12-Cy5 (100 nM). A fluorescent shift was also seen for B12-Cy5 yet different than IF-B12-Cy5. This indicates functional CUBN expression is expressed on FHs 74 Int. cells. Ex: 640 nm Em: 660/20 nm. P2 defines a positive result. 103

**Figure 8.** Western Blot for Megalin. Lane 1: CHO-K1 cell lysate (negative control), Lane 2: FHs 74 Int. cell lysate, Lane 3: BioRad Kaleidoscope Protein Markers, Lane 4: BN16 cell lysate (positive control) on a PDVF membrane. 104

**Figure 9.** Flow cytometry analysis of FHs 74 Int. cells treated with TCII-B12-Cy5 or B12-Cy5 (1  $\mu$ M) in HBSS for 1 h at 37°C. A fluorescence shift was seen in TCII-B12-Cy5 treated cells compared to non-treated and B12-Cy5 treated cells. This indicates supports functional megalin expression is expressed on FHs 74 Int. cells. Ex: 640 nm Em: 660/20 nm. P2 defines a positive result. 105

**Figure 10.** A) Synthesis of B12-Ex4 as previously reported I: EDC and HOBT in anhydrous DMSO with aminobutyne, overnight at RT, and II: 107

Cu/TBTA in DMF and H<sub>2</sub>O, overnight and B) Synthesis of B12-Ex4-Cy5, I: Purified B12-Ex4 was reacted with sulfo-cyanine5-NHS-ester in PBS pH 7.6. Predicted conjugation site is the N-terminus and the lysine 27 (lysine 12 was modified to have an azido group for click chemistry), yield: 94%.

**Figure 11.** A) RP-HPLC of B12-Ex4-Cy5 showing purity  $\geq 91\%$ . It is suspected that some of the compound is degrading on the column.  $R_t$ : 12.1 min. Detection at 371 and 640 nm. B) LC-MS Analysis of B<sub>12</sub>-Ex4-Cy5. ESMS Expected  $m/z = 6284$  (M1; B12-Ex4+Cy5) and  $6923$  (M2; B12-Ex4+2xCy5), observed  $m/z = 1258$   $[M1+5H]^{+5}$ ,  $1572$   $[M1+4H]^{+4}$ ,  $1383$   $[M2+5H]^{+5}$ ,  $1728$   $[M2+4H]^{+4}$ . 108

**Figure 12.** Excitation and Emission for B12-Ex4-Cy5. Excitation in green and emission in red. Solvent: H<sub>2</sub>O, excitation: 648 nm, emission: 670 nm. 109

**Figure 13.** B12-Ex4-Cy5 Agonism at the GLP-1R. Cells were infected with the H188 FRET cAMP reporter. Agonism shows the fluorescent compound retains function at the GLP-1R. Points are in triplicate.  $EC_{50}$ : 13 nM. Full sigmoidal curve could not be obtained due to the solubility of the conjugate. 110

**Figure 14.** Systemically delivered fluorescently labeled Ex-4 (F-Ex-4) highly penetrates within the DVC and the PVN. A) DVC uptake of F-Ex-4, B) Inset of A, C) PVN uptake of F-Ex-4, D) Inset of C. Ex4 (yellow), 111



astrocytes (GFAP; green) and neurons (NeuN; red). Sections were counterstained using DAPI (blue) to visualize cell nuclei. AP, area postrema; CC, central canal; DVC, dorsal vagal complex; NTS, nucleus tractus solitaries; 3V, third ventricle; PVN paraventricular hypothalamic nucleus. Images were acquired at 10-20x (A,C) or 63x (with 2-3x optical zoom) (B,D) magnifications.

**Figure 15.** Systemically-delivered fluorescently labeled B12-Cy5 does not penetrate the DVC or the PVN. A) DVC uptake of B12-Cy5, B) Inset of A, C) PVN uptake of B12-Cy5, D) Inset of C. B12-Cy5 (yellow), astrocytes (GFAP; green) and neurons (NeuN; red). Sections were counterstained using DAPI (blue) to visualize cell nuclei. AP, area postrema; CC, central canal; DVC, dorsal vagal complex; NTS, nucleus tractus solitaries; 3V, third ventricle; PVN paraventricular hypothalamic nucleus. Images were acquired at 10-20x (A,C) or 63x (with 2-3x optical zoom) (B,D) magnifications.

**Figure 16.** Systemically-delivered fluorescently labeled B12-Ex4-Cy5 does not penetrate the DVC or the PVN. A) DVC uptake of B12-Ex4-Cy5, B) Inset of A, C) PVN uptake of B12-Ex4-Cy5, D) Inset of C. B12-Cy5 (yellow), astrocytes (GFAP; green) and neurons (NeuN; red). Sections were counterstained using DAPI (blue) to visualize cell nuclei. AP, area postrema; CC, central canal; DVC, dorsal vagal complex; NTS, nucleus tractus solitaries; 3V, third ventricle; PVN paraventricular hypothalamic

nucleus. Images were acquired at 10-20x (A,C) or 63x (with 2-3x optical zoom) (B,D) magnifications.

## Chapter 5

**Figure 1.** Chemical structures of the anesthetics A) ketamine and B) xylazine. 122

**Figure 2.** An example of baseline hearing in guinea pigs through ABR. 124  
Hearing determined at 8 kHz, 6 kHz, and click (in descending order) for both the left and right ear for guinea pig 1. The seven characteristic peaks between 10 and 50 ms are at all frequencies. Baseline hearing was determined between -10 and 0 mV for all guinea pigs.

**Table 1.** Results of the ABR test using kanamycin over 23 days for guinea pigs 1-4. ABR's guinea pigs 2-3 were tested at 3, 5, and 6 weeks. No hearing loss was observed in any guinea pigs. 125

**Figure 3.** An example of ABR hearing test in guinea pigs administered kanamycin for 23 days. ABR results of guinea pigs 4's left ear. Hearing determined at 8 kHz, 6 kHz, and click (in descending order) for guinea pig 4 at 0 and 41 days. There was no observable hearing loss. 126

**Table 2.** Results of the ABR test using kanamycin and IF for 23 days for guinea pigs 5-8. Hearings tests were conducted at 3, 5 and 6 weeks p.i. using ABR's. There was no hearing loss observed for all guinea pigs. 128

**Figure 4.** An example of ABR hearing test in guinea pigs administered kanamycin and IF for 23 days. ABR comparison of guinea pig 7's left ear 128

between day 0 and week 4 p.i. Hearing determined at 8 kHz, 6 kHz, and click (in descending order). There was no hearing loss seen.

**Figure 5.** Daily weights of guinea pigs **1-8** during 23 days. Guinea pigs **1-4** had no IF injected and **5-8** had IF injected twice daily. \* Two injections of 13  $\mu\text{g}/\text{day}$ . Weights for each cohort increased steadily over time showing no difference in weight in each study. 129

**Figure 6.** ELISA IF antigenicity results for **2, 3, 6, 12,** and **18**. Guinea pigs that had no IF injected (**2, 3,** and **12**) show no antigenicity while guinea pigs (**6** and **18**) showed high indication of antigens in their blood. 130

## Chapter 7

**Figure 1.** Synthetic scheme for Cbi-Ex4. Dicyano-Cbi was functionalized with a terminal alkyne through CDT activation of the secondary alcohol with subsequent addition of aminobutyne in a one-pot reaction. Once purified the Cbi-alkyne and azido-Ex4 were linked using CuAAC chemistry. Final yield of 95%, based on B12-Ex4 starting material. 160

**Figure 2.** Characterization of Cbi-alkyne. A) RP-HPLC of Cbi-alkyne using an Eclipse XDB-C18 column. 0.1% TFA/H<sub>2</sub>O with MeCN gradient of 1 – 70% MeCN over 15 min,  $t_r = 8.0$  and 8.4 min. Analysis shows compound is 97% pure. B) LC-MS: Shimadzu LCMS-8040, ESMS Expected  $m/z = 1129$ , observed  $m/z = 556 [M-H_2O+2H]^{+2}$ , 1110  $[M-H_2O]^+$ . 160

**Figure 3.** A) RP-HPLC of Cbi-Ex4 using an Eclipse XDB-C18 column. 161

0.1% TFA/H<sub>2</sub>O with MeCN gradient of 1 – 70% MeCN over 15 min,  $t_r$  = 8.9 min. Analysis shows compound is 96% pure. B) LC-MS: Shimadzu LCMS-8040, ESMS Expected  $m/z$  = 5354, observed  $m/z$  = 1784 [M+3H]<sup>+3</sup>, 1338 [M+4H]<sup>+4</sup>, 1071 [M+5H]<sup>+5</sup>, 893 [M+6H]<sup>+6</sup>. No detection of free exendin-4 was seen.

**Figure 4.** Dose response of cAMP binding to the H188 reporter in real 162

time after administration of Cbi-Ex4 ranging from 1 nM – 3 pM. SES: standard extracellular solution with 0.01% BSA and 0.1 mM glucose. F/IBMX: forskolin and (3-isobutyl-1-methylxanthine) (IBMX) as a positive control.

**Figure 5.** Cbi-Ex4 agonsim at the GLP-1 receptor using the FRET H188 163

reporter in stability transfected HEK-GLP-1 cells. EC<sub>50</sub> of Cbi-Ex4 was determined to be 120 pM.

**Figure 6.** Dose response of cAMP binding to the H188 reporter in real 164

time after administration of HC-Cbi-Ex4 ranging from 1 nM – 3 pM. SES: standard extracellular solution with 0.01% BSA and 0.1 mM glucose. F/IBMX: forskolin and IBMX as a positive control.

**Figure 7.** HC-Cbi-Ex4 agonsim at the GLP-1 receptor using the FRET 165

H188 reporter in stability transfected HEK-GLP-1 cells. EC<sub>50</sub> of Cbi-Ex4 was determined to be 3 nM. Full sigmoidal curve could not be obtained due to the assay limits.

**Figure 8.** Western Blot of Asian Tree Shrew Blood. HC primary antibody (lanes 1-4) and TCII primary antibody (lanes 5-8). 1: recombinant human HC, 2: shrew serum, 3: recombinant pig TCII, 4 and 5: BioRad Kaleidoscope Protein Markers (10-250 kDa), 6: recombinant pig TCII, 7: shrew serum, 8: recombinant human HC.

## Chapter 1: Introduction

### 1.1 Vitamin B12

Vitamin B12 (B12, cobalamin) is an essential vitamin, one of thirteen required in the human diet (Table 1).<sup>1,2,3</sup> B12 is produced naturally by select bacteria (and likely certain archea).<sup>4,5</sup> Organisms that cannot produce B12 must acquire the vitamin through their diet, with the human requirement being 2.5 µg per day.<sup>1</sup>

Vitamin	Molecular Weight (g/mol)	Solubility	Primary Biological Function
A	286.4	Fat	Vision Health
C	176.1	Water	Protein metabolism
D	384.6	Fat	Ca <sup>2+</sup> Storage
E	430.7	Fat	Antioxidant
K	450.7	Fat	Blood Clotting
Thiamin (B1)	300.1	Water	Energy Metabolism
Riboflavin (B2)	376.3	Water	Energy Metabolism
Niacin (B3)	123.1	Water	Energy Metabolism
Pantothenic Acid (B5)	219.2	Water	Energy Metabolism
Pyridoxine (B6)	168.1	Water	Protein Metabolism
Biotin (B7)	244.3	Water	Energy Metabolism
Folate (B9)	441.4	Water	DNA and Cell Production
Cobalamin (B12)	1355.3	Water	Cell Production

**Table 1.** A list of all thirteen essential vitamins, molecular weight, solubility, and primary biological function.

However, unlike other water-soluble vitamins, the body can store B12, in the liver and kidneys, making identification of intake deficiency difficult.<sup>3,6</sup> B12 deficiency can lead to

pernicious and megaloblastic anemias, as well as various neurological disorders.<sup>1,7</sup> There are no known cases of B12 toxicity and there is no upper limit to dosing. B12 is an organometallic, composed of a Co(III)-carbon bond, with the biological activity is based on the bond dissociation energies of such are modulated by the presence of the cobalt in a corrin ring with a 5,6-dimethylbenzimidazole base (see Section 1.1.2).<sup>1,8-10</sup>

### 1.1.1 History of B12

In 1920, George Whipple discovered that an ‘extrinsic’ factor (later identified as B12) in liver was responsible for anemia recovery in dogs.<sup>11</sup> Then in 1926, George Minot and William Murphy, while studying pernicious anemia in humans, showed a liver supplemented diet reversed pernicious anemia in patients.<sup>12</sup> These discoveries won Whipple, Minot, and Murphy the Nobel Prize in Physiology or Medicine in 1934.<sup>13</sup> It wasn’t until 1948 that B12 itself was purified from liver.<sup>14</sup> In 1956 Dorothy Hodgkin determined the structure of B12 through single-crystal X-ray crystallography, winning her the 1964 Nobel Prize in Chemistry.<sup>8</sup>

### 1.1.2 Structure of B12

B12 has a midplanar corrin ring composed of four pyrrole rings linked to a central cobalt(III) atom.<sup>8</sup> The corrin ring is similar to the more commonly known porphyrin structure, but with key differences in terms of degree of saturation, symmetry and planarity (Figure 1). The f-side chain has a 5,6-dimethylbenzimidazole base that coordinates the central cobalt at the  $\alpha$ -axial position, producing the so-called ‘base-on’ form of B12.<sup>7,8</sup> The corrin ring, which has a greater number of sp<sup>3</sup> carbons than a porphyrin (10 rather than 0) rendering it less planar and

less conjugated. The corrin ring also has one less carbon (19 rather than 20) compared to a porphyrin due to the lack of a methylene spacer unit between the 'C' and 'D' rings (Figure 1).

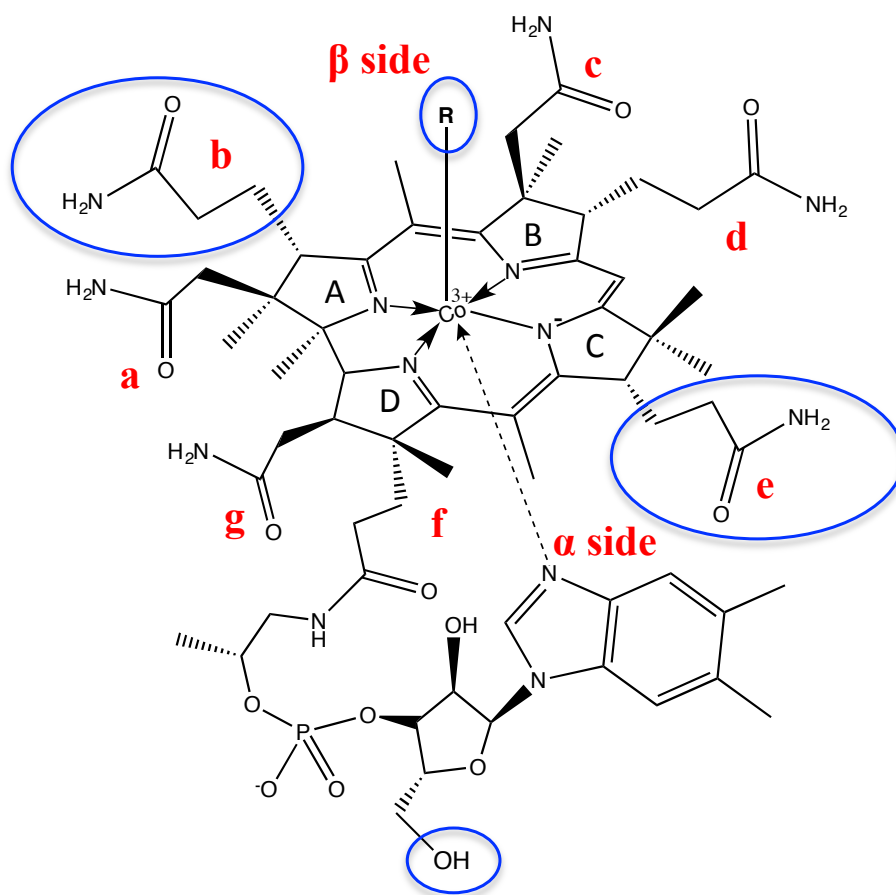


**Figure 1.** Structure of B12. Highlighted (blue) are the major modifiable sites on B12 for conjugation to small molecules or peptides/proteins, whereby binding by the dietary uptake proteins can be minimally affected, or selected for.

B12 has a variable  $\beta$ -axial ligand, common forms being methyl, adenosyl, hydroxyl, and cyano.<sup>1,7</sup> Cyanocobalamin is the form commonly found in B12 supplements and is the form used in all synthesis in this thesis.<sup>15</sup> The major modifiable sites on B12, for conjugation to small



molecules or peptides/proteins, whereby binding by the dietary uptake proteins can be minimally affected or selected for, are the  $\beta$ -axial ligand, the b-, and d-side chains and the 5'-hydroxyl group on the ribose ring (Section 1.1.5).<sup>16-21</sup>

### 1.1.3 Metabolism of B12

B12 is a cofactor for two enzymes, methionine synthase and methylmalonyl-CoA mutase (Figure 2).<sup>1,9,10,22,23</sup> There are two primary biologically active forms of B12: methylcobalamin and adenosylcobalamin. Cytosolic methionine synthase uses methylcobalamin to produce the amino acid methionine from homocysteine.<sup>23</sup> In the mitochondria, methylmalonyl-CoA mutase uses adenosylcobalamin as a cofactor to produce succinyl-CoA.<sup>9</sup>

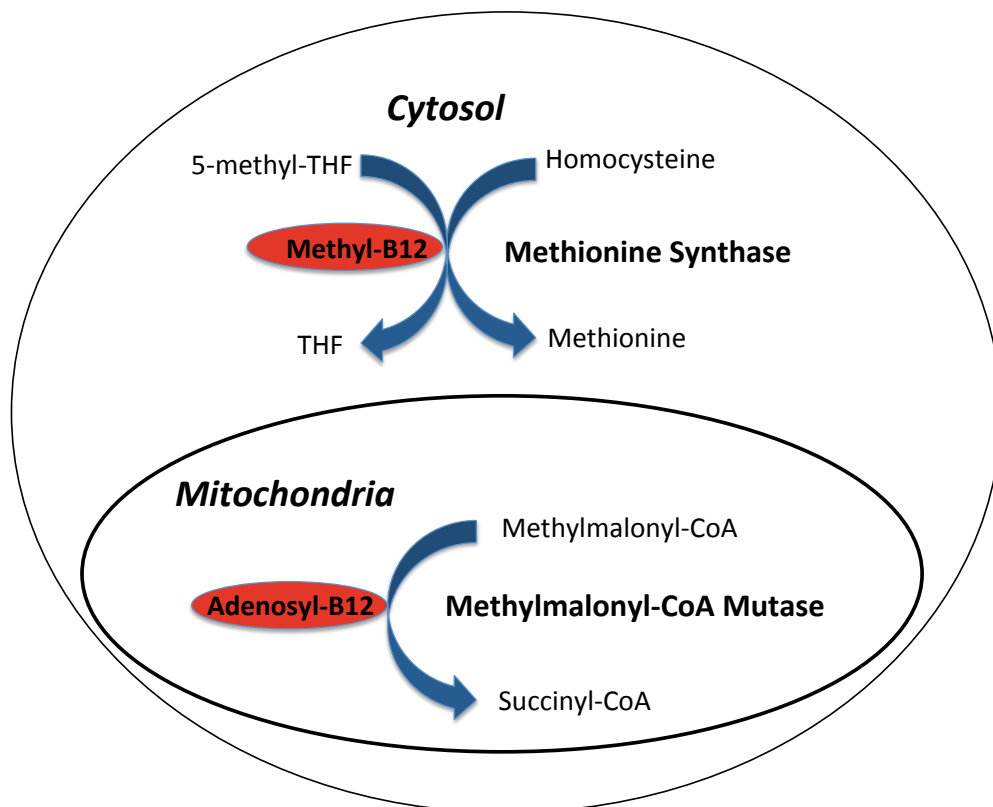


**Figure 2.** B12 function in the cell as a co-factor with methionine synthase and methylmalonyl-CoA Mutase.

Both enzymes use the cobalt-carbon bond to catalyze a methyl transfer to homocysteine and a radical-isomerization of methylmalonyl-CoA.<sup>7,9,23</sup> The oxidation state of the central cobalt, which can be Co(I), Co(II), or Co(III) at physiological conditions, determines B12's function as a cofactor.<sup>7</sup> Cyanocobalamin is not biologically active, but can be readily converted into methyl- or adenosyl-cobalamin for function.<sup>15</sup>

#### 1.1.4 Dietary Uptake of B12

Mammals have developed a complex dietary uptake pathway for B12 involving a series of transport proteins and specific receptors across various tissues and organs (Figure 3).<sup>1,7</sup> Transport and delivery of B12 is dependent on three primary carrier proteins: haptocorrin (HC;  $K_d = 0.01$  pM), intrinsic factor (IF;  $K_d = 1$  pM), and transcobalamin II (TCII;  $K_d = 0.005$  pM), each responsible for carrying a single B12 molecule.<sup>24</sup> B12 is initially released from food by the action of peptic enzymes and the acidic environment of the gastrointestinal system and bound by HC [also known as transcobalamin I or R-binder (TCI)].<sup>1,25</sup> Holo-HC travels from the stomach to the duodenum, where the increase in pH (>5) decreases the affinity of HC for B12 and, combined with pancreatic digestion of HC, causes B12 release, whereupon it is bound by gastric intrinsic factor (IF).<sup>24,26-28</sup>

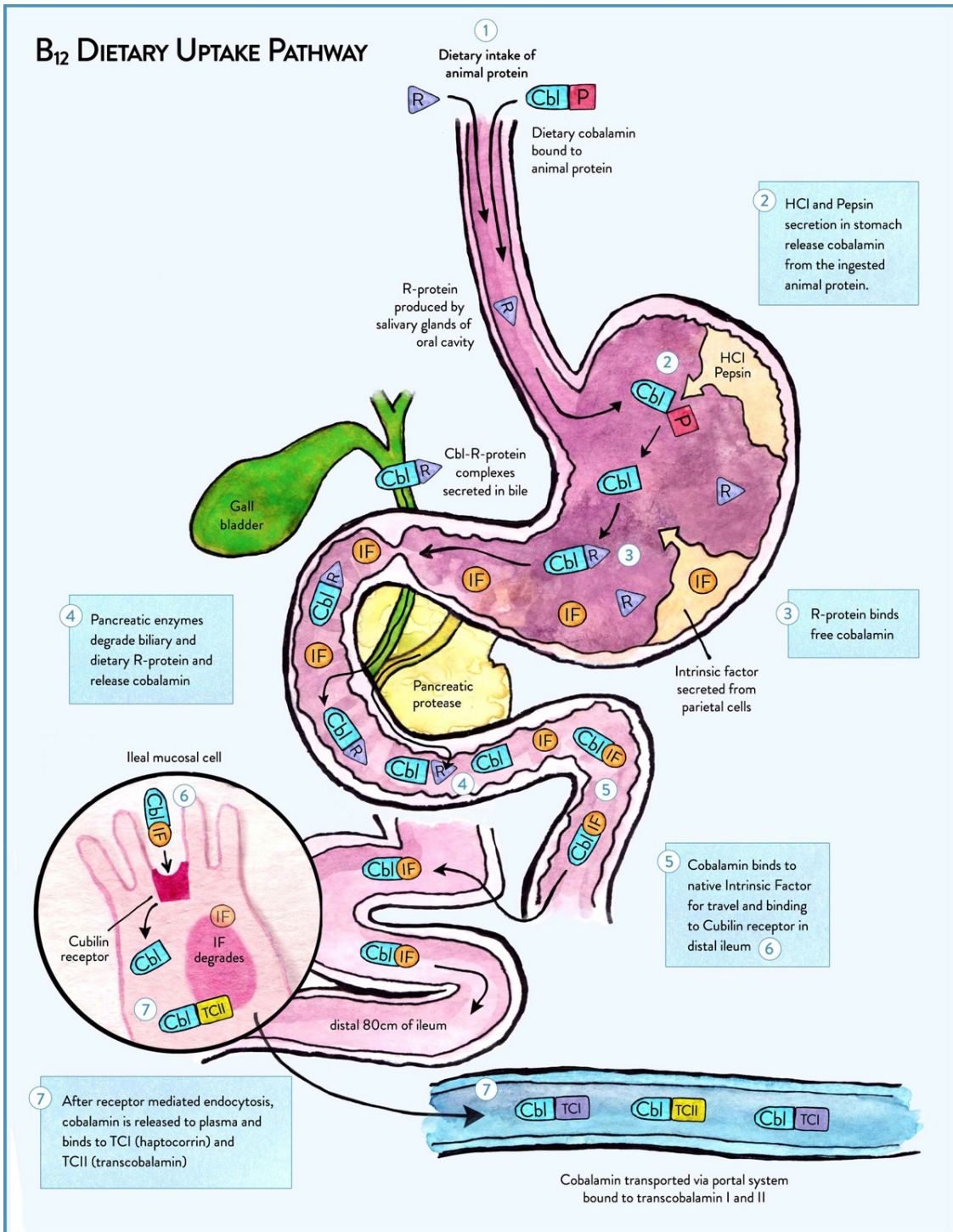


**Figure 3.** Dietary uptake pathway for B12 in humans. Abbreviations used: R-protein/TCI: Haptocorrin (HC); IF: Intrinsic factor; TCII: Transcobalamin II; Cbl: cobalamin/B12. Image used with permission of Xeragenx LLC (St. Louis, MO, USA).

Once B12 is bound to IF, it facilitates intestinal transport and passage across ileal enterocyte. This passage occurs via receptor-mediated endocytosis through the IF-B12 receptor cubilin (CUBN).<sup>27,29</sup> CUBN transports holo-IF in concert with a transmembrane protein amnionless (CUBAM).<sup>30</sup> Following internalization, IF is degraded by lysosomal proteases, such as cathepsin L, and B12 is released into the blood stream, either as free B12 or pre-bound to transcobalamin II (TCII).<sup>1,31</sup> There is some controversy in this area as to whether both occur or one dominates over the other, and indeed whether there is third mechanism at play. Cells that require B12 express the holo-TCII receptor, CD320.<sup>1,22,32</sup> Upon internalization, TCII is degraded and B12 is transported from the lysosome for cellular use. Kidney cells also express the megalin receptor, which in part reabsorbs filtered holo-TCII from urine for TCII recirculation.<sup>33,34</sup>

#### 1.1.4.1 Transport Proteins of B12

HC is a glycoprotein with a molecular mass of between 60-70 kDa and is secreted by the salivary glands (crystal structure shown in Figure 4).<sup>35</sup> HC is resistant to low pH and has a high affinity for B12 ( $K_d = 0.01$  pM) under acidic conditions ( $\text{pH} < 3$ ), allowing it to protect B12 from acidic hydrolysis.<sup>1,7</sup> HC is also found within the bloodstream where it binds ~80% of total serum B12, with a half-life of ~9 days.<sup>16,36</sup> The role of holo-HC in the bloodstream is not clear as there is no known receptor for holo-HC, albeit it may play a role in bacteriostasis.<sup>37,38</sup> IF is a ~50 kDa glycosylated protein that is secreted from the gastric mucosa and is resistant to pancreatic enzymes, such as trypsin and chymotrypsin (see Section 1.2).<sup>28,39</sup>

TCII, ~50 kDa, is a non-glycosylated protein that is secreted into the blood primarily from liver cells and bone marrow (crystal structure shown in Figure 4).<sup>40-42</sup> Holo-TCII is recognized by CD230 and megalin (within the kidney), where upon binding it is rapidly

internalized into proliferating cells (within minutes).<sup>1,7,43</sup> TCII concentrations found in humans are in average of 0.6-1.5 nmol/L.<sup>44</sup> TCII concentrations found in rats are 2 nmol/L and in mice are 20 nmol/L in mice, important to consider during in vivo experiments.<sup>45</sup>

All three transport proteins (HC, IF and TCII) bind to B12 with affinities in the pM range but their specificity varies. IF shows the highest specificity for B12, followed closely by TCII, with HC having a broad substrate base including B12 analogs such as cobinamide.<sup>17,24</sup> It is thought because of the affinity of HC for many inactive B12 analogs that it acts as a scavenger, removing such from the blood and partially digested B12 from the intestine, preventing bacterial access (thus suggesting a role for B12 in bacteriostasis).<sup>17,24,35,41</sup> Viewed synthetically, this implies that B12 can be readily modified and retain recognition by HC, whereas IF and TCII offer significantly less range for modification (for more detail see Chapter 7, Section 7.2).

Knowledge of the binding between B12 and its various transport proteins is critical if the system is to be successfully exploited from bench-top to bedside. In the last 10 years there has been a huge advance in critical understanding of transport protein structure as it relates to the B12 uptake pathway, with the publication of HC, IF, TCII, and cubilin-IF-B12 structures (Figure 4).<sup>35,39,42</sup> HC, TCII, and IF have similar protein structure and bind B12 in a similar manner, at the interface of two domains.

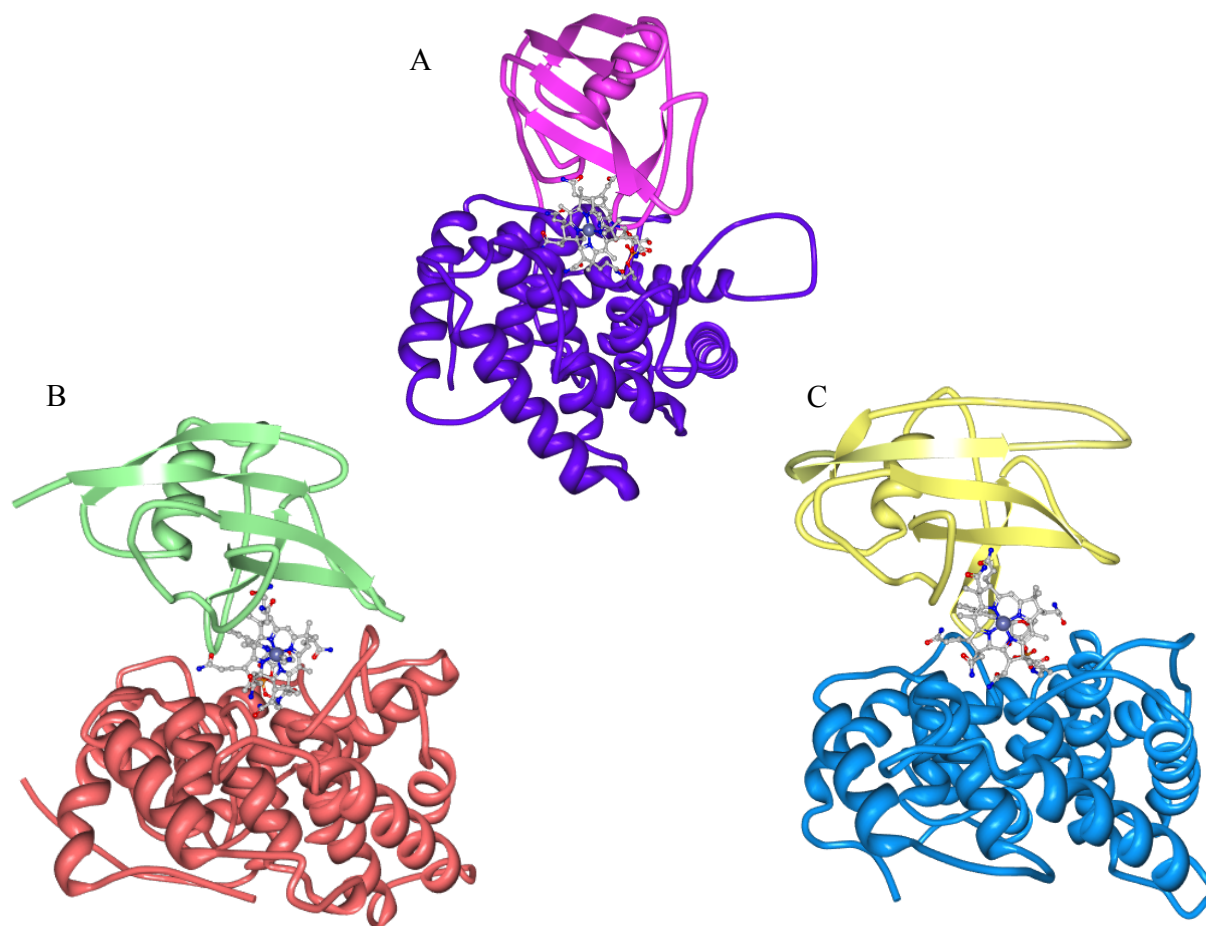


**Figure 4.** Transport Proteins Bound to B12. A) TCII, B) HC, and C) IF. PDB code 2BB5, 4KK1, 2PMV, respectively.

### 1.1.5 B12 Modification

B12 modification, essential for the development of B12 chemistry, ideally should have 1) an ease of synthesis and 2) retention of recognition of B12 transport proteins.<sup>46</sup> B12 modification resulting in the recognition of HC, IF, and TCII have been successful with four major sites to date: 1) the peripheral corrin ring e-side chain; 2) the peripheral corrin ring b-side chain; 3) the 5'-hydroxyl group of the ribose ring on the dimethylbenzimidazole base; and 4) the cobalt cation (Figure 1, Section 1.1.2).<sup>16,19,20,47-49</sup>

The crystal structure of holo-TCII provides a rationale for why these positions are available for modification.<sup>42</sup> The phosphate moiety, 2'-hydroxyl group, and a, c, d, and g-side chains have various hydrogen bonds between multiple TCII residues and the solvent molecules indicating any modifications would disrupt that bonding and stability of the TCII-B12 complex (Figure 4). In addition, TCII does not completely encompass B12 and leaves a 1.4 nm solvent-accessible pocket, showing the phosphate and the ribose moieties protruding. Both the phosphate and the ribose moieties have been exploited in conjugate design whereby TCII and IF binding was maintained at the nM level.<sup>50,51</sup>

Modification to the b- and e-side chains have been a popular choice for chemists.<sup>16,48,49</sup> Such a route requires acid hydrolysis of the amides, typically using 1 N HCl, creating multiple mono-acids at the b, d and e-positions, which makes access to targeted specific acids low yielding ( $\leq 15\%$ ) and complex to purify.<sup>52</sup> A recent result exploiting this approach however, is that of Schubiger *et al.*, who showed that, based on the tether length off of the b-acid side chain, selectively towards specific transport proteins (IF over TCII, for example) could be achieved (see Section 1.1.6 and 1.3.4).<sup>16</sup>

The most common site for modification has, however, become the 5'-hydroxyl group, for three main reasons: 1) conjugation still allows binding retention of the transport proteins; and 2) conjugation to this site is highly facile and selective; and 3) a wide range of modifications have been developed for this site, expanding scope for substrate conjugation.<sup>19,20,47,50,53,54</sup> The “classic” activation with 1,1'-carbonyldiimidazole or 1,1'-carbonyldi(1,2,4-triazole) with an addition of a primary amine, producing a carbamate linked conjugation, allows for a wide range of molecules to be used.<sup>55</sup> Doyle *et al.* directly modified this position, using 2-iodoxybenzoic

acid and 2-hydroxypyridine, to create a carboxylic acid at this position, which could then be readily used to produce amide linked conjugates.<sup>47</sup>

Later, Gryko *et al.* developed a “clickable” B12 conjugate, replacing the 5'-hydroxyl with an azide, which allows for a high yielding Huisgen-Sharpless copper-azide-alkyl reaction, creating a stable triazole linker with alkyne containing molecules.<sup>19</sup> Most recently, Gryko also developed a reactive pyridyl disulfide group at this site, allowing the possibility of direct disulfide bonds to proteins and molecules, opening up a new area for conjugation that readily exploits redox for the first time.<sup>20</sup>

#### 1.1.6 B12 in Drug Delivery

There are several excellent reviews in this area that the reader is referred to here. In particular the reader is referred to a 2017 review by this author provided in Appendix A of this document.<sup>56-58</sup> This section will serve as a brief summary of the B12 drug development field.

Few peptide/protein-based drugs have the ability to survive the gastrointestinal tract and/or cross the intestinal wall to make it to the systemic circulation.<sup>59</sup> The B12 pathway has naturally developed a complex mechanism for this uptake. Researchers can “hijack” this pathway to deliver B12-drugs in an oral manner. Early research in B12-peptide/protein oral drug delivery was conducted by Russell-Jones and co-workers in the 1990's focusing on B12 conjugates of granulocyte colony stimulating factor, erythropoietin, luteinizing hormone-releasing hormone, ANTIDE-1, and ANTIDE-3.<sup>60,61</sup> Since then other groups have shown B12-molecules being transported via the B12 pathway across intestine cell lines in vitro and in vivo<sup>53,54,62,63</sup>.



In 2016, Mishra *et al.* showed a B12-chitosan layered nanoparticle that encapsulated insulin had a 10-fold increase in effective insulin duration *in vivo* when administered orally, achieving a maximum drop in glucose of ~40%.<sup>63</sup> Although data suggests drugs can be delivered orally through this pathway there are some limitations. There is a limited pool of CUB expressed in the terminal ileum, which limits IF-mediated absorption to ~1.5 µg per meal (1 nmole/dose).<sup>64</sup> Survival of enterocyte passage by a peptide bound to B12 is also unknown, as is whether such a conjugate would arrive in serum bound or unbound to TCII (with implications for subsequent function).

In 2015, Doyle *et al.* published on a subcutaneously administered B12-PYY<sub>3-36</sub>.<sup>65</sup> Peptide YY<sub>3-36</sub> (PYY<sub>3-36</sub>) is an endogenous appetite suppressing peptide that is an agonist for the neuropeptide Y2 receptor in the intestines and arcuate nucleus of the hypothalamus. Food intake (FI) was significantly reduced over a five day course for B12-PYY<sub>3-36</sub> (24%) compared to PYY<sub>3-36</sub> (13%), In addition, reduction of FI was more consistent after each dose through the course of the rats feeding cycle for B12-PYY<sub>3-36</sub> (26%, 29%, and 27%) compared with PYY<sub>3-36</sub> treatment (3%, 21%, and 16%).<sup>65</sup> These findings demonstrate significant pharmacodynamic improvement upon simple conjugation of B12 to PYY<sub>3-36</sub> for subcutaneous delivery.

In 2015, Doyle *et al.* focused on the stability (as defined by retention of peptide/protein agonist receptor function) of a B12 conjugate of the glucose controlling (GLP-1R agonist), exendin-4 (Ex-4) (see Section 1.5).<sup>50,66</sup> Either as the B12-conjugate, or bound by IF, function at the GLP-1R relative to undigested controls was investigated using proteases from both the gastrointestinal tract (trypsin and chymotrypsin) and kidney (meprin β).<sup>50</sup> The addition of IF produced up to a four-fold increase in function compared to Ex-4 alone, when digested by trypsin, and no statistical decrease in function when challenged by meprin β. These results offer

a significant opportunity for exploitation. Increase in gastric stability, even on a small percentage scale, could provide a route to achieving the desired effect orally. This work also suggests the possibility of utilizing an IF-B12-drug complex in serum, thus expanding use of IF beyond oral administration.

## 1.2 Intrinsic Factor Protein

IF is secreted from gastric parietal cells and binds B12 ( $K_d = 1.0 \text{ pM}$ ) once released from HC, after HC is degraded by pancreatic enzymes.<sup>17,67</sup> IF is a glycosylated protein making it resistant to pancreatic enzymes, protecting B12 until it reaches the ileum where CUBN is expressed and it is internalized.<sup>1</sup> When IF is internalized into ileal enterocyte and it is degraded in the lysosome by enzymes, such as cathepsin L.<sup>68</sup>

### 1.2.1 History of IF

IF was initially discovered in 1929 by William Castle. Experiments indicated that patients, who had pernicious anemia, showed improvement when administered human gastric juices.<sup>69</sup> The treatment of gastric juices indicated an '*intrinsic factor*' was treating the anemia. Castle showed that while an increase in '*extrinsic factor*' (B12) helped treat anemia, another lack of '*intrinsic factor*' reduced the bodies' ability to access B12, hence the name (IF).<sup>70</sup>

### 1.2.2 The Receptor Cubilin

CUBN (~500 kDa) is the only known receptor for holo-IF. CUBN binds other ligands such as albumin, holo-transferrin, cholesterol, receptor-associated protein, aminoglycosides, and holo-vitamin B binding protein (Figure 5).<sup>71-76</sup> CUBN is limited in expression and is expressed in the

renal brush boarder, placental membrane, yolk sac, small intestine, gallbladder, and the inner ear.<sup>76-80</sup> CUBN is a peripheral membrane protein and is expressed with two transmembrane proteins amnionless and megalin that work in concert with CUBN to internalize CUBN ligands.<sup>78,79,81</sup>

#### 1.2.2.1 Structure of Cubilin

CUBN is a peripheral membrane protein that has three distinct domains. It has a C-terminal region, eight epidermal growth factor-related domains, and 27 CUB domains. The 27 CUB domains are where CUBN ligands are recognized, with CUB5-8 recognizing IF.<sup>82,39</sup> The C-terminal domain anchors CUBN to the membrane and also has been shown create CUBN trimmers.<sup>83</sup>

#### 1.2.2.2 Amnionless

Amnionless is a transmembrane protein (40-50 kDa) and is always expressed with CUBN (CUBAM).<sup>76,84,85</sup> Mutations in the amnionless gene or CUBN gene do not allow either protein to be expressed.<sup>76,85</sup> Amnionless assists CUBN in the internalization of CUBN ligands and does not recognize any substrates.

#### 1.2.2.3 Megalin

Megalin is a transmembrane protein (600 kDa) that can be expressed with CUBN.<sup>34</sup> Megalin has shown to be expressed with CUBN in the kidney, placental membrane, inner ear, and visceral yolk sac.<sup>71,76,86</sup> Megalin can be expressed without CUBN and is more widely expressed than CUBN in tissues such as thyroid, parathyroid gland, and choroid plexus. Megalin

recognizes a considerably greater number of substrates than CUBN, while a select few substrates bind to both (Figure 5).<sup>34</sup>

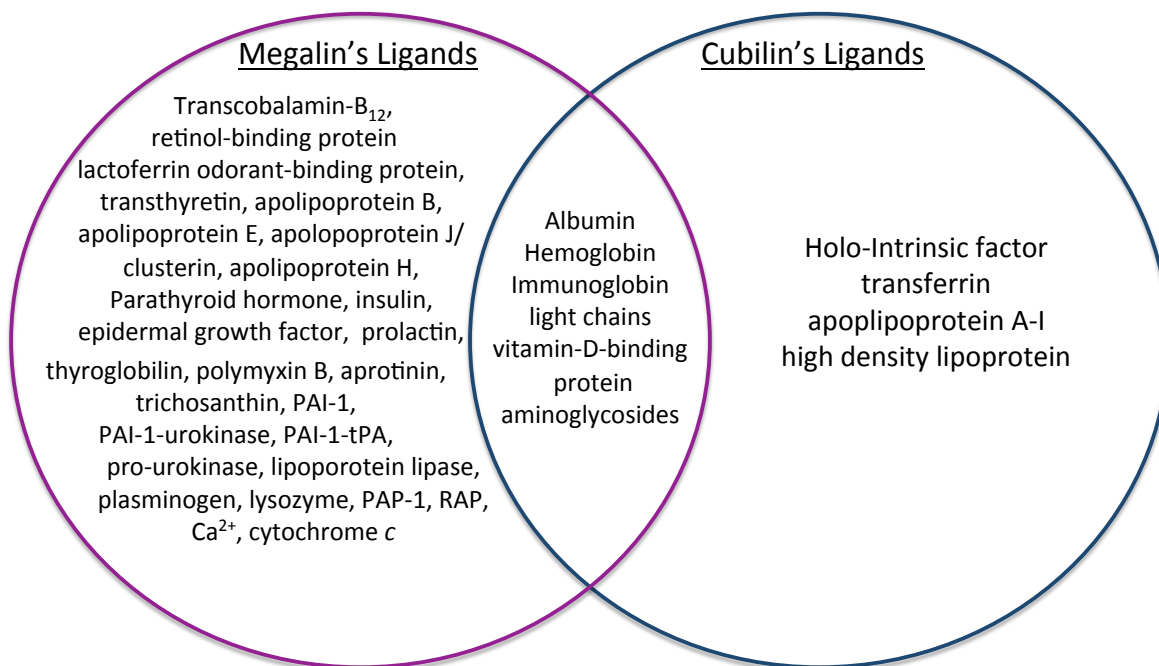


**Figure 5.** Megalin and cubilin's binding substrates, substrates in the center are recognized by both receptors.

#### 1.2.2.4 The Crystal Structures of Holo-IF and Cubilin Bound to Holo-IF

In 2007, Mathew *et al.* published the crystal structure of IF (produced in *Pichia pastoris*) bound to B12 (Figure 4).<sup>39</sup> Results showed IF having two domains,  $\alpha$  (~270 residues) and  $\beta$  (~110 residues), with B12 bound between the two domain interfaces. All but 19% of B12 is buried in the complex. There are nine residues that bind to B12 directly and there are equal hydrogen bonds to B12 from each domain. Histidine was not found coordinated to the central cobalt of IF, unlike such observed in the TCII crystal structure.<sup>42</sup> The glycosylation site was determined to be on asparagine-395.<sup>39</sup>

In 2010, Andersen *et al.* published holo-IF (produced in *P. pastoris*) bound to CUB domains 5-8.<sup>27</sup> The structure shows that both the  $\alpha$  and  $\beta$  domains bind to CUBN, supporting IF has to be bound by B12 to be recognized by CUBN. The  $\alpha$  domain binds directly to CUB-6 (25-299 residues on IF) and the  $\beta$  domain binds to CUB-8 (308-417 residues on IF). CUB-5 and CUB-7 do not interact with IF but plays a structural role in combination with  $\text{Ca}^{2+}$ , which binds to all four CUB domains.<sup>27</sup> The crystal structure also shows holo-IF remains structurally similar to unbound holo-IF.

### 1.3 Radioimaging Utilizing the B12 Dietary Pathway

#### 1.3.1 Single Photon Emission Computed Tomography and Positron Emission Tomography Imaging

Single Photon Emission Computed Tomography (SPECT) is a form of three-dimensional nuclear imaging that creates an image by tracing a radioisotope's gamma ray emissions.<sup>87</sup> Positron Emission Tomography (PET) is also a three-dimensional imaging tool that detects a radioisotope's positron emissions by detecting gamma rays emitted when positrons are released and react with electrons.<sup>87</sup> The key differences between SPECT and PET imaging are 1) the radioisotopes used, 2) PET is higher in sensitivity (two-three orders). PET's increase in sensitivity allows for shorter imaging time, less radio-dose injected, and improved diagnoses.<sup>87</sup> With that said PET has been gaining popularity especially in cancer detection.<sup>88</sup> Experiments in this thesis use the SPECT radioisotope <sup>99m</sup>Tc and the PET radioisotopes <sup>64</sup>Cu and <sup>89</sup>Zr to investigate B12 and IF uptake in vivo (Chapters 2 and 3).<sup>89-91</sup>

### 1.3.1.1 Radioisotope $^{99m}\text{Tc}$

$^{99m}\text{Tc}$  (Technetium-99m) was discovered in 1938 by Seaborg and Segrè.<sup>92</sup> Since then it has become the most commonly used radioisotope in nuclear imaging, due to its half-life of 6 h and is easily generated on site.<sup>89</sup>  $^{99m}\text{Tc}$  uniquely emits a gamma ray while not emitting a beta ray.<sup>93</sup> In combination with its half-life (6 h) and lack of beta ray decay makes  $^{99m}\text{Tc}$  a safer radioisotope compared to isotopes that have longer half-lives and emit beta rays, such as  $^{131}\text{I}$ .<sup>94</sup>  $^{99m}\text{Tc}$  is primarily used for medical imaging in bone scans and cardiac function.<sup>95,96</sup>

### 1.3.1.2 Radioisotope $^{64}\text{Cu}$

$^{64}\text{Cu}$  (Copper-64) is a radioisotope for PET imaging, has a half-life of 12.7 h, and decays through three mechanisms, positron, beta, and electron capture.<sup>97,98</sup> This half-life allows  $^{64}\text{Cu}$  to be utilized on small molecules as well on large proteins that have a slow clearance rate (2-4 days) such as antibodies.<sup>90,99</sup>  $^{64}\text{Cu}$  is a popular PET isotope due to its well-established coordination chemistry allowing ease of radiolabeling to multiple ligands.<sup>97,98</sup>

### 1.3.1.3 Radioisotope $^{89}\text{Zr}$

$^{89}\text{Zr}$  (Zirconium-89) is a radioisotope for PET imaging and has a half-life of 3.27 d, and decays through positron and electron capture.<sup>91,100</sup>  $^{89}\text{Zr}$  has become increasingly popular due the conception of immuno-PET imaging.<sup>101</sup> Immuno-PET imaging is based on the premise that monoclonal antibodies allow for disease-specific agents in diagnostic imaging. In cancer research these antibodies allow targeting to specific cancer tumors and, due to PET's sensitivity, can also detect a response to treatment.<sup>101</sup>  $^{89}\text{Zr}$  has an ideal half-life for antibodies targeting, as

they are large and therefore slow to accumulate in the tumor (2-4 days), thus  $^{89}\text{Zr}$  allows for a longer visualization time (1-5 days) and improved background/tumor ratio.

### 1.3.2 Specific Targeting Using Radio-B12 Conjugates

A B12 conjugate injected in the systemic circulation can be bound by HC or TCII. Initially, it was hypothesized that cancer therapy/imaging using a B12 based delivery mechanism would work based on a projected increase in the TCII receptor, CD320, in a variety of cancer types such as breast, ovarian, thyroid, uterine, testis, and brain cancer.<sup>51,102-104</sup> This overexpression of CD320 would provide sufficient uptake of a tracer bound to endogenous TCII vs uptake in healthy tissue. Such studies, however, suffered from high background accumulation in the liver and kidneys, primarily due to megalin expression.

The use of HC binding was not investigated until 2008, when Schubiger *et al.* made a series of B12 conjugates that would selectively bind HC (and IF), but not TCII.<sup>16,105,106</sup> The hypothesis here was that, given the presence of TCII and HC in serum, and assigning the high background to TCII mediated cell entry, targeting only HC would offer improved results. Membrane associated HC, expressed *de novo*, in certain cancer cell lines offered a possible route to selectivity, absent from the approach to CD320 uptake. In 2014,  $^{99\text{m}}\text{Tc}$ -PAMA-cobalamin, capable of selectively binding HC in blood serum, used in the detection of breast, colon, lung, and pharyngeal cancers in human patients.<sup>105</sup> This conjugate showed greater tumor uptake and reduced TCII-based background, relative to preceding reports so far. This publication is highly significant for B12 drug development, especially since it was performed in human patients.

### 1.3.2.1 A History of SPECT B12 Conjugates

Table 2 lists the B12-imaging agents reported to date. Historically, imaging using B12 targeted the CD320 receptor, based on the premise that overexpression of CD320 on rapidly proliferating tumor cells would provide necessary tumor to background ratio's. However, this technique proved highly limited due to observed high background uptake across tissues. Early investigators used cobalt radioisotopes ( $^{57}\text{Co}$ ,  $^{58}\text{Co}$ ,  $^{60}\text{Co}$ ) to radiolabel B12 for imaging, due to the naturally occurring cobalt center.<sup>107,108</sup> However, the half-life of the radionuclides (272 days, 71 days, and 77 days, respectively) are too long for successful external images. Since then other radioisotopes,  $^{111}\text{In}$  (2.8 days),  $^{131}\text{I}$  (8 h), and  $^{99\text{m}}\text{Tc}$  (6 h), have been conjugated to B12.<sup>51,103,109,110</sup> Unfortunately, they still resulted in undesired organ accumulation, limiting their use due to high background uptake in healthy cells.



Molecule	Conjugation Site	Linker	Ref
<sup>99m</sup> Tc-DTPA	b-side chain	1,4diaminobutane	51
<sup>111</sup> In-DTPA	b-side chain	1,4diaminobutane	103
[ <sup>99m</sup> TcO <sub>4</sub> ] <sup>-</sup>	Beta ligand	Imidazolecarboxylic acid	110
		Picolinic acid	
		2,4-dipicolinic acid	
		Serine	
		N,N-dimethylglycine	
<sup>131</sup> I	Beta ligand	Cisplatin	109
[ <sup>99m</sup> Tc(CO) <sub>3</sub> (OH <sub>2</sub> ) <sub>3</sub> ]	b-side chain	Propyl-PAMA-OEt	16
		Ethyl-PAMA-OEt	
		Butyl-PAMA-OEt*	105/106
		Pentyl-PAMA-OEt	
		Hexyl-PAMA-OEt	
	b-side chain	3-c-Histidinate	102
	d-side chain	3-c-Histidinate	
	b-side chain	4-c-Histidinate	
	c-side chain	4-c-Histidinate	
<sup>64</sup> Cu-NOTA	Ribose 5'-OH	En-SCN-Bn	111

**Table 2.** All B12-radioimaing agents reported to date. DTPA: diethylenetriamine-N,N;N',N'', N''''-pentaacetic acid; PAMA: [pyridine-2-ylmethyl-amino]-acetic acid; 3-c-Histidinate: 1,3-propanamine-1-carboxymethyl-N-histidinate; 4-c-Histidinate: 1,4-aminobutane-1-carboxymethyl-N-histidinate; SCN-Bn-NOTA; isothiocyanatobenzyl-1,4,7- triazacyclononane-N,N',N''-triacetic acid. \*Conjugate was selected for human studies targeting tumors.

### 1.3.2.2 A History of PET B12 Conjugates

Only one PET B12 conjugate has been reported to date, in 2014, Doyle *et al.* published a B12-PET imaging probe using a B12-NOTA conjugate labeled with <sup>64</sup>Cu.<sup>111</sup> PET imaging and

ex vivo biodistribution were conducted with four cancer cell lines: pancreatic (MIA PaCa2), ovarian (SKOV-3), colorectal (HCT116), and murine melanoma (B16-F10). The highest percent injected dose per gram (%ID/g) reported was  $4.84 \pm 0.32$  at 6 h in the colorectal tumor model. However, as was observed with previous studies, the same high background trend was seen, with high accumulation in the liver and kidneys.

#### 1.4 Human and Plant N-Glycosylation

Protein glycosylation is an important post-translational modification in all eukaryote cells. It has been shown that initial steps of N-glycosylation are similar between plants and mammals.<sup>112,113</sup> Later steps deviate, creating distinct glycosylation profiles for each (Figure 6). Plant glycosylation tends to be less sophisticated without branching or being sialylated, in comparison to mammal glycosylation.

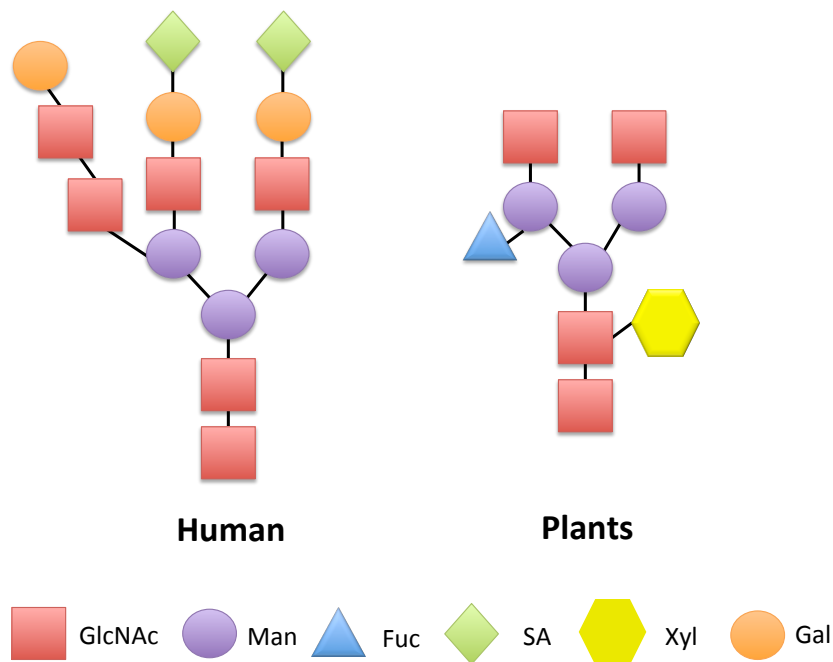


**Figure 6.** Comparing typical N-glycosylation of Human and Plants. GlcNAc: *n*-acetylglucosamine, Man: mannose, Fuc: fucose, SA: sialic acid, Xyl: xylose, Gal: galactose.

#### 1.4.1 Human N- Glycosylation

Most Eukaryotes, including humans, utilize glucoseamine (Glc), mannose, and *n*-acetylglucoseamine (GlcNAc) as a base for glycosylation, which is attached to select asparagine (N) residues.<sup>113</sup> Glycosylation can be highly complex with multiple branched sugars (Figure 6). Human glycoproteins are terminally sialylated.<sup>114</sup> Removal of the terminal sialic acid usually exposes galactose, a sugar recognized by the liver, which degrades asialylated glycoproteins.<sup>115</sup>

#### 1.4.2 Plant N- Glycosylation

Plants, similarly to humans, also have a base of Glc, mannose, and GlcNAc attached to N residues on proteins (Figure 6).<sup>112</sup> However, plant glycosylation is less sophisticated than humans, typically not branched, and is not terminally sialylated. Lack of terminal sialic acid can facilitate liver based degradation and immune response to plant glycoproteins.<sup>116</sup> In addition, plants can incorporate different sugars, such as xylose (not seen in humans).

#### 1.4.3 Asialoglycoprotein receptor

Asialoglycoprotein (ASGPR) is a glycoprotein that clears glycoproteins, which have a terminal galactose, *n*-acetylgalactoseamine from blood serum.<sup>115</sup> ASGPR has also been shown to remove cholesterol. ASGPR is highly expressed in the liver sinusoidal endothelial (liver capillary lining) cells, and is the receptor responsible for clearing endogenous proteins for recycling.

#### 1.4.4 Mannose Receptor Family

The mannose receptor family (MRF) is a group of four glycosylated receptor proteins that are expressed in mice and humans.<sup>117</sup> They are CD206, CD205, Endo180, and phospholipase A2 receptor (PLA<sub>2</sub>R).<sup>117-120</sup> Endo 180 is involved in the turn over of extracellular matrix.<sup>119</sup> PLA<sub>2</sub>R is activated by PLA<sub>2</sub> molecules and has been shown to be involved with membranous nephropathy, an autoimmune disorder that prevents the kidney from functioning properly<sup>120</sup>. The MRF are all type 1 transmembrane proteins, part of the C-lectin family and have a common motif with N-terminal cysteine rich domain, fibronectin II domain, and eight-ten carbohydrate recognition domains.<sup>117</sup>

##### 1.4.4.1 CD205 Receptor

Cluster of differentiation 205 (CD205) is a member of the MRF and is predominantly expressed on hepatic dendritic cells and thymic epithelium.<sup>118</sup> CD205 can recognize mannose, fucose, *n*-actylglucosamine, and glucose. However, CD205's expression can be inconstant depending on the stage of the dendritic cell.<sup>121</sup>

##### 1.4.4.2 CD206 Receptor

Cluster of differentiation 206 (CD206) is a transmembrane glycoprotein predominantly expressed by macrophages, dendritic cells, and select lymphatic and liver endothelial cells.<sup>117,122</sup> CD206 is expressed in the liver sinusoidal endothelial (liver capillary lining) cells. CD206 recognizes mannose, fucose, *n*-actylglucosamine, and glucose. Its extracellular regions include N-terminal cysteine rich domain (binds to *n*-actylglucosamine and glucose), fibronectin II domain, and eight carbohydrate recognition domains (binds mannose and fucose). CD206's main

role is to remove unwanted mannose linked glycoproteins from circulation. Due to many microbes, such as *Mycobacterium tuberculosis*, having a mannan-coated cell wall, CD206 plays a large role in the immune response.<sup>123</sup>

## 1.5 Glucagon-like-peptide Receptor Peptide Agonists

### 1.5.1 Glucagon-like Peptide-1

Glucagon-like Peptide-1 (GLP-1) is produced in the intestinal L cells and is released after a meal.<sup>124</sup> GLP-1 is an incretin hormone in humans, which is primarily responsible for controlling insulin levels in response to a rise in glucose levels in the blood.<sup>125</sup> Most humans have a typical fasting plasma level of GLP-1 of 5-10 pmol/L, which can increase upon glucose addition.<sup>126</sup> The enzyme dipeptidyl peptidase IV (DPP-IV) quickly degrades GLP-1, as it cleaves any peptide with an alanine or proline at the second position from the N-terminus, resulting in rapid clearance (half-life being 2 minutes).<sup>127</sup> The GLP-1 receptor (GLP-1R) is located in the pancreatic  $\beta$ - cells as well as the brain, stomach and adipose tissue.<sup>128-130</sup>

### 1.5.2 Exendin-4

During the late 1980s and early 1990s Eng *et al.*, was researching peptides found in the *Heloderma* family of lizards. The team initially discovered exendin-3, a GLP-1R agonist.<sup>131</sup> In 1992, exendin-4 (Ex-4) was discovered as a more potent agonist to GLP-1R. Ex-4 is an incretin mimetic, sharing 53% amino acid sequence similarity with GLP-1, and acts similarly to GLP-1 (Figure 7).<sup>132</sup> However, unlike GLP-1, Ex-4 is resistant to the enzyme DPP-IV, with a glycine in place of alanine, as the second amino acid. This degradation resistance allows Ex-4 to have a half-life of 2.4 h.<sup>133</sup> Such resistance to DPP-IV does not, however, translate to other proteases,

and exenatide (synthetic Ex-4) therefore must be administered subcutaneously. Exenatide was approved as a pharmaceutical as the first incretin mimetic under the name Byetta in 2005.<sup>134</sup> Common side effects of Ex-4 include pronounced nausea, vomiting, and malaise, occurring in ~50% of patients.<sup>135-137</sup>

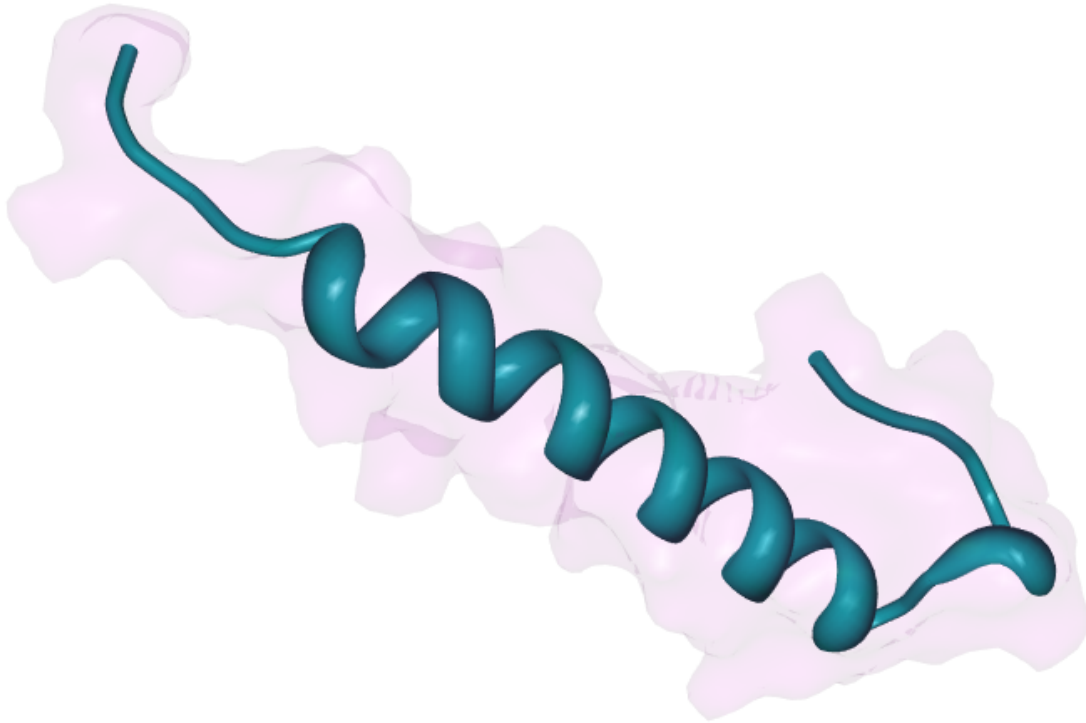


**Figure 7.** Structure of Ex-4. Note significant helical content (46%) and a C-terminal hair-pin (1JRJ).

### 1.5.3 Glucagon Receptor Family

The glucagon receptor superfamily includes the glucagon receptor, GLP-1R, glucagon-like peptide 2, and glucose-dependent insulinotropic peptide receptor.<sup>138,139</sup> Although the glucagon receptor family and corresponding peptide agonists share many similarities, each receptor maintains a high affinity for only one peptide.<sup>138</sup> This family is part of the G protein-

coupled receptors (GPCR).<sup>140,141</sup> GPCRs are classified into three classes; class A, B, and C.<sup>142</sup> The glucagon receptor superfamily is part of class B. Class B GPCRs are part of the secretin family and are activated by endocrine hormones.<sup>141</sup> Upon agonist binding a GPCR undergoes a conformational change resulting in the active state, signaling a cascade.<sup>143</sup> There are three G protein subunits,  $\alpha$ ,  $\beta$ , and  $\gamma$  and each subunit can be tied to a number of different pathways with the most well know being  $G_s$ ,  $G_q$ , and  $G_i$ .<sup>144</sup> Members of the glucagon receptor superfamily activate the  $G_s$  pathway resulting in an increase in cyclic adenosine monophosphate (cAMP), which can be used to follow agonism in receptor assays.<sup>144</sup>

#### 1.5.4 B12-Exendin-4

In 2017, it was shown that B12-Exendin-4 (B12-Ex4) had 1) a reduced effect on feeding, 2) no significant change in body weight gain and 3) suppresses blood glucose in an oral glucose tolerance test (OGTT) and 4) does not elicit malaise and nausea in rats compared to the controls (see Appendix A). B12-Ex-4 was administered in two doses 5  $\mu\text{g}/\text{kg}$  and 20  $\mu\text{g}/\text{kg}$ , both doses showed glycemic control during an OGTT, while only 20  $\mu\text{g}/\text{kg}$  had a significant ( $p < 0.05$ ) reduced effect on food intake. The overall 24 h body weight change was not significant from the controls. In a conditioned taste avoidance test, rats administered B12-Ex4, at 5  $\mu\text{g}/\text{kg}$ , showed no aversion compared to the controls, Ex-4 (5  $\mu\text{g}/\text{kg}$ ) and lithium chloride (0.15M).

Ex-4 is an agonist for the GLP-1R located on the pancreas and in the central nervous system (CNS).<sup>66,135,137</sup> CNS activation mediates the body weight-suppressive effects and also contributes to the common side effects such as nausea and malaise. Due to the unique effects of B12-Ex4 (i.e. lack of weight loss and no taste aversion) it was hypothesized that B12-Ex4 was

acting at the GLP-1R in the pancreas, as proven by glycemic control, but not activating the GLP-1R in the CNS, supported by the lack of nausea. This was explored further in Chapter 4, Part II.

#### 1.5.5 H188 FRET Assay to Detect cAMP Levels

To determine the agonism of B12-Ex4 conjugates an exchange protein directly activated by cAMP-based (EPAC) fluorescence resonance energy transfer (FRET) sensor was used.<sup>145,146</sup> This sensor consists of a cAMP binding activating protein that is sandwiched between a suitable donor and acceptor fluorescent proteins. The EPAC used in this assay detects initial cAMP levels as it is catalytically dead and cannot produce a response. In 2015, the H188 EPAC was developed with a donor cyanine fluorescent protein (CFP) and an acceptor yellow fluorescent protein (YFP).<sup>146</sup> When cAMP binds the EPAC a conformational change occurs, causing the two proteins, CFP and YFP, to move away, creating an increase in FRET response (Figure 8). This EPAC was chosen based on its higher sensitivity (~70%) than other FRET assays such as AKAR3 (~20%).



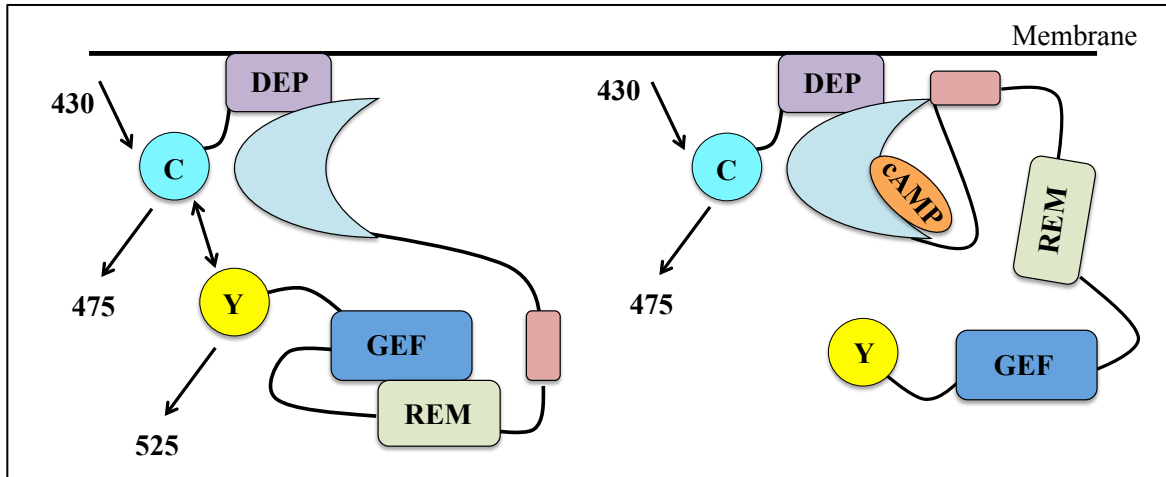


**Figure 8.** Conformational change of EPAC after cAMP binding. DEP: disheveled, Egl-10, and pleckstrin, GEF: guanine nucleotide exchange factor, REM: ras exchange motif, C: cyanine fluorescent protein, Y: yellow fluorescent protein.

## 1.6 Cubilin and Aminoglycosides

In 2009, a study by Christensen *et al.* showed that the receptor CUBN, co-expressed with megalin, binds to six different AGA (gentamicin, tobramycin, streptomycin, neomycin, kanamycin, and netilmicin) with  $K_d$  values ranging from 1.3-3.4 mM.<sup>79</sup> The role of CUBN and megalin in the inner ear is unknown, but it is hypothesized to help with fluid homeostasis. CUBN could also contribute to the ototoxic side effect commonly seen in ~50% of AGA receiving patients (explored further in Chapter 5).<sup>147-149</sup>

### 1.6.1 Aminoglycosides Antibiotics

Aminoglycosides antibiotics (AGA) are a class of antibiotics that target the 30s ribosome in bacteria.<sup>149</sup> AGAs are isolated from *Streptomyces* or *Micromonospora* bacteria and have the suffix 'micin' or 'mycin'. Their structures are similar in nature with connected rings (2 or 3) with

variable side chains. AGA's possess a broad spectrum of antibacterial activity including bacteria that are gram-negative and gram-positive.<sup>150</sup> AGAs were first discovered in 1944, and first put into use, are still widely used today, particularly in the treatment of life-threatening infections, such as sepsis, methicillin-resistant *Staphylococcus aureus* (MRSA) infection or meningitis.<sup>149-151</sup> However, AGAs are not usually a first line drug, primarily due to their renal- and oto-toxicity which can occur in ~50% of all patients, especially those receiving large or prolonged doses.<sup>147,148</sup>

### 1.6.2 Kanamycin

Kanamycin is an AGA that was discovered in 1957 when it was isolated from *S. kanamyceticus* (Figure 8).<sup>152</sup> It has a broad antibacterial spectrum and is cheap to manufacture (0.85 – 1.52 \$/dose in 2014) making it an important medicine throughout the world. This importance can be seen in kanamycin being placed on the World Health Organization's list of essential medicines.<sup>153</sup> However, due to kanamycin's severe renal- and oto-toxicity (higher than all AGAs, except neomycin) it is not a first line treatment.<sup>148</sup> Kanamycin is mainly used as a last-resort to treat very severe bacterial infections and tuberculosis.<sup>154</sup>

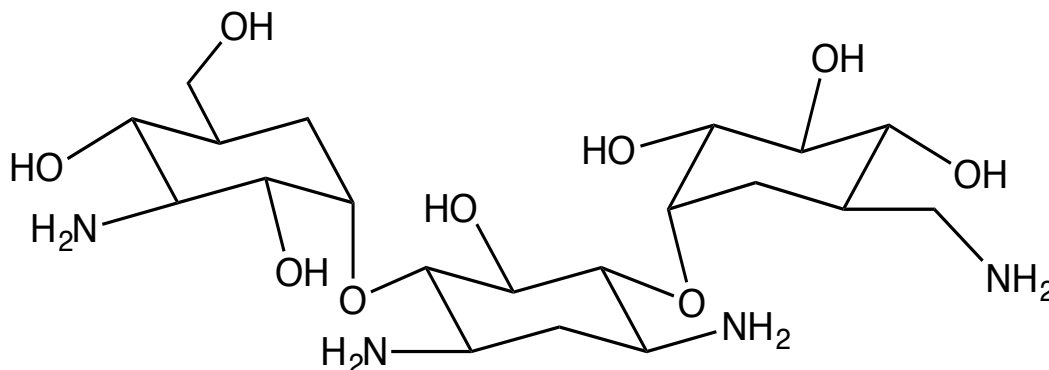


**Figure 9.** Chemical structure of the AGA kanamycin.

## 1.6 Summary

B12-radio probes, while being studied through SPECT have yet to be fully explored through PET imaging. Since PET imaging allows for better sensitivity, a new B12-radio probe with a longer half-life could improve the background/tumor uptake (Chapter 2). Previous studies, while using radiochemistry, have exploited the properties of TCII and HC. IF, being found only in the gastro-intestinal tract, when systemically administered could allow for the systemic targeting of CUBN, IF's only known receptor (Chapter 3). The exploitation of the B12 dietary uptake pathway in drug discovery research has been increasing in the past few years. Promising results warranting further investigation of what "cobalaminating" peptides and drugs will accomplish. In exploring this area new assays and probes to explore B12 transport proteins, receptors and B12-drug pharmacokinetic profiles have proven essential in these efforts (Chapter 4). AGA, while proven to be essential medicines, are less commonly used due to their nephro- and oto-toxicity. CUBN, capable of binding AGA and expressed in the inner ear, could be playing a role in AGA toxicity, warranting further investigation (Chapter 5).

## 1.7 References

- (1) Nielsen, M. J.; Rasmussen, M. R.; Andersen, C. B. F.; Nexø, E.; Moestrup, S. K. Vitamin B12 Transport from Food to the Body's Cells—a Sophisticated, Multistep Pathway. *Nat. Rev. Gastroenterol. Hepatol.* **2012**, 9 (6), 345–354.
- (2) E, S. *The Essential Guide to Vitamins and Minerals. Nutrition as a Way of Life -- Vitamins, Minerals, and the Body --The Vitamins -- The Minerals -- Vitamins, Minerals, and Disease -- How Medications, Alcohol, and Tobacco Affect Vitamin and Mineral Status -- Vitamins, Minerals, and Food -- Understanding Supplements. 2nd Ed.*; 1995.

- (3) Folate, I. of M. (US) S. C. on the S. E. of D. R. I. and its P. on; Vitamins, O. B.; Choline, A. *Estimation of the Period Covered by Vitamin B12 Stores*; National Academies Press (US), 1998.
- (4) Doxey, A. C.; Kurtz, D. A.; Lynch, M. D.; Sauder, L. A.; Neufeld, J. D. Aquatic Metagenomes Implicate Thaumarchaeota in Global Cobalamin Production. *ISME J.* **2015**, *9* (2), 461–471.
- (5) Martens, J.-H.; Barg, H.; Warren, M.; Jahn, D. Microbial Production of Vitamin B12. *Appl. Microbiol. Biotechnol.* **2002**, *58* (3), 275–285.
- (6) Swendseid, M. E.; Hvolboll, E.; Schick, G.; Halsted, J. A. The Vitamin B<sub>12</sub> Content of Human Liver Tissue and Its Nutritional Significance. *Blood* **1957**, *12* (1), 24–28.
- (7) Gherasim, C.; Lofgren, M.; Banerjee, R. Navigating the B12 Road: Assimilation, Delivery, and Disorders of Cobalamin. *J. Biol. Chem.* **2013**, *288* (19), 13186–13193.
- (8) Hodgkin, D. C.; Pickworth, J.; Robertson, J. H.; Trueblood, K. N.; Prosen, R. J.; White, J. G. Structure of Vitamin B12 : The Crystal Structure of the Hexacarboxylic Acid Derived from B12 and the Molecular Structure of the Vitamin. *Nature* **1955**, *176* (4477), 325–328.
- (9) Takahashi-Iñiguez, T.; García-Hernandez, E.; Arreguín-Espinosa, R.; Flores, M. E. Role of Vitamin B12 on Methylmalonyl-CoA Mutase Activity. *J. Zhejiang Univ. Sci. B* **2012**, *13* (6), 423–437.
- (10) Toohey, J. I. Vitamin B12 and Methionine Synthesis: A Critical Review. Is Nature’s Most Beautiful Cofactor Misunderstood? *BioFactors Oxf. Engl.* **2006**, *26* (1), 45–57.
- (11) Whipple, G. H.; Hooper, C. H.; Robscheit, F. S. BLOOD REGENERATION FOLLOWING SIMPLE ANEMIA. *American Journal of Physiology*, **1920**, *53*, 167-205.
- (12) Minot, G. R.; Murphy, W. P. Treatment of Pernicious Anemia by a Special Diet. 1926. *Yale J. Biol. Med.* **2001**, *74* (5), 341–353.
- (13) Okuda, K. Discovery of Vitamin B12 in the Liver and Its Absorption Factor in the Stomach: A Historical Review. *J. Gastroenterol. Hepatol.* **1999**, *14* (4), 301–308.
- (14) Smith, L. Purification of Anti-pernicious Anæmia Factors from Liver. *Nature.* **1948**, *161*, 638-639.

- (15) Obeid, R.; Fedosov, S. N.; Nexø, E. Cobalamin Coenzyme Forms Are Not Likely to Be Superior to Cyano- and Hydroxyl-Cobalamin in Prevention or Treatment of Cobalamin Deficiency. *Mol. Nutr. Food Res.* **2015**, *59* (7), 1364–1372.
- (16) Waibel, R.; Treichler, H.; Schaefer, N. G.; Staveren, D. R. van; Mundwiler, S.; Kunze, S.; Küenzi, M.; Alberto, R.; Nüesch, J.; Knuth, A.; et al. New Derivatives of Vitamin B12 Show Preferential Targeting of Tumors. *Cancer Res.* **2008**, *68* (8), 2904–2911.
- (17) Fedosov, S. N.; Fedosova, N. U.; Kräutler, B.; Nexø, E.; Petersen, T. E. Mechanisms of Discrimination between Cobalamins and Their Natural Analogues during Their Binding to the Specific B12-Transporting Proteins. *Biochemistry (Mosc.)* **2007**, *46* (21), 6446–6458.
- (18) Tran, M. T. Q.; Stürup, S.; Lambert, I. H.; Gammelgaard, B.; Furger, E.; Alberto, R. Cellular Uptake of Metallated Cobalamins. *Metallomics* **2016**, *8* (3), 298–304.
- (19) Chromiński, M.; Gryko, D. “Clickable” Vitamin B12 Derivative. *Chem. – Eur. J.* **2013**, *19* (16), 5141–5148.
- (20) Wierzba, A.; Wojciechowska, M.; Trylska, J.; Gryko, D. Vitamin B12 Suitably Tailored for Disulfide-Based Conjugation. *Bioconjug. Chem.* **2016**, *27* (1), 189–197.
- (21) Chromiński, M.; Lewalska, A.; Karczewski, M.; Gryko, D. Vitamin B12 Derivatives for Orthogonal Functionalization. *J. Org. Chem.* **2014**, *79* (16), 7532–7542.
- (22) Kräutler, B. Vitamin B12: Chemistry and Biochemistry. *Biochem. Soc. Trans.* **2005**, *33* (4), 806–810.
- (23) Banerjee, R. V.; Matthews, R. G. Cobalamin-Dependent Methionine Synthase. *FASEB J. Off. Publ. Fed. Am. Soc. Exp. Biol.* **1990**, *4* (5), 1450–1459.
- (24) Fedosov, S. N.; Berglund, L.; Fedosova, N. U.; Nexø, E.; Petersen, T. E. Comparative Analysis of Cobalamin Binding Kinetics and Ligand Protection for Intrinsic Factor, Transcobalamin, and Haptocorrin. *J. Biol. Chem.* **2002**, *277* (12), 9989–9996.
- (25) Neale, G. B12 Binding Proteins. *Gut* **1990**, *31* (1), 59–63.
- (26) GLASS, G. B. J. Gastric intrinsic factor and its function in the metabolism of vitamin B12. *Physiol. Rev.* **1963**, *43*, 529–849.
- (27) Andersen, C. B. F.; Madsen, M.; Storm, T.; Moestrup, S. K.; Andersen, G. R. Structural Basis for Receptor Recognition of Vitamin-B12–intrinsic Factor Complexes. *Nature* **2010**, *464* (7287), 445–448.

- (28) Marcoullis, G.; Parmentier, Y.; Nicolas, J. P.; Jimenez, M.; Gerard, P. Cobalamin Malabsorption due to Nondegradation of R Proteins in the Human Intestine. Inhibited Cobalamin Absorption in Exocrine Pancreatic Dysfunction. *J. Clin. Invest.* **1980**, *66* (3), 430–440.
- (29) Christensen, E. I.; Nielsen, R.; Birn, H. From Bowel to Kidneys: The Role of Cubilin in Physiology and Disease. *Nephrol. Dial. Transplant.* **2013**, *28* (2), 274–281.
- (30) Fyfe, J. C.; Madsen, M.; Højrup, P.; Christensen, E. I.; Tanner, S. M.; Chapelle, A. de la; He, Q.; Moestrup, S. K. The Functional Cobalamin (Vitamin B12)–intrinsic Factor Receptor Is a Novel Complex of Cubilin and Amnionless. *Blood* **2004**, *103* (5), 1573–1579.
- (31) Beedholm-Ebsen, R.; Wetering, K. van de; Hardlei, T.; Nexø, E.; Borst, P.; Moestrup, S. K. Identification of Multidrug Resistance Protein 1 (MRP1/ABCC1) as a Molecular Gate for Cellular Export of Cobalamin. *Blood* **2010**, *115* (8), 1632–1639.
- (32) Collins, D. A.; Hogenkamp, H. P.; O'Connor, M. K.; Naylor, S.; Benson, L. M.; Hardyman, T. J.; Thorson, L. M. Biodistribution of Radiolabeled Adenosylcobalamin in Patients Diagnosed with Various Malignancies. *Mayo Clin. Proc.* **2000**, *75* (6), 568–580.
- (33) Moestrup, S. K.; Birn, H.; Fischer, P. B.; Petersen, C. M.; Verroust, P. J.; Sim, R. B.; Christensen, E. I.; Nexø, E. Megalin-Mediated Endocytosis of Transcobalamin-Vitamin-B12 Complexes Suggests a Role of the Receptor in Vitamin-B12 Homeostasis. *Proc. Natl. Acad. Sci.* **1996**, *93* (16), 8612–8617.
- (34) Christensen, E. I.; Birn, H. Megalin and Cubilin: Multifunctional Endocytic Receptors. *Nat. Rev. Mol. Cell Biol.* **2002**, *3* (4), 258–268.
- (35) Furger, E.; Frei, D. C.; Schibli, R.; Fischer, E.; Prota, A. E. Structural Basis for Universal Corrinoid Recognition by the Cobalamin Transport Protein Haptocorrin. *J. Biol. Chem.* **2013**, *288* (35), 25466–25476.
- (36) Burger, R. L.; Schneider, R. J.; Mehlman, C. S.; Allen, R. H. Human Plasma R-Type Vitamin B12-Binding Proteins. II. The Role of Transcobalamin I, Transcobalamin III, and the Normal Granulocyte Vitamin B12-Binding Protein in the Plasma Transport of Vitamin B12. *J. Biol. Chem.* **1975**, *250* (19), 7707–7713.

- (37) Jensen, H. R.; Laursen, M. F.; Lildballe, D. L.; Andersen, J. B.; Nexø, E.; Licht, T. R. Effect of the Vitamin B12-Binding Protein Haptocorrin Present in Human Milk on a Panel of Commensal and Pathogenic Bacteria. *BMC Res. Notes* **2011**, *4*, 208.
- (38) Samson, R. R.; Mirtle, C.; McClelland, D. B. Secretory IgA Does Not Enhance the Bacteriostatic Effects of Iron-Binding or Vitamin B12-Binding Proteins in Human Colostrum. *Immunology* **1979**, *38* (2), 367–373.
- (39) Mathews, F. S.; Gordon, M. M.; Chen, Z.; Rajashankar, K. R.; Ealick, S. E.; Alpers, D. H.; Sukumar, N. Crystal Structure of Human Intrinsic Factor: Cobalamin Complex at 2.6-Å Resolution. *Proc. Natl. Acad. Sci.* **2007**, *104* (44), 17311–17316.
- (40) Savage, C. R.; Green, P. D. Biosynthesis of Transcobalamin II by Adult Rat Liver Parenchymal Cells in Culture. *Arch. Biochem. Biophys.* **1976**, *173* (2), 691–702.
- (41) Christensen, P. A.; Brynskov, J.; Gimsing, P.; Petersen, J. Vitamin B12 Binding Proteins (Transcobalamin and Haptocorrin) in Serum and Synovial Fluid of Patients with Rheumatoid Arthritis and Traumatic Synovitis. *Scand. J. Rheumatol.* **1983**, *12* (3), 268–272.
- (42) Wuerges, J.; Garau, G.; Geremia, S.; Fedosov, S. N.; Petersen, T. E.; Randaccio, L. Structural Basis for Mammalian Vitamin B12 Transport by Transcobalamin. *Proc. Natl. Acad. Sci. U. S. A.* **2006**, *103* (12), 4386–4391.
- (43) Quadros, E. V.; Sequeira, J. M. Cellular Uptake of Cobalamin: Transcobalamin and the TCbIR/CD320 Receptor. *Biochimie* **2013**, *95* (5), 1008–1018.
- (44) Nexø, E.; Christensen, A.-L.; Hvas, A.-M.; Petersen, T. E.; Fedosov, S. N. Quantification of Holo-Transcobalamin, a Marker of Vitamin B<sub>12</sub> Deficiency. *Clin. Chem.* **2002**, *48* (3), 561–562.
- (45) Hygum, K.; Lildballe, D. L.; Greibe, E. H.; Morkbak, A. L.; Poulsen, S. S.; Sorensen, B. S.; Petersen, T. E.; Nexø, E. Mouse Transcobalamin Has Features Resembling Both Human Transcobalamin and Haptocorrin. *PLOS ONE* **2011**, *6* (5), e20638.
- (46) Proinsias, K. ó; Giedyk, M.; Gryko, D. Vitamin B12: Chemical Modifications. *Chem. Soc. Rev.* **2013**, *42* (16), 6605–6619.
- (47) Clardy-James, S.; Bernstein, J.; Kerwood, D.; Doyle, R. Site-Selective Oxidation of Vitamin B12 Using 2-Iodoxybenzoic Acid. *Synlett* **2012**, *23* (16), 2363–2366.

- (48) van Staveren, D. R.; Waibel, R.; Mundwiler, S.; Schubiger, P. A.; Alberto, R. Conjugates of Vitamin B12 with N $\epsilon$ -Functionalized Histidine for Labeling with [ $^{99m}\text{Tc}(\text{OH}_2)_3(\text{CO})_3$ ] $^{+}$ : Synthesis and Biodistribution Studies in Tumor Bearing Mice. *J. Organomet. Chem.* **2004**, *689* (25), 4803–4810.
- (49) Alsenz, J.; Russell-Jones, G. J.; Westwood, S.; Levet-Trafit, B.; de Smidt, P. C. Oral Absorption of Peptides through the Cobalamin (Vitamin B12) Pathway in the Rat Intestine. *Pharm. Res.* **2000**, *17* (7), 825–832.
- (50) Bonaccorso, R. L.; Chepurny, O. G.; Becker-Pauly, C.; Holz, G. G.; Doyle, R. P. Enhanced Peptide Stability Against Protease Digestion Induced by Intrinsic Factor Binding of a Vitamin B12 Conjugate of Exendin-4. *Mol. Pharm.* **2015**, *12* (9), 3502–3506.
- (51) Collins, D. A.; Hogenkamp, H. P. C. Transcobalamin II Receptor Imaging via Radiolabeled Diethylene-Triaminepentaacetate Cobalamin Analogs. *J. Nucl. Med.* **1997**, *38* (5), 717–723.
- (52) Pathare, P. M.; Wilbur, D. S.; Heusser, S.; Quadros, E. V.; McLoughlin, P.; Morgan, A. C. Synthesis of Cobalamin–Biotin Conjugates That Vary in the Position of Cobalamin Coupling. Evaluation of Cobalamin Derivative Binding to Transcobalamin II. *Bioconjug. Chem.* **1996**, *7* (2), 217–232.
- (53) Fazen, C. H.; Valentin, D.; Fairchild, T. J.; Doyle, R. P. Oral Delivery of the Appetite Suppressing Peptide hPYY(3–36) through the Vitamin B12 Uptake Pathway. *J. Med. Chem.* **2011**, *54* (24), 8707–8711.
- (54) Petrus, A. K.; Vortherms, A. R.; Fairchild, T. J.; Doyle, R. P. Vitamin B12 as a Carrier for the Oral Delivery of Insulin. *ChemMedChem* **2007**, *2* (12), 1717–1721.
- (55) McEwan, J. F.; Veitch, H. S.; Russell-Jones, G. J. Synthesis and Biological Activity of Ribose-5'-Carbamate Derivatives of Vitamin B12. *Bioconjug. Chem.* **1999**, *10* (6), 1131–1136.
- (56) Zelder, F.; Sonnay, M.; Prieto, L. Antivitamins for Medicinal Applications. *ChemBioChem* **2015**, *16* (9), 1264–1278.
- (57) Petrus, A. K.; Fairchild, T. J.; Doyle, R. P. Traveling the Vitamin B12 Pathway: Oral Delivery of Protein and Peptide Drugs. *Angew. Chem. Int. Ed.* **2009**, *48* (6), 1022–1028.
- (58) Obeid, R. *Vitamin B12: Advances and Insights*; 2017.



- (59) Ziv, E.; Bendayan, M. Intestinal Absorption of Peptides through the Enterocytes. *Microsc. Res. Tech.* **2000**, *49* (4), 346–352.
- (60) Russell-Jones, G. J.; Westwood, S. W.; Habberfield, A. D. Vitamin B12 Mediated Oral Delivery Systems for Granulocyte-Colony Stimulating Factor and Erythropoietin. *Bioconjug. Chem.* **1995**, *6* (4), 459–465.
- (61) Russell-Jones, G.; Westwood, S.; Farnworth, P.; Findlay, J.; Burger, H. Synthesis of LHRH Antagonists Suitable for Oral Administration via the Vitamin B12 Uptake System. *Bioconjug. Chem.* **1995**, *6* (1), 34–42.
- (62) Dix, C. J.; Hassan, I. F.; Obray, H. Y.; Shah, R.; Wilson, G. The Transport of Vitamin B12 through Polarized Monolayers of Caco-2 Cells. *Gastroenterology* **1990**, *98* (5 PART 1), 1272–1279.
- (63) Verma, A.; Sharma, S.; Gupta, P. K.; Singh, A.; Teja, B. V.; Dwivedi, P.; Gupta, G. K.; Trivedi, R.; Mishra, P. R. Vitamin B12 Functionalized Layer by Layer Calcium Phosphate Nanoparticles: A Mucoadhesive and pH Responsive Carrier for Improved Oral Delivery of Insulin. *Acta Biomater.* **2016**, *31*, 288–300.
- (64) Schjønby, H. Vitamin B12 Absorption and Malabsorption. *Gut* **1989**, *30* (12), 1686–1691.
- (65) Henry, K. E.; Elfers, C. T.; Burke, R. M.; Chepurny, O. G.; Holz, G. G.; Blevins, J. E.; Roth, C. L.; Doyle, R. P. Vitamin B12 Conjugation of Peptide-YY3–36 Decreases Food Intake Compared to Native Peptide-YY3–36 Upon Subcutaneous Administration in Male Rats. *Endocrinology* **2015**, *156* (5), 1739–1749.
- (66) Kanoski, S. E.; Rupperecht, L. E.; Fortin, S. M.; De Jonghe, B. C.; Hayes, M. R. The Role of Nausea in Food Intake and Body Weight Suppression by Peripheral GLP-1 Receptor Agonists, Exendin-4 and Liraglutide. *Neuropharmacology* **2012**, *62* (5–6), 1916–1927.
- (67) Agunod, M.; Yamaguchi, N.; Lopez, R.; Luhby, A. L.; Glass, G. B. J. Correlative Study of Hydrochloric Acid, Pepsin, and Intrinsic Factor Secretion in Newborns and Infants. *Am. J. Dig. Dis.* **1969**, *14* (6), 400–414.
- (68) Gordon, M. M.; Howard, T.; Becich, M. J.; Alpers, D. H. Cathepsin L Mediates Intracellular Ileal Digestion of Gastric Intrinsic Factor. *Am. J. Physiol. - Gastrointest. Liver Physiol.* **1995**, *268* (1), G33–G40.
- (69) Castle, W. B. Observations On The Etiologic Relationship Of Achylia Gastrica To Pernicious Anemia. *Am. J. Med. Sci.* **1929**, *178* (6), 748–763.

- (70) Castle, W. B.; Ham, T. H. OBSERVATIONS ON THE ETIOLOGIC RELATIONSHIP OF ACHYLIA GASTRICA TO PERNICIOUS ANEMIA: V. FURTHER EVIDENCE FOR THE ESSENTIAL PARTICIPATION OF EXTRINSIC FACTOR IN HEMATOPOIETIC RESPONSES TO MIXTURES OF BEEF MUSCLE AND GASTRIC JUICE AND TO HOG STOMACH MUCOSA. *J. Am. Med. Assoc.* **1936**, *107* (18), 1456–1463.
- (71) Seetharam, B.; Christensen, E. I.; Moestrup, S. K.; Hammond, T. G.; Verroust, P. J. Identification of Rat Yolk Sac Target Protein of Teratogenic Antibodies, gp280, as Intrinsic Factor-Cobalamin Receptor. *J. Clin. Invest.* **1997**, *99* (10), 2317–2322.
- (72) Nykjaer, A.; Fyfe, J. C.; Kozyraki, R.; Leheste, J. R.; Jacobsen, C.; Nielsen, M. S.; Verroust, P. J.; Aminoff, M.; de la Chapelle, A.; Moestrup, S. K.; et al. Cubilin Dysfunction Causes Abnormal Metabolism of the Steroid Hormone 25(OH) Vitamin D(3). *Proc. Natl. Acad. Sci. U. S. A.* **2001**, *98* (24), 13895–13900.
- (73) Kozyraki, R.; Fyfe, J.; Verroust, P. J.; Jacobsen, C.; Dautry-Varsat, A.; Gburek, J.; Willnow, T. E.; Christensen, E. I.; Moestrup, S. K. Megalin-Dependent Cubilin-Mediated Endocytosis Is a Major Pathway for the Apical Uptake of Transferrin in Polarized Epithelia. *Proc. Natl. Acad. Sci.* **2001**, *98* (22), 12491–12496.
- (74) Gburek, J.; Verroust, P. J.; Willnow, T. E.; Fyfe, J. C.; Nowacki, W.; Jacobsen, C.; Moestrup, S. K.; Christensen, E. I. Megalin and Cubilin Are Endocytic Receptors Involved in Renal Clearance of Hemoglobin. *J. Am. Soc. Nephrol.* **2002**, *13* (2), 423–430.
- (75) Kozyraki, R.; Fyfe, J.; Kristiansen, M.; Gerdes, C.; Jacobsen, C.; Cui, S.; Christensen, E. I.; Aminoff, M.; Chapelle, A. de la; Krahe, R.; et al. The Intrinsic Factor|ndash|vitamin B12 Receptor, Cubilin, Is a High-Affinity Apolipoprotein A-I Receptor Facilitating Endocytosis of High-Density Lipoprotein. *Nat. Med.* **1999**, *5* (6), 656–661.
- (76) Amsellem, S.; Gburek, J.; Hamard, G.; Nielsen, R.; Willnow, T. E.; Devuyst, O.; Nexø, E.; Verroust, P. J.; Christensen, E. I.; Kozyraki, R. Cubilin Is Essential for Albumin Reabsorption in the Renal Proximal Tubule. *J. Am. Soc. Nephrol. JASN* **2010**, *21* (11), 1859–1867.

- (77) Burke, K. A.; Jauniaux, E.; Burton, G. J.; Cindrova-Davies, T. Expression and Immunolocalisation of the Endocytic Receptors Megalin and Cubilin in the Human Yolk Sac and Placenta across Gestation. *Placenta* **2013**, *34* (11), 1105–1109.
- (78) Tsaroucha, A. K.; Chatzaki, E.; Lambropoulou, M.; Despoudi, K.; Laftsidis, P.; Charsou, C.; Polychronidis, A.; Papadopoulos, N.; Simopoulos, C. E. Megalin and Cubilin in the Human Gallbladder Epithelium. *Clin. Exp. Med.* **2008**, *8* (3), 165–170.
- (79) Tauris, J.; Christensen, E. I.; Nykjaer, A.; Jacobsen, C.; Petersen, C. M.; Ovesen, T. Cubilin and Megalin Co-Localize in the Neonatal Inner Ear. *Audiol. Neurootol.* **2009**, *14* (4), 267–278.
- (80) He, Q.; Madsen, M.; Kilkenney, A.; Gregory, B.; Christensen, E. I.; Vorum, H.; Højrup, P.; Schäffer, A. A.; Kirkness, E. F.; Tanner, S. M.; et al. Amnionless Function Is Required for Cubilin Brush-Border Expression and Intrinsic Factor-Cobalamin (Vitamin B12) Absorption in Vivo. *Blood* **2005**, *106* (4), 1447–1453.
- (81) Fyfe, J. C.; Madsen, M.; Højrup, P.; Christensen, E. I.; Tanner, S. M.; de la Chapelle, A.; He, Q.; Moestrup, S. K. The Functional Cobalamin (Vitamin B12)-Intrinsic Factor Receptor Is a Novel Complex of Cubilin and Amnionless. *Blood* **2004**, *103* (5), 1573–1579.
- (82) Kozyraki, R. Cubilin, a Multifunctional Epithelial Receptor: An Overview. *J. Mol. Med. Berl. Ger.* **2001**, *79* (4), 161–167.
- (83) Lindblom, A.; Quadt, N.; Marsh, T.; Aeschlimann, D.; Mörgelin, M.; Mann, K.; Maurer, P.; Paulsson, M. The Intrinsic Factor-Vitamin B12 Receptor, Cubilin, Is Assembled into Trimers via a Coiled-Coil  $\alpha$ -Helix. *J. Biol. Chem.* **1999**, *274* (10), 6374–6380.
- (84) He, Q.; Madsen, M.; Kilkenney, A.; Gregory, B.; Christensen, E. I.; Vorum, H.; Højrup, P.; Schäffer, A. A.; Kirkness, E. F.; Tanner, S. M.; et al. Amnionless Function Is Required for Cubilin Brush-Border Expression and Intrinsic Factor-Cobalamin (Vitamin B12) Absorption in Vivo. *Blood* **2005**, *106* (4), 1447–1453.
- (85) Tanner, S. M.; Aminoff, M.; Wright, F. A.; Liyanarachchi, S.; Kuronen, M.; Saarinen, A.; Massika, O.; Mandel, H.; Broch, H.; de la Chapelle, A. Amnionless, Essential for Mouse Gastrulation, Is Mutated in Recessive Hereditary Megaloblastic Anemia. *Nat. Genet.* **2003**, *33* (3), 426–429.

- (86) Tauris, J.; Christensen, E. I.; Nykjaer, A.; Jacobsen, C.; Petersen, C. M.; Ovesen, T. Cubilin and Megalin Co-Localize in the Neonatal Inner Ear. *Audiol. Neurootol.* **2009**, *14* (4), 267–278.
- (87) Rahmim, A.; Zaidi, H. PET versus SPECT: Strengths, Limitations and Challenges. *Nucl. Med. Commun.* **2008**, *29* (3), 193–207.
- (88) Tsukamoto, E.; Ochi, S. PET/CT Today: System and Its Impact on Cancer Diagnosis. *Ann. Nucl. Med.* **2006**, *20* (4), 255.
- (89) Eckelman, W. C. Unparalleled Contribution of Technetium-99m to Medicine Over 5 Decades. *JACC Cardiovasc. Imaging* **2009**, *2* (3), 364–368.
- (90) Anderson, C. J.; Ferdani, R. Copper-64 Radiopharmaceuticals for PET Imaging of Cancer: Advances in Preclinical and Clinical Research. *Cancer Biother. Radiopharm.* **2009**, *24* (4), 379–393.
- (91) Severin, G. W.; Engle, J. W.; Nickles, R. J.; Barnhart, T. E. <sup>89</sup>Zr Radiochemistry for PET. *Med. Chem. Shariqah United Arab Emir.* **2011**, *7* (5), 389–394.
- (92) Segrè, E.; Seaborg, G. T. Nuclear Isomerism in Element 43. *Phys. Rev.* **1938**, *54* (9), 772–772.
- (93) Pillai, M. R. A.; Dash, A.; Knapp, F. F. (Russ). Sustained Availability of <sup>99m</sup>Tc: Possible Paths Forward. *J. Nucl. Med.* **2013**, *54* (2), 313–323.
- (94) Ravichandran, R.; Binukumar, J.; Saadi, A. A. Estimation of Effective Half Life of Clearance of Radioactive Iodine (<sup>131</sup>I) in Patients Treated for Hyperthyroidism and Carcinoma Thyroid. *Indian J. Nucl. Med. IJNM Off. J. Soc. Nucl. Med. India* **2010**, *25* (2), 49–52.
- (95) Corbett, J. R.; Ficaro, E. P. Clinical Review of Attenuation-Corrected Cardiac SPECT. *J. Nucl. Cardiol.* **1999**, *6* (1), 54–68.
- (96) Buckley O.; O'keeffe, S.; Geoghegan, T.; Lyburn, I. D.; Munk, P. L.; Worsley, D. torregginani, W. C. <sup>99m</sup>Tc bone scintigraphy superscans: a review. *Nuclear Medicine Communications*, **2007**, *28*, 521-7.
- (97) Szymański, P.; Frączek, T.; Markowicz, M.; Mikiciuk-Olasik, E. Development of Copper Based Drugs, Radiopharmaceuticals and Medical Materials. *BioMetals* **2012**, *25* (6), 1089–1112.

- (98) Niccoli Asabella, A.; Cascini, G. L.; Altini, C.; Paparella, D.; Notaristefano, A.; Rubini, G. The Copper Radioisotopes: A Systematic Review with Special Interest to  $^{64}\text{Cu}$ . *BioMed Res. Int.* **2014**, *2014*, e786463.
- (99) Dearling, J. L. J.; Paterson, B. M.; Akurathi, V.; Betanzos-Lara, S.; Treves, S. T.; Voss, S. D.; White, J. M.; Huston, J. S.; Smith, S. V.; Donnelly, P. S.; et al. The Ionic Charge of Copper-64 Complexes Conjugated to an Engineered Antibody Affects Biodistribution. *Bioconjug. Chem.* **2015**, *26* (4), 707–717.
- (100) Deri, M. A.; Zeglis, B. M.; Francesconi, L. C.; Lewis, J. S. PET Imaging with  $^{89}\text{Zr}$ : From Radiochemistry to the Clinic. *Nucl. Med. Biol.* **2013**, *40* (1), 3–14.
- (101) Dongen, G. A. M. S. van; Visser, G. W. M.; Hooge, M. N. L.; Vries, E. G. de; Perk, L. R. Immuno-PET: A Navigator in Monoclonal Antibody Development and Applications. *The Oncologist* **2007**, *12* (12), 1379–1389.
- (102) van Staveren, D. R.; Waibel, R.; Mundwiler, S.; Schubiger, P. A.; Alberto, R. Conjugates of Vitamin B12 with N $\epsilon$ -Functionalized Histidine for Labeling with  $[\text{}^{99m}\text{Tc}(\text{OH})_2\text{CO}_3]^+$ : Synthesis and Biodistribution Studies in Tumor Bearing Mice. *J. Organomet. Chem.* **2004**, *689* (25), 4803–4810.
- (103) Collins, D. A.; Hogenkamp, H. P. C.; Gebhard, M. W. Tumor Imaging Via Indium 111–Labeled DTPA– Adenosylcobalamin. *Mayo Clin. Proc.* **1999**, *74* (7), 687–691.
- (104) Mundwiler, S.; Waibel, R.; Spingler, B.; Kunze, S.; Alberto, R. Picolyamine-Methylphosphonic Acid Esters as Tridentate Ligands for the Labeling of Alcohols with the Fac- $[\text{M}(\text{CO})_3]^+$  Core (M= $^{99m}\text{Tc}$ , Re): Synthesis and Biodistribution of Model Compounds and of a  $^{99m}\text{Tc}$ -Labeled Cobinamide. *Nucl. Med. Biol.* **2005**, *32* (5), 473–484.
- (105) Sah, B.-R.; Schibli, R.; Waibel, R.; Boehmer, L. von; Bläuenstein, P.; Nexø, E.; Johayem, A.; Fischer, E.; Müller, E.; Soyka, J. D.; et al. Tumor Imaging in Patients with Advanced Tumors Using a New  $^{99m}\text{Tc}$ -Radiolabeled Vitamin B12 Derivative. *J. Nucl. Med.* **2014**, *55* (1), 43–49.
- (106) Baldoni, D.; Waibel, R.; Bläuenstein, P.; Galli, F.; Iodice, V.; Signore, A.; Schibli, R.; Trampuz, A. Evaluation of a Novel Tc- $^{99m}$  Labelled Vitamin B12 Derivative for Targeting Escherichia Coli and Staphylococcus Aureus In Vitro and in an Experimental Foreign-Body Infection Model. *Mol. Imaging Biol.* **2015**, *17* (6), 829–837.

- (107) Cooperman, J. M. Distribution of Radioactive and Nonradioactive Vitamin B<sub>12</sub> in Normal and Malignant Tissues of an Infant with Neuroblastoma. *Cancer Res.* **1972**, *32* (1), 167–172.
- (108) Bose, S.; Komorowski, R.; Seetharam, S.; Gilfix, B.; Rosenblatt, D. S.; Seetharam, B. In Vitro and in Vivo Inactivation of Transcobalamin II Receptor by Its Antiserum. *J. Biol. Chem.* **1996**, *271* (8), 4195–4200.
- (109) Ruiz-Sánchez, P.; Mundwiler, S.; Medina-Molner, A.; Spingler, B.; Alberto, R. Iodination of Cisplatin Adduct of Vitamin B<sub>12</sub> [ $\{B_{12}\}-CN-\{cis-PtCl(NH_3)_2\}^+$ ]. *J. Organomet. Chem.* **2007**, *692* (6), 1358–1362.
- (110) Kunze, S.; Zobi, F.; Kurz, P.; Spingler, B.; Alberto, R. Vitamin B<sub>12</sub> as a Ligand for Technetium and Rhenium Complexes. *Angew. Chem. Int. Ed Engl.* **2004**, *43* (38), 5025–5029.
- (111) Ikotun, O. F.; Marquez, B. V.; Fazen, C. H.; Kahkoska, A. R.; Doyle, R. P.; Lapi, S. E. Investigation of a Vitamin B<sub>12</sub> Conjugate as a PET Imaging Probe. *ChemMedChem* **2014**, *9* (6), 1244–1251.
- (112) Strasser, R. Plant Protein Glycosylation. *Glycobiology* **2016**, *26* (9), 926–939.
- (113) Schwarz, F.; Aebi, M. Mechanisms and Principles of N-Linked Protein Glycosylation. *Curr. Opin. Struct. Biol.* **2011**, *21* (5), 576–582.
- (114) Clerc, F.; Reiding, K. R.; Jansen, B. C.; Kammeijer, G. S. M.; Bondt, A.; Wuhrer, M. Human Plasma Protein N-Glycosylation. *Glycoconj. J.* **2016**, *33* (3), 309–343.
- (115) Roggenbuck, D.; Mytilinaiou, M. G.; Lapin, S. V.; Reinhold, D.; Conrad, K. Asialoglycoprotein Receptor (ASGPR): A Peculiar Target of Liver-Specific Autoimmunity. *Auto-Immun. Highlights* **2012**, *3* (3), 119–125.
- (116) Garcia-Casado, G.; Sanchez-Monge, R.; Chrispeels, M. J.; Armentia, A.; Salcedo, G.; Gomez, L. Role of Complex Asparagine-Linked Glycans in the Allergenicity of Plant Glycoproteins. *Glycobiology* **1996**, *6* (4), 471–477.
- (117) East, L.; Isacke, C. M. The Mannose Receptor Family. *Biochim. Biophys. Acta* **2002**, *1572* (2–3), 364–386.
- (118) Shrimpton, R. E.; Butler, M.; Morel, A.-S.; Eren, E.; Hue, S. S.; Ritter, M. A. CD205 (DEC-205): A Recognition Receptor for Apoptotic and Necrotic Self. *Mol. Immunol.* **2009**, *46* (6), 1229–1239.

- (119) Sheikh, H.; Yarwood, H.; Ashworth, A.; Isacke, C. M. Endo180, an Endocytic Recycling Glycoprotein Related to the Macrophage Mannose Receptor Is Expressed on Fibroblasts, Endothelial Cells and Macrophages and Functions as a Lectin Receptor. *J. Cell Sci.* **2000**, *113 (Pt 6)*, 1021–1032.
- (120) Hihara, K.; Iyoda, M.; Tachibana, S.; Iseri, K.; Saito, T.; Yamamoto, Y.; Suzuki, T.; Wada, Y.; Matsumoto, K.; Shibata, T. Anti-Phospholipase A2 Receptor (PLA2R) Antibody and Glomerular PLA2R Expression in Japanese Patients with Membranous Nephropathy. *PLOS ONE* **2016**, *11 (6)*, e0158154.
- (121) Takahashi, K.; Donovan, M. J.; Rogers, R. A.; Ezekowitz, R. A. Distribution of Murine Mannose Receptor Expression from Early Embryogenesis through to Adulthood. *Cell Tissue Res.* **1998**, *292 (2)*, 311–323.
- (122) De Leeuw, A. M.; Brouwer, A.; Knook, D. L. Sinusoidal Endothelial Cells of the Liver: Fine Structure and Function in Relation to Age. *J. Electron Microsc. Tech.* **1990**, *14 (3)*, 218–236.
- (123) Ernst, J. D. Macrophage Receptors for Mycobacterium Tuberculosis. *Infect. Immun.* **1998**, *66 (4)*, 1277–1281.
- (124) Elliott, R. M.; Morgan, L. M.; Tredger, J. A.; Deacon, S.; Wright, J.; Marks, V. Glucagon-like Peptide-1 (7-36)amide and Glucose-Dependent Insulinotropic Polypeptide Secretion in Response to Nutrient Ingestion in Man: Acute Post-Prandial and 24-H Secretion Patterns. *J. Endocrinol.* **1993**, *138 (1)*, 159–166.
- (125) Kreymann, B.; Williams, G.; Ghatei, M. A.; Bloom, S. R. Glucagon-like Peptide-1 7-36: A Physiological Incretin in Man. *Lancet Lond. Engl.* **1987**, *2 (8571)*, 1300–1304.
- (126) Kim, W.; Egan, J. M. The Role of Incretins in Glucose Homeostasis and Diabetes Treatment. *Pharmacol. Rev.* **2008**, *60 (4)*, 470–512.
- (127) Holst, J. J.; Deacon, C. F. Glucagon-like Peptide-1 Mediates the Therapeutic Actions of DPP-IV Inhibitors. *Diabetologia* **2005**, *48 (4)*, 612–615.
- (128) Mérida, E.; Delgado, E.; Molina, L. M.; Villanueva-Peñacarrillo, M. L.; Valverde, I. Presence of Glucagon and Glucagon-like Peptide-1-(7-36)amide Receptors in Solubilized Membranes of Human Adipose Tissue. *J. Clin. Endocrinol. Metab.* **1993**, *77 (6)*, 1654–1657.

- (129) Göke, R.; Larsen, P. J.; Mikkelsen, J. D.; Sheikh, S. P. Distribution of GLP-1 Binding Sites in the Rat Brain: Evidence That Exendin-4 Is a Ligand of Brain GLP-1 Binding Sites. *Eur. J. Neurosci.* **1995**, *7* (11), 2294–2300.
- (130) Hörsch, D.; Göke, R.; Eissele, R.; Michel, B.; Göke, B. Reciprocal Cellular Distribution of Glucagon-like Peptide-1 (GLP-1) Immunoreactivity and GLP-1 Receptor mRNA in Pancreatic Islets of Rat. *Pancreas* **1997**, *14* (3), 290–294.
- (131) Eng, J.; Andrews, P. C.; Kleinman, W. A.; Singh, L.; Raufman, J. P. Purification and Structure of Exendin-3, a New Pancreatic Secretagogue Isolated from Heloderma Horridum Venom. *J. Biol. Chem.* **1990**, *265* (33), 20259–20262.
- (132) Eng, J.; Kleinman, W. A.; Singh, L.; Singh, G.; Raufman, J. P. Isolation and Characterization of Exendin-4, an Exendin-3 Analogue, from Heloderma Suspectum Venom. Further Evidence for an Exendin Receptor on Dispersed Acini from Guinea Pig Pancreas. *J. Biol. Chem.* **1992**, *267* (11), 7402–7405.
- (133) Furman, B. L. The Development of Byetta (Exenatide) from the Venom of the Gila Monster as an Anti-Diabetic Agent. *Toxicon Off. J. Int. Soc. Toxinology* **2012**, *59* (4), 464–471.
- (134) Bond, A. Exenatide (Byetta) as a Novel Treatment Option for Type 2 Diabetes Mellitus. *Proc. Bayl. Univ. Med. Cent.* **2006**, *19* (3), 281–284.
- (135) De Jonghe, B. C.; Holland, R. A.; Olivos, D. R.; Rupprecht, L. E.; Kanoski, S. E.; Hayes, M. R. Hindbrain GLP-1 Receptor Mediation of Cisplatin-Induced Anorexia and Nausea. *Physiol. Behav.* **2016**, *153*, 109–114.
- (136) Kanoski, S. E.; Hayes, M. R.; Skibicka, K. P. GLP-1 and Weight Loss: Unraveling the Diverse Neural Circuitry. *Am. J. Physiol. Regul. Integr. Comp. Physiol.* **2016**, *310* (10), R885-895.
- (137) Hayes, M. R.; De Jonghe, B. C.; Kanoski, S. E. Role of the Glucagon-like-Peptide-1 Receptor in the Control of Energy Balance. *Physiol. Behav.* **2010**, *100* (5), 503–510.
- (138) Brubaker, P. L.; Drucker, D. J. Structure-Function of the Glucagon Receptor Family of G Protein-Coupled Receptors: The Glucagon, GIP, GLP-1, and GLP-2 Receptors. *Receptors Channels* **2002**, *8* (3–4), 179–188.
- (139) Reimann, F.; Gribble, F. M. G Protein-Coupled Receptors as New Therapeutic Targets for Type 2 Diabetes. *Diabetologia* **2016**, *59* (2), 229–233.



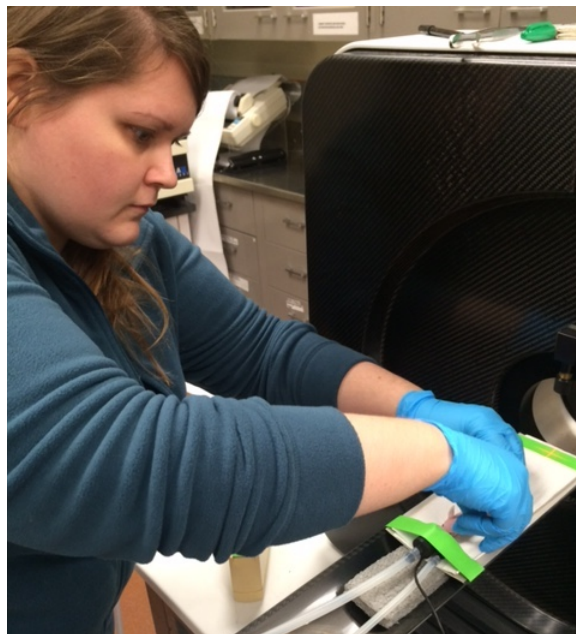
- (140) Siu, F. Y.; He, M.; de Graaf, C.; Han, G. W.; Yang, D.; Zhang, Z.; Zhou, C.; Xu, Q.; Wacker, D.; Joseph, J. S.; et al. Structure of the Human Glucagon Class B G-Protein-Coupled Receptor. *Nature* **2013**, *499* (7459), 444–449.
- (141) Kirkpatrick, A.; Heo, J.; Abrol, R.; Goddard, W. A. Predicted Structure of Agonist-Bound Glucagon-like Peptide 1 Receptor, a Class B G Protein-Coupled Receptor. *Proc. Natl. Acad. Sci.* **2012**, *109* (49), 19988–19993.
- (142) Lee, S.-M.; Booe, J. M.; Pioszak, A. A. Structural Insights into Ligand Recognition and Selectivity for Classes A, B, and C GPCRs. *Eur. J. Pharmacol.* **2015**, *763* (Pt B), 196–205.
- (143) Li, Y.; Sun, J.; Li, D.; Lin, J. Activation and Conformational Dynamics of a Class B G-Protein-Coupled Glucagon Receptor. *Phys. Chem. Chem. Phys.* **2016**, *18* (18), 12642–12650.
- (144) Neves, S. R.; Ram, P. T.; Iyengar, R. G Protein Pathways. *Science* **2002**, *296* (5573), 1636–1639.
- (145) Holz, G. G. Epac: A New cAMP-Binding Protein in Support of Glucagon-Like Peptide-1 Receptor-Mediated Signal Transduction in the Pancreatic  $\beta$ -Cell. *Diabetes* **2004**, *53* (1), 5–13.
- (146) Klarenbeek, J.; Goedhart, J.; Batenburg, A. van; Groenewald, D.; Jalink, K. Fourth-Generation Epac-Based FRET Sensors for cAMP Feature Exceptional Brightness, Photostability and Dynamic Range: Characterization of Dedicated Sensors for FLIM, for Ratiometry and with High Affinity. *PLOS ONE* **2015**, *10* (4), e0122513.
- (147) Huth, M. E.; Ricci, A. J.; Cheng, A. G. Mechanisms of Aminoglycoside Ototoxicity and Targets of Hair Cell Protection. *Int. J. Otolaryngol.* **2011**, *2011*, e937861.
- (148) Clark, C. H. Toxicity of Aminoglycoside Antibiotics. *Mod. Vet. Pract.* **1977**, *58* (7), 594–598.
- (149) Begg, E. J.; Barclay, M. L. Aminoglycosides--50 Years On. *Br. J. Clin. Pharmacol.* **1995**, *39* (6), 597–603.
- (150) Mingeot-Leclercq, M.-P.; Glupczynski, Y.; Tulkens, P. M. Aminoglycosides: Activity and Resistance. *Antimicrob. Agents Chemother.* **1999**, *43* (4), 727–737.
- (151) Forge, A.; Schacht, J. Aminoglycoside Antibiotics. *Audiol. Neurootol.* **2000**, *5* (1), 3–22.

- (152) Umezawa, H. KANAMYCIN: ITS DISCOVERY . *Annals of the New York Academy of Sciences*. **1958**, 76, 20-26.
- (153) WHO | Essential Medicines List and WHO Model Formulary  
[http://www.who.int/selection\\_medicines/list/en/](http://www.who.int/selection_medicines/list/en/) (accessed Jun 22, 2017).
- (154) Maus, C. E.; Plikaytis, B. B.; Shinnick, T. M. Molecular Analysis of Cross-Resistance to Capreomycin, Kanamycin, Amikacin, and Viomycin in Mycobacterium Tuberculosis. *Antimicrob. Agents Chemother.* **2005**, 49 (8), 3192–3197.

## Chapter 2: A Vitamin B12 Conjugate of Desferrioxamine-<sup>89</sup>Zirconium as a PET Imaging Agent to Detect CD320 Positive Tumors

The work reported in this chapter resulted in the paper “<sup>89</sup>Zr-Cobalamin PET Tracer: Synthesis, Cellular Uptake, and Use for Tumor Imaging” in ACS Omega in October 2017 with authors Jayne L. Workinger, Akhila N. Kuda-Wedagedara, Ebba Nexo, Nerissa T. Viola-Villegas, and Robert P. Doyle.

Work in this chapter was performed by the author unless otherwise indicated. Where indicated work was performed in collaboration with Dr. Nerissa Viola-Villegas at Wayne State University, Detroit, MI.



In vivo studies using <sup>89</sup>Zr-B12 were completed by the author (shown above) while visiting Dr. Nerissa Viola-Villages group at Wayne State University (Detroit, MI).

## 2.1 Introduction

One of the essential nutrients needed for cell homeostasis and proliferative activity is B12 due to its involvement in DNA synthesis and protein production (for more detail on B12, see Chapter 1, Section 1.1.3).<sup>1,2</sup> In particular, the CD320 receptor, responsible for B12 (bound to TCII, see Chapter 1, Section 1.1.4) entry to proliferating cells, has been shown to be up-regulated in cancer cells.<sup>3,4</sup> Herein, we explore the feasibility of a <sup>89</sup>Zirconium-labeled B12 (<sup>89</sup>Zr-B12) as a new positron emission tomography (PET) tracer. The **hypothesis** of this work is that a <sup>89</sup>Zr-B12 conjugate will allow for optimal signal-to-noise ratio for tumor imaging through the CD320 receptor. Previous CD320 targeting studies have primarily used single photon emission computed tomography (SPECT) with only one PET tracer reported to date.<sup>5-10</sup> Doyle *et al.* reported a <sup>64</sup>Cu-B12 PET imaging agent that had tumor uptake of 2.20 - 4.84 %ID/g at 6 h post injection (p.i.) in various tumor lines including ovarian, pancreatic, colorectal, and melanoma.<sup>5</sup> Using <sup>89</sup>Zr ( $t_{1/2} \sim 3.27$  d, for more detail on <sup>89</sup>Zr see Chapter 1, Section 1.3.1.3) allows for a longer visualization window to optimize signal-to-noise ratio in tumor imaging.<sup>11,12</sup> Herein, the synthesis, characterization, and in vitro, in vivo, and ex vivo analyses of <sup>89</sup>Zr-B12 in a breast cancer cell line MDA-MB-453 at 4, 24, and 48 h was investigated.

## 2.2 Design, Synthesis, and Characterization of <sup>89</sup>Zr-B12

B12-desferrioxamine (B12-DFO) was synthesized by activating the 5'-hydroxyl group on the deoxyribose moiety of B12 with 1,1'-carbonyl-di-(1,2,4-triazole) (CDT) (Figure 1).<sup>13</sup> Once conversion was observed through RP-HPLC, DFO was added and the mixture was allowed to stir overnight at room temperature (RT) to yield B12-DFO (35-45%, based on B12 starting

material). B12-DFO was purified with RP-HPLC to >95%. LC-MS showed an observed  $m/z$  of  $942[M+2H]^{2+}$ , and  $648[M+3H]^{3+}$ , expected  $m/z$  1942 (Figure 2).

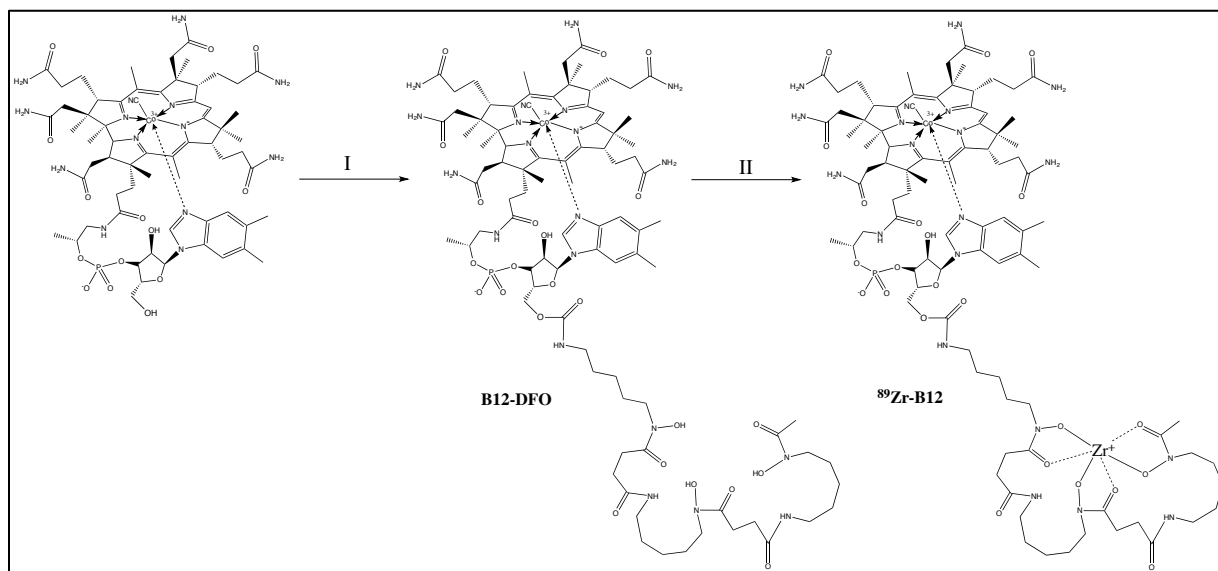


**Figure 1.** The synthesis and radiolabeling of B12-DFO. Reaction conditions: I) CDT (7.2 eq.) was added to B12 (1 eq.) in anhydrous DMSO at 40°C for 2 h, then DFO (7.4 eq.) was added to the reaction mixture and allowed to stir overnight at RT, and II) Radiolabeling was achieved by incubating  $^{89}\text{Zr}(\text{C}_2\text{O}_4)_2$  (1  $\mu\text{Ci}$ ) with B12-DFO (0.004  $\mu\text{mol}$ ) for 20 min at pH 7–7.5.

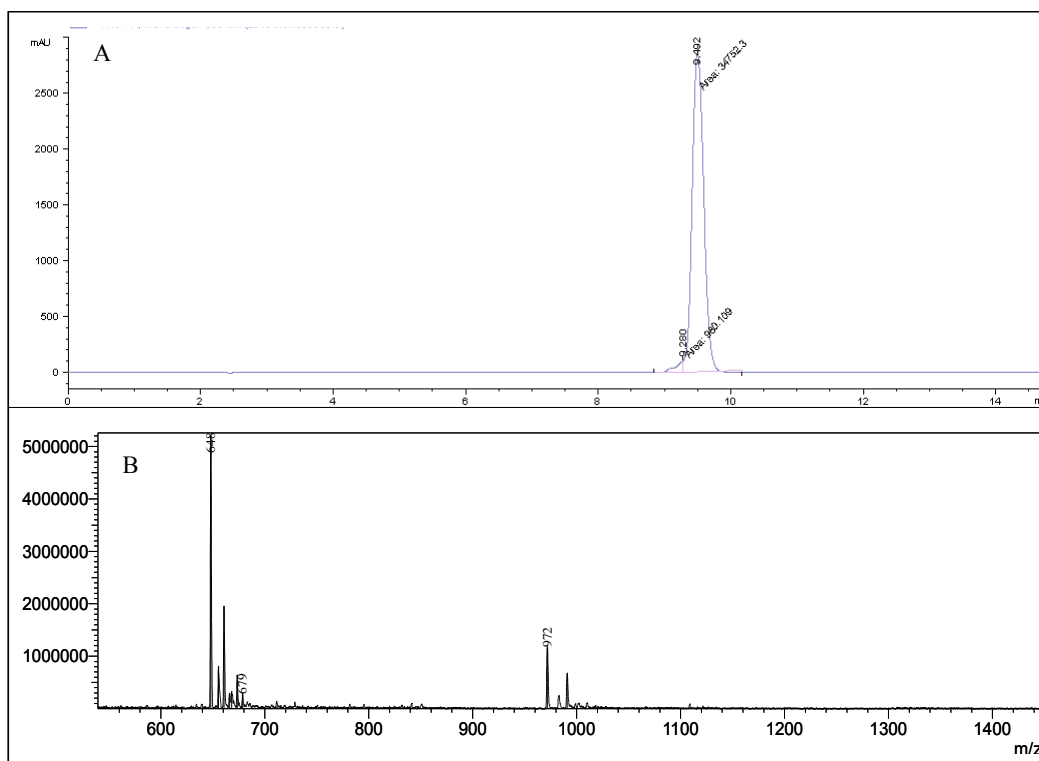


**Figure 2.** Characterization of B12-DFO. A) RP-HPLC:  $R_t = 9.4$  min. Detection at 360 nm. Integrated purity is 97%. B) LC-MS showed  $942[M+2H]^{2+}$  and  $648[M+3H]^{3+}$ , expected  $m/z$  1942.

### 2.2.1 Labeling and Stability of $^{89}\text{Zr}$ -B12

B12-DFO was labeled with  $^{89}\text{Zr}(\text{C}_2\text{O}_4)_2$  to provide ( $^{89}\text{Zr}$ -B12) using previously established protocols for zirconium-DFO metalation (Figure 1).<sup>14</sup> A radiolabeling efficiency of >97% was determined by instant thin layer chromatography (iTLC). The specific activity of the tracer was determined by titrating  $^{89}\text{Zr}^{4+}$  and B12 at different mole ratios with an optimum specific activity of  $250 \pm 20$  mCi/ $\mu\text{mol}$ . Figure 3 shows complete metalation of B12-DFO used in the experiments herein.

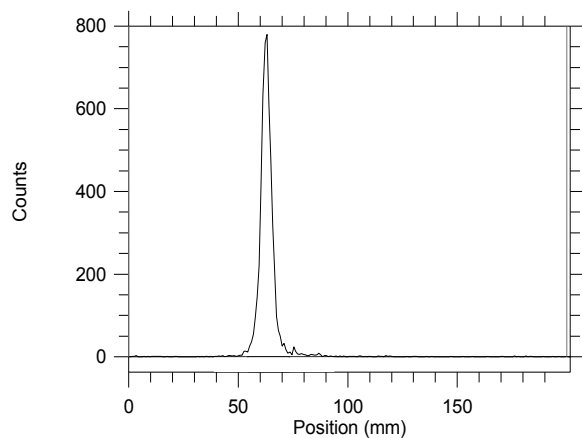


**Figure 3.** iTLC of  $^{89}\text{Zr}$ -B12 binding. The peak around 60 mm shows completely labeled B12-DFO.

Stability of the tracer was analyzed by incubating the  $^{89}\text{Zr}$ -B12 in saline and in human serum at  $37^\circ\text{C}$  and analyzing fractions at 4, 24, and 48 h using iTLC (Figure 4). There was 0% unbound  $^{89}\text{Zr}^{4+}$  observed over 48 h; therefore, the  $^{89}\text{Zr}$ -Cbl tracer was stable to demetallation during 0–48 h period.

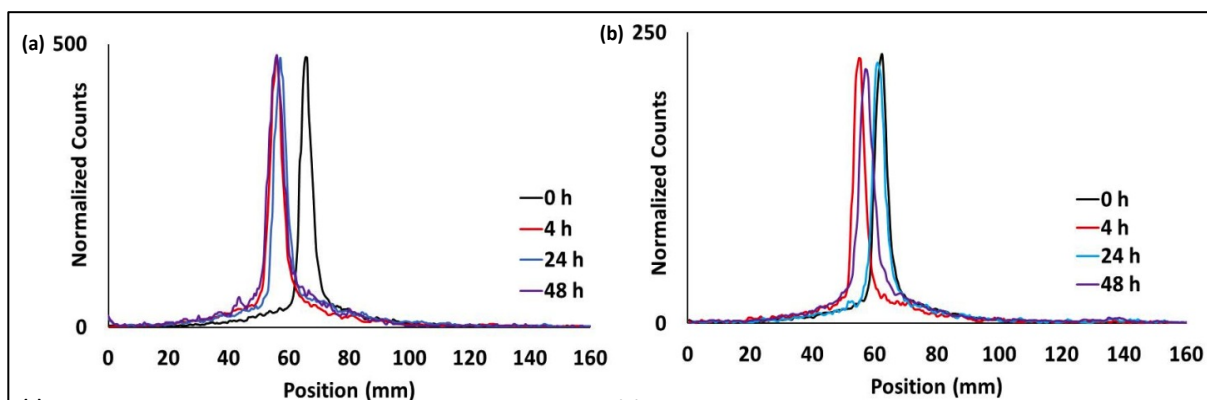


**Figure 4.**  $^{89}\text{Zr}$ -B12 stability in A) saline and B) human serum at  $37^\circ\text{C}$  at 4, 24, and 48 h. Analysis shows the  $^{89}\text{Zr}$ -B12 tracer was stable to demetallation up to 48 h, using iTLC.

### 2.2.2 Confirmation of Mouse TCII Binding to Zr-B12

Mouse TCII binding of  $^{91}\text{Zr}$ -B12 (non-radioisotope) was confirmed by radiometric chase assay (performed in the lab of Dr. Ebba Nexø, Aarhus University, Aarhus, Denmark) using  $^{57}\text{Co}$ -labeled B12 and compared to free B12.  $^{15}\text{Zr}$ -B12 was metalated as above using  $^{91}\text{ZrCl}_4$ . Mouse TCII binding of  $^{91}\text{Zr}$ -B12 (1.6 nM) was maintained in comparison from unmodified B12 (1.3 nM) (Figure 5).

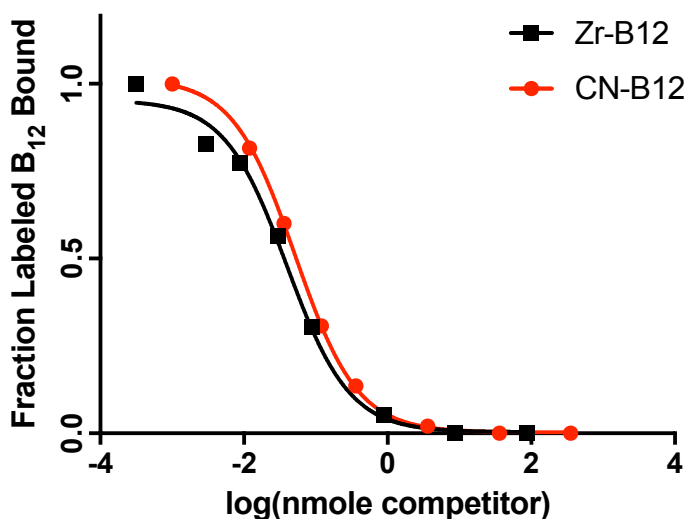


**Figure 5.** Mouse TCII binding of  $^{91}\text{Zr}$ -B12 (metalated with cold  $^{91}\text{ZrCl}_4$ ) and B12. TCII binding of  $^{91}\text{Zr}$ -B12 (1.6 nM) was maintained in comparison with unmodified B12 (1.3 nM).

### 2.3 In Vitro Uptake of $^{89}\text{Zr}$ -B12 in MDA-MD-453 Human Breast Cancer Cells

Initially, in vitro  $^{89}\text{Zr}$ -B12 uptake was tested through a modified internalization assay in MDA-MD-453 cells (Figure 6). MDA-MD-453 cells are a mammary gland breast cancer model.<sup>16,17</sup> Results showed increasing uptake over 24 h with the highest uptake at 37°C (1 h:  $144 \pm 20$ ; 4 h:  $210 \pm 64$ ; and 24 h:  $304 \pm 25$  CPM/ $10^5$  cells, data is shown as mean and standard deviation,  $n \geq 3$ ). Incubation at 4°C shows a significant decrease in uptake at all time points



indicating receptor-mediated uptake (1 h:  $36 \pm 29$ ; 4 h:  $30 \pm 8$ ; and 24 h:  $83 \pm 15$  CPM). A competitive assay with a co-administration of  $^{89}\text{Zr}$ -B12 and cold B12 (100 fold excess) showed a decrease in  $^{89}\text{Zr}$ -B12 uptake at all time points (1 h:  $15 \pm 6$ ; 4 h:  $30 \pm 5$ ; and 24 h:  $46 \pm 4$  CPM), indicating that  $^{89}\text{Zr}$ -B12 internalization is B12 dependent. This data supports that MDA-MD-453 tumors can be detected via the CD230 receptor and, as such, these cells were utilized in in vivo studies.

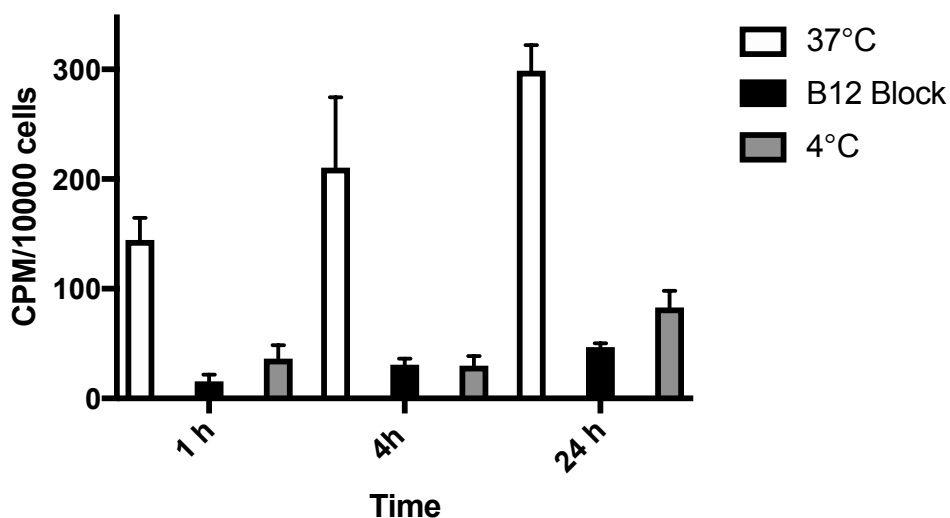


**Figure 6.** Internalization of  $^{89}\text{Zr}$ -B12 (1  $\mu\text{Ci}$ , 4 pmol/well) at 1, 4, 24 h time points incubated at 4 and 37°C in MDA-MB-453 cells. A competition assay was also performed at each time point using unlabeled B12 (40 pmol/well). The fraction of  $^{89}\text{Zr}$ -Cbl internalized in MDA-MB-453 cells is expressed as counts per minute in  $10^5$  cells (CPM/ $10^5$ ).

### 2.3.1 CD320 Immunohistochemistry on MDA-MD-453 Human Breast Cancer Cells and Tumors

Immunohistochemistry (IHC) results showed CD320 was largely expressed on MDA-MD-453 cells, supporting the hypothesis that  $^{89}\text{Zr}$ -B12 uptake in the tumors is CD320 mediated

(Figure 7). Sysel *et al.* reported similar IHC results for breast cancer xenografts and reported high expression of CD320 in breast tumor xenografts (mammary adenocarcinoma) compared to other tumor types (i.e. intestinal lymphoma and splenic mass cell tumor).<sup>4</sup> The CD320 expression supports the practicability of using <sup>89</sup>Zr-B12 to detect breast cancer tumors in vivo.

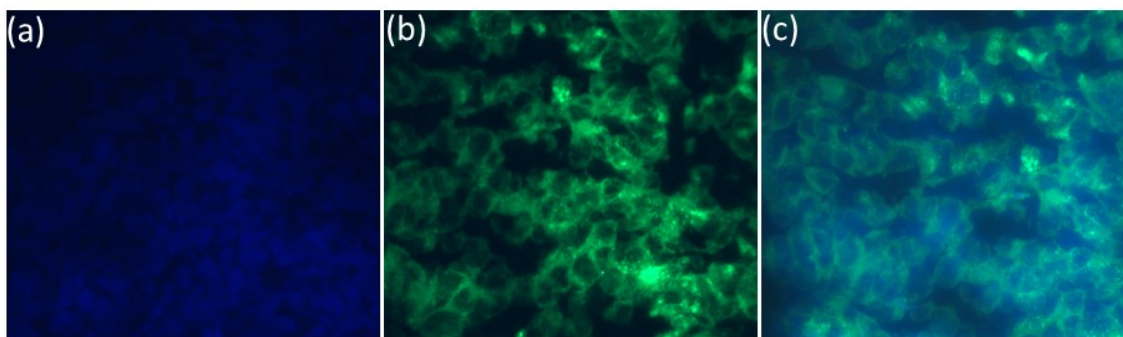


**Figure 7.** IHC staining of MDA-MB-453 tumor sections showing (a) DAPI, (b) CD320-AF488, and (c) overlay.

## 2.4 In Vivo Uptake of <sup>89</sup>Zr-B12 in a Nude Athymic Female Murine Model

### 2.4.1 PET Imaging of <sup>89</sup>Zr-B12 Uptake in Nude Athymic Female Mice

PET imaging was completed in nude athymic female mice at 4, 24 and 48 h p.i. (200-250  $\mu$ Ci/mouse via the tail vein) of <sup>89</sup>Zr-B12. As shown in Figure 8, there was high kidney uptake, relative to all other tissues, at 4 h that persisted over 48 h. Liver uptake was also observed, albeit significantly less than observed in the kidneys. The change in tissue uptake at 24 h was not apparent using PET imaging alone, however, the high contrast images were promising for tumor models as was hypothesized.

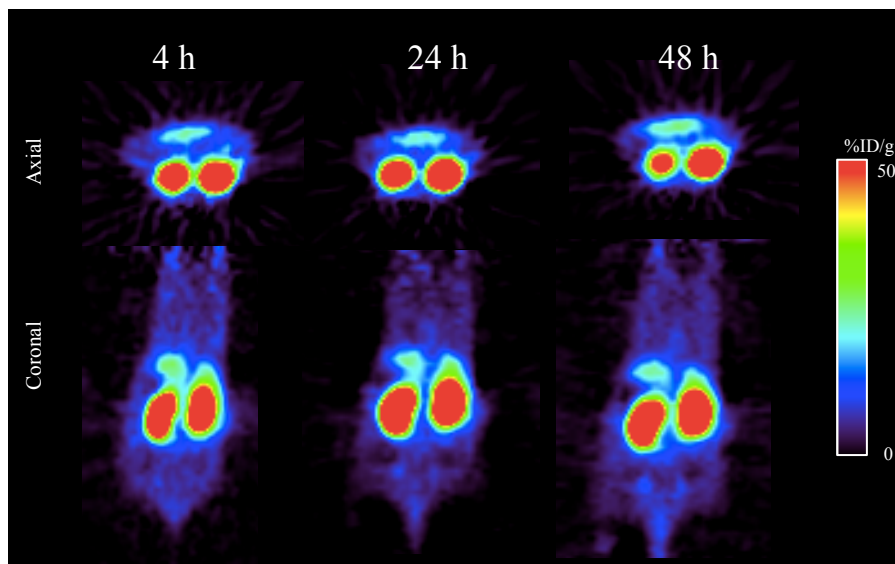


**Figure 8.** PET imaging of  $^{89}\text{Zr}$ -B12 at 4, 24, and 48 h in nude athymic female mice.  $^{89}\text{Zr}$ -B12 (200-250  $\mu\text{Ci}/\text{mouse}$ ) showed high uptake in the kidneys that did not change over 48 h. All other tissues assayed had relatively low uptake (see also Table 1, section 2.4.4).

#### 2.4.2 Biodistribution of $^{89}\text{Zr}$ -B12 Uptake in Nude Athymic Female Mice

To more closely examine the uptake of  $^{89}\text{Zr}$ -B12 ex vivo biodistribution was completed on mice 24 h p.i (Figure 9). Uptake in the liver and kidneys for  $^{89}\text{Zr}$ -B12 was  $19.19 \pm 2.18$  and  $88.34 \pm 4.49$  %ID/g, respectively. Other notable uptake was seen in the pancreas with  $5.94 \pm 1.22$  %ID/g. Notably little uptake was seen in the bone, which is commonly seen with  $^{89}\text{Zr}$  experiments as the tracer accumulates due to high phosphate content. Lack of bone uptake supports that our tracer is stable in vivo.<sup>12</sup> The ex vivo results show that, while tracer accumulation in the kidney was very high in comparison to other tissues, said tissues were low, defined as under 10 %ID/g. Due to the promising uptake in healthy mouse models the investigation of  $^{89}\text{Zr}$ -B12 as a PET imaging probe for CD320 receptor positive tumors detection was therefore warranted (*vide infra*).

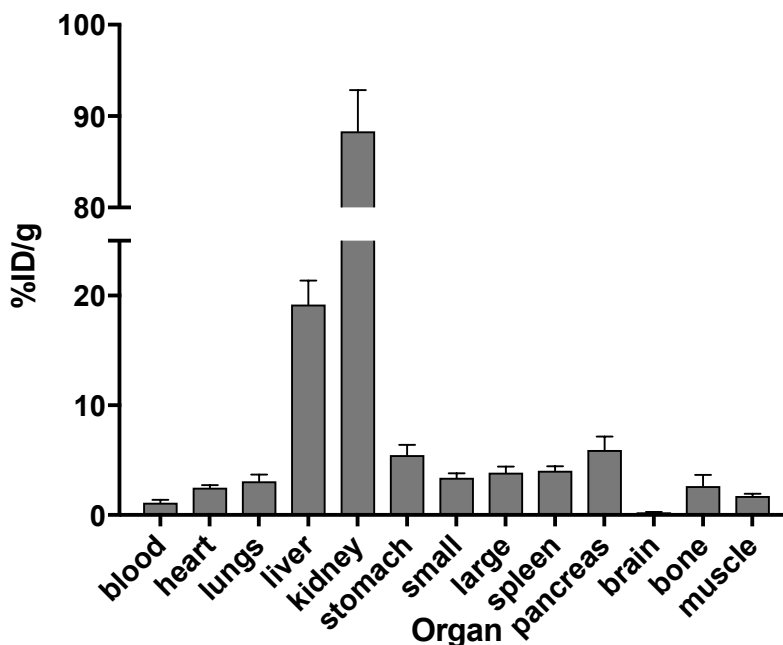


**Figure 9.** Ex vivo tissue distribution of  $^{89}\text{Zr}$ -B12 at 24 h in nude athymic female mice at 24 h.  $^{89}\text{Zr}$ -B12 showed high uptake in the kidney ( $130.26 \pm 14.05$  %ID/g) and moderate uptake in the liver ( $21.5 \pm 3.91$  %ID/g).  $n = 4$ .

#### 2.4.3 PET Imaging of $^{89}\text{Zr}$ -B12 in Nude Athymic Female Mice Bearing MDA-MD-453 Human Breast Tumors.

To investigate if  $^{89}\text{Zr}$ -B12 is a feasible PET imaging agent to detect cancer tumors, mice were used bearing MDA-MD-453 tumors. PET imaging of nude athymic female mice bearing MDA-MD-453 tumors and on a B12 deplete diet for 21 days prior to  $^{89}\text{Zr}$ -B12 administration was completed. A B12 deplete diet was used to increase tracer uptake by lowering endogenous B12 levels.  $^{89}\text{Zr}$ -B12 showed high kidney and moderate liver uptake that appeared to decrease over 48 h (Figure 10). Tumor uptake appeared moderately high and the tracer was retained over the 48 h. Regions of interest (ROI) of the tumors showed uptake of  $1.09 \pm 0.15$  at 24 h. Cohorts that were co-injected with 200-fold excess unlabeled B12 showed significantly less uptake in the

tumors ( $0.2 \pm 0.05$  %ID/g). It is important to note that mice used were on a B12 deplete diet for 21 days to increase tracer uptake. This data showed that  $^{89}\text{Zr}$ -B12, while having high kidney uptake, had clear and high contrast in MDA-MD-453 tumors, demonstrating its feasibility as a PET imaging agent to detect cancer tumors.

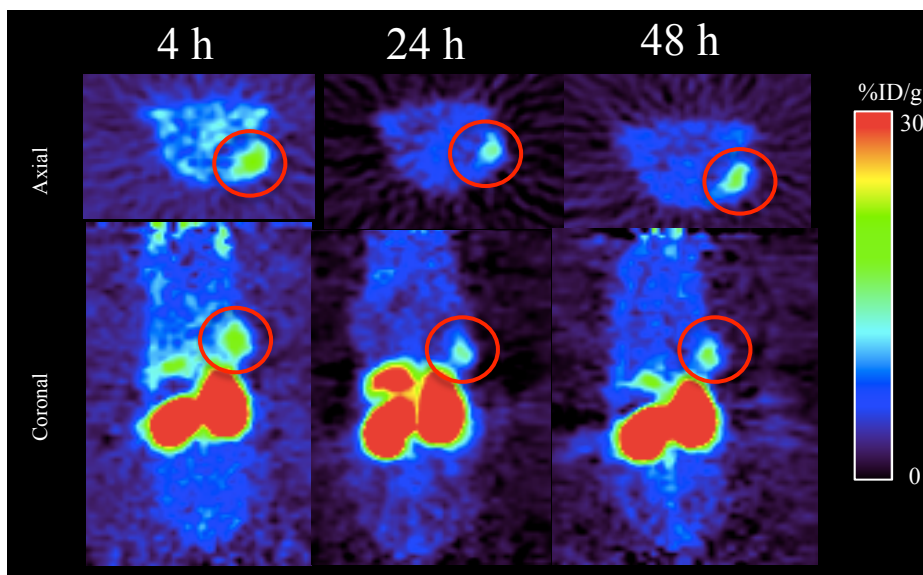


**Figure 10.** PET images of representative mice bearing MDA-MB-453 tumors imaged with  $^{89}\text{Zr}$ -B12 (1 nmol/mouse) at 4, 24, and 48 h p.i. time points, and co-injected  $^{89}\text{Zr}$ -B12 and cold B12 (~200 nmol/mouse) at 4 and 24 h p.i. time points. Mice were on a B12 deplete diet for 21 days pre-injection. The tumor location is indicated by a red circle.

#### 2.4.4 Biodistribution of $^{89}\text{Zr}$ -B12 in Nude Athymic Female Mice Bearing MDA-MD-453 Human Breast Cancer Tumors

Ex vivo tissue analysis showed  $5.11 \pm 1.33$  %ID/g tumor uptake in MDA-MD-453 tumors at 4 h and persisted over 48 h (24 h:  $4.16 \pm 1.09$ ; 48 h:  $3.78 \pm 0.77$  %ID/g) (Figure 11 and Table 1). Kidney showed the highest uptake of  $^{89}\text{Zr}$ -B12 with  $94.42 \pm 4.27$  %ID/g 4 h p.i. (24 h:

103.32 ± 11.50; 48 h: 72.74 ± 8.41 %ID/g) and liver showed uptake of 20.15 ± 3.42 %ID/g at 4 h p.i. (24 h: 16.75 ± 1.44; 48 h: 17.99 ± 2.54 %ID/g) To determine if such tumor uptake was B12 pathway dependent a competitive binding assay using excess cold-B12 was performed. This competitive study demonstrated more than a three-fold decrease in tracer uptake in tumors (Table 1), compared to unblocked cohorts at 48 h, when <sup>89</sup>Zr-B12 was co-administered with cold-B12 (0.04 ± 0.01 %ID/g), consistent with B12 dependent uptake. Liver (0.08 ± 0.01 %ID/g) and kidney (1.39 ± 0.18 %ID/g) were also significantly decreased with the co-administration with cold-B12. Blood clearance of <sup>89</sup>Zr-B12 was 83% after 20 h by which time tumor uptake has also decreased but by 20%. Importantly, the tumor uptake observed is comparatively higher than any other B12-based PET tracers reported thus far.<sup>5-10</sup>

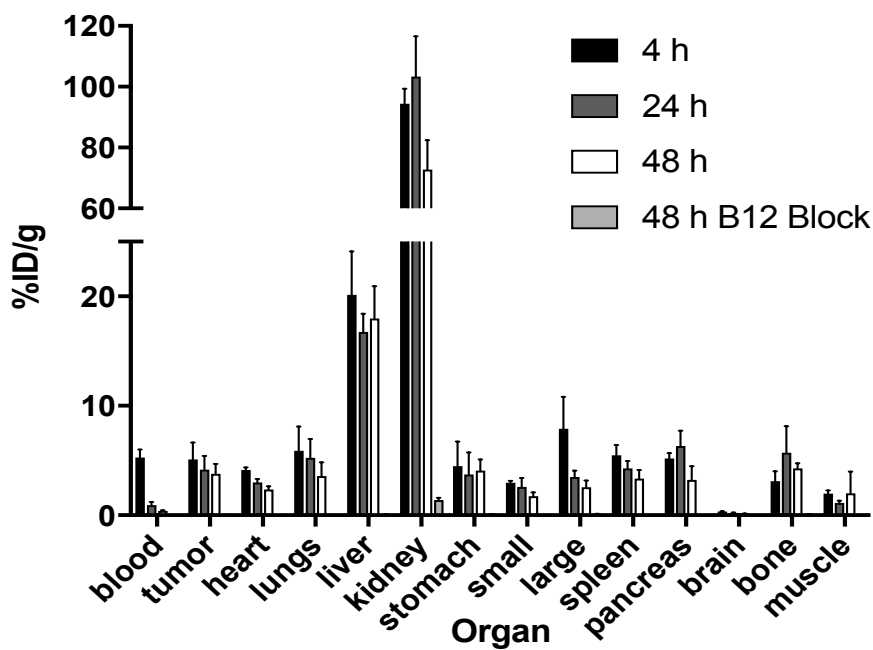


**Figure 11.** Ex vivo tissue distribution of <sup>89</sup>Zr-B12 (0.1 nmol/mouse), in nude athymic female mice bearing MDA-MD-453 tumors, at 4, 24, and 48 h. A blocking study with 100-fold (20 nmol/mouse, co-injected with tracer) of unmodified B12 displayed a significant decrease in

uptake in all tissues. Mice were on a B12 deplete diet for 21 days pre-injection. Data is shown as mean and standard deviation, n = 4.

One of the limitations noted in this study in using  $^{89}\text{Zr}$ -B12 was high kidney uptake (defined as  $>50\%ID/g$ ), a common problem across all tracers targeting CD320 to date.<sup>5-10</sup> This kidney uptake is due to the receptor megalin that is highly expressed in the kidneys, which binds and reabsorbs to holo-TCII and hence the TCII- $^{89}\text{Zr}$ -B12 complex tracer, is likely causing high uptake in the kidneys.<sup>24</sup> It is hypothesized that the higher kidney uptake and retention, compared to previous tracers, is due to a combination of the overall positive charge of the  $^{89}\text{Zr}$ -B12 and a higher injected concentrations compared to the negatively charged  $^{64}\text{Cu}$ -B12, neutral  $^{111}\text{In}$ -B12 complex and the similarly charged  $^{99m}\text{Tc}$ -B12 complex.<sup>5,7,10</sup> It has been shown that cationic species can be retained within the kidney for longer periods compared to neutral or anion complex's.<sup>18,19</sup> A positively charged  $^{99m}\text{Tc}$ -B12 complex reported in 2004 showed moderate uptake in the kidneys (15 – 50 %ID/g), however, only 0.5 – 1 ng was injected into the mouse model.<sup>10</sup> The  $^{89}\text{Zr}$ -B12 concentration used herein was 177 – 221 ng, which may account for the higher kidney retention seen with this tracer.

Organs	4 h	24 h	48h	48 h-Block
Blood	5.28 ± 0.62	0.92 ± 0.25	0.39 ± 0.06	0.009 ± 0.003
<b>Tumor</b>	<b>5.11 ± 1.33</b>	<b>4.16 ± 1.09</b>	<b>3.78 ± 0.77</b>	<b>0.04 ± 0.01</b>
Heart	4.12 ± 0.22	2.98 ± 0.29	2.34 ± 0.26	0.01 ± 0.002
Lungs	5.88 ± 1.92	5.23 ± 1.49	3.58 ± 1.08	0.04 ± 0.005
Liver	20.15 ± 3.42	16.75 ± 1.44	17.99 ± 2.54	0.08 ± 0.01
Kidney	94.42 ± 4.27	103.32 ± 11.50	72.74 ± 8.41	1.39 ± 0.18
Stomach	4.47 ± 1.95	3.74 ± 1.74	4.08 ± 0.88	0.06 ± 0.04
Small Int.	2.95 ± 0.16	2.59 ± 0.71	1.73 ± 0.31	0.03 ± 0.011
Large Int.	7.89 ± 2.55	3.49 ± 0.50	2.56 ± 0.53	0.10 ± 0.02
Spleen	5.47 ± 0.81	4.28 ± 0.57	3.35 ± 0.67	0.04 ± 0.009
Pancreas	5.17 ± 0.43	6.33 ± 1.21	3.24 ± 1.09	0.02 ± 0.001
Brain	0.33 ± 0.04	0.20 ± 0.05	0.14 ± 0.02	0.001 ± 0.0002
Bone	3.11 ± 0.77	5.70 ± 2.12	4.28 ± 0.39	0.09 ± 0.018
Muscle	1.96 ± 0.25	1.12 ± 0.19	2.00 ± 1.71	0.009 ± 0.003

Reported as %ID/g n ≥3

**Table 1.** Biodistribution of <sup>89</sup>Zr-B12 at 4, 24, and 48 h p.i. in MDA-MD-453 mouse models.

Data is shown as mean and standard deviation, n ≥ 3.

#### 2.4.5 CD320 Immunohistochemistry on Ex Vivo MDA-MD-453 Human Breast Cancer Tumors

Ex vivo MDA-MD-453 tumors were analyzed with IHC, results show CD320 was largely expressed on MDA-MD-453 tumor slices, supporting the hypothesis that <sup>89</sup>Zr-B12 uptake is CD320 mediated in the tumors (Figure 12).

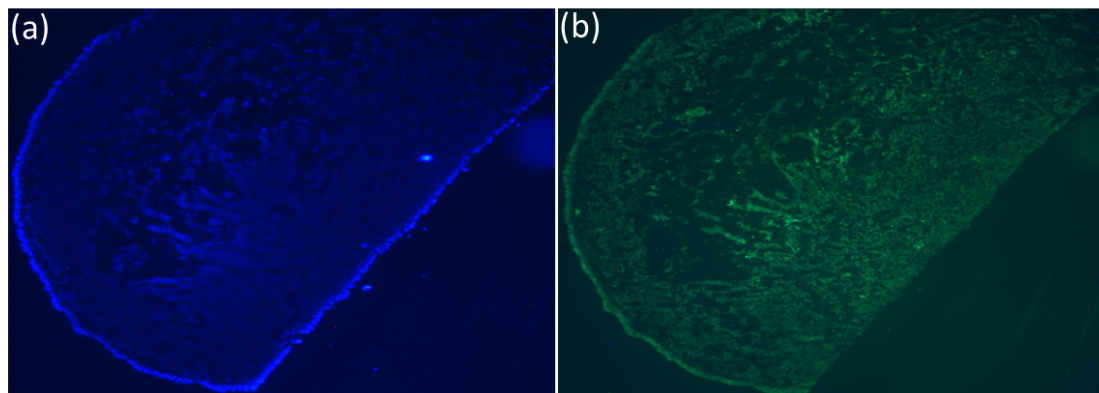


**Figure 12.** IHC staining of MDA-MD-453 tumor slices (a) with DAPI and (b) CD320-AF488, showing the tumors express CD320.



## 2.5 Comparing $^{89}\text{Zr}$ -B12 to Previous Radio-B12 Experiments

Doyle *et al.* reported  $^{64}\text{Cu}$ -labeled B12 with pancreatic, ovarian, mouse melanoma, and colorectal tumor models and the highest %ID/g reported was  $4.84 \pm 0.32$  at 6 h p.i. in the colorectal tumor model.<sup>5</sup> After 24 h, tumor uptake decreased by 23% with  $^{64}\text{Cu}$ -B12 in the melanoma model while our uptake decreased by 20%.<sup>5</sup> The  $^{64}\text{Cu}$ -B12 probe also showed high kidney uptake ( $36.15 \pm 2.10$  %ID/g at 6 h), which persisted after 24 h; whereas kidney retention of our tracer is 3 fold higher at all time points. The blood associated activity decreased by almost 90% after 24 h for the  $^{64}\text{Cu}$ -B12 tracer while  $^{89}\text{Zr}$ -B12 blood clearance is 83% after 20 h.<sup>5</sup>

Compared to the only B12-based PET tracer reported to date, namely  $^{64}\text{Cu}$ -B12, the tracer described in this report shows a higher %ID/g in tumor uptake, that persisted throughout a 48 h period.<sup>5,18-20</sup> Using  $^{89}\text{Zr}$  as the isotope is therefore overall advantageous as the background uptake decreases significantly overtime, suited to the  $^{89}\text{Zr}$  half-life.

## 2.6 Conclusions

Herein, a  $^{89}\text{Zr}$ -labeled B12 tracer was successfully developed and evaluated as a viable tool for visualizing the CD320 receptor mediated pathway in a breast cancer model.  $^{89}\text{Zr}$ -B12 displayed retained tumor uptake up to 48 h p.i. allowing for a longer imaging window and high contrast images. Most notably the achieved tumor uptake, to the best of our knowledge and after thorough review of previous literature, in our tumor model is comparatively higher than the other B12-based tracers reported thus far.<sup>5-10</sup> These studies showed that  $^{89}\text{Zr}$ -B12 can be a practical PET imaging agent in the detection of breast cancer models.

## 2.7 References

- (1) Nielsen, M. J.; Rasmussen, M. R.; Andersen, C. B. F.; Nexø, E.; Moestrup, S. K. Vitamin B12 Transport from Food to the Body's Cells—a Sophisticated, Multistep Pathway. *Nat. Rev. Gastroenterol. Hepatol.* **2012**, *9* (6), 345–354.
- (2) Gherasim, C.; Lofgren, M.; Banerjee, R. Navigating the B12 Road: Assimilation, Delivery, and Disorders of Cobalamin. *J. Biol. Chem.* **2013**, *288* (19), 13186–13193.
- (3) Quadros, E. V.; Sequeira, J. M. Cellular Uptake of Cobalamin: Transcobalamin and the TCbIR/CD320 Receptor. *Biochimie* **2013**, *95* (5), 1008–1018.
- (4) Sysel, A. M.; Valli, V. E.; Nagle, R. B.; Bauer, J. A. Immunohistochemical Quantification of the Vitamin B12 Transport Protein (TCII), Cell Surface Receptor (TCII-R) and Ki-67 in Human Tumor Xenografts. *Anticancer Res.* **2013**, *33* (10), 4203–4212.
- (5) Ikotun, O. F.; Marquez, B. V.; Fazen, C. H.; Kahkoska, A. R.; Doyle, R. P.; Lapi, S. E. Investigation of a Vitamin B12 Conjugate as a PET Imaging Probe. *ChemMedChem* **2014**, *9* (6), 1244–1251.
- (6) Collins, D. A.; Hogenkamp, H. P. C. Transcobalamin II Receptor Imaging via Radiolabeled Diethylene-Triaminepentaacetate Cobalamin Analogs. *J. Nucl. Med.* **1997**, *38* (5), 717–723.
- (7) Collins, D. A.; Hogenkamp, H. P. C.; Gebhard, M. W. Tumor Imaging Via Indium 111–Labeled DTPA–Adenosylcobalamin. *Mayo Clin. Proc.* **1999**, *74* (7), 687–691.
- (8) Waibel, R.; Treichler, H.; Schaefer, N. G.; Staveren, D. R. van; Mundwiler, S.; Kunze, S.; Küenzi, M.; Alberto, R.; Nüesch, J.; Knuth, A.; et al. New Derivatives of Vitamin B12 Show Preferential Targeting of Tumors. *Cancer Res.* **2008**, *68* (8), 2904–2911.
- (9) Ruiz-Sánchez, P.; Mundwiler, S.; Medina-Molner, A.; Spingler, B.; Alberto, R. Iodination of Cisplatin Adduct of Vitamin B12 [ $\{B12\}-CN-\{cis-PtCl(NH_3)_2\}^+$ ]. *J. Organomet. Chem.* **2007**, *692* (6), 1358–1362.
- (10) van Staveren, D. R.; Waibel, R.; Mundwiler, S.; Schubiger, P. A.; Alberto, R. Conjugates of Vitamin B12 with N $\epsilon$ -Functionalized Histidine for Labeling with [ $^{99m}Tc(OH_2)_3(CO)_3$ ] $^+$ : Synthesis and Biodistribution Studies in Tumor Bearing Mice. *J. Organomet. Chem.* **2004**, *689* (25), 4803–4810.
- (11) Severin, G. W.; Engle, J. W.; Nickles, R. J.; Barnhart, T. E.  $^{89}Zr$  Radiochemistry for PET. *Med. Chem. Shariqah United Arab Emir.* **2011**, *7* (5), 389–394.

- (12) Deri, M. A.; Zeglis, B. M.; Francesconi, L. C.; Lewis, J. S. PET Imaging with  $^{89}\text{Zr}$ : From Radiochemistry to the Clinic. *Nucl. Med. Biol.* **2013**, *40* (1), 3–14.
- (13) McEwan, J. F.; Veitch, H. S.; Russell-Jones, G. J. Synthesis and Biological Activity of Ribose-5'-Carbamate Derivatives of Vitamin B12. *Bioconjug. Chem.* **1999**, *10* (6), 1131–1136.
- (14) Perk, L. R.; Vosjan, M. J. W. D.; Visser, G. W. M.; Budde, M.; Jurek, P.; Kiefer, G. E.; van Dongen, G. A. M. S. P-Isothiocyanatobenzyl-Desferrioxamine: A New Bifunctional Chelate for Facile Radiolabeling of Monoclonal Antibodies with Zirconium-89 for Immuno-PET Imaging. *Eur. J. Nucl. Med. Mol. Imaging* **2010**, *37* (2), 250–259.
- (15) Stupperich, E.; Nexø, E. Effect of the Cobalt-N Coordination on the Cobamide Recognition by the Human Vitamin B12 Binding Proteins Intrinsic Factor, Transcobalamin and Haptocorrin. *Eur. J. Biochem.* **1991**, *199* (2), 299–303.
- (16) Hall, R. E.; Birrell, S. N.; Tilley, W. D.; Sutherland, R. L. MDA-MB-453, an Androgen-Responsive Human Breast Carcinoma Cell Line with High Level Androgen Receptor Expression. *Eur. J. Cancer* **1994**, *30* (4), 484–490.
- (17) Vranic, S.; Gatalica, Z.; Wang, Z.-Y. Update on the Molecular Profile of the MDA-MB-453 Cell Line as a Model for Apocrine Breast Carcinoma Studies. *Oncol. Lett.* **2011**, *2* (6), 1131–1137.
- (18) Akizawa, H.; Arano, Y.; Mifune, M.; Iwado, A.; Saito, Y.; Mukai, T.; Uehara, T.; Ono, M.; Fujioka, Y.; Ogawa, K.; et al. Effect of Molecular Charges on Renal Uptake of  $^{111}\text{In}$ -DTPA-Conjugated Peptides. *Nucl. Med. Biol.* **2001**, *28* (7), 761–768.
- (19) Ferdani, R.; Stigers, D. J.; Fiamengo, A. L.; Wei, L.; Li, B. T. Y.; Golen, J. A.; Rheingold, A. L.; Weisman, G. R.; Wong, E. H.; Anderson, C. J. Synthesis, Cu(II) Complexation,  $^{64}\text{Cu}$ -Labeling and Biological Evaluation of Cross-Bridged Cyclam Chelators with Phosphonate Pendant Arms. *Dalton Trans. Camb. Engl. 2003* **2012**, *41* (7), 1938–1950.

### **Chapter 3: The Use of Systemically Administered Intrinsic Factor in Radio-Imaging**

The work reported in this chapter will be submitted titled “Pre-binding of Vitamin B12 Conjugates to Gastric Intrinsic Factor is Not Effected by Endogenous B12 levels” by authors Jayme L. Workinger, Akhila N. Kuda-Wedagedara, Ebba Nexo, Nerissa T. Viola-Villegas, and Robert P. Doyle.

Work in this chapter was performed by the author unless otherwise indicated. Where indicated work was performed in collaboration with Dr. Nerissa Viola-Villegas at Wayne State University, Detroit, MI.

#### 3.1 Introduction

The American Cancer Society (ACS) predicts 64,000 new cases of renal (kidney) cancer to occur in 2017.<sup>1</sup> Stage IV, metastasized renal cancer patients have an 8% 5-year survival rate.<sup>2</sup> As with most cancers, the key for survival is in early detection.<sup>3,4</sup> The low 5-year survival rate has been attributed to small tumor size, the location of the tumors, and patients showing little or no symptoms.<sup>3-5</sup> The renal proximal tubule, where CUBN is highly expressed, is the origin of 90% of all renal cancer.<sup>5-7</sup>

The receptor CUBN recognizes multiple ligands, including holo-IF (for more detail see Chapter 1, Section 1.2.2).<sup>7-10</sup> However, there are limited reports of CUBN being expressed (mainly the kidney and small intestine) in tissues and none that suggest it is overexpressed in cancer tissues.<sup>7,10-15</sup> Targeting CUBN then should produce low background due to CUBN's limited expression.<sup>10-15</sup> The **hypothesis** of this work is that systemically administered gastric holo-IF protein bound to a radiolabelled B12 conjugate will allow targeting, with specific uptake

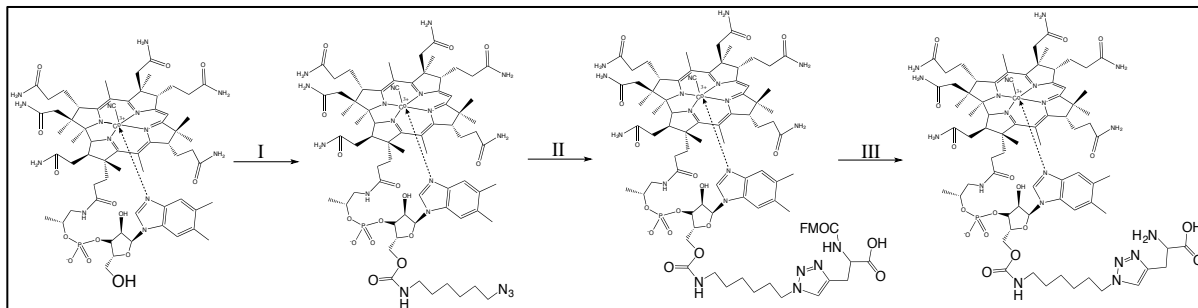
and low background, of CUBN. The goals of this chapter are to 1) evaluate the distribution of CUBN through systemic administration of a radiolabeled IF-B12 complex, and 2) determine mechanism of uptake in primary accumulating organs.

### 3.2 In vivo Analysis of $^{99m}\text{Tc}$ -B12 and IF- $^{99m}\text{Tc}$ -B12

This work was done in collaboration with Dr. John Valliant's research group at McMaster University, Hamilton, ON, Canada.

#### 3.2.1 Synthesis and Characterization of B12-propargylglycine (B12-PG)

B12-propargylglycine was synthesized by activating the 5'-hydroxyl group on the deoxyribose moiety of B12 with CDT in anhydrous DMSO followed by addition of 1-amine-6-azidohexane priming it for copper-alkyne-azide 'click' (CuAAC) chemistry creating B12-azide-linker.<sup>16</sup> B12-azide-linker was 'clicked' to fmoc-propargylglycine (FPG) (0.0492 mmol) with Cu(I)/TBTA (0.0216 mmol and 0.043 mmol, respectively) in DMF/H<sub>2</sub>O (4:1) (v/v) overnight to produce B12-FPG, which was subsequently deprotected with a 30% piperidine mixture for the final compound, B12-PG (Scheme 1).<sup>17,18,19</sup> The final yield was 95%, based on B12 starting material. CuAAC reactions were attempted with PG without success (data not shown). LC-MS analysis showed an observed m/z 1637 [M]<sup>+</sup> and the expected being 1636.



**Scheme 1.** Synthesis of B12-PG. I: B12 was activated with CDT and reacted forward with 1-amine-6-azido-hexane. II: B12-azide-linker ‘clicked’ to FPG with Cu(I)/TBTA in DMF/H<sub>2</sub>O. III: B12-FPG was deprotected with 30% piperidine mixture. Overall yield based on B12 starting material was 95%.

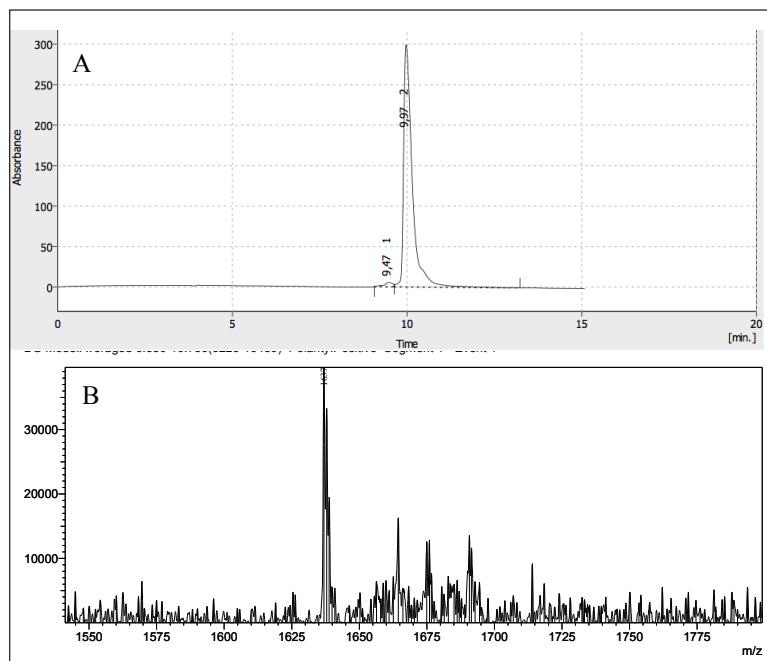


**Figure 1.** RP-HPLC and LC-MS of B12-PG. A) HPLC shows > 95%,  $R_t = 9.9$  min and B) LC-MS: m/z observed m/z 1637  $[M]^+$ , expected m/z 1636.

### 3.2.1.1 Labeling and Stability of $^{99m}\text{Tc}$ -B12 and IF- $^{99m}\text{Tc}$ -B12

B12-PG was metalated with  $^{99m}\text{Tc}$  at equal molar ratios for 30 min 30 min at 40 C and pH 7 to yield  $^{99m}\text{Tc}$ -B12. Figure 2 shows RP-HPLC of  $^{99m}\text{Tc}$ -B12 and full metalation was achieved.  $^{99m}\text{Tc}$ -B12 was purified and reconstituted for IF binding and biodistribution studies.

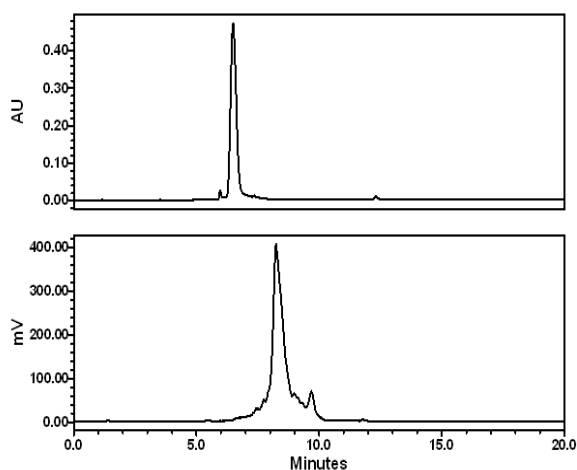


**Figure 2.** Labeling of B12-PG with  $^{99m}\text{Tc}$  showing full metalation. A) ultraviolet detection at 360 nm, and B) gamma detection.

$^{99m}\text{Tc}$ -B12 was then pre-bound by IF and stability was examined (Figure 3). Gamma and ultraviolet detection (360 nm) of IF- $^{99m}\text{Tc}$ -B12 (1 nM) confirmed that  $^{99m}\text{Tc}$ -B12 was bound by IF within 30 min.<sup>20</sup>

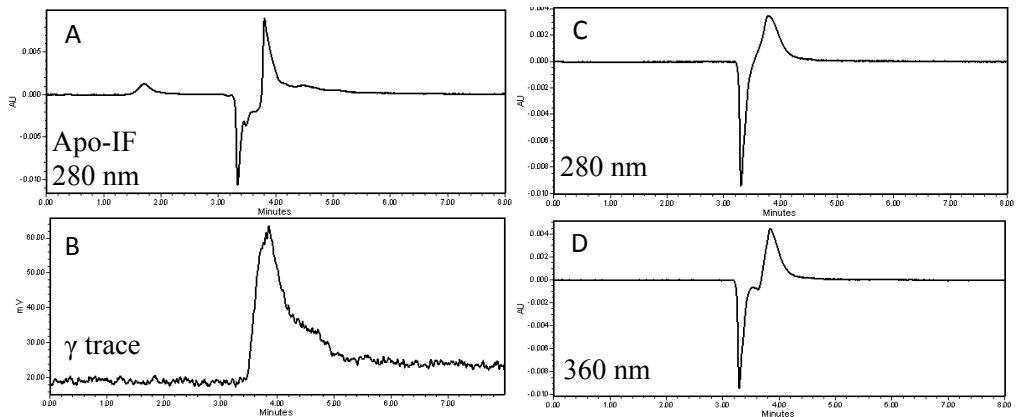


**Figure 3.** Size exclusion chromatograph of IF-<sup>99m</sup>Tc-B12 (1 nM) confirms IF binding to <sup>99m</sup>Tc-B12. A) detection of apo-IF,  $R_t$ : 4 min, B) detection of IF-<sup>99m</sup>Tc-B12 through gamma, C) detection of IF-<sup>99m</sup>Tc-B12 at 280 nm, D) detection of IF-<sup>99m</sup>Tc-B12 at 360 nm. Column: Zorbax GF-250, 4  $\mu$ m, 4.6 x 250 mm, Elution Buffer: 20 mM sodium phosphate and 300 mM sodium chloride at pH 7.

### 3.2.2 Biodistribution of IF-<sup>99m</sup>Tc-B12 in Male CD-1 Mice

Initially, <sup>99m</sup>Tc-B12 was injected into CD-1 mice to establish a B12 control (Figure 4). As shown rapid uptake in the kidney ( $41.96 \pm 2.28$ ,  $63.21 \pm 4.93$ , and  $69.05 \pm 3.28$  %ID/g at 3, 6, and 24 h, respectively) with low uptake in all other tissue was observed, as previously reported for B12 radio-probes.<sup>21–25</sup> Next, IF-<sup>99m</sup>Tc-B12 was injected in male CD-1 mice at 500 nM (0.1 nmol/mouse) at 1, 3, and 6 h (Figure 5). The 500 nM concentration was based on the max concentration before IF is known to aggregate.<sup>8,26</sup>



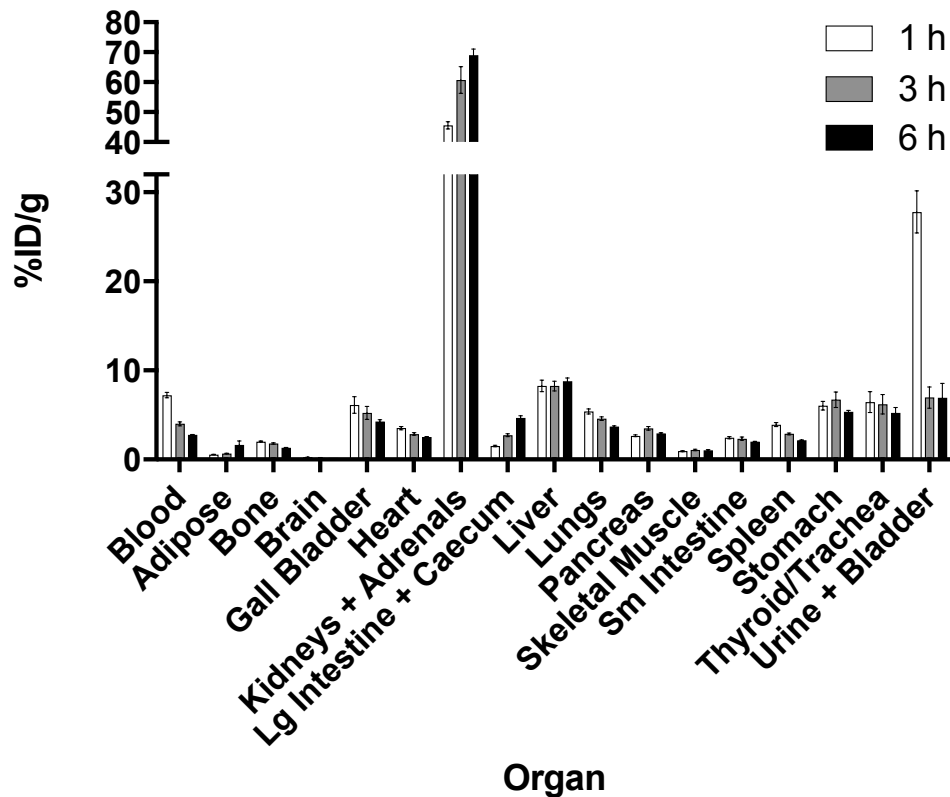


**Figure 4.** Ex vivo tissue distribution of A)  $^{99m}\text{Tc}$ -B12 at 1, 3, and 6 h in CD-1 mice. Highest uptake observed is within the kidney with low tracer uptake in all other tissues. n = 3

Figure 5 shows IF- $^{99m}\text{Tc}$ -B12, at 500 nM, has a clear tissue distribution shift from the kidney to the liver (kidney:  $13.15 \pm 1.58$ ,  $19.28 \pm 3.01$ , and  $28.64 \pm 1.67$  and liver:  $27.46 \pm 3.18$ ,  $32.82 \pm 6.11$ , and  $30.8 \pm 1.55$  at 1, 3, and 6 h, respectively). In comparing the data of IF- $^{99m}\text{Tc}$ -B12 with  $^{99m}\text{Tc}$ -B12 it is clear that there is a significant change in the liver and kidney uptake, with a 4-fold increase in liver and three-fold decrease in the kidney observed.

The switch in liver uptake could be due to a) IF being degraded or b) possible receptor recognition of IF in the liver. Figure 5 shows that the liver uptake is consistent from 1 – 6 h,

suggesting it is not degrading (accumulation would increase over time) and is likely due to receptor recognition.

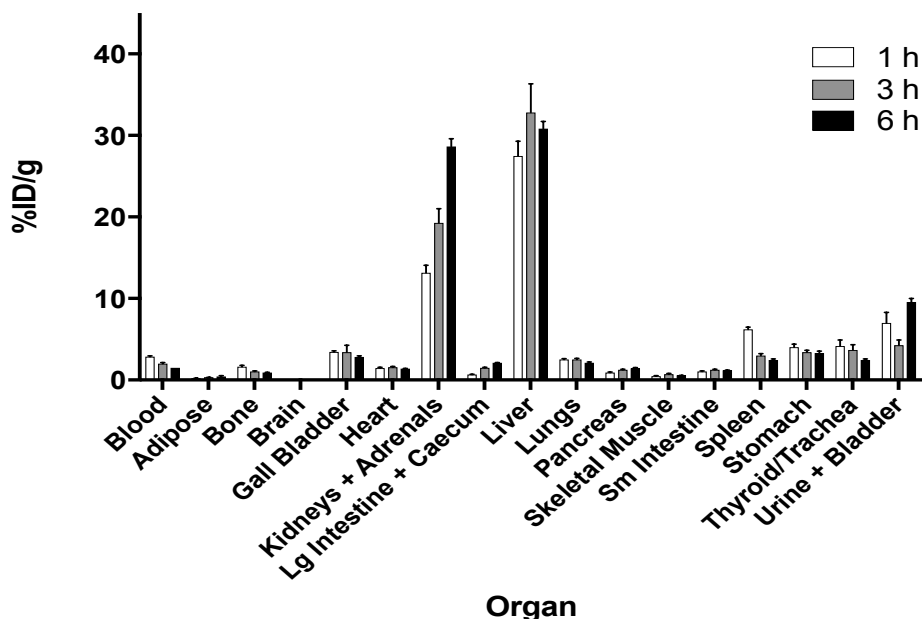


**Figure 5.** Ex vivo tissue distribution of IF-<sup>99m</sup>Tc-B12 (500 nM) at 1, 3, and 6 h in CD-1 mice. Highest uptake is in the kidney and liver. Kidney: 13.15 ± 1.58, 19.28 ± 3.01, and 28.64 ± 1.67 at 1, 3, and 6 h respectively. Liver: 27.46 ± 3.18, 32.82 ± 6.11, and 30.8 ± 1.55 at 1, 3, and 6 h, respectively. n = 3 for each time point.

### 3.3 In vivo Uptake of IF-<sup>64</sup>Cu-B12 in Nude Athymic Female Mice

This work was done in collaboration with Dr. Nerissa Viola-Villegas research group at Wayne State University.

#### 3.3.1 PET Imaging of IF-<sup>64</sup>Cu-B12 in Nude Athymic Female Mice

Once the shift in liver uptake with IF-<sup>99m</sup>Tc-B12 was observed this work was continued with <sup>64</sup>Cu to do PET imaging. B12-NOTA was made as previously reported and IF-<sup>64</sup>Cu-B12

was injected into nude athymic female mice and imaged 1, 3, 16 and 20 h.<sup>22</sup> Figure 6 shows IF-<sup>64</sup>Cu-B12 uptake at 1 and 20 h p.i. The same increasing trend is seen with liver uptake (seen in biodistribution) IF-<sup>99m</sup>Tc-B12 uptake was similar to the PET imaging of IF-<sup>64</sup>Cu-B12. However, the specific activity (60 mCi/ $\mu$ mol) for <sup>64</sup>Cu-B12 was not feasible for continued use and therefore only two mice were imaged. This low activity was suspected to be due to isotopic decay of <sup>64</sup>Cu to Ni during isotope delivery, as three half-lives (half-life being 12.7 h) passed once activity was required.<sup>27</sup>

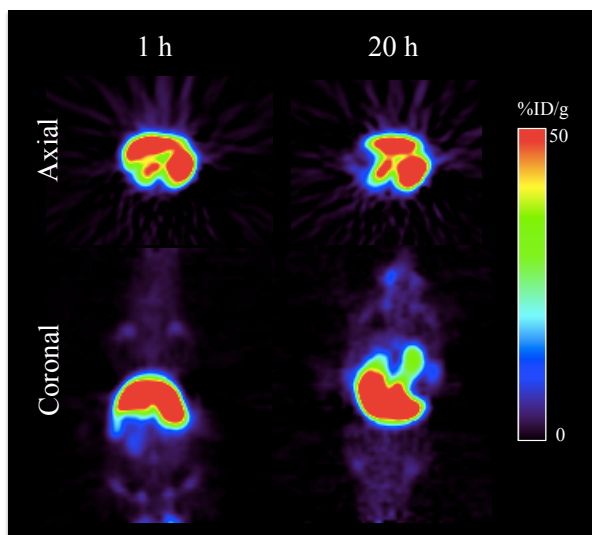


**Figure 6.** PET imaging of IF-<sup>64</sup>Cu-B12 (~200  $\mu$ Ci/mouse) at 1 and 20 h p.i. High uptake in the liver and kidney is observed with little uptake in all other tissues.

### 3.3.2 Biodistribution of IF-<sup>64</sup>Cu-B12 in Nude Athymic Female Mice

After the PET imaging was completed the two mice were sacrificed and ex vivo tissue distribution of IF-<sup>64</sup>Cu-B12 at 24 h was completed (Figure 7). Biodistribution shows the same high liver and kidney trend ( $24.31 \pm 12.31$  and  $51.31 \pm 2.46$  %ID/g, respectively). Spleen uptake is also high ( $5.55 \pm 3.98$  %ID/g) compared to all other tissues but was not seen using <sup>99m</sup>Tc. It is

important to note that comparing uptake between different radio-tracers and even experiments is difficult as amounts, concentrations, activity, and strain of mouse vary. In comparing the different data the trends are primarily the focus and not exact numbers. The trends seen herein show IF administration is reproducible.

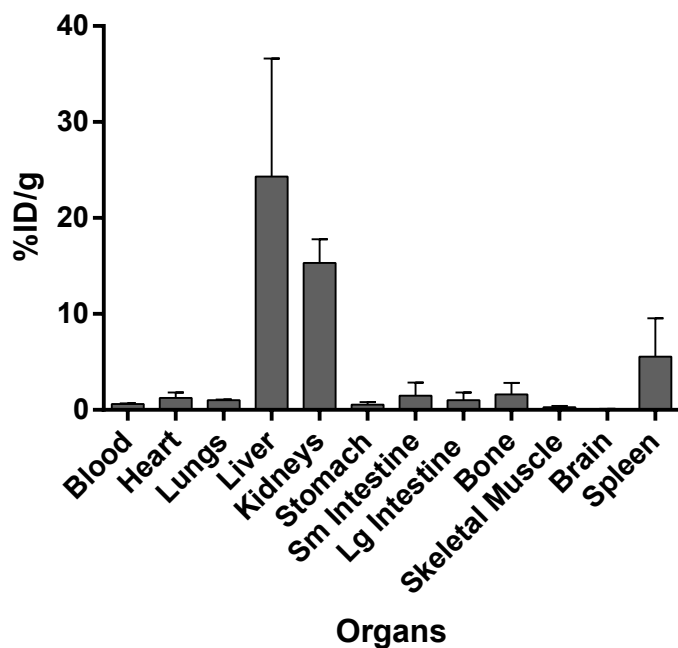


**Figure 7.** Ex vivo tissue distribution of IF-<sup>64</sup>Cu-B12 at 24 h in nude athymic female mice. n = 2.

### 3.4 In vivo Uptake of IF-<sup>89</sup>Zr-B12 in Nude Athymic Female Mice

This work was done in collaboration with Dr. Nerissa Viola-Villegas research group at Wayne State University.

Using IF-<sup>64</sup>Cu-B12 and IF-<sup>99m</sup>Tc-B12 showed a rapid and significant uptake in the liver and to a lesser degree the kidneys. It was decided, due to the low specific activity with IF-<sup>64</sup>Cu-B12, a new radio-isotope, <sup>89</sup>Zr, would be used. IF-<sup>89</sup>Zr-B12 was used to fully explore IF uptake

in a mouse model through PET and biodistribution (for more detail on  $^{89}\text{Zr}$ -B12 see Chapter 2, Section 2.2).

### 3.4.1 Human Gastric IF Binding to $^{91}\text{Zr}$ -B12

To confirm that  $^{89}\text{Zr}$ -B12 will bind to IF a radiometric chase assay, using  $^{57}\text{Co}$ -B12, was completed with a cold tracer ( $^{91}\text{Zr}$ -B12) and compared to free B12, as cyanocobalamin (CN-B12).<sup>28</sup>  $^{91}\text{Zr}$ -B12 was made using B12-DFO and chelated to  $^{91}\text{ZrCl}_4$  at pH 7-7.5. Human gastric IF binding of Zr-B12 (1.57 nM) was maintained and was similar to free B12 (1.36 nM) (Figure 8).

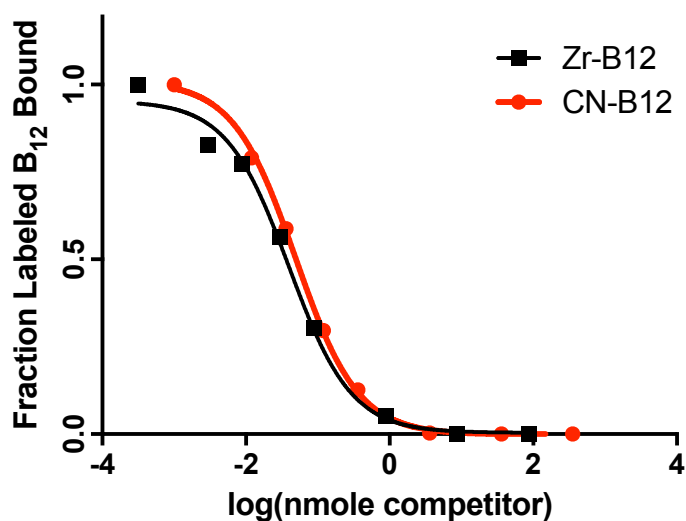


**Figure 8.** Binding Affinities of Zr-B12 and B12 to human gastric IF with a  $K_d$ : 1.57 nM and 1.36 nM, respectively.

### 3.4.2 PET Imaging of IF-<sup>89</sup>Zr-B12 in Nude Athymic Female Mice on B12 Replete Chow

Initially, PET imaging was completed in nude athymic female mice on B12 replete chow (has B12 within) at 1, 6 and 24 h p.i. (200-250  $\mu$ Ci/mouse via the tail vein) of IF-<sup>89</sup>Zr-B12. As shown in Figure 9 there was significant liver uptake at 1 h, which did not change over the subsequent 24 h. Overall, the highest uptake was observed in the liver, compared to the control (<sup>89</sup>Zr-B12 alone), which showed primary uptake in the kidneys. The change in tissue uptake from 1 to 24 h was not apparent using PET imaging alone and hence biodistribution studies were conducted.

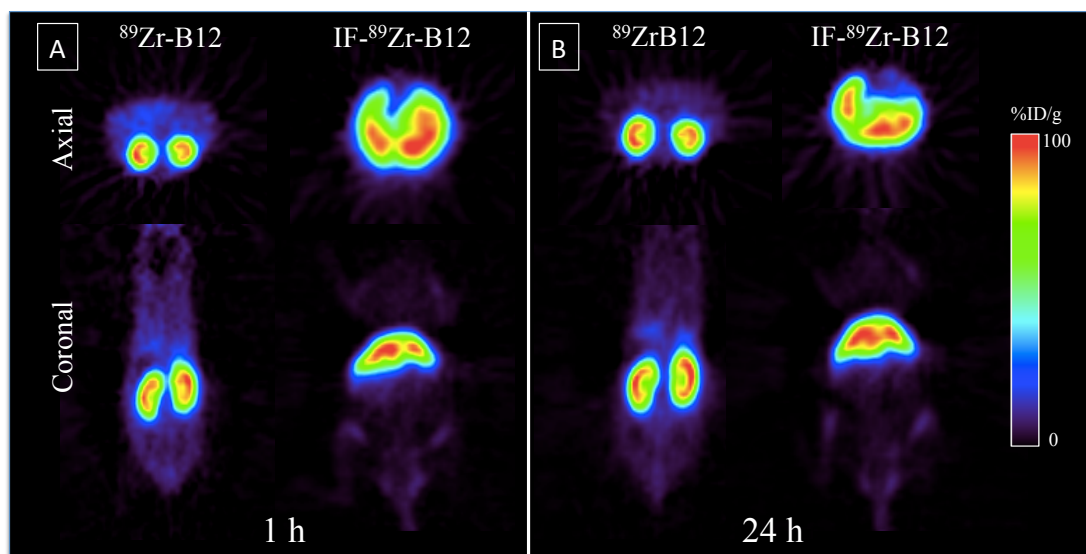


**Figure 9.** PET imaging of IF-<sup>89</sup>Zr-B12 and <sup>89</sup>Zr-B12 at 1 and 24 h in nude athymic mice on a B12 replete diet. In comparison to the control (<sup>89</sup>Zr-B12) IF-<sup>89</sup>Zr-B12 showed rapid and significant uptake in the liver, which did not change over 24 h.

### 3.4.3 Biodistribution of IF-<sup>89</sup>Zr-B12 in Nude Athymic Female Mice on Normal Chow

To more closely examine the uptake of IF-<sup>89</sup>Zr-B12 ex vivo biodistribution was completed on mice 24 h p.i. Figure 10 (see Table 1, Section 3.4.4) shows the biodistribution for

IF-<sup>89</sup>Zr-B12 and the control <sup>89</sup>Zr-B12. For IF-<sup>89</sup>Zr-B12 the highest uptake was seen in the liver and kidneys with  $18.46 \pm 1.90$  and  $17.01 \pm 5.36$  %ID/g (s.d), respectively. In comparison, the uptake in the liver and kidneys for <sup>89</sup>Zr-B12 was  $13.45 \pm 2.24$  and  $81.51 \pm 8.67$  %ID/g (s.d), respectively. Other notable uptake for IF-<sup>89</sup>Zr-B12 was seen in the spleen and bone ( $6.53 \pm 0.39$  and  $3.53 \pm 1.91$  %ID/g (s.d)) with similar uptake in the control (<sup>89</sup>Zr-B12). Uptake in all other tissues was significantly decreased compared to <sup>89</sup>Zr-B12.

A similar trend emerges from using all three radio-tracers (<sup>99m</sup>Tc, <sup>64</sup>Cu, and <sup>89</sup>Zr) that pre-binding a radiolabeled B12 conjugate to IF causes a clear shift in uptake with a decrease in kidney and an increase in the liver. It can be noted that we do not see the 3-fold increase in liver uptake as observed before but the significant decrease, 4-fold, in the kidney uptake was similar. The overall decrease in uptake across all other tissues points to IF-<sup>89</sup>Zr-B12 not being recognized through the endogenous B12 CD320 receptor that internalizes <sup>89</sup>Zr-B12. Bone uptake is commonly seen with <sup>89</sup>Zr as the tracer due to the high phosphate content.<sup>29</sup> The spleen (which has been shown to be CUBN negative)<sup>30</sup> uptake could possibly indicate an immune response to IF, which warrants further investigation (see Chapter 5, Section 5.4).

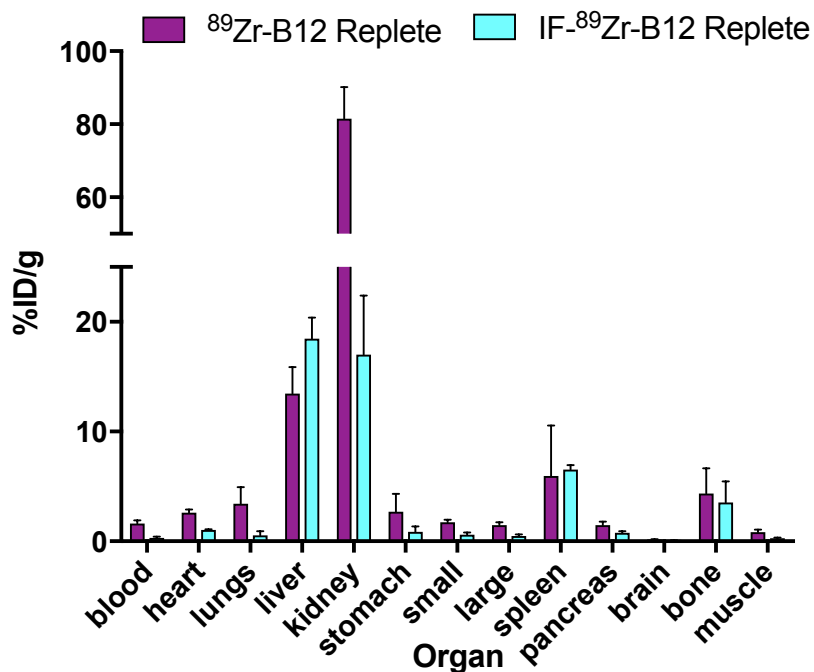


**Figure 10.** Ex vivo tissue distribution of IF- $^{89}\text{Zr-B12}$  and  $^{89}\text{Zr-B12}$  at 24 h in nude athymic female mice on a B12 replete diet. In compared to the control ( $^{89}\text{Zr-B12}$ ) IF- $^{89}\text{Zr-B12}$  showed high uptake in the liver and a decrease in uptake in the kidney. Data is shown as mean and standard deviation,  $n \geq 3$ .

While these initial observations with IF showed promise, the investigation using mice on a B12 deplete diet warranted further investigation. All B12 based radio-tracers that have been reported to date have used rodent models on a B12 deficient (deplete) diet.<sup>21,22,24</sup> A report on using mice on a normal diet was not found.

### 3.4.4 PET Imaging of IF- $^{89}\text{Zr-B12}$ in Nude Athymic Female Mice on B12 Deficient Chow

To more closely examine the effects of a B12 diet IF- $^{89}\text{Zr-B12}$  or  $^{89}\text{Zr-B12}$  was injected into nude athymic female mice on a B12 deplete diet for 21 days and PET imaging was completed on mice 24 h p.i. Figure 11 shows PET imaging of IF- $^{89}\text{Zr-B12}$  and the control  $^{89}\text{Zr-B12}$ .



B12. For IF-<sup>89</sup>Zr-B12 the highest uptake was seen in the liver and kidneys and was not significantly different than mice on normal diets. However, with <sup>89</sup>Zr-B12 a change was observed with higher uptake in the liver.

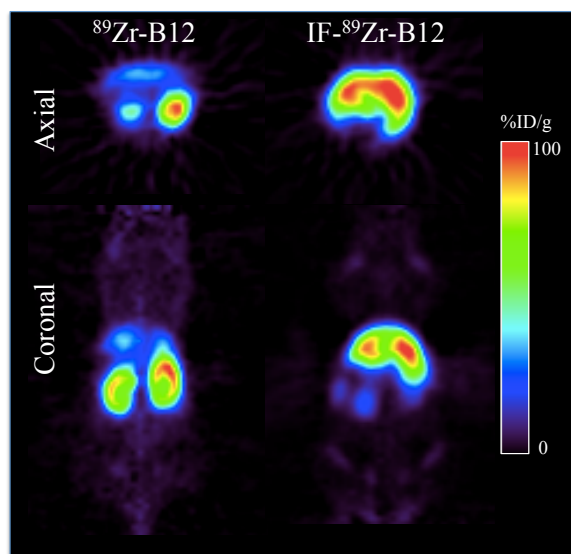


**Figure 11.** PET imaging of IF-<sup>89</sup>Zr-B12 and <sup>89</sup>Zr-B12 at 24 h in nude athymic female mice on a B12 deplete diet for 21 days. IF-<sup>89</sup>Zr-B12 in mice on normal chow (Figure 9) showed similar uptake at 24 h. A higher uptake in the liver was observed for <sup>89</sup>Zr-B12 than in mice on a replete diet.

### 3.4.5 Biodistribution of IF-<sup>89</sup>Zr-B12 in Nude Athymic Female Mice on B12 Deficient Chow

To more closely examine the uptake of IF-<sup>89</sup>Zr-B12 in mice on a B12 deplete diet ex vivo biodistribution was completed 24 h p.i. Figure 12 (see Table 1 in Section 3.4.4) shows the biodistribution for IF-<sup>89</sup>Zr-B12 and the control <sup>89</sup>Zr-B12. For IF-<sup>89</sup>Zr-B12 the highest uptake was seen in the liver and kidneys with  $58.21 \pm 8.71$  and  $61.04 \pm 1.69$  %ID/g, respectively. In comparison the uptake in the liver and kidneys for <sup>89</sup>Zr-B12 was  $19.19 \pm 2.18$  and  $88.34 \pm 4.49$

%ID/g, respectively. Other notable uptake for IF-<sup>89</sup>Zr-B12 was seen in the spleen and bone (16.90 ± 3.10 and 4.47 ± 1.26 %ID/g (s.d.), respectively). Uptake in all other tissues was significantly decreased compared to <sup>89</sup>Zr-B12.

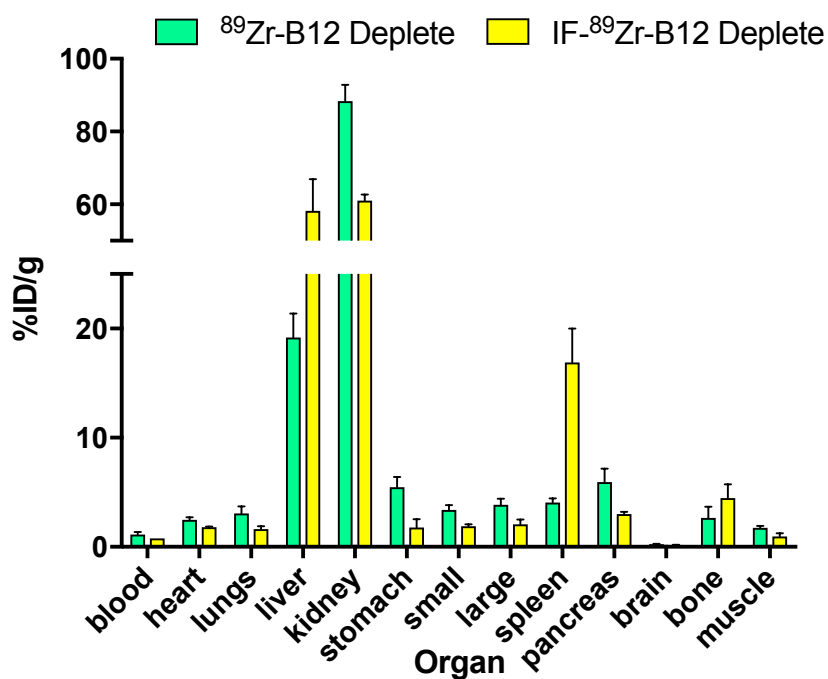


**Figure 12.** Ex vivo tissue distribution of IF-<sup>89</sup>Zr-B12 and <sup>89</sup>Zr-B12 at 24 h in nude athymic female mice on a B12 deplete diet for 21 days. Comparison to the control (<sup>89</sup>Zr-B12) IF-<sup>89</sup>Zr-B12 show a high uptake in liver and decrease uptake in the kidney. Data is shown as mean and standard deviation, n ≥ 3.

In reviewing the data, there appeared to be a notable effect on uptake of IF-<sup>89</sup>Zr-B12 when using mice on a B12 deplete (Figure 13 and Table 1). The overall trend observed was a decrease in uptake in most tissues (except liver, spleen, and bone) in comparison to <sup>89</sup>Zr-B12.

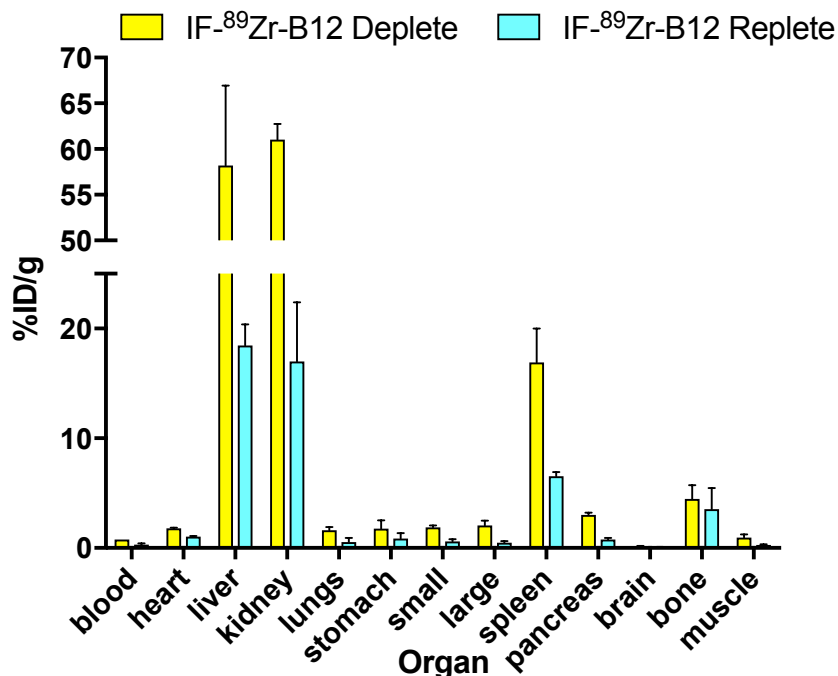


**Figure 13.** Comparing the effects of mice on a B12 deplete and replete diet 24 h p.i of IF-<sup>89</sup>Zr-B12. A 3-fold increase in uptake is seen in both the liver, kidney, and spleen in deplete mice.

Organs	89Zr-B12	IF-89Zr-B12	89Zr-B12	IF-89Zr-B12
	Replete	Replete	Deplete	Deplete
Blood	1.60 ± 0.29	0.30 ± 0.10	1.13 ± 0.24	0.77 ± 0.01
Heart	2.6 ± 0.30	1.04 ± 0.04	2.48 ± 0.24	1.80 ± 0.05
Lungs	3.42 ± 1.51	0.52 ± 0.40	3.07 ± 0.61	1.62 ± 0.27
Liver	13.45 ± 2.24	18.46 ± 1.90	19.19 ± 2.18	58.21 ± 8.71
Kidney	81.51 ± 8.67	17.01 ± 5.36	88.34 ± 4.49	61.04 ± 1.69
Stomach	2.70 ± 1.61	0.87 ± 0.48	5.46 ± 0.92	1.76 ± 0.75
Small Int.	1.72 ± 0.23	0.59 ± 0.19	3.39 ± 0.41	1.87 ± 0.17
Large Int.	1.47 ± 0.25	0.47 ± 0.15	3.85 ± 0.56	2.05 ± 0.44
Spleen	5.95 ± 4.59	6.53 ± 0.39	4.04 ± 0.38	16.90 ± 3.10
Pancreas	1.48 ± 0.30	0.77 ± 0.15	5.93 ± 1.22	3.0 ± 0.21
Brain	0.15 ± 0.04	0.08 ± 0.01	0.25 ± 0.01	0.16 ± 0.02
Bone	4.34 ± 2.29	3.53 ± 1.91	2.65 ± 1.01	4.47 ± 1.26
Muscle	0.82 ± 0.24	0.27 ± 0.06	1.74 ± 0.18	0.95 ± 0.29

Reported as %ID/g n ≥ 3

**Table 1.** Biodistribution of <sup>89</sup>Zr-B12 and IF-<sup>89</sup>Zr-B12 on B12 replete and deplete diets. Data reported in %ID/g.

### 3.5 Utilizing IF to Step Outside of the B12 Pathway

#### 3.5.1 IF-<sup>89</sup>Zr-B12 and <sup>89</sup>Zr-B12 Biodistribution in Nude Athymic Female Mice on B12 Deplete and Replete Chow

Due to the interesting rate in uptake of IF-<sup>89</sup>Zr-B12 in mice on a B12 replete or deplete diet it was decided to re-plot the ex vivo distribution data to account for the experiments retention differences (i.e. more activity rather than actual differences) and to hence base the uptake on the organ and not grams. By accounting for the amount of activity retained in each organ, for each experiment and normalizing to activity, a new trend occurs (Figure 14 and 15 and Table 2).

In looking at the uptake for <sup>89</sup>Zr-B12 we can see a notable change in uptake in the liver, kidneys, and blood (liver:  $32.18 \pm 2.61$  vs  $36.24 \pm 1.88$ , kidney:  $53.58 \pm 2.72$  vs  $48.89 \pm 1.01$ , blood:  $1.60 \pm 1.07$  vs  $0.19 \pm 0.05$  %recovered/organ for replete vs deplete, respectively). The pancreas also showed a change in uptake ( $0.49 \pm 0.18$  vs  $1.19 \pm 0.15$  %recovered/organ for replete vs deplete, respectively).

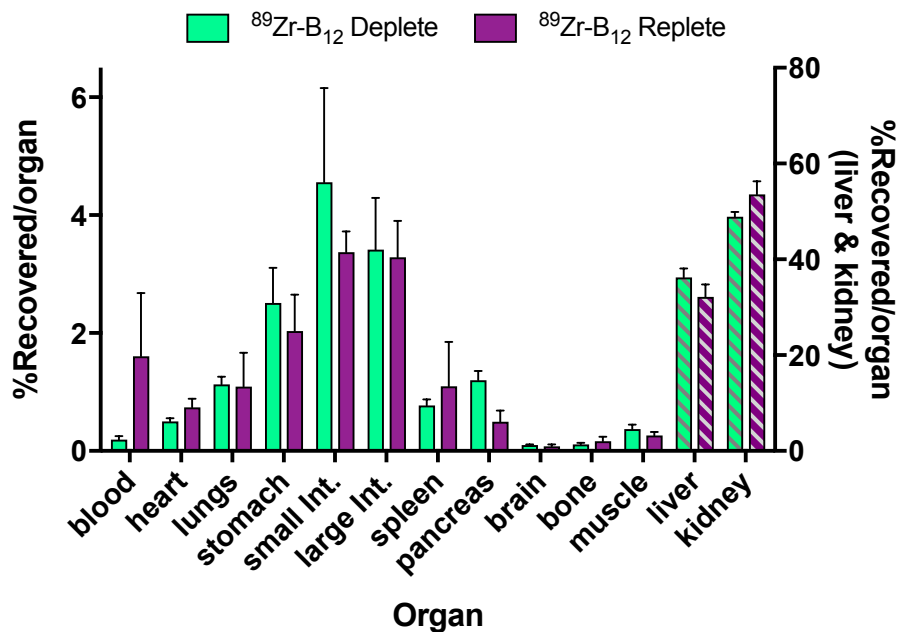


**Figure 14.** Ex vivo tissue distribution of <sup>89</sup>Zr-B12 in mice on a deplete or replete diet at 24 h plotted as %recovered/organ. Changes in uptake occurred in the liver, kidneys, and blood. Data is represented as mean and standard deviation, n ≥ 3.

IF-<sup>89</sup>Zr-B12 showed the most notable change in tissue uptake in the blood and heart (blood:  $0.72 \pm 0.26$  vs  $0.10 \pm 0.01$ , heart:  $0.51 \pm 0.09$  vs  $0.23 \pm 0.04$  %recovered/organ for replete vs deplete) (Figure 15 and Table 2). The uptake in the liver, kidneys, spleen, and pancreas were not significantly different in the two models. Liver uptake:  $69.67 \pm 7.34$  vs  $72.22 \pm 2.02$ , kidneys:  $20.56 \pm 5.90$  vs  $20.61 \pm 1.81$ , spleen:  $2.37 \pm 0.40$  vs  $2.07 \pm 0.14$ , and pancreas:  $0.43 \pm 0.12$  vs  $0.39 \pm 0.03$  %recovered/organ for replete vs deplete.

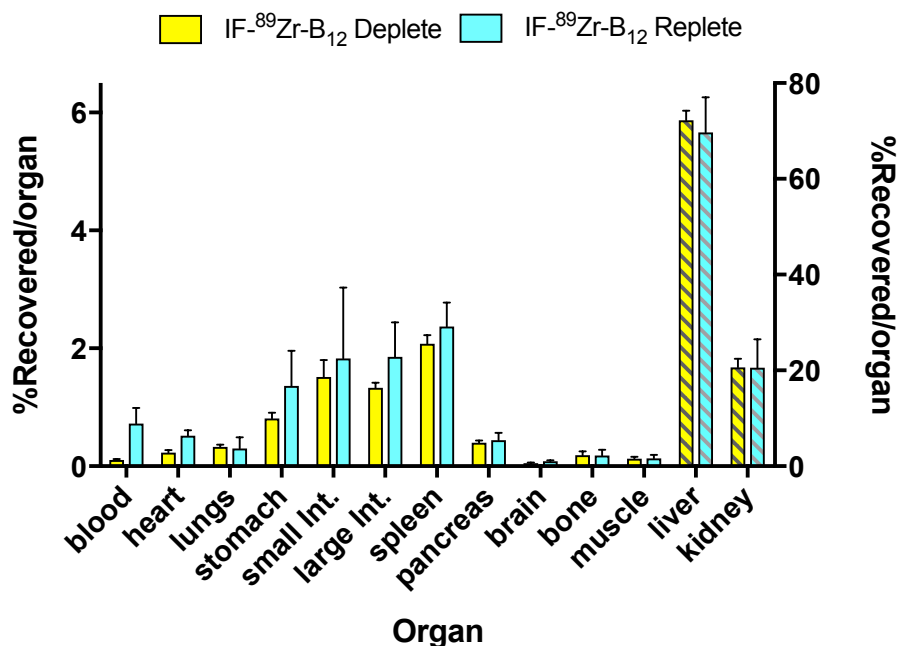


**Figure 15.** Ex vivo tissue distribution of IF-<sup>89</sup>Zr-B<sub>12</sub> in mice on a B<sub>12</sub> deplete or replete diet at 24 h plotted as %recovered/organ. The significant changes occurred in the blood, stomach, and large intestine, while the liver, kidneys, spleen and pancreas stayed the same. Data is represented as mean and standard deviation, n ≥ 3.

In comparing the two graphs with the new units, again the same trends are seen as before. The liver is increased and the kidney and all other tissue decreased, compared to <sup>89</sup>Zr-B<sub>12</sub>, in the IF experiments. Focusing on the liver and kidney uptake where the most significant changes occurred, a trend between the two models (deplete vs replete) is apparent (Figure 16 and Table 2). When using <sup>89</sup>Zr-B<sub>12</sub> significant changes in liver and kidney uptake were observed in comparing both models (deplete and replete) (p = 0.05) (Figure 18). The opposite trend is seen when using IF-<sup>89</sup>Zr-B<sub>12</sub>, the liver and kidneys are not affected by the endogenous B<sub>12</sub> levels in the two models, and is supported by the lack of change in most of the other tissues that are commonly affected by depleted B<sub>12</sub> levels.<sup>22-24</sup>

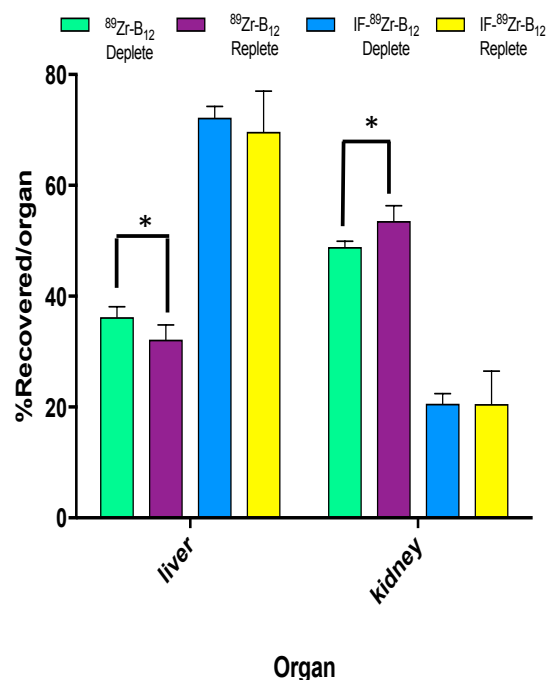


**Figure 16.** Select ex vivo tissue distribution of IF-<sup>89</sup>Zr-B12 and <sup>89</sup>Zr-B12 in mice on a B12 deplete or replete diet at 24 h plotted as %recovered/organ. The significant changes occurred with <sup>89</sup>Zr-B12 in the liver and kidney, while they were not significantly changed in the IF-<sup>89</sup>Zr-B12. n ≥ 3, \*p = 0.05.

These results support the hypothesis that pre-binding B12 conjugates to IF allows for the utilization of B12 conjugate chemistry without effecting critical endogenous B12 levels. Interest in B12 in drug development has been on the rise in recent years.<sup>25,31–36</sup> However, it is important to note that while these reports are promising, a concern arises in what prolonged dosing of a B12-pharmaceutical conjugate would ultimately do to endogenous B12 levels. In 2012, Nexo *et al.* published points of concern for possible B12 deficiency after long B12 dosing periods.<sup>37</sup> Using IF as a platform technology would allow for the use of these established drugs while removing the concern for this deficiency because it would be removed from the natural pathway

for B12 uptake (for more detail see Chapter 1, Section 1.1.4). In short, in the blood stream TCII carries B12 to all cells expressing the CD320 receptor, where it is then internalized and used within the cell (this is what is affecting the  $^{89}\text{Zr}$ -B12 uptake), while IF- $^{89}\text{Zr}$ -B12 is removed from this pathway.

Organs	$^{89}\text{Zr}$ -B12	IF- $^{89}\text{Zr}$ -B12	$^{89}\text{Zr}$ -B12	IF- $^{89}\text{Zr}$ -B12
	Replete	Replete	Deplete	Deplete
Blood	1.60 ± 1.07	0.72 ± 0.26	0.19 ± 0.05	0.106 ± 0.01
Heart	0.74 ± 0.14	0.51 ± 0.09	0.50 ± 0.05	0.23 ± 0.04
Lungs	1.09 ± 0.57	0.29 ± 0.19	1.12 ± 0.12	0.32 ± 0.03
Liver	32.18 ± 2.61	69.67 ± 7.34	36.24 ± 1.88	72.22 ± 2.02
Kidney	53.58 ± 2.72	20.56 ± 5.90	48.88 ± 1.01	20.61 ± 1.81
Stomach	2.03 ± 0.61	1.36 ± 0.60	2.51 ± 0.59	0.80 ± 0.09
Small Int.	3.37 ± 0.35	1.82 ± 1.20	4.55 ± 1.59	1.51 ± 0.28
Large Int.	3.28 ± 0.61	1.85 ± 0.58	3.41 ± 0.87	1.33 ± 0.08
Spleen	1.09 ± 0.75	2.37 ± 0.40	0.77 ± 0.10	2.07 ± 0.14
Pancreas	0.49 ± 0.18	0.43 ± 0.12	1.19 ± 0.15	0.39 ± 0.03
Brain	0.08 ± 0.03	0.08 ± 0.02	0.09 ± 0.01	0.05 ± 0.01
Bone	0.16 ± 0.07	0.18 ± 0.10	0.11 ± 0.02	0.18 ± 0.06
Muscle	0.26 ± 0.06	0.13 ± 0.06	0.37 ± 0.07	0.12 ± 0.03

**Reported as %recovered/organ n ≥ 3**

**Table 2.** Ex vivo tissue distribution of IF- $^{89}\text{Zr}$ -B12 and  $^{89}\text{Zr}$ -B12 in mice on a B12 deplete or replete diet at 24 h plotted as %recovered/organ.

### 3.6 Investigating the Role of Glycosylation in the Liver Accumulation Observed When Using Human Recombinant IF Expressed in the Plant *Arabidopsis thaliana*

As shown in earlier Section 3.4, using IF- $^{89}\text{Zr}$ -B12 in animal models had a surprising uptake in the liver that had very rapid (within 1 h) and significant (compared to  $^{89}\text{Zr}$ -B12). Yet, the questions remained of why this uptake is occurring and what is causing this uptake. The liver uptake of IF was most likely due to receptor-mediated uptake. This is supported by the rapid nature of this uptake (within 1 h) that did not change overtime (within 24 h). If degradation were the cause the uptake would be a gradual accumulation over time.



The IF that has been used in these experiments is recombinant human IF (rhIF) that is expressed in the plant *Arabidopsis thaliana*. This IF is used because of the amount and quality of protein needed. The rhIF is a commercial product of pure apo-IF, as opposed to other commercial human IF that is not purely apo (data completed in house and not shown). Glycoproteins in plants are known to have different endogenous sugars than in animals.<sup>38</sup> As IF is a highly glycosylated protein, the sugars on this rhIF are likely different than endogenously IF in humans. Most importantly, plants are known to have the terminal sugars of either mannose or galactose while humans always have terminal sialic acid.<sup>38,39</sup> It is **hypothesized** that the terminal sugar on rhIF is being recognized by a receptor in the liver. The most likely receptors would be the asialoglycoprotein receptor (ASGPR) or the mannose receptor (CD205 or CD206), which are highly expressed in the liver, and such sugars (i.e. galactose, mannose, fucose, *n*-acetylglucosamine) are found in *A. thaliana*.<sup>38,40-43</sup> The glycosylation profile was determined through GC-MS and then uptake in cells expressing either the ASGPR, CD205, and CD206 were used to assay IF uptake mediated through specific glycosylation profile.

### 3.6.1 GC-MS Analyses of the Glycosylation on Recombinant Human IF Expressed in Plants

The glycosylation of IF was examined by GC-MS (Table 3) by SGS M-Scan Inc. The rhIF showed a different glycosylation profile than endogenous human proteins have.<sup>38</sup> The sugars identified were fucose, xylose, mannose and *n*-acetylglucosamine with the ratios of 0.17:0.18:1.0:0.24, respectively. Since galactose was not detected the most likely receptor causing the liver internalization of IF is the mannose receptor as the ASGPR does not recognize any of the sugars above.<sup>40</sup>

Sugar	Peak Area Ave.	[nmol] Detected	Ratio (Man = 1.0)
Fucose	8471	11.2	0.17
Xylose	6156	11.8	0.18
Mannose	81654	66.7	1.0
<i>n</i> -acetylglucosamine	4508	16.0	0.24

**Table 3.** GC-MS analysis of hrIF showing that fucose, xylose, mannose and *n*-acetylglucosamine are present.

### 3.6.2 IF-B12-Cy5 Uptake in Human Liver HEPG2 cells

HEPG2 cells were used as a cell model for expressing ASGPR as it is the standard in vitro cell model for this receptor.<sup>44,45</sup> Uptake of IF in HEPG2 cells were investigated through fluorescence and flow cytometry. B12-Cy5 (ex: 645 nm em: 682 nm) (for more detail see Chapter 4, Section 4.2) was used as the fluorophore and was bound to IF to create the fluorescent complex IF-B12-Cy5 (incubated with IF in excess and at 4°C overnight to ensure complete binding). IF-B12-Cy5 (100 nM) was incubated at 37°C for 1 h in hanks balanced salt solution (HBSS). HBSS was used in these experiments to prevent any leaching of the B12-Cy5 from IF to TCII found in complete media.<sup>46</sup> Cells were analyzed by flow cytometry. IF-B12-Cy5 uptake in HEPG2 cells is shown in Figure 17. IF-B12-Cy5 was not internalized in HEPG2 cells supporting the GC-MS results that galactose or *n*-acetylglucoseamine was not present on IF and ASGPR is not the cause of liver uptake.

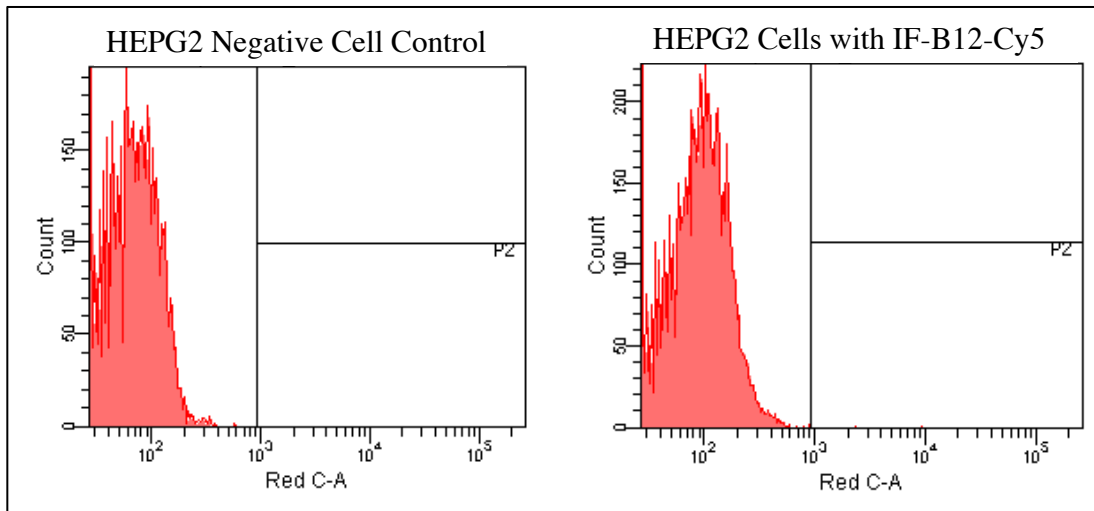


**Figure 17.** Flow cytometry analyses of HEPG2 cells treated with IF-B12-Cy5 (100 nM) in HBSS for 1 h at 37°C. There was no shift in fluorescence with the treated cells compared to non-treated cells indicating no uptake of the complex. Ex: 640 nm Em: 660/20 nm. P2 defines a positive result.

### 3.6.3 IF-B12-Cy5 Uptake Murine Dendritic JAWII Cells

JAWII cells are a murine dendritic cell line derived from bone marrow.<sup>47</sup> JAWII are known to express the mannose receptor CD205, which is a member of the mannose receptor family (for more detail see Chapter 1, Section 1.4.4.1).<sup>41</sup> The recognition and uptake of IF-B12-Cy5 through CD205 was investigated by flow cytometry (Figure 18). IF-B12-Cy5 (100 nM) treated cells showed a broadening in fluorescence without a defined shift in compared to the untreated cells. A control using B12-Cy5 at equal concentration showed the same broadening indicating the shift for IF-B12-Cy5 was not an IF dependent uptake. This lack of uptake could be due to CD205 being selectively expressed depending on the age of the cell.<sup>48</sup>

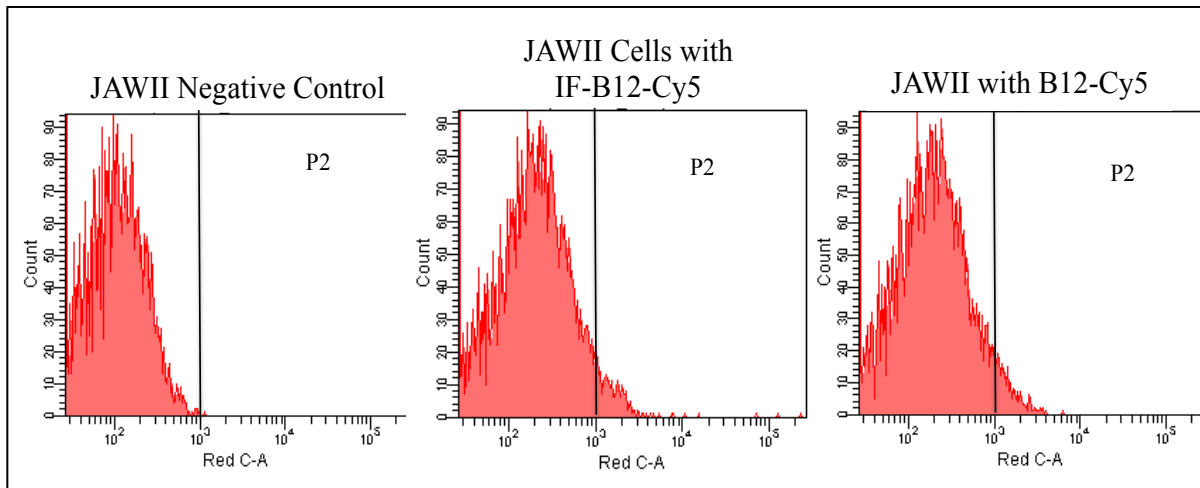


**Figure 18.** Flow cytometry analyses of JAWII cells treated with IF-B12-Cy5 or B12-Cy5 (100 nM each) in HBSS for 1 h at 37°C. A broadening in fluorescence was seen using IF-B12-Cy5 and B12-Cy5 treated cells compared to non-treated cells indicating a non-IF specific uptake/association of the complex. Ex: 640 nm Em: 660/20 nm. P2 defines a positive result.

### 3.6.4 IF-B12-Cy5 Uptake in Murine Macrophage J774A.1 Cells

J774A.1 cells are a murine macrophage cell line that is known to express the mannose receptor CD206 (for more details see Chapter 1, Section 1.4.4.2).<sup>49,42</sup> The recognition and uptake of IF-B12-Cy5 through CD205 was investigated by flow cytometry (Figure 19). IF-B12-Cy5 (200 nM) treated cells for 1 h showed a clear shift compared to untreated cells, while B12-Cy5 treated cells did not show a shift in fluorescence. This indicates that IF-B12-Cy5 is being recognized through IF specific recognition and supports the GC-MS sugar profile, since CD206 will recognize and internalize fucose, mannose, and *n*-acetylglucosamine.<sup>42,43</sup> Literature supports the results, with the same shift in fluorescence observed when a fluorescent-monoclonal antibody for the CD206 receptor was incubated with J774A.1 cells.<sup>50,51</sup> A block of the CD206 receptor was completed by pre-incubating the cells with mannan (2 mg/mL) 45 min before and during the

incubation with IF-B12-Cy5. A 50% decrease in uptake was observed (Figure 19) with the block indicating that the IF-B12-Cy5 uptake is mediated by the CD206 receptor in the J774A.1 cells.

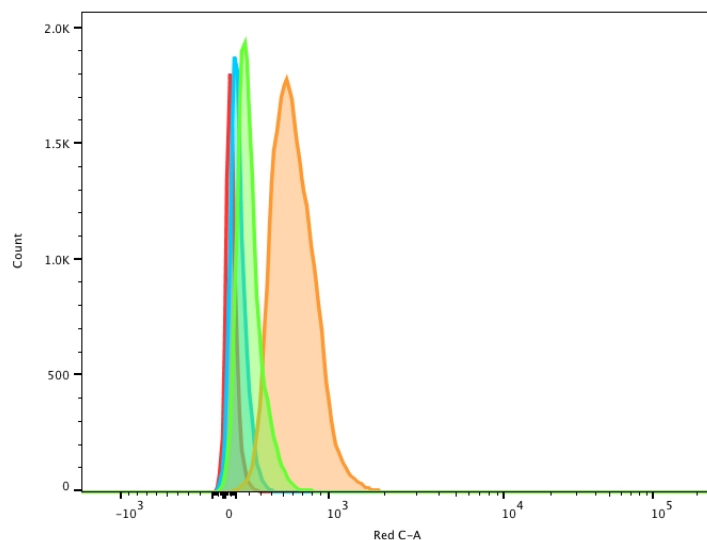


**Figure 19.** Flow cytometry analysis of J774A.1 cells treated with IF-B12-Cy5 (orange), B12-Cy5 (blue) (200 nM each), and IF-B12-Cy5 with mannan (green) (2 mg/mL administered 45 min before and during probe) in HBSS for 1 h at 37°C. Untreated cells are red. A shift in fluorescence was seen in the IF-B12-Cy5 uptake indicating IF specific uptake/association of the complex and a 50% decrease in uptake during a mannan block indicating the CD206 is mediating this uptake. Ex: 640 nm Em: 660/20 nm.

### 3.7 Conclusions

PET imaging and *ex vivo* tissue distribution had a marked difference of IF-B12 uptake compared to the control of B12 only using the radio-tracers  $^{99m}\text{Tc}$ ,  $^{64}\text{Cu}$ , and  $^{89}\text{Zr}$ . High liver uptake and a decrease in kidney uptake with all other tissues markedly lower was a trend seen using all three tracers including in two mice models (B12 replete and deplete). The absence of affect on IF uptake by endogenous B12 levels indicates that IF can allow for the use of B12 conjugate chemistry (i.e. B12 drug conjugates) while stepping out of the B12 pathway. This

would diminish the concern of developing B12 deficiency in subjects being dosed with B12.<sup>37</sup> The liver uptake seen in the PET imaging and biodistribution was determined to be due to the terminal sugar on the IF, which was recognized by the CD206 receptor that is highly expressed in the liver.<sup>42,43</sup> Still, further exploration into IF-89Zr-B12 detecting cubilin positive tumors needs to be accomplished (Chapter 7, Section 1.1).<sup>52</sup>

### 3.8 References

- (1) What Are the Key Statistics About Kidney Cancer? <https://www.cancer.org/cancer/kidney-cancer/about/key-statistics.html> (accessed Jun 21, 2017).
- (2) Survival Rates for Kidney Cancer by Stage <https://www.cancer.org/cancer/kidney-cancer/detection-diagnosis-staging/survival-rates.html> (accessed Jun 21, 2017).
- (3) Prasad, S. R.; Humphrey, P. A.; Catena, J. R.; Narra, V. R.; Srigley, J. R.; Cortez, A. D.; Dalrymple, N. C.; Chintapalli, K. N. Common and Uncommon Histologic Subtypes of Renal Cell Carcinoma: Imaging Spectrum with Pathologic Correlation. *Radiogr. Rev. Publ. Radiol. Soc. N. Am. Inc* **2006**, *26* (6), 1795-1806-1810.
- (4) Low, G.; Huang, G.; Fu, W.; Moloo, Z.; Girgis, S. Review of Renal Cell Carcinoma and Its Common Subtypes in Radiology. *World J. Radiol.* **2016**, *8* (5), 484–500.
- (5) Cairns, P. Renal Cell Carcinoma. *Cancer Biomark.* **2011**, *9* (1–6), 461–473.
- (6) What Is Kidney Cancer? <https://www.cancer.org/cancer/kidney-cancer/about/what-is-kidney-cancer.html> (accessed Jun 21, 2017).
- (7) Christensen, E. I.; Nielsen, R.; Birn, H. From Bowel to Kidneys: The Role of Cubilin in Physiology and Disease. *Nephrol. Dial. Transplant.* **2013**, *28* (2), 274–281.
- (8) Mathews, F. S.; Gordon, M. M.; Chen, Z.; Rajashankar, K. R.; Ealick, S. E.; Alpers, D. H.; Sukumar, N. Crystal Structure of Human Intrinsic Factor: Cobalamin Complex at 2.6-Å Resolution. *Proc. Natl. Acad. Sci.* **2007**, *104* (44), 17311–17316.
- (9) Kozyraki, R.; Fyfe, J.; Kristiansen, M.; Gerdes, C.; Jacobsen, C.; Cui, S.; Christensen, E. I.; Aminoff, M.; Chapelle, A. de la; Krahe, R.; et al. The Intrinsic Factor[ndash]vitamin

- B12 Receptor, Cubilin, Is a High-Affinity Apolipoprotein A-I Receptor Facilitating Endocytosis of High-Density Lipoprotein. *Nat. Med.* **1999**, *5* (6), 656–661.
- (10) Amsellem, S.; Gburek, J.; Hamard, G.; Nielsen, R.; Willnow, T. E.; Devuyst, O.; Nexø, E.; Verroust, P. J.; Christensen, E. I.; Kozyraki, R. Cubilin Is Essential for Albumin Reabsorption in the Renal Proximal Tubule. *J. Am. Soc. Nephrol.* **2010**, *21* (11), 1859–1867.
- (11) Tauris, J.; Christensen, E. I.; Nykjaer, A.; Jacobsen, C.; Petersen, C. M.; Ovesen, T. Cubilin and Megalin Co-Localize in the Neonatal Inner Ear. *Audiol. Neurootol.* **2009**, *14* (4), 267–278.
- (12) Erranz, B.; Miquel, J. F.; Argraves, W. S.; Barth, J. L.; Pimentel, F.; Marzolo, M.-P. Megalin and Cubilin Expression in Gallbladder Epithelium and Regulation by Bile Acids. *J. Lipid Res.* **2004**, *45* (12), 2185–2198.
- (13) Tsaroucha, A. K.; Chatzaki, E.; Lambropoulou, M.; Despoudi, K.; Laftsidis, P.; Charsou, C.; Polychronidis, A.; Papadopoulos, N.; Simopoulos, C. E. Megalin and Cubilin in the Human Gallbladder Epithelium. *Clin. Exp. Med.* **2008**, *8* (3), 165–170.
- (14) Burke, K. A.; Jauniaux, E.; Burton, G. J.; Cindrova-Davies, T. Expression and Immunolocalisation of the Endocytic Receptors Megalin and Cubilin in the Human Yolk Sac and Placenta across Gestation. *Placenta* **2013**, *34* (11), 1105–1109.
- (15) Vortherms, A. R.; Kahkoska, A. R.; Rabideau, A. E.; Zubieta, J.; Andersen, L. L.; Madsen, M.; Doyle, R. P. A Water Soluble Vitamin B12-ReI Fluorescent Conjugate for Cell Uptake Screens: Use in the Confirmation of Cubilin in the Lung Cancer Line A549. *Chem. Commun. Camb. Engl.* **2011**, *47* (35), 9792–9794.
- (16) McEwan, J. F.; Veitch, H. S.; Russell-Jones, G. J. Synthesis and Biological Activity of Ribose-5'-Carbamate Derivatives of Vitamin B12. *Bioconjug. Chem.* **1999**, *10* (6), 1131–1136.
- (17) Huisgen, R. 1,3-Dipolar Cycloadditions. Past and Future. *Angew. Chem. Int. Ed. Engl.* **1963**, *2* (10), 565–598.
- (18) Kolb, H. C.; Finn, M. G.; Sharpless, K. B. Click Chemistry: Diverse Chemical Function from a Few Good Reactions. *Angew. Chem. Int. Ed.* **2001**, *40* (11), 2004–2021.
- (19) Isidro-Llobet, A.; Álvarez, M.; Albericio, F. Amino Acid-Protecting Groups. *Chem. Rev.* **2009**, *109* (6), 2455–2504.

- (20) Eckelman, W. C. Unparalleled Contribution of Technetium-99m to Medicine Over 5 Decades. *JACC Cardiovasc. Imaging* **2009**, *2* (3), 364–368.
- (21) Baldoni, D.; Waibel, R.; Bläuenstein, P.; Galli, F.; Iodice, V.; Signore, A.; Schibli, R.; Trampuz, A. Evaluation of a Novel Tc-99m Labelled Vitamin B12 Derivative for Targeting Escherichia Coli and Staphylococcus Aureus In Vitro and in an Experimental Foreign-Body Infection Model. *Mol. Imaging Biol.* **2015**, *17* (6), 829–837.
- (22) Ikotun, O. F.; Marquez, B. V.; Fazen, C. H.; Kahkoska, A. R.; Doyle, R. P.; Lapi, S. E. Investigation of a Vitamin B12 Conjugate as a PET Imaging Probe. *ChemMedChem* **2014**, *9* (6), 1244–1251.
- (23) Ruiz-Sánchez, P.; Mundwiler, S.; Medina-Molner, A.; Spingler, B.; Alberto, R. Iodination of Cisplatin Adduct of Vitamin B12 [ $\{B12\}-CN-\{cis-PtCl(NH_3)_2\}^+$ ]. *J. Organomet. Chem.* **2007**, *692* (6), 1358–1362.
- (24) Collins, D. A.; Hogenkamp, H. P. C. Transcobalamin II Receptor Imaging via Radiolabeled Diethylene-Triaminepentaacetate Cobalamin Analogs. *J. Nucl. Med.* **1997**, *38* (5), 717–723.
- (25) Sah, B.-R.; Schibli, R.; Waibel, R.; Boehmer, L. von; Bläuenstein, P.; Nexø, E.; Johayem, A.; Fischer, E.; Müller, E.; Soyka, J. D.; et al. Tumor Imaging in Patients with Advanced Tumors Using a New  $^{99m}Tc$ -Radiolabeled Vitamin B12 Derivative. *J. Nucl. Med.* **2014**, *55* (1), 43–49.
- (26) Fedosov, S. N.; Fedosova, N. U.; Berglund, L.; Moestrup, S. K.; Nexø, E.; Petersen, T. E. Composite Organization of the Cobalamin Binding and Cubilin Recognition Sites of Intrinsic Factor. *Biochemistry (Mosc.)* **2005**, *44* (9), 3604–3614.
- (27) Niccoli Asabella, A.; Cascini, G. L.; Altini, C.; Paparella, D.; Notaristefano, A.; Rubini, G. The Copper Radioisotopes: A Systematic Review with Special Interest to  $^{64}Cu$ . *BioMed Res. Int.* **2014**, *2014*, e786463.
- (28) Stupperich, E.; Nexø, E. Effect of the Cobalt-N Coordination on the Cobamide Recognition by the Human Vitamin B12 Binding Proteins Intrinsic Factor, Transcobalamin and Haptocorrin. *Eur. J. Biochem.* **1991**, *199* (2), 299–303.
- (29) Deri, M. A.; Zeglis, B. M.; Francesconi, L. C.; Lewis, J. S. PET Imaging with  $^{89}Zr$ : From Radiochemistry to the Clinic. *Nucl. Med. Biol.* **2013**, *40* (1), 3–14.



- (30) He, Q.; Madsen, M.; Kilkenney, A.; Gregory, B.; Christensen, E. I.; Vorum, H.; Højrup, P.; Schäffer, A. A.; Kirkness, E. F.; Tanner, S. M.; et al. Amnionless Function Is Required for Cubilin Brush-Border Expression and Intrinsic Factor-Cobalamin (Vitamin B12) Absorption in Vivo. *Blood* **2005**, *106* (4), 1447–1453.
- (31) Waibel, R.; Treichler, H.; Schaefer, N. G.; Staveren, D. R. van; Mundwiler, S.; Kunze, S.; Küenzi, M.; Alberto, R.; Nüesch, J.; Knuth, A.; et al. New Derivatives of Vitamin B12 Show Preferential Targeting of Tumors. *Cancer Res.* **2008**, *68* (8), 2904–2911.
- (32) Henry, K. E.; Elfers, C. T.; Burke, R. M.; Chepurny, O. G.; Holz, G. G.; Blevins, J. E.; Roth, C. L.; Doyle, R. P. Vitamin B12 Conjugation of Peptide-YY3–36 Decreases Food Intake Compared to Native Peptide-YY3–36 Upon Subcutaneous Administration in Male Rats. *Endocrinology* **2015**, *156* (5), 1739–1749.
- (33) Verma, A.; Sharma, S.; Gupta, P. K.; Singh, A.; Teja, B. V.; Dwivedi, P.; Gupta, G. K.; Trivedi, R.; Mishra, P. R. Vitamin B12 Functionalized Layer by Layer Calcium Phosphate Nanoparticles: A Mucoadhesive and pH Responsive Carrier for Improved Oral Delivery of Insulin. *Acta Biomater.* **2016**, *31*, 288–300.
- (34) Henry, K. E.; Kerwood, D. J.; Allis, D. G.; Workinger, J. L.; Bonaccorso, R. L.; Holz, G. G.; Roth, C. L.; Zubieta, J.; Doyle, R. P. Solution Structure and Constrained Molecular Dynamics Study of Vitamin B<sub>12</sub> Conjugates of the Anorectic Peptide PYY(3-36). *ChemMedChem* **2016**, *11*, 1015, 1021.
- (35) Smith, W. J.; Oien, N. P.; Hughes, R. M.; Marvin, C. M.; Rodgers, Z. L.; Lee, J.; Lawrence, D. S. Cell-Mediated Assembly of Phototherapeutics. *Angew. Chem. Int. Ed.* **2014**, *53* (41), 10945–10948.
- (36) Bonaccorso, R. L.; Chepurny, O. G.; Becker-Pauly, C.; Holz, G. G.; Doyle, R. P. Enhanced Peptide Stability Against Protease Digestion Induced by Intrinsic Factor Binding of a Vitamin B12 Conjugate of Exendin-4. *Mol. Pharm.* **2015**, *12* (9), 3502–3506.
- (37) Lildballe, D. L.; Mutti, E.; Birn, H.; Nexø, E. Maximal Load of the Vitamin B12 Transport System: A Study on Mice Treated for Four Weeks with High-Dose Vitamin B12 or Cobinamide. *PLOS ONE* **2012**, *7* (10), e46657.
- (38) Strasser, R. Plant Protein Glycosylation. *Glycobiology* **2016**, *26* (9), 926–939.
- (39) Schwarz, F.; Aebi, M. Mechanisms and Principles of N-Linked Protein Glycosylation. *Curr. Opin. Struct. Biol.* **2011**, *21* (5), 576–582.

- (40) Roggenbuck, D.; Mytilinaiou, M. G.; Lapin, S. V.; Reinhold, D.; Conrad, K. Asialoglycoprotein Receptor (ASGPR): A Peculiar Target of Liver-Specific Autoimmunity. *Auto-Immun. Highlights* **2012**, *3* (3), 119–125.
- (41) Shrimpton, R. E.; Butler, M.; Morel, A.-S.; Eren, E.; Hue, S. S.; Ritter, M. A. CD205 (DEC-205): A Recognition Receptor for Apoptotic and Necrotic Self. *Mol. Immunol.* **2009**, *46* (6), 1229–1239.
- (42) Wollenberg, A.; Mommaas, M.; Oppel, T.; Schottdorf, E.-M.; Günther, S.; Moderer, M. Expression and Function of the Mannose Receptor CD206 on Epidermal Dendritic Cells in Inflammatory Skin Diseases. *J. Invest. Dermatol.* **2002**, *118* (2), 327–334.
- (43) De Leeuw, A. M.; Brouwer, A.; Knook, D. L. Sinusoidal Endothelial Cells of the Liver: Fine Structure and Function in Relation to Age. *J. Electron Microsc. Tech.* **1990**, *14* (3), 218–236.
- (44) Li, Y.; Huang, G.; Diakur, J.; Wiebe, L. I. Targeted Delivery of Macromolecular Drugs: Asialoglycoprotein Receptor (ASGPR) Expression by Selected Hepatoma Cell Lines Used in Antiviral Drug Development. *Curr. Drug Deliv.* **2008**, *5* (4), 299–302.
- (45) Schwartz, A. L. The Hepatic Asialoglycoprotein Receptor. *CRC Crit. Rev. Biochem.* **1984**, *16* (3), 207–233.
- (46) Polak, D. M.; Elliot, J. M.; Haluska, M. Vitamin B12 Binding Proteins in Bovine Serum1. *J. Dairy Sci.* **1979**, *62* (5), 697–701.
- (47) Pajtasz-Piasecka, E.; Rossowska, J.; Szyda, A.; Krawczenko, A.; Dus, D. Generation of Anti-Tumor Response by JAWS II Mouse Dendritic Cells Transduced with Murine Interleukin 12 Genes. *Oncol. Rep.* **2007**, *17* (5), 1249–1257.
- (48) Takahashi, K.; Donovan, M. J.; Rogers, R. A.; Ezekowitz, R. A. Distribution of Murine Mannose Receptor Expression from Early Embryogenesis through to Adulthood. *Cell Tissue Res.* **1998**, *292* (2), 311–323.
- (49) D’Addio, S. M.; Baldassano, S.; Shi, L.; Cheung, L.; Adamson, D. H.; Bruzek, M.; Anthony, J. E.; Laskin, D. L.; Sinko, P. J.; Prud’homme, R. K. Optimization of Cell Receptor-Specific Targeting through Multivalent Surface Decoration of Polymeric Nanocarriers. *J. Control. Release Off. J. Control. Release Soc.* **2013**, *168* (1), 41–49.
- (50) Bio-Rad. Anti Mouse CD206 Antibody - clone MR5D3 <https://www.bio-rad-antibodies.com/mouse-cd206-antibody-mr5d3-mca2235.html> (accessed Jun 22, 2017).

- (51) Zamze, S.; Martinez-Pomares, L.; Jones, H.; Taylor, P. R.; Stillion, R. J.; Gordon, S.; Wong, S. Y. C. Recognition of Bacterial Capsular Polysaccharides and Lipopolysaccharides by the Macrophage Mannose Receptor. *J. Biol. Chem.* **2002**, *277* (44), 41613–41623.
- (52) Burmeister, R.; Bøe, I.-M.; Nykjaer, A.; Jacobsen, C.; Moestrup, S. K.; Verroust, P.; Christensen, E. I.; Lund, J.; Willnow, T. E. A Two-Receptor Pathway for Catabolism of Clara Cell Secretory Protein in the Kidney. *J. Biol. Chem.* **2001**, *276* (16), 13295–13301.

## **Chapter 4: Development and Validation of B12-Based Fluorescent Probes for B12 Dependent Receptor Function**

This data was submitted as part of a paper titled “A Vitamin B12 conjugate of Exendin-4 Produces Hypoglycemia Without Associated Hypophagia or Nausea in Male Rats” with coauthors: Elizabeth G. Mietlicki-Baase, Claudia G. Liberini, Jayne L. Workinger, Ron L. Bonaccorso, David J. Reiner, Kieran Koch-Laskowski, Lauren E. McGrath, Rinzin Lhamo, Lauren M. Stein, Bart C. De Jonghe, George G. Holz, Christian L. Roth, Matthew R. Hayes\* and Robert P. Doyle\*. In revision (June 2017) for ‘*Diabetes, Obesity, and Metabolism*’

Work in this chapter was completed by the author unless stipulated. Where indicated work was performed in collaboration with Prof. Matthew Hayes, Department of Psychiatry, University of Pennsylvania, Philadelphia, PA.

### 4.1 Introduction

The B12 dietary uptake pathway is complex with multiple transport proteins and associated receptors (see Chapter 1, Section 1.1.4). Despite its complexity, and in large part because of it, the B12 pathway has become increasingly popular in drug delivery.<sup>1-9</sup> Probes to explore B12 transport proteins, receptors and B12-drug pharmacokinetic profiles have proven essential in these efforts. Herein, the design, synthesis and characterization of B12-based fluorescent probes are discussed and validated for biological function.

## Part I: Use of a New Fluorescent Vitamin B12 (B12-Cy5) Probe in the Screening of FHs 74

### Int. Cells for Cubilin and Megalin

#### 4.2. Design, Synthesis, and Characterization of B12-Cy5

B12-cyanine5 (B12-Cy5) was synthesized by activating the ribose 5'-hydroxyl group with  $N_3$ , priming it for 'Click' chemistry (Figure 1).<sup>10-12</sup> This was done as previously reported by first activating B12 with mesyl chloride in *n*-methyl-2-pyrrolidone (NMP) and diisopropylamine (DIPA) for 1 h at RT, producing B12-MsCl (yield 65%).<sup>10</sup> Once B12-MsCl was purified it was reacted forward with  $NaN_3$  in hexamethylphosphoramide (HMPA) overnight at RT, creating B12- $N_3$  (yield: 52%).<sup>10</sup>

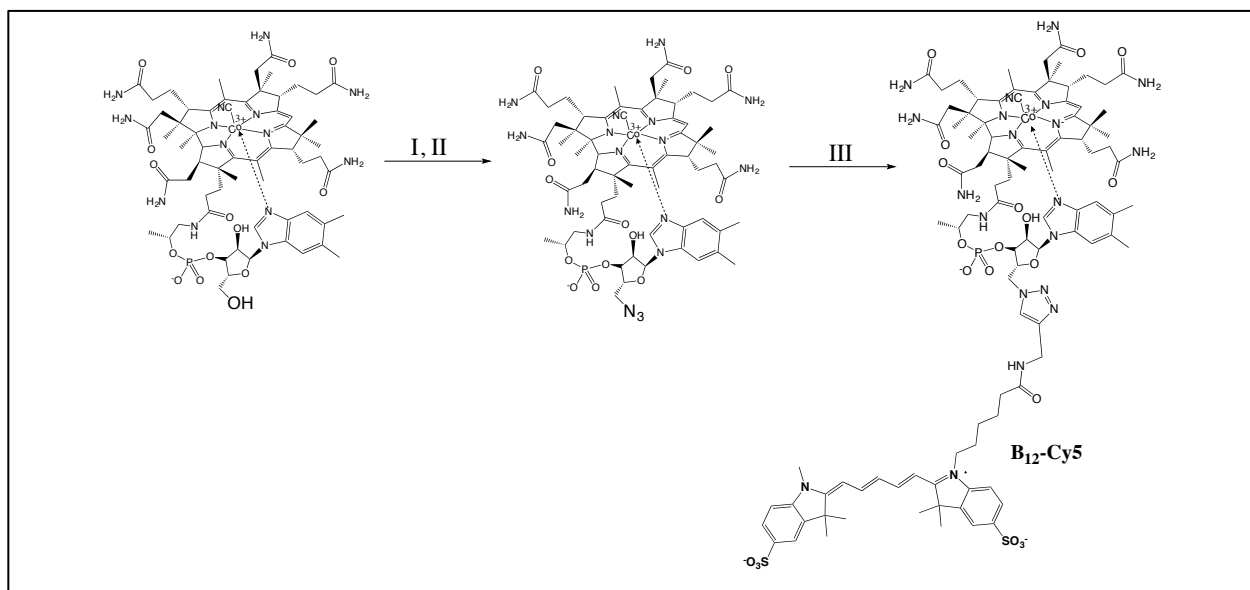


**Figure 1.** Synthesis of B12-Cy5. B12 was activated by replacing the terminal ribose 5'OH with an azide for 'Click' chemistry as previously reported. I: B12 was dissolved in NMP. A solution of MSCl in NMP and DIPEA were added in separately, at the same time, in three intervals 1 h apart then stirred for 1 hour at RT. II: B12-MsCl was dissolved in HMPA and  $NaN_3$  was added and stirred overnight at 40°C. III: Huisgen/Sharpless CuAAC chemistry was implemented using

Sulfo-Cy5 Alkyne and Cu(I)/TBTA in DMF/H<sub>2</sub>O (4:1) overnight. Final yield: 98%, based on B12 starting material.

Purified B12-N<sub>3</sub> was then reacted with cyanine5 alkyne (purchased commercially) with Cu(I)/TBTA (1 mg, 0.005 mmol and 3.5 mg, 0.006 mmol, respectively) in DMF/H<sub>2</sub>O (4:1 ratio, respectively) overnight at RT to yield B12-Cy5 (yield 90%).<sup>10-12</sup> B12-Cy5 purified on a RP-HPLC and characterized by LC-MS and fluorescence (Figure 2 and 3). LC-MS showed 688 [M+3H]<sup>+</sup>, 2031 [M+2H]<sup>2+</sup> with the expected m/z of 2059. Fluorescence analysis showed an emission and excitation of 645 and 682 nm. This indicated that the Cy5 molecule was not quenched by B12 conjugation, which has been observed in previous B12-fluorophores.<sup>13-15</sup>

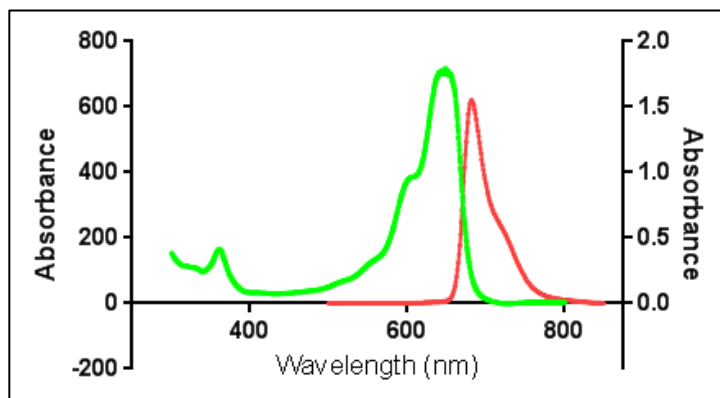


**Figure 2.** Excitation and Emission for B12-Cy5. The excitation and emission are similar to Cy5 without conjugation (646 and 662 nm, respectively) indicating B12-Cy5 was made and B12 did not quench Cy5 fluorescence.<sup>15</sup> Excitation in green and emission in red. Solvent: H<sub>2</sub>O, excitation: 645 nm, emission: 682 nm.

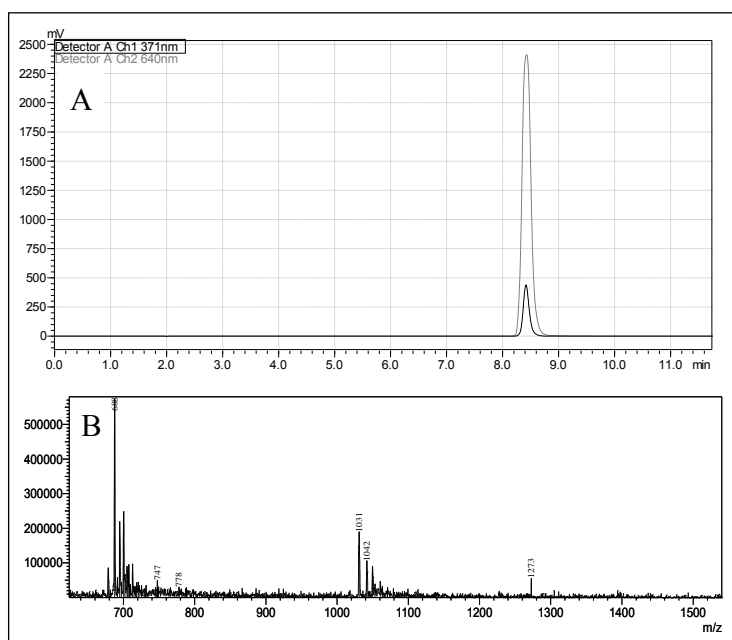


**Figure 3.** A) RP-HPLC of purified B12-Cy5.  $R_t$ : 8.41 min. Purity: 99%. Detection at 371 and 640 nm. B) LC-MS Analysis of B12-Cy5 showing the compound was made. Expected  $m/z = 2059$ , observed  $m/z = 688 [M+3H]^{+3}$ ,  $2031 [M+2H]^{+2}$ ,  $695 [M+Na]^{+3}$ ,  $700 [M+K]^{+3}$ ,  $1042 [M+Na]^{+2}$ .

#### 4.2.1 IF-B12-Cy5 Uptake in the Cubilin Positive control cell line BN16

Binding B12-Cy5 with IF allows for a fluorescent IF complex to investigate the expression of CUBN *in vitro*. To validate IF-B12-Cy5 as a viable probe for CUBN expression, uptake in BN16 (brown Norway rat yolk sac cells) cells were investigated. BN16 cells were used because they are the gold standard for CUBN and megalin expression *in vitro*.<sup>16-19</sup>

BN16 cells were incubated with IF-B12-Cy5 in HBSS for 1h at 100 nM. IF was incubated overnight with B12-Cy5 with IF in excess (ratio 0.8:1, respectively). Figure 4 shows IF-B12-Cy5 and B12-Cy5 uptake in BN16 cells at 37°C and 4°C. IF-B12-Cy5 incubated at 100

nM for 1 h at 37°C shows a three-log order increase in fluorescence. When B12-Cy5 is incubated at the same conditions no shift is observed. IF-B12-Cy5 incubated at 100 nM for 1 h at 4°C shows a decrease (two-log order) in fluorescence compared to cells treated with IF-B12-Cy5 at 37°C. This uptake shows 1) uptake is IF mediated and 2) receptor mediated, namely CUBN dependent.

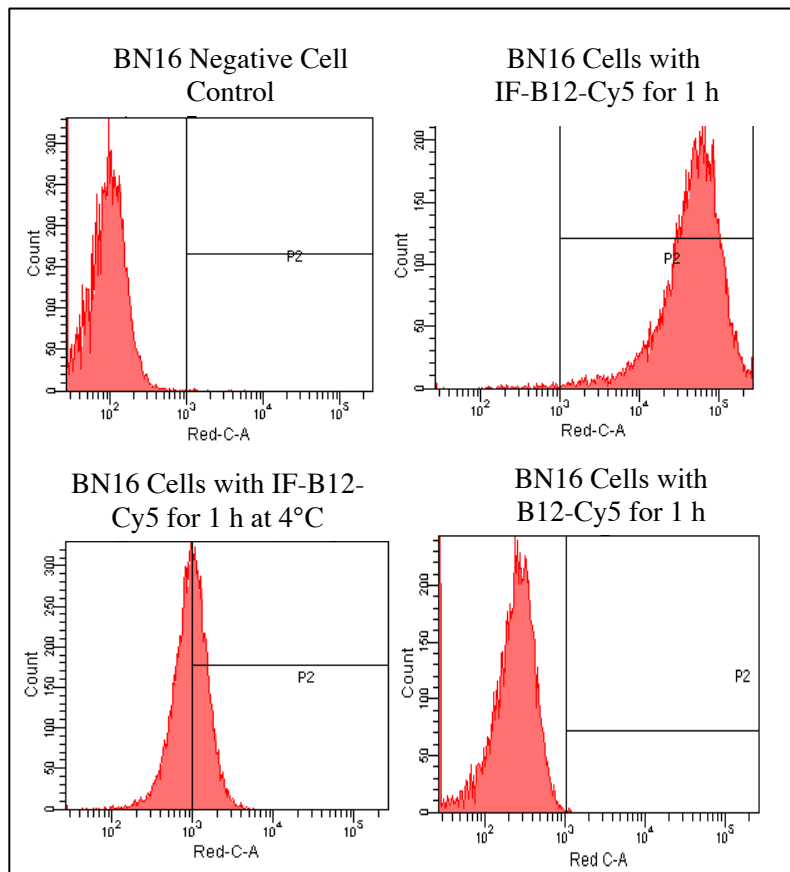


**Figure 4.** Flow cytometry analyses of BN16 cells treated with IF-B12-Cy5 (100 nM) in HBSS for 1 h at 37°C. A three-log shift in fluorescence was seen using IF-B12-Cy5 treated cells compared to non-treated cells indicating an IF specific uptake/association of the complex, namely CUBN. The decrease in uptake at 4°C supports a receptor mediated mechanism. Ex: 640 nm Em: 660/20 nm. P2 defines a positive result.



#### 4.2.2 IF-B12-Cy5 Uptake in the Cubilin Negative control cell line CHO-K1

Since a positive control for CUBN uptake was established, a negative control cell line was also investigated.<sup>20</sup> Uptake of IF-B12-Cy5 in the CHO-K1 cell line, known not to express CUBN or megalin, was investigated.

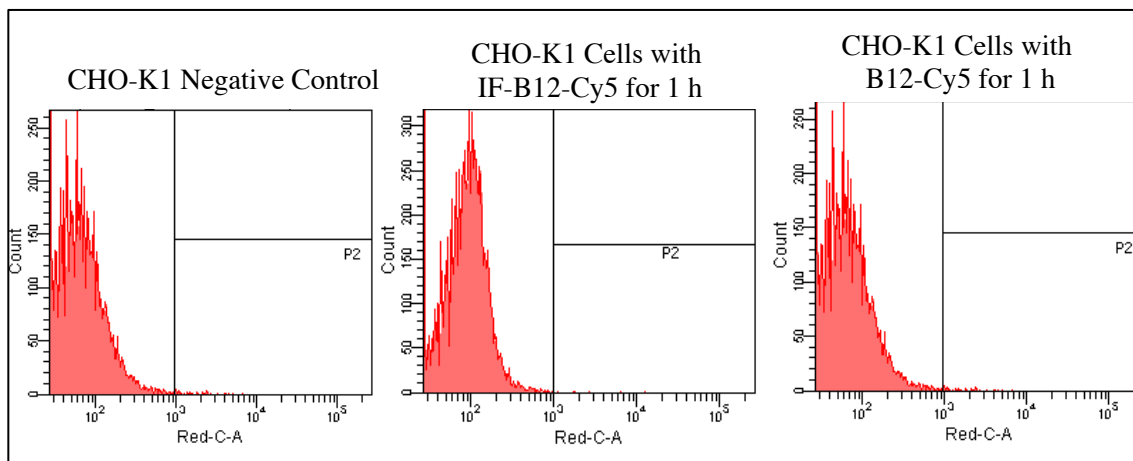


**Figure 5.** Flow cytometry analyses of CHO-K1 cells treated with IF-B12-Cy5 or B12-Cy5 (100 nM) in HBSS for 1 h at 37°C. A no fluorescence change was seen in IF-B12-Cy5 or B12-Cy5 treated cells compared to non-treated cells indicating a IF was not internalized. Ex: 640 nm Em: 660/20 nm. P2 defines a positive result.

IF-B12-Cy5 and B12-Cy5 was not internalized by CHO-K1 cells when incubated at 100 nM for 1 h at 37°C (Figure 5). The lack in fluorescent shift in the CHO-K1 negative cell line along with the uptake seen in BN16 cells validated IF-B12-Cy5 as a valid probe for CUBN expression in vitro.

### 4.3 Using B12-Cy5 to Explore the Expression of Cubilin and Megalin in Human Fetal Intestinal Cells (FHs 74 Int.)

In 2014 Madsen *et al.* showed that megalin is not expressed in adult terminal ileum and is not needed for B12 absorption (in concert with CUBN).<sup>21</sup> Interestingly, they also showed that a biopsy of fetal ileum (16-20 weeks) had low amount of mRNA CUBN and relatively higher amounts of mRNA megalin through reverse transcription-polymerase chain reaction.<sup>21</sup> They then investigated the mRNA levels in a commercially available fetal small intestinal cell line (3–4 months) (FHs 74 Int., ATCC#: CCL-241), showing both CUBN and megalin.<sup>21</sup> However, they did not investigate the expression of said receptors. While mRNA levels correlate to protein expression it can be variable and even end in non-functional protein.<sup>22,23</sup> The **hypothesis** of this work is that there is both functional CUBN and megalin in human small intestinal cells. Herein, expression of functional CUBN and megalin in FHs 74 Int. cells are investigated through flow cytometry using IF-B12-Cy5 and TCII-B12-Cy5.

#### 4.3.1 Investigating Cubilin Expression in FHs 74 Int. Cells

##### 4.3.1.1 Western Blot of Cubilin in FHs 74 Int. Cells

FHs 74 Int. cells were investigated for CUBN expression by western blot analysis. FHs 74 Int., BN16 and CHO-K1 cell lysates were run on a 6% SDS-PAGE gel. The membrane fractions of FHs 74 Int. and BN16 cells were included as CUBN is a membrane protein. BN16 cells show a clear hit for CUBN while CHO-K1 and FHs 74 Int. cells do not hit for the protein (Figure 6) after incubation with the primary antibody (Santa Cruz) for 24 h. The lack of CUBN hit in FHs 74 Int. cells indicate that either 1) CUBN is not expressed or 2) CUBN is expressed in very small amounts below detection limit.

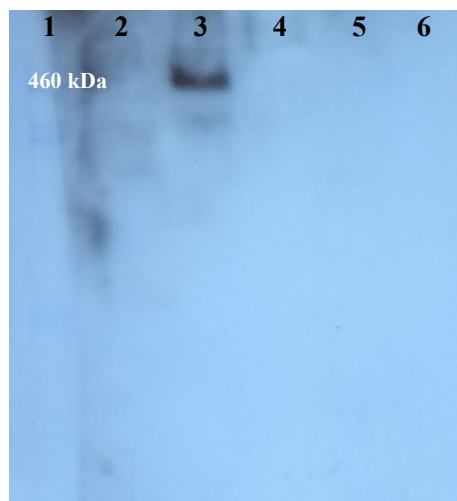


**Figure 6.** Western blot for CUBN. Lane 1: Thermo Fisher Scientific HiMark Pre-Stained HMW Protein Standard, Lane 2: CHO-K1 lysate (negative control), Lane 3: BN16 lysate (positive control), Lane 4: BN16 (membrane), Lane 5: FHs 74 Int., Lane 6: FHs 74 Int. (membrane).

#### 4.3.1.2 Flow Cytometry Uptake of IF-B12-Cy5 in FHs 74 Int. Cells

To further investigate CUBN expression, flow cytometry was used due to its high sensitivity and quantification of uptake.<sup>24,25</sup> IF-B12-Cy5 or B12-Cy5 was incubated with FHs 74 Int. cells for up to 2 h and ranging concentration of 100 nM – 1  $\mu$ M. Figure 7 shows IF-B12-Cy5 uptake at 1  $\mu$ M for 2 h at 37°C. IF-B12-Cy5 showed a half-log order increase in fluorescence and B12-Cy5, incubated under the same conditions as IF-B12-Cy5, showed the same half-log order increase. Results at lower concentrations did not show a significant shift (Figure 7). This uptake of IF-B12-Cy5 indicates that functional CUBN is expressed in a small amount on FHs 74 Int. cells.

This low expression observed could be due to the environment of the cells and select expression, thereof. Precautions were taken to account for this such as repeating these

experiments at various passage numbers (low and high) and allowing the cells to grow on the plate for 48-72 h to allow for expression but results did not differ from shown.

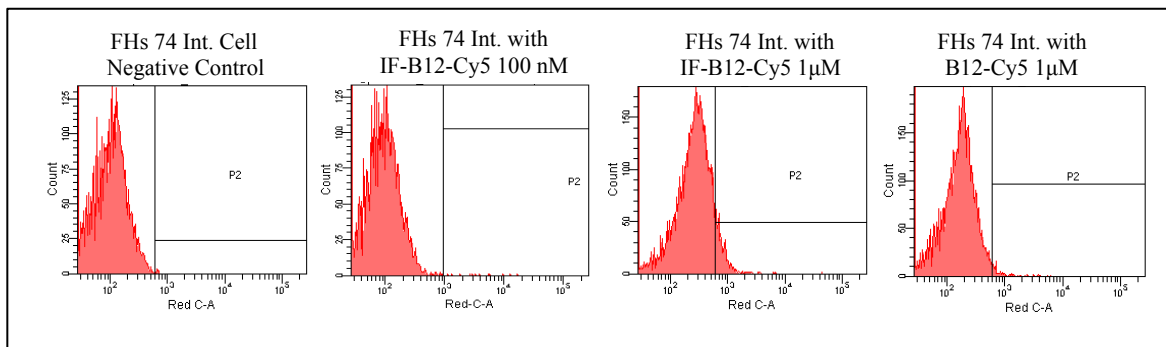


**Figure 7.** Flow cytometry analysis of FHs 74 Int. cells treated with IF-B12-Cy5 or B12-Cy5 (100 nM, and 1  $\mu$ M) in HBSS for 2 h at 37°C. A fluorescence change was seen in IF-B12-Cy5 (1  $\mu$ M) treated cells compared to non-treated or IF-B12-Cy5 (100 nM). A fluorescent shift was also seen for B12-Cy5 yet different than IF-B12-Cy5. This indicates functional CUBN expression is expressed on FHs 74 Int. cells. Ex: 640 nm Em: 660/20 nm. P2 defines a positive result.

#### 4.3.2 Investigating Functional Megalin Expression in FHs 74 Int. Cells

Functional megalin was investigated on FHs 74 Int. cells. To do this TCII-B12-Cy5 was used, as holo-TCII is a substrate of megalin (for more detail see Chapter 1, Section 1.2.2.3). Megalin expression was investigated using western blots and flow cytometry.

##### 4.3.2.1 Western Blot of Megalin in FHs 74 Int. Cells

FHs 74 Int. cells were investigated for megalin expression by western blot analysis. FHs 74 Int., BN16 and CHO-K1 cell lysates were run on a 6% SDS-PAGE gel. BN16 and FHs 74 Int. cells show a clear hit for megalin while CHO-K1 cells do not cross-react for the protein after

incubation with the primary antibody (anti-megalin) for 24 h (Figure 8). The megalin cross-react in FHs 74 Int. cells and the positive control, BN16 cells, (and lack of a cross-react in the negative control) supports the idea that megalin is expressed in FHs 74 Int. cells.

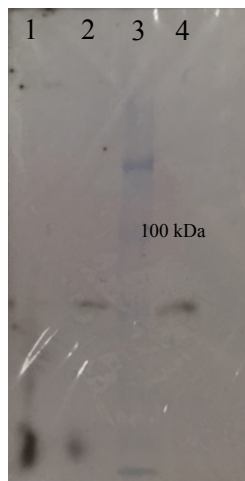


**Figure 8.** Western Blot for Megalin. Lane 1: CHO-K1 cell lysate (negative control), Lane 2: FHs 74 Int. cell lysate, Lane 3: BioRad Kaleidoscope Protein Markers, Lane 4: BN16 cell lysate (positive control) on a PDVF membrane.

#### 4.3.2.2 Flow Cytometry Uptake of TCII-B12-Cy5 in FHs 74 Int. Cells

To further look at megalin expression in FHs 74 Int. cells, flow cytometry was used. TCII-B12-Cy5 or B12-Cy5 was incubated with FHs 74 Int. cells for up to 2 h and ranging concentration of 100 nM – 1  $\mu$ M. Figure 9 shows TCII-B12-Cy5 uptake at 1  $\mu$ M for 2 h at 37°C. TCII-B12-Cy5 showed over a log order increase in fluorescence, however, the peak was very broad ranging over four-log orders. B12-Cy5 treated cells showed a small shift in fluorescence. Results at lower concentrations did not show a significant shift (data not shown). This uptake of TCII-B12-Cy5, along with the positive western blot, strongly indicates that functional megalin is expressed on FHs 74 Int. cells.

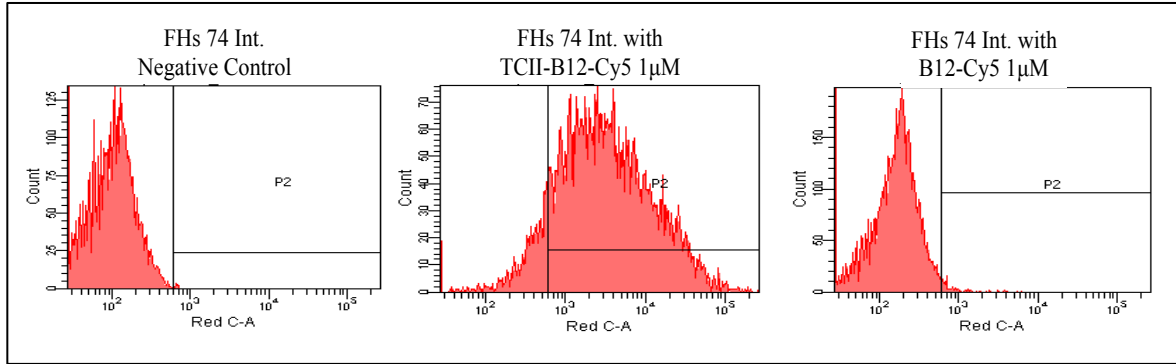


**Figure 9.** Flow cytometry analysis of FHs 74 Int. cells treated with TCII-B12-Cy5 or B12-Cy5 (1 µM) in HBSS for 1 h at 37°C. A fluorescence shift was seen in TCII-B12-Cy5 treated cells compared to non-treated and B12-Cy5 treated cells. This indicates supports functional megalin expression is expressed on FHs 74 Int. cells. Ex: 640 nm Em: 660/20 nm. P2 defines a positive result.

The question now becomes why is functional megalin and (to a lesser degree) CUBN expressed in the fetal small intestine while megalin is not expressed and CUBN is highly expressed in the adult small intestine.<sup>21,26</sup> Megalin, being a multi-substrate receptor (see Chapter 1, Section 1.2.2.3), could be playing a role in nutrient uptake from the amniotic fluid during gestation as the fetus drinks the fluid.<sup>27,28</sup> The fetus is known to urinate during gestation, the nutrients would then be re-circulated by megalin back into the fetus.<sup>28</sup> This would give the small intestine a ‘kidney-like’ function in the fetus without a need for CUBN (i.e. the fetus gets B12 from the mother). The expression in the small intestine would then change in adults from predominantly megalin to CUBN (a reduced substrate binder, see Chapter 1, Section 1.2.2) to allow for B12 uptake after birth.<sup>26,29</sup>

## **Part II: Use of a New Fluorescent B12-Ex4 (B12-Ex4-Cy5) in the Screening of Rat CNS**

### **Penetrance**

#### 4.4 Introduction

In 2017, it was shown that B12-Ex4 promotes improved glycemia in the absence of visceral malaise and anorexia in male rats (see Chapter 1, Section 1.5.2 and Appendix A). The rat being a unique model to test these effects, as rats display stress-mediated hyperglycemia to Ex4 and pronounced anorexia and malaise due to action within the central nervous system (CNS).<sup>30</sup> In addition, B12-Ex4 (5 µg/kg) had no significant effects on feeding, and did not produce the nausea/malaise elicited by Ex4, as measured by conditioned taste avoidance.<sup>31,32</sup> The **hypothesis** of this work is that B12-Ex4 does not cause taste avoidance due to limited penetrance of the dorsal vagal complex and paraventricular hypothalamic nucleus in the rat CNS. Therefore, to evaluate whether this difference is due to altered CNS penetrance, animals received systemic injections of either fluorescein-Ex-4 (F-Ex-4), B12-Cy5 or B12-Ex4-Cy5. B12-Ex4-Cy5 was designed to investigate B12-Ex4 uptake in the brain using confocal microscopy.

#### 4.4.1 Synthesis and Characterization of B12-Ex4-Cy5

B12-Ex4-Cy5 was synthesized by functionalizing B12 through activating the ribose 5'-hydroxyl group with 2-iodoxybenzoic acid (IBX) as previously reported (yield 15%, based on B12 starting material).<sup>33</sup> B12 was then reacted with 1-ethyl-3-(3-dimethylaminopropyl)carbodiimide (EDC), hydroxybenzotriazole (HOBT), and aminobutyrine in anhydrous DMSO overnight to create B12-AB (yield 80%).<sup>1,5,8</sup> Purified B12-AB was then reacted with azido-Ex-4 to make B12-Ex4 (Figure 10, A) using CuAAC chemistry with

Cu(I)/TBTA (1 mg, 0.005 mmol and 3.5 mg, 0.006 mmol, respectively) in DMF/H<sub>2</sub>O (4:1 ratio, respectively) overnight at RT (yield 94%).<sup>1,11,12</sup>

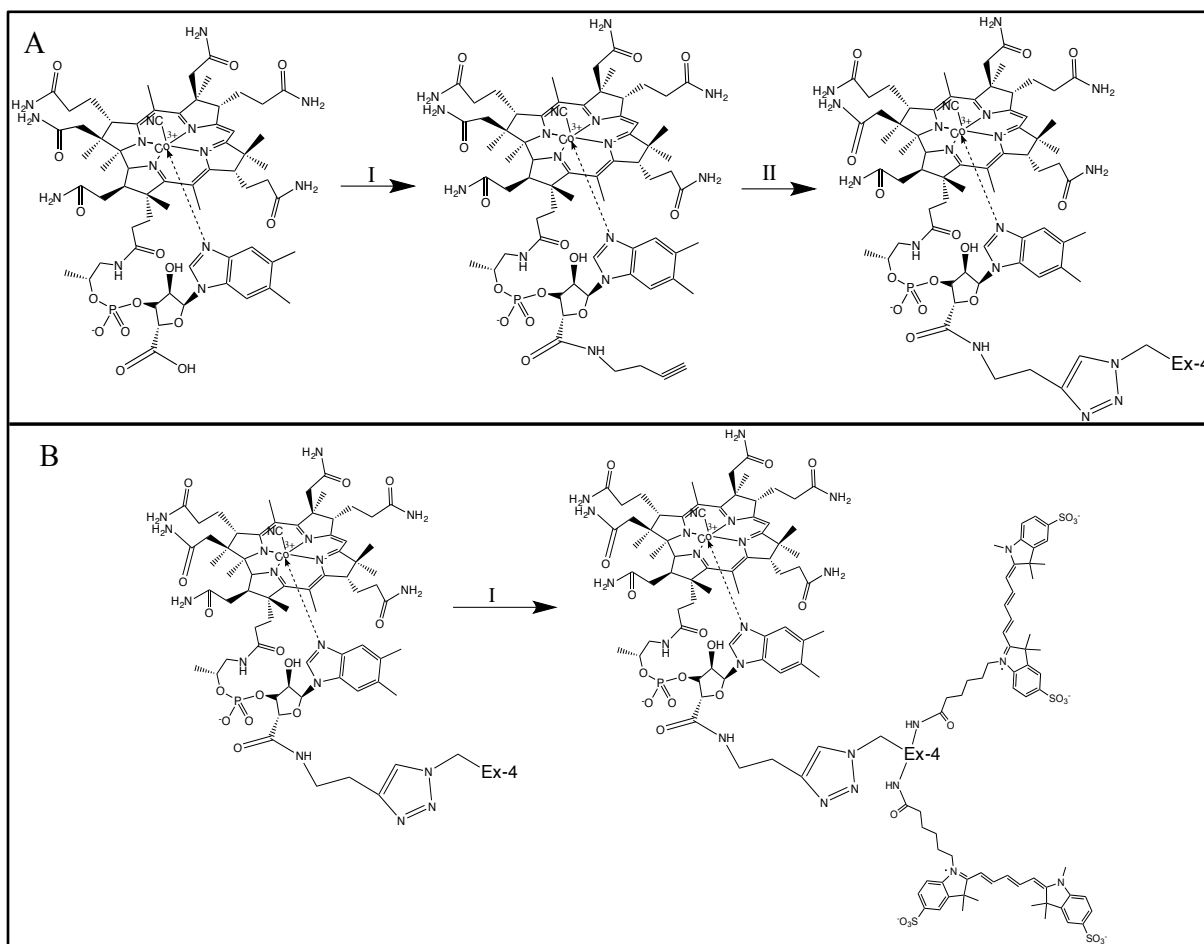


**Figure 10.** A) Synthesis of B12-Ex4 as previously reported I: EDC and HOBT in anhydrous DMSO with aminobutynes, overnight at RT, and II: Cu/TBTA in DMF and H<sub>2</sub>O, overnight and B) Synthesis of B12-Ex4-Cy5, I: Purified B12-Ex4 was reacted with sulfo-cyanine5-NHS-ester in PBS pH 7.6. Predicted conjugation site is the N-terminus and the lysine 27 (lysine 12 was modified to have an azido group for click chemistry), yield: 94%.

B12-Ex4 (0.5 mg, 0.0001mmol) was dissolved in PBS buffer pH 7.6 and then sulfo-cyanine5-NHS-ester (1 mg, 0.001mmol) was added to find a volume of 0.5 mL.<sup>34</sup> The resulting



solution was allowed to mix for 2h at room temperature, protected from light, and then purified through RP-HPLC (Figure 11, A). LC-MS analysis (Figure 11, B) showed the indication of B12-Ex4-Cy5 with 1 and 2 Cy5 molecules with an expected m/z of 6284 (M1; B12-Ex4+Cy5) or 6923 (M2; B12-Ex4+2xCy5). It is believed that there is loss of a Cy5 during ionization, which is why both mono-Cy5 and bi-Cy5 products are observed.

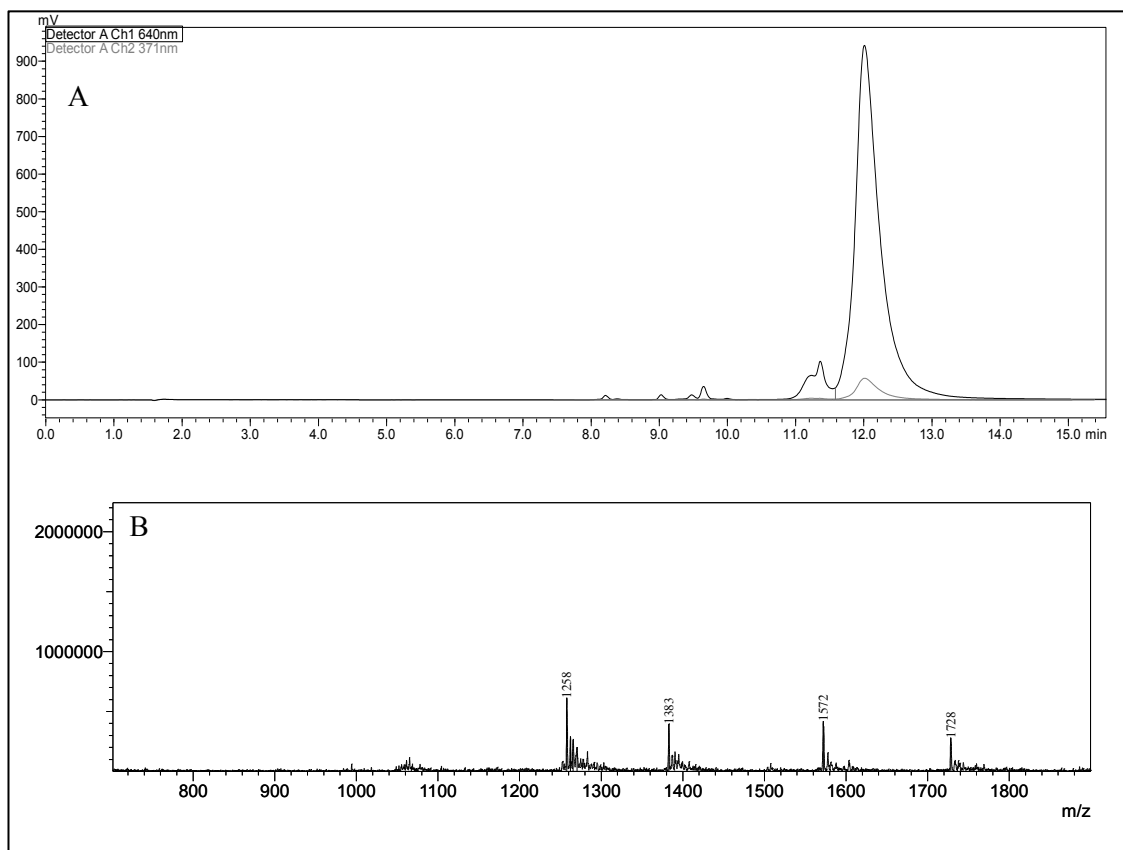


**Figure 11.** A) RP-HPLC of B12-Ex4-Cy5 showing purity  $\geq 91\%$ . It is suspected that some of the compound is degrading on the column.  $R_t$ : 12.1 min. Detection at 371 and 640 nm. B) LC-MS Analysis of B<sub>12</sub>-Ex4-Cy5. ESMS Expected m/z = 6284 (M1; B12-Ex4+Cy5) and 6923 (M2; B12-Ex4+2xCy5), observed m/z = 1258 [M1+5H]<sup>+5</sup>, 1572 [M1+4H]<sup>+4</sup>, 1383 [M2+5H]<sup>+5</sup>, 1728 [M2+4H]<sup>+4</sup>.

Fluorescent and UV analysis showed an excitation and emission profile of 648 and 670 nm, respectively (Figure 12). This indicated that B12-Ex4 conjugation had no effect on the emission/excitation profile of Cy5.

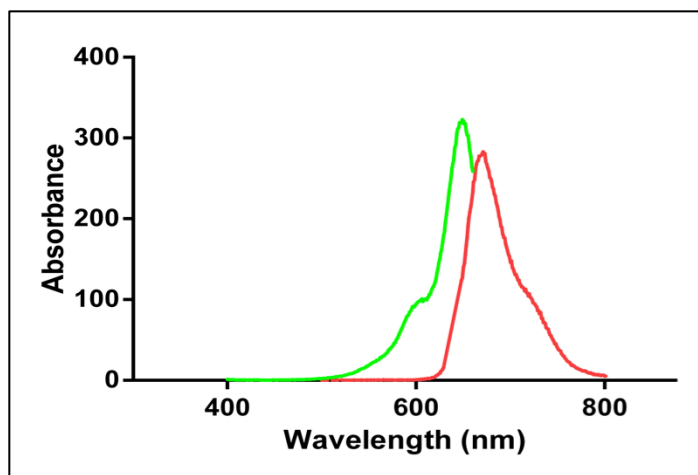


**Figure 12.** Excitation and Emission for B12-Ex4-Cy5. Excitation in green and emission in red. Solvent: H<sub>2</sub>O, excitation: 648 nm, emission: 670 nm.

#### 4.4.2 Agonism of B12-Ex4-Cy5 at the GLP-1R using H188 FRET Reporter Assay

Once B12-Ex4-Cy5 was synthesized and characterized the agonism at the GLP-1R, Ex-4's endogenous receptor, was determined to confirm functionality (for more detail see Chapter 1, Section 1.5).<sup>1,35,36</sup> A H188 FRET assay that reports the cAMP binding to an EPAC (exchange protein directly activated by cAMP) that increases the FRET ratio.<sup>37,38</sup> Figure 13 shows the EC<sub>50</sub> of B12-Ex4-Cy5 to be 13 nM.

There was a decrease in GLP-1R agonism with B12-Ex4-Cy5 compared to B12-Ex4 (68 pM), reported previously.<sup>1</sup> This decrease was expected as two Cy5 molecules were added to Ex4 directly, one being on a lysine in the middle of the protein. This conjugation would no doubt cause possible interference in receptor recognition or a shift in the protein structure causing it to

be less potent. However, the conjugate was still active at low nM range and was used in in vivo experiments.

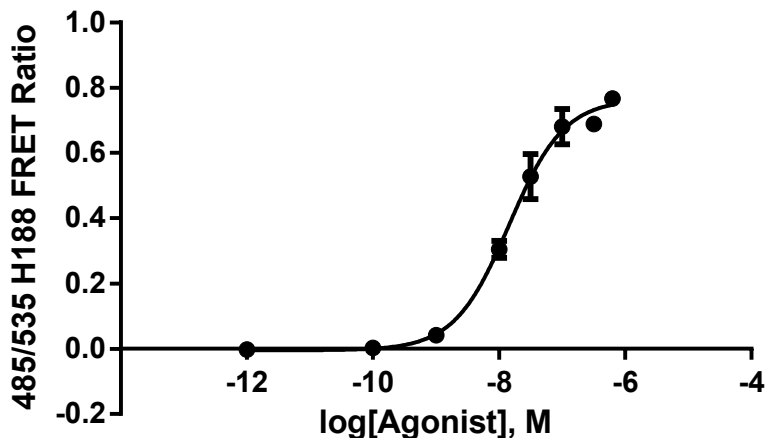


**Figure 13.** B12-Ex4-Cy5 Agonism at the GLP-1R. Cells were infected with the H188 FRET cAMP reporter. Agonism shows the fluorescent compound retains function at the GLP-1R. Points are in triplicate. EC<sub>50</sub>: 13 nM. Full sigmoidal curve could not be obtained due to the solubility of the conjugate.

#### 4.4.3 Sprague Dawley Rat Brain Uptake of B12-Cy5 and B12-Ex4-Cy5

Confocal microscopy was completed in collaboration with Dr. Matt Hayes group at University of Pennsylvania.

Previous work has shown that Ex4 crosses the blood-brain barrier to exert effects on energy balance and nausea.<sup>32,39,40</sup> B12-Ex4 dosing produces the glycemic benefits associated with Ex4 without producing the brain mediated effects of hypophagia and nausea. Thus, it is hypothesized that B12-Ex4 is not penetrating the central nervous system (CNS) and therefore not causing nausea and weight loss. The investigation of B12-Ex4 penetrating the brain was

completed in Sprague Dawley Rats treated with F-Ex-4 (previously made fluorescent Ex-4) (Figure 14), B12-Cy5 (Figure 15), and B12-Ex4-Cy5 (Figure 16) and evaluated using confocal microscopy.<sup>41</sup>

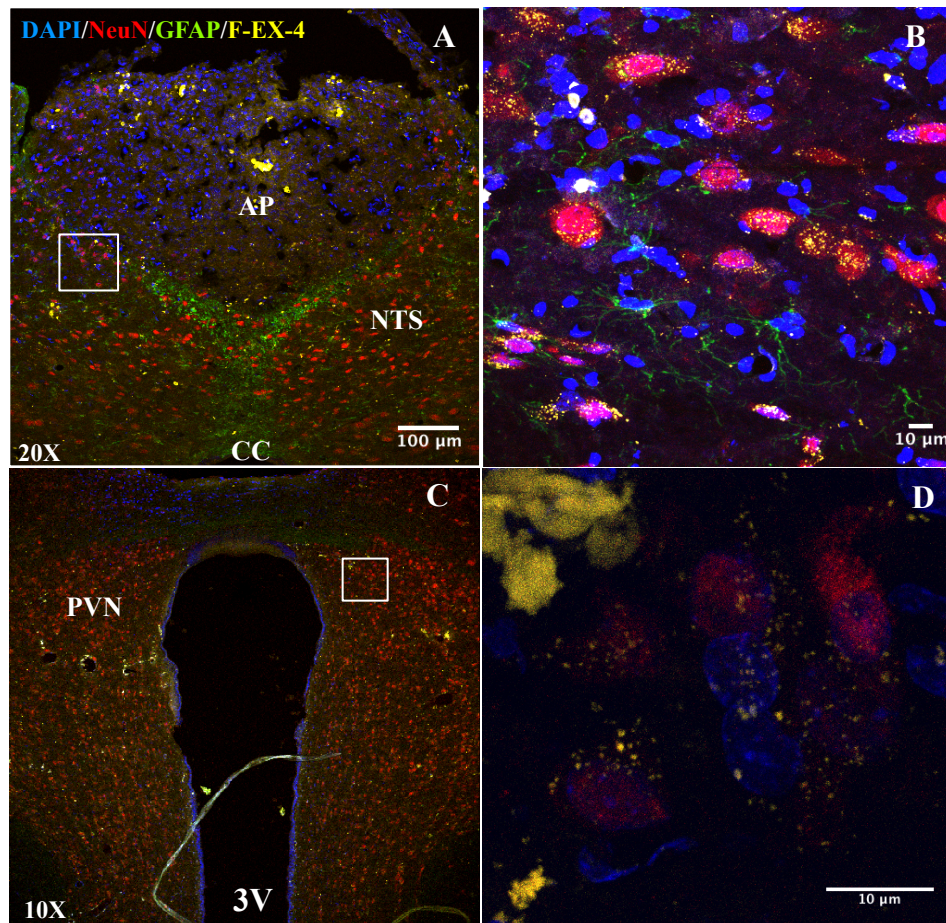


**Figure 14.** Systemically-delivered fluorescently labeled Ex-4 (F-Ex-4) highly penetrates within the DVC and the PVN. A) DVC uptake of F-Ex-4, B) Inset of A, C) PVN uptake of F-Ex-4, D) Inset of C. Ex4 (yellow), astrocytes (GFAP; green) and neurons (NeuN; red). Sections were counterstained using DAPI (blue) to visualize cell nuclei. AP, area postrema; CC, central canal; DVC, dorsal vagal complex; NTS, nucleus tractus solitaries; 3V, third ventricle; PVN

paraventricular hypothalamic nucleus. Images were acquired at 10-20x (A,C) or 63x (with 2-3x optical zoom) (B,D) magnifications.

F-Ex-4 has been shown to penetrate the brain and Figure 14 confirms that uptake.<sup>41</sup> The yellow (F-Ex-4) shows that Ex4 is in the dorsal vagal complex (DVC) and paraventricular hypothalamic nucleus (PVN). The DVC and PVN were highlighted due to the known significance of these areas in mediating the feeding effects of GLP-1R activation.<sup>42,43</sup> The green is astrocyte staining (GFAP) and the red is neuron staining (NeuN) with a counterstain of DAPI (blue) to visualize cell nuclei. B12-Cy5 and B12-Ex4-Cy5 injected into rats show a lack of B12 and B12-Ex4 in the brain, specifically the DVC and PVN (Figure 15 and 16).

This lack of penetrance of B12-Cy5 and B12-Ex4-Cy5 suggests that injected B12, and therefore B12-Ex4, does not readily penetrate into the CNS.<sup>44</sup> This also supports the hypothesis that B12 conjugation to Ex4 dramatically reduces, or prevents, Ex4 from entering the DVC and PVN and therefore does not cause nausea typically seen after Ex4 treatment.

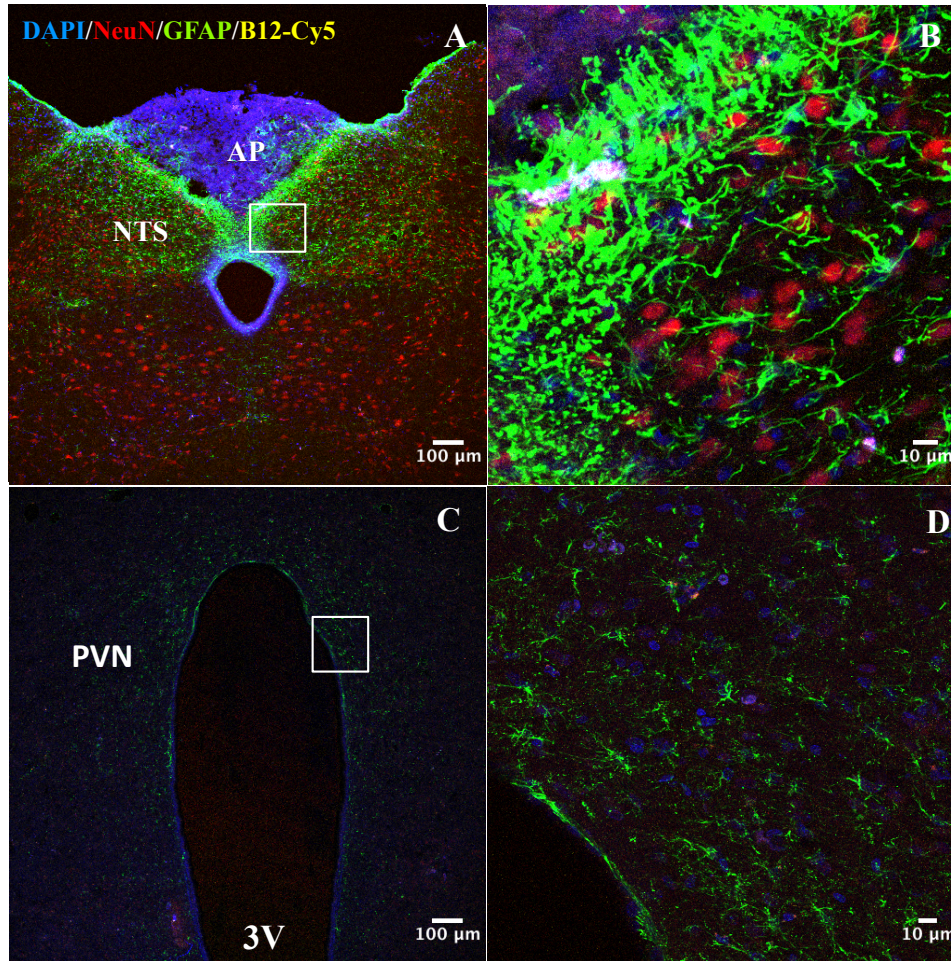


**Figure 15.** Systemically-delivered fluorescently labeled B12-Cy5 does not penetrate the DVC or the PVN. A) DVC uptake of B12-Cy5, B) Inset of A, C) PVN uptake of B12-Cy5, D) Inset of C. B12-Cy5 (yellow), astrocytes (GFAP; green) and neurons (NeuN; red). Sections were counterstained using DAPI (blue) to visualize cell nuclei. AP, area postrema; CC, central canal; DVC, dorsal vagal complex; NTS, nucleus tractus solitaries; 3V, third ventricle; PVN paraventricular hypothalamic nucleus. Images were acquired at 10-20x (A,C) or 63x (with 2-3x optical zoom) (B,D) magnifications.

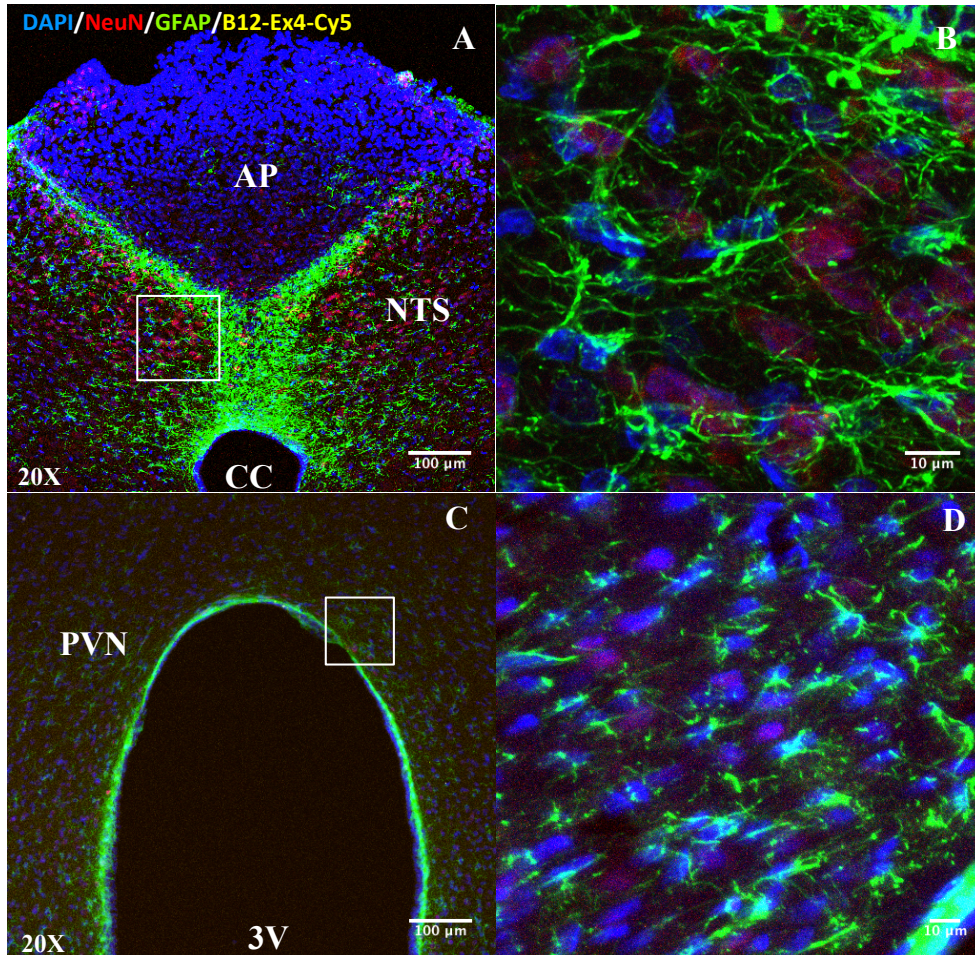


**Figure 16.** Systemically-delivered fluorescently labeled B12-Ex4-Cy5 does not penetrate the DVC or the PVN. A) DVC uptake of B12-Ex4-Cy5, B) Inset of A, C) PVN uptake of B12-Ex4-Cy5, D) Inset of C. B12-Cy5 (yellow), astrocytes (GFAP; green) and neurons (NeuN; red). Sections were counterstained using DAPI (blue) to visualize cell nuclei. AP, area postrema; CC, central canal; DVC, dorsal vagal complex; NTS, nucleus tractus solitarius; 3V, third ventricle; PVN paraventricular hypothalamic nucleus. Images were acquired at 10-20x (A,C) or 63x (with 2-3x optical zoom) (B,D) magnifications.

#### 4.5. Conclusions

The B12-fluorophores, B12-Cy5 and B12-Ex4-Cy5, were designed, synthesized and characterized. In Part I, B12-Cy5 was used to create fluorescent IF and TCII to investigate the functional expression of CUBN and megalin in FHs 74 Int. cells. IF-B12-Cy5 showed that CUBN is likely expressed minimally, while TCII-B12-Cy5 indicated that megalin expression is more prevalent in FHs 74 Int. cells.

In Part II, B12-Ex4-Cy5 and B12-Cy5 were used in in vivo studies to investigate B12 and B12-Ex4 penetrance into the rat brain, specifically the PVN and DVC. Both B12-Cy5 and B12-Ex4-Cy5 showed reduced uptake in DVC and PVN, relative to Ex-4, suggesting that B12 conjugation to Ex-4 prevents it from producing a CNS based response.

#### 4.6 References

- (1) Bonaccorso, R. L.; Chepurny, O. G.; Becker-Pauly, C.; Holz, G. G.; Doyle, R. P. Enhanced Peptide Stability Against Protease Digestion Induced by Intrinsic Factor Binding of a Vitamin B12 Conjugate of Exendin-4. *Mol. Pharm.* **2015**, *12* (9), 3502–3506.
- (2) Baldoni, D.; Waibel, R.; Bläuenstein, P.; Galli, F.; Iodice, V.; Signore, A.; Schibli, R.; Trampuz, A. Evaluation of a Novel Tc-99m Labelled Vitamin B12 Derivative for Targeting Escherichia Coli and Staphylococcus Aureus In Vitro and in an Experimental Foreign-Body Infection Model. *Mol. Imaging Biol.* **2015**, *17* (6), 829–837.
- (3) Smith, W. J.; Oien, N. P.; Hughes, R. M.; Marvin, C. M.; Rodgers, Z. L.; Lee, J.; Lawrence, D. S. Cell-Mediated Assembly of Phototherapeutics. *Angew. Chem. Int. Ed.* **2014**, *53* (41), 10945–10948.
- (4) Kräutler, B. Antivitamins B12—A Structure- and Reactivity-Based Concept. *Chem. – Eur. J.* **2015**, *21* (32), 11280–11287.
- (5) Henry, K. E.; Kerwood, D. J.; Allis, D. G.; Workinger, J. L.; Bonaccorso, R. L.; Holz, G. G.; Roth, C. L.; Zubieta, J.; Doyle, R. P. Solution Structure and Constrained Molecular



- Dynamics Study of Vitamin B<sub>12</sub> Conjugates of the Anorectic Peptide PYY(3-36).  
*ChemMedChem* **2016**, *11*, 1015-1021.
- (6) Sah, B.-R.; Schibli, R.; Waibel, R.; Boehmer, L. von; Bläuenstein, P.; Nexo, E.; Johayem, A.; Fischer, E.; Müller, E.; Soyka, J. D.; et al. Tumor Imaging in Patients with Advanced Tumors Using a New <sup>99m</sup>Tc-Radiolabeled Vitamin B12 Derivative. *J. Nucl. Med.* **2014**, *55* (1), 43–49.
- (7) Shell, T. A.; Shell, J. R.; Rodgers, Z. L.; Lawrence, D. S. Tunable Visible and Near-IR Photoactivation of Light-Responsive Compounds by Using Fluorophores as Light-Capturing Antennas. *Angew. Chem. Int. Ed.* **2014**, *53* (3), 875–878.
- (8) Henry, K. E.; Elfers, C. T.; Burke, R. M.; Chepurny, O. G.; Holz, G. G.; Blevins, J. E.; Roth, C. L.; Doyle, R. P. Vitamin B12 Conjugation of Peptide-YY3–36 Decreases Food Intake Compared to Native Peptide-YY3–36 Upon Subcutaneous Administration in Male Rats. *Endocrinology* **2015**, *156* (5), 1739–1749.
- (9) Verma, A.; Sharma, S.; Gupta, P. K.; Singh, A.; Teja, B. V.; Dwivedi, P.; Gupta, G. K.; Trivedi, R.; Mishra, P. R. Vitamin B12 Functionalized Layer by Layer Calcium Phosphate Nanoparticles: A Mucoadhesive and pH Responsive Carrier for Improved Oral Delivery of Insulin. *Acta Biomater.* **2016**, *31*, 288–300.
- (10) Chromiński, M.; Gryko, D. “Clickable” Vitamin B12 Derivative. *Chem. – Eur. J.* **2013**, *19* (16), 5141–5148.
- (11) Kolb, H. C.; Finn, M. G.; Sharpless, K. B. Click Chemistry: Diverse Chemical Function from a Few Good Reactions. *Angew. Chem. Int. Ed.* **2001**, *40* (11), 2004–2021.
- (12) Huisgen, R. 1,3-Dipolar Cycloadditions. Past and Future. *Angew. Chem. Int. Ed. Engl.* **1963**, *2* (10), 565–598.
- (13) Vaishnavi, E.; Renganathan, R. CdTe Quantum Dot as a Fluorescence Probe for Vitamin B(12) in Dosage Form. *Spectrochim. Acta. A. Mol. Biomol. Spectrosc.* **2013**, *115*, 603–609.
- (14) Shang, Z. B.; Wen, Y. J.; Yan, X. Q.; Sun, H. H.; Wang, Y.; Jin, W. J. Synthesis of a Novel Fluorescent Probe Based on 7-Nitrobenzo-2-Oxa-1,3-Diazole Skeleton for the Rapid Determination of Vitamin B12 in Pharmaceuticals. *Lumin. J. Biol. Chem. Lumin.* **2014**, *29* (6), 598–602.

- (15) Burnham-Marusich, A. R.; Plechaty, A. M.; Berninsone, P. M. Size-Matched Alkyne-Conjugated Cyanine Fluorophores to Identify Differences in Protein Glycosylation. *ELECTROPHORESIS* **2014**, *35* (18), 2621–2625.
- (16) Burmeister, R.; Bøe, I.-M.; Nykjaer, A.; Jacobsen, C.; Moestrup, S. K.; Verroust, P.; Christensen, E. I.; Lund, J.; Willnow, T. E. A Two-Receptor Pathway for Catabolism of Clara Cell Secretory Protein in the Kidney. *J. Biol. Chem.* **2001**, *276* (16), 13295–13301.
- (17) Le Panse, S.; Verroust, P.; Christensen, E. Internalization and Recycling of Glycoprotein 280 in Epithelial Cells of Yolk Sac. *Eur. J. Cell Biol.* **1997**, *72* (3), 257–267.
- (18) Chun, R. F.; Lauridsen, A. L.; Suon, L.; Zella, L. A.; Pike, J. W.; Modlin, R. L.; Martineau, A. R.; Wilkinson, R. J.; Adams, J.; Hewison, M. Vitamin D-Binding Protein Directs Monocyte Responses to 25-Hydroxy- and 1,25-Dihydroxyvitamin D. *J. Clin. Endocrinol. Metab.* **2010**, *95* (7), 3368–3376.
- (19) Vegt, E.; Eek, A.; Oyen, W. J. G.; de Jong, M.; Gotthardt, M.; Boerman, O. C. Albumin-Derived Peptides Efficiently Reduce Renal Uptake of Radiolabelled Peptides. *Eur. J. Nucl. Med. Mol. Imaging* **2010**, *37* (2), 226–234.
- (20) Kozyraki, R.; Fyfe, J.; Kristiansen, M.; Gerdes, C.; Jacobsen, C.; Cui, S.; Christensen, E. I.; Aminoff, M.; Chapelle, A. de la; Krahe, R.; et al. The Intrinsic Factor–vitamin B12 Receptor, Cubilin, Is a High-Affinity Apolipoprotein A-I Receptor Facilitating Endocytosis of High-Density Lipoprotein. *Nat. Med.* **1999**, *5* (6), 656–661.
- (21) Jensen, L. L.; Andersen, R. K.; Hager, H.; Madsen, M. Lack of Megalin Expression in Adult Human Terminal Ileum Suggests Megalin-Independent Cubilin/Amnionless Activity during Vitamin B12 Absorption. *Physiol. Rep.* **2014**, *2* (7).
- (22) Greenbaum D, Colangelo C, Williams K, Gerstein M. Comparing protein abundance and mRNA expression levels on a genomic scale. *Genome Biol.* **2003**, *4*, 117.
- (23) Maier, T.; Güell, M.; Serrano, L. Correlation of mRNA and Protein in Complex Biological Samples. *FEBS Lett.* **2009**, *583* (24), 3966–3973.
- (24) Marjanovič, I.; Kandušer, M.; Miklavčič, D.; Keber, M. M.; Pavlin, M. Comparison of Flow Cytometry, Fluorescence Microscopy and Spectrofluorometry for Analysis of Gene Electrotransfer Efficiency. *J. Membr. Biol.* **2014**, *247* (12), 1259–1267.
- (25) Hogg, K.; Thomas, J.; Ashford, D.; Cartwright, J.; Coldwell, R.; Weston, D. J.; Pillmoor, J.; Surry, D.; O’Toole, P. Quantification of Proteins by Flow Cytometry: Quantification of

- Human Hepatic Transporter P-Gp and OATP1B1 Using Flow Cytometry and Mass Spectrometry. *Methods San Diego Calif* **2015**, *82*, 38–46.
- (26) Christensen, E. I.; Nielsen, R.; Birn, H. From Bowel to Kidneys: The Role of Cubilin in Physiology and Disease. *Nephrol. Dial. Transplant.* **2013**, *28* (2), 274–281.
- (27) Pritchard, J. A. Fetal Swallowing and Amniotic Fluid Volume. *Obstetrics & Gynecology.* **1966**, *28*, 606-10.
- (28) Underwood, M. A.; Gilbert, W. M.; Sherman, M. P. Amniotic Fluid: Not Just Fetal Urine Anymore. *J. Perinatol.* **2005**, *25* (5), 341–348.
- (29) Nielsen, M. J.; Rasmussen, M. R.; Andersen, C. B. F.; Nexø, E.; Moestrup, S. K. Vitamin B12 Transport from Food to the Body's Cells—a Sophisticated, Multistep Pathway. *Nat. Rev. Gastroenterol. Hepatol.* **2012**, *9* (6), 345–354.
- (30) Pérez-Tilve, D.; González-Matías, L.; Aulinger, B. A.; Alvarez-Crespo, M.; Gil-Lozano, M.; Alvarez, E.; Andrade-Olivie, A. M.; Tschöp, M. H.; D'Alessio, D. A.; Mallo, F. Exendin-4 Increases Blood Glucose Levels Acutely in Rats by Activation of the Sympathetic Nervous System. *Am. J. Physiol. - Endocrinol. Metab.* **2010**, *298* (5), E1088–E1096.
- (31) Kanoski, S. E.; Rupprecht, L. E.; Fortin, S. M.; De Jonghe, B. C.; Hayes, M. R. The Role of Nausea in Food Intake and Body Weight Suppression by Peripheral GLP-1 Receptor Agonists, Exendin-4 and Liraglutide. *Neuropharmacology* **2012**, *62* (5–6), 1916–1927.
- (32) Hayes, M. R.; De Jonghe, B. C.; Kanoski, S. E. Role of the Glucagon-like-Peptide-1 Receptor in the Control of Energy Balance. *Physiol. Behav.* **2010**, *100* (5), 503–510.
- (33) Clardy-James, S.; Berstein, J. L.; Kerwood, D. J.; Doyle, R. P. Site-Selective Oxidation of Vitamin B12 Using 2-Iodoxybenzoic Acid. *Synlett.* **2012**, *23*, 2363-2366.
- (34) Fischer, M. E. Amine Coupling Through EDC/NHS: A Practical Approach. In *Surface Plasmon Resonance*; Mol, N. J., Fischer, M. J. E., Eds.; Methods in Molecular Biology; Humana Press, 2010; 55–73.
- (35) Nielsen, L. L.; Young, A. A.; Parkes, D. G. Pharmacology of Exenatide (Synthetic Exendin-4): A Potential Therapeutic for Improved Glycemic Control of Type 2 Diabetes. *Regul. Pept.* **2004**, *117* (2), 77–88.
- (36) Doyle, M. E.; Theodorakis, M. J.; Holloway, H. W.; Bernier, M.; Greig, N. H.; Egan, J. M. The Importance of the Nine-Amino Acid C-Terminal Sequence of Exendin-4 for Binding

- to the GLP-1 Receptor and for Biological Activity. *Regul. Pept.* **2003**, *114* (2–3), 153–158.
- (37) Klarenbeek, J.; Goedhart, J.; Batenburg, A. van; Groenewald, D.; Jalink, K. Fourth-Generation Epac-Based FRET Sensors for cAMP Feature Exceptional Brightness, Photostability and Dynamic Range: Characterization of Dedicated Sensors for FLIM, for Ratiometry and with High Affinity. *PLOS ONE* **2015**, *10* (4), e0122513.
- (38) Holz, G. G. Epac: A New cAMP-Binding Protein in Support of Glucagon-Like Peptide-1 Receptor-Mediated Signal Transduction in the Pancreatic  $\beta$ -Cell. *Diabetes* **2004**, *53* (1), 5–13.
- (39) De Jonghe, B. C.; Holland, R. A.; Olivos, D. R.; Rupprecht, L. E.; Kanoski, S. E.; Hayes, M. R. Hindbrain GLP-1 Receptor Mediation of Cisplatin-Induced Anorexia and Nausea. *Physiol. Behav.* **2016**, *153*, 109–114.
- (40) Kanoski, S. E.; Hayes, M. R.; Skibicka, K. P. GLP-1 and Weight Loss: Unraveling the Diverse Neural Circuitry. *Am. J. Physiol. Regul. Integr. Comp. Physiol.* **2016**, *310* (10), R885-895.
- (41) Reiner, D. J.; Mietlicki-Baase, E. G.; McGrath, L. E.; Zimmer, D. J.; Bence, K. K.; Sousa, G. L.; Konanur, V. R.; Krawczyk, J.; Burk, D. H.; Kanoski, S. E.; et al. Astrocytes Regulate GLP-1 Receptor-Mediated Effects on Energy Balance. *J. Neurosci.* **2016**, *36* (12), 3531–3540.
- (42) McMahon, L. R.; Wellman, P. J. PVN Infusion of GLP-1-(7-36) Amide Suppresses Feeding but Does Not Induce Aversion or Alter Locomotion in Rats. *Am. J. Physiol.* **1998**, *274* (1 Pt 2), R23-29.
- (43) Hayes, M. R.; Leichner, T. M.; Zhao, S.; Lee, G. S.; Chowansky, A.; Zimmer, D.; De Jonghe, B. C.; Kanoski, S. E.; Grill, H. J.; Bence, K. K. Intracellular Signals Mediating the Food Intake-Suppressive Effects of Hindbrain Glucagon-like Peptide-1 Receptor Activation. *Cell Metab.* **2011**, *13* (3), 320–330.
- (44) Ikotun, O. F.; Marquez, B. V.; Fazen, C. H.; Kahkoska, A. R.; Doyle, R. P.; Lapi, S. E. Investigation of a Vitamin B12 Conjugate as a PET Imaging Probe. *ChemMedChem* **2014**, *9* (6), 1244–1251.

## Chapter 5: Mitigation of Aminoglycoside Toxicity in Pigmented Guinea Pigs Using Intrinsic Factor Expressed in *Arabidopsis thaliana*

Work in this chapter was performed by the author unless otherwise indicated. Where indicated the work was performed in collaboration with Stefania Arduini, Au.D. and Dr. Beth Prieve, Department of Communication Sciences and Disorders, Syracuse University, Syracuse, NY.

### 5.1 Introduction

#### 5.1.1 Mitigating Hearing Loss from Aminoglycosides using Human Gastric Intrinsic Factor

In 2009, a study by Christensen *et al.* showed that the receptor CUBN binds to six different AGA (gentamicin, tobramycin, streptomycin, neomycin, kanamycin, and netilmicin) (for more detail on AGA see Chapter 1, Section 1.6.1) with K<sub>d</sub> values ranging from 1.3-3.4 mM.<sup>1</sup> CUBN is a multi-ligand binding receptor with limited expression (mainly within the kidney and small intestine) (for more detail see Chapter 1, Section 1.2.2). Of particular relevance here, CUBN is also found within the inner ear co-expressed with megalin.<sup>1</sup> The role of CUBN in the inner ear is unknown, but it is hypothesized to help with fluid homeostasis.<sup>1,2</sup> This work **hypothesizes** that CUBN's binding of AGA contributes to their ototoxicity and the aim of this work is to inhibit CUBN mediated AGA uptake into cells of the inner ear and mitigate associated hearing damage.

The inhibition of CUBN mediated AGA uptake will be investigated through the administration of Intrinsic Factor (IF) with AGA in pigmented guinea pigs (see section 5.2.1 for rationale).<sup>2</sup> IF is a '*bona fide*' substrate of CUBN and is found only in the gastrointestinal tract where it plays a critical role in dietary uptake of B12 (for more detail see Chapter 1, Section

1.1.4). CUBN is the only known receptor for holo-IF and has a  $K_d$  of 1 pM.<sup>3,4</sup> Thus, systemically administered holo-IF will target CUBN expressed within the inner ear with high specificity.

## 5.2 Inducing Hearing Loss in Pigmented Guinea Pigs using Kanamycin

### 5.2.1 Pigmented Guinea Pigs

Guinea pigs are a common animal model used when doing hearing studies, as their ear structure and hearing ranges are similar to humans.<sup>5,6,7,8</sup> Pigmented guinea pigs were specifically chosen based on reports of kanamycin induced hearing damage.<sup>5,6,9</sup>

### 5.2.2 A Discussion on Anesthesia in Pigmented Guinea Pigs

Ketamine is a commonly used injectable anesthetic with rodents and small animal models (Figure 1, left).<sup>10,11</sup> Ketamine is a Schedule III controlled substance in the U.S.A. Ketamine is a *N*-methyl-D-aspartate receptor agonist.<sup>12</sup> With most rodents, ketamine alone will cause sufficient sedation to handle and examine.<sup>10</sup> However, guinea pigs are among the most difficult rodents to achieve effective anesthesia due to their highly variable response and post-anesthetic complications.<sup>13,14</sup> Therefore, a large dose of injectable anesthesia is needed to adequately sedate guinea pigs for handling/examinations.<sup>15</sup> In our early studies a dose of ketamine at 55 mg/kg was used to sedate the guinea pigs, but this alone was not sufficient for the placement of the subdermal needles needed to collect auditory brainstem response's (ABR) (data not shown).

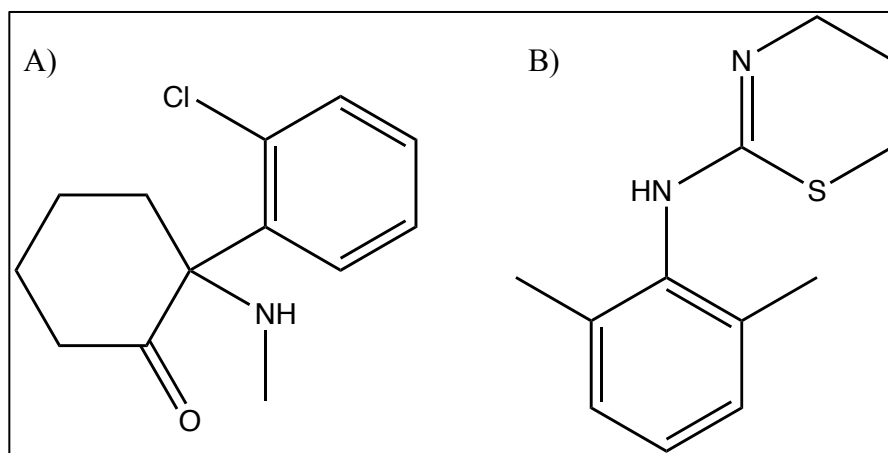


**Figure 1.** Chemical structures of the anesthetics A) ketamine and B) xylazine.

After these initial failed attempts at sedating the guinea pigs, a combination anesthetic cocktail of ketamine and xylazine was used (Figure 1, right). Xylazine is an alpha-2 agonist that inhibits norepinephrine release and blocks its uptake in the locus ceruleus section of the brainstem, which causes sedation and muscle relaxation.<sup>13,15</sup> This cocktail of ketamine/xylazine (55 and 5 mg/kg, respectively, via intraperitoneal injection (IP)) showed appropriate sedation and time of sedation for the experiments performed. After experiments that lead to guinea pig death due to respiratory failure, atipamezole, was added to the anesthesia regiment. Atipamezole (1 mg/kg via intramuscular injections (IM)) is an alpha-2 antagonist and reverses the effects of xylazine.<sup>15</sup>

Thus, a new protocol was designed by this author to enable the safe and effective anesthesia for guinea pigs necessary for the studies performed herein. All experiments were conducted under permission of the NY Dept. of Health and U.S. Drug Enforcement Agency (License # RD0494928). All animal handling and manipulations were conducted in accordance with the guidelines set by Syracuse University Animal Care and Use Committee (IACUC) and Research Animal Resource Center.

### 5.2.3 Experimental Design

#### 5.2.3.1 Administering Kanamycin for 23 days

Pigmented guinea pigs ( $n = 4$ ) were injected with kanamycin (250 mg/kg via IP) injections for 23 days. Campbell *et al.* previously reported that this dosage administered via subcutaneous (SC) injections induced 60-80 dB hearing loss at 8 kHz.<sup>5,9</sup> The administration route was changed to IP to keep the route consistent with the injections of IF in later experiments, and was necessary due to IF's unknown pharmacokinetic profile in guinea pigs. IP injections allow for a greater serum uptake of IF and therefore potential effectiveness. Hearing tests were performed at 3, 5 and 6 weeks after first injection as per literature.<sup>5,9</sup>

### 5.2.4 Auditory Brainstem Response Hearing Tests on Guinea Pigs Using Kanamycin

#### 5.2.4.1 Auditory Brainstem Response Test

An ABR is a neurological test that detects auditory brainstem function in response to auditory stimuli.<sup>16</sup> ABR is detected with electrodes that can be placed directly on the skin or subdermal needles under the skin. Stimuli from an acoustic transducer in the form of an insert earphone or headphone evokes a potential waveform.<sup>16</sup> The amplitude (mV) of the signal is averaged over multiple scans and charted against time (ms). ABR's are a common test to perform on new-born babies to determine their hearing.<sup>17</sup> This experiment herein used ABR to determine the hearing of guinea pigs.

#### 5.2.4.2 Auditory Brainstem Response Hearing Baseline for Pigmented Guinea Pigs

While there is extensive research on guinea pigs and their hearing it is important to establish a baseline hearing for all subjects before any experiment. This is due to different



individuals animals having different hearing baselines. Therefore, to properly determine hearing loss, comparisons between starting and ending hearing tests for each animal individually is empirical. In addition, it was important to establish a typical guinea pig waveform for reference to our studies.

Figure 2 is an example of baseline hearing in guinea pigs at 8 kHz, 6 kHz, and ‘click’ (in descending order). A characteristic waveform profile for guinea pig hearing was established. A typical waveform had seven peaks between 20 and 50 ms (Figure 2). Hearing baselines were also determined to be between -10 and 0 mV for most guinea pigs.

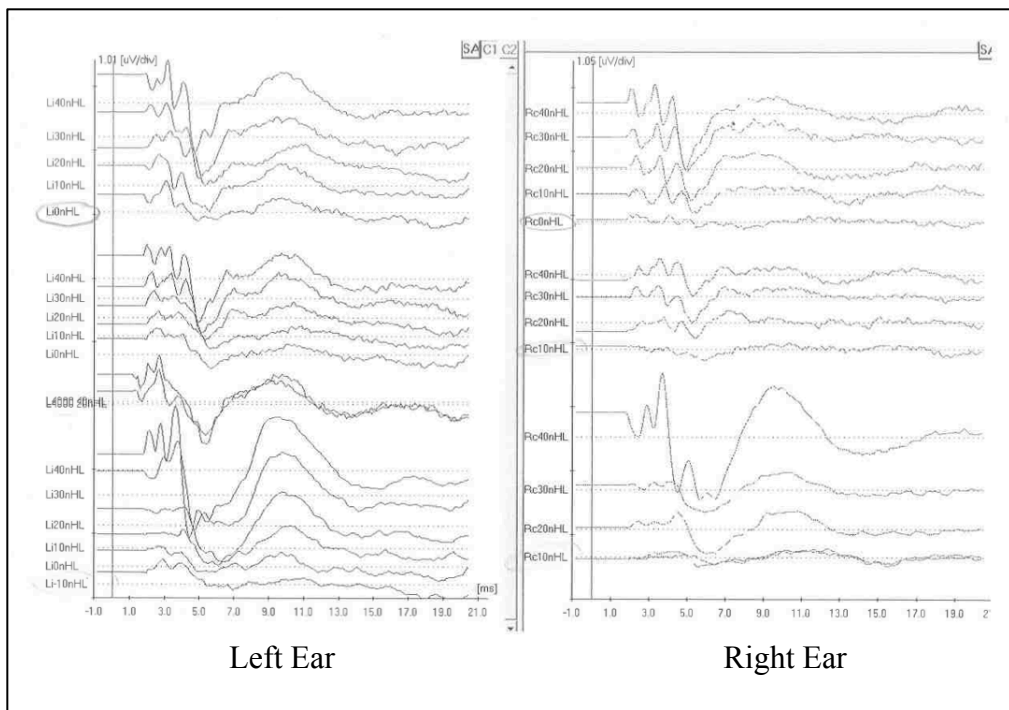


**Figure 2.** An example of baseline hearing in guinea pigs through ABR. Hearing determined at 8 kHz, 6 kHz, and ‘click’ (in descending order) for both the left and right ear for guinea pig 1. The seven characteristic peaks between 10 and 50 ms are at all frequencies. Baseline hearing was determined between -10 and 0 mV for all guinea pigs.

### 5.2.4.3 Kanamycin Induced Hearing Loss in Pigmented Guinea Pigs

Hearing loss was determined by examining this characteristic profile of the seven peaks and a loss of all peaks, not magnitude, was deemed as hearing loss. Table 1 shows a summary of hearing loss with guinea pigs **1-4** after a 23-day administration of kanamycin. Guinea pig **1** died before any hearing tests were performed. Guinea pigs **2-4** were tested at 3, 5, and 6 weeks. Figure 3 shows an example of baseline hearing compared to hearing at week 6 for guinea pig **4**.

<b>GP ID #</b>	<b>Drug and Dose</b>	<b>Hearing Loss</b>
<b>1</b>	Kanamycin 250 mg/kg 23 days	N/A
<b>2</b>	Kanamycin 250 mg/kg 23 days	No
<b>3</b>	Kanamycin 250 mg/kg 23 days	No
<b>4</b>	Kanamycin 250 mg/kg 23 days	No

**Table 1.** Results of the ABR test after kanamycin dosing over 23 days for guinea pigs **1-4**. ABR's guinea pigs **2-3** were tested at 3, 5, and 6 weeks. No hearing loss was observed in any guinea pigs.

Analysis of the ABR's showed interesting results for guinea pigs **2-4**. Results showed either the same hearing dB as on day 0 or better hearing dB. Thus, no guinea pig was deemed to have hearing loss, under our criteria here. However, it is important to note that it was decided to base hearing loss on the complete loss of the waveforms as is normal for human hearing analysis. The question of whether to actually assign hearing loss to a complete lack of waveform or to some of the waveform in the guinea pig studies now comes into play.

Unfortunately, there is limited information regarding 1) what a normal waveform for a guinea pig looks like and 2) what that waveform should look like to indicate hearing loss. Most papers cite hearing loss differences without publishing the ABR waveforms. In this experiment, there was an observed loss in part of the waveforms for some of the guinea pigs as well as a decrease in intensity for those waveforms when compared to day 0, yet the significance of this is unknown. Interestingly however, such differences were not seen in the IF administered guinea pigs (see Figure 4).

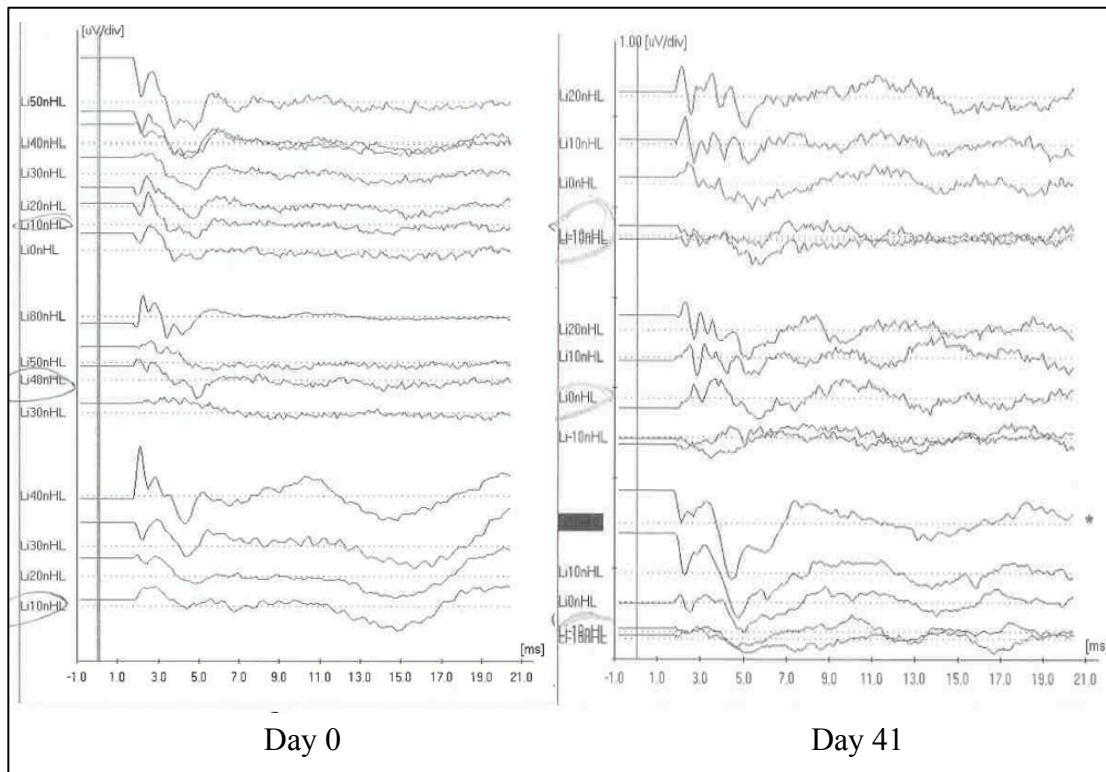


**Figure 3.** An example of ABR hearing test in guinea pigs administered kanamycin for 23 days. ABR results of guinea pig 4's left ear. Hearing determined at 8 kHz, 6 kHz, and 'click' (in descending order) for guinea pig 4 at 0 and 41 days. There was no observable hearing loss.

## 5.3 Using IF to Mitigate Hearing Loss from Aminoglycoside Toxicity

### 5.3.1 Experimental Design

#### 5.3.1.1 Kanamycin with IF Induced Hearing loss in Pigmented Guinea Pigs

Pigmented guinea pigs (n = 4) (**5-8**) were injected with kanamycin (250 mg/kg via IP) for 23 days with 6.25 µg of IF injected at 15 min pre-kanamycin and again at 30 min post-kanamycin. Hearing tests were performed at 3, 5, and 6 weeks.

#### 5.3.2 Auditory Brainstem Response Hearing Tests in Guinea Pigs on Kanamycin and IF for 23 days

Hearings tests were conducted at 3, 5 and 6 weeks after the first injection of kanamycin and IF (250 mg/kg/day and 13 µg/day, respectively, via IP). Table 2 shows the results of ABR hearing tests for guinea pigs **5-8**. Figure 4 shows an example of baseline (day 0) hearing for guinea pig **7** compared to hearing at week 4 (day 35).

There was no observed hearing loss for guinea pigs **5-8**. This lack in hearing loss was a targeted outcome but since a positive control could not be established the results are debatable. However, it can be noted that the overall waveform for **5-8** was better retained than **1-4**, which points to IF mitigating AGA toxicity, but cannot be definitively confirmed at this time. The inconclusive results are perplexing due to proclaimed literature results. In fact the paper that was being followed, Campbell *et al.* showed a 40 dB shift in hearing after kanamycin injections over 23 days.<sup>5</sup>

GP ID #	Drug and Dose	Hearing Loss
5	Kanamycin 250 mg/kg + IF (13 µg/day) 23 days	No
6	Kanamycin 250 mg/kg + IF (13 µg/day) 23 days	No
7	Kanamycin 250 mg/kg + IF (13 µg/day) 23 days	No
8	Kanamycin 250 mg/kg + IF (13 µg/day) 23 days	No

**Table 2.** Results of the ABR test using kanamycin and IF for 23 days for guinea pigs 5-8. Hearings tests were conducted at 3, 5 and 6 weeks p.i. using ABR's. There was no hearing loss observed for all guinea pigs.

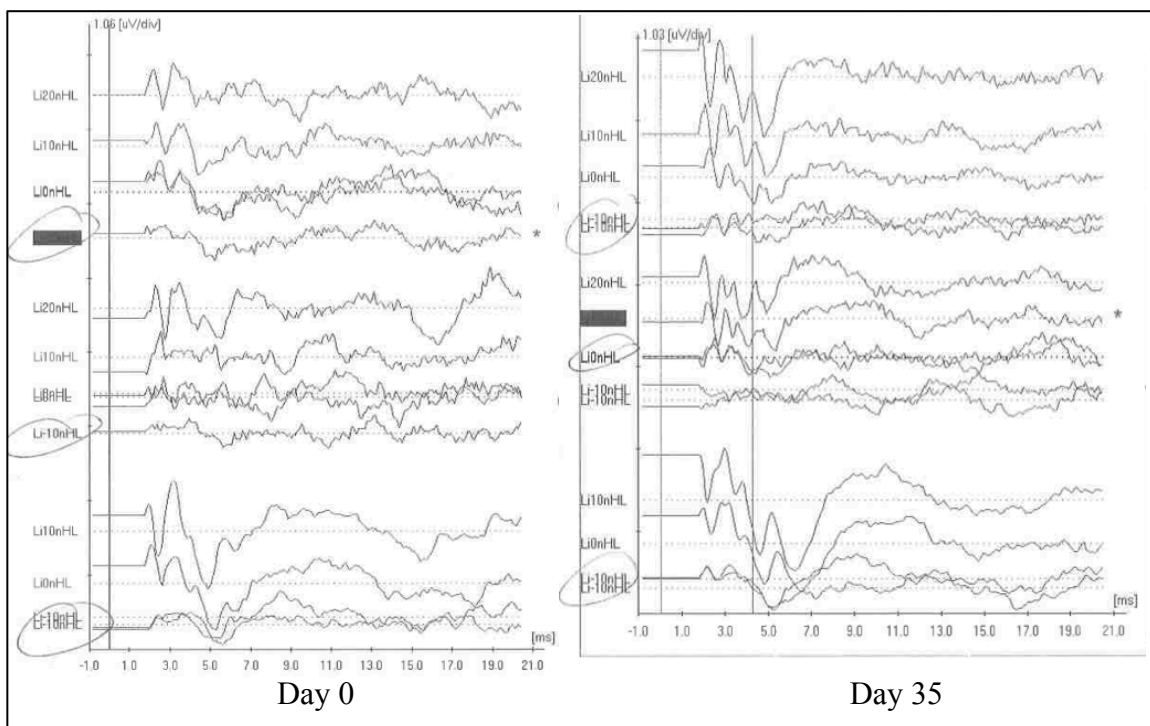


**Figure 4.** An example of ABR hearing test in guinea pigs administered kanamycin and IF for 23 days. ABR comparison of guinea pig 7's left ear between day 0 and week 4 p.i. Hearing determined at 8 kHz, 6 kHz, and 'click' (in descending order). There was no hearing loss seen.

## 5.4 Antigenicity of IF expressed in *Arabidopsis thaliana* in Guinea Pigs

The IF used in these experiments is recombinant human IF expressed in *A. thaliana* (for more detail see Chapter 3, Section 3.6). Plant based proteins are well known to be antigenic.<sup>18,19</sup> Since this is the first time IF has been systemically injected, and it was injected over a prolonged period time the possibility of antigenicity was investigated.

### 5.4.1 Effect of IF on Guinea Pig Weight

To determine if the IF was causing adverse side effects on guinea pigs their weights were monitored for the 23 days and compared to the control models (no IF administered). Figure 5 shows the weights of the guinea pigs over 23 days. No weight difference was seen in the two different cohorts (with or without IF). This indicates that IF is not causing notable side effects on the guinea pigs normal behavior.

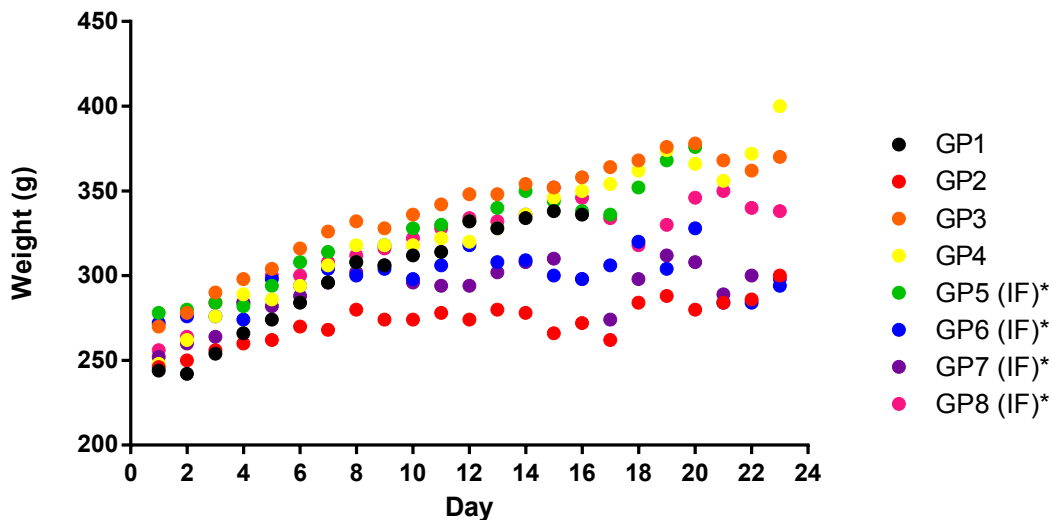


**Figure 5.** Daily weights of guinea pigs 1-8 during 23 days. Guinea pigs 1-4 had no IF injected and 5-8 had IF injected twice daily. \*Two injections of 13  $\mu\text{g}/\text{day}$ . Weights for each cohort increased steadily over time showing no difference in weight in each study.

#### 5.4.2 ELISA of Guinea Pig Blood to Detect for IF Antibodies Raised by Guinea Pigs

Once experiments were completed on the remaining guinea pigs (**2**, **3**, **6**, **12**, and **18**) was sacked and blood samples were collected. Guinea pigs **12** and **18** were from a separate experiment using kanamycin and IF for a shorter time (data is not shown). IF antigens in the blood samples were determined using a commercial ELISA kit. Figure 6 shows the results of the ELISA. Guinea pigs **2**, **3**, and **12** show no antigens in their blood as expected. Guinea pigs **6** (IF injection of 136  $\mu\text{g}/\text{day}$  for 23 days) and **18** (0.25 mg once) show a high amount of antigens in their blood serum compared to those without IF injected, which indicates that IF causes an antigenic response, albeit without appearing to cause harm to the guinea pigs.

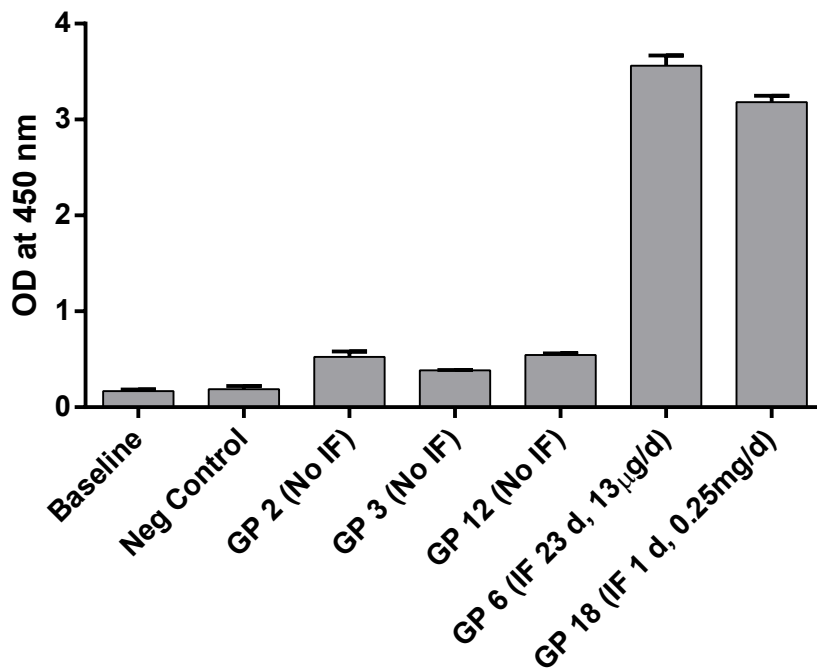


**Figure 6.** ELISA IF antigenicity results for **2**, **3**, **6**, **12**, and **18**. Guinea pigs that had no IF injected (**2**, **3**, and **12**) show no antigenicity while guinea pigs (**6** and **18**) showed high indication of antigens in their blood.

## 5.5 Summary and Conclusions

The results herein, while not confirming IF protection of AGA induced hearing damage, produced significant information.

1. A characteristic waveform profile was shown to have seven peaks for a pigmented guinea pig with the lab equipment used.
2. The standard normal hearing threshold for guinea pigs is around -10 and 0 dB.
3. A standard and safe anesthesia protocol was developed using a combination cocktail (ketamine and xylazine) with the recovery agent (atipamezole).
4. The prolonged use of IF at short doses does not affect guinea pig development and weight gain in comparison to control.
5. All guinea pigs that had IF injections, whether at large single doses (0.25 mg) or small doses over prolonged periods (13 µg/day), showed antigens for IF in their blood serum. This result was expected as IF is produced in plants and their glycosylation profile is different than in humans triggering an immune response. However, it's important to note that this response was not harmful to the animals.

In conclusion these experiments allowed a wealth new of information to be obtained regarding in vivo guinea pig research. One important observation is that the highest frequency observed in these experiments was 8 kHz. AGA are known to effect the higher hearing frequencies (12 kHz and higher) more readily.<sup>6</sup> Therefore the control experiments could of caused hearing damage but it was not seen due to those higher frequencies not being looked at. With this said in moving forward the baseline hearing and new anesthesia protocols allow for



experiments to be repeated with minimal loss of subjects, observation at higher frequencies will be also completed (up to 18 kHz) (see Chapter 7, Section 7.3.2).

## 5.6 References

- (1) Tauris, J.; Christensen, E. I.; Nykjaer, A.; Jacobsen, C.; Petersen, C. M.; Ovesen, T. Cubilin and Megalin Co-Localize in the Neonatal Inner Ear. *Audiol. Neurootol.* **2009**, *14* (4), 267–278.
- (2) Christensen, E. I.; Birn, H. Megalin and Cubilin: Multifunctional Endocytic Receptors. *Nat. Rev. Mol. Cell Biol.* **2002**, *3* (4), 258–268.
- (3) Fedosov, S. N.; Fedosova, N. U.; Berglund, L.; Moestrup, S. K.; Nexø, E.; Petersen, T. E. Composite Organization of the Cobalamin Binding and Cubilin Recognition Sites of Intrinsic Factor. *Biochemistry (Mosc.)* **2005**, *44* (9), 3604–3614.
- (4) Nielsen, M. J.; Rasmussen, M. R.; Andersen, C. B. F.; Nexø, E.; Moestrup, S. K. Vitamin B12 Transport from Food to the Body's Cells—a Sophisticated, Multistep Pathway. *Nat. Rev. Gastroenterol. Hepatol.* **2012**, *9* (6), 345–354.
- (5) Campbell, K. C. M.; Martin, S. M.; Meech, R. P.; Hargrove, T. L.; Verhulst, S. J.; Fox, D. J. D-Methionine (D-Met) Significantly Reduces Kanamycin-Induced Ototoxicity in Pigmented Guinea Pigs. *Int. J. Audiol.* **2016**, *55* (5), 273–278.
- (6) Havenith, S.; Klis, S. F. L.; Versnel, H.; Grolman, W. A Guinea Pig Model of Selective Severe High-Frequency Hearing Loss. *Otol. Neurotol.* **2013**, *34* (8), 1510–1518.
- (7) Mujica-Mota, M. A.; Gasbarrino, K.; Rappaport, J. M.; Shapiro, R. S.; Daniel, S. J. The Effect of Caffeine on Hearing in a Guinea Pig Model of Acoustic Trauma. *Am. J. Otolaryngol.* **2014**, *35* (2), 99–105.
- (8) Tanaka, C.; Nguyen-Huynh, A.; Loera, K.; Stark, G.; Reiss, L. Factors Associated with Hearing Loss in a Normal-Hearing Guinea Pig Model of Hybrid Cochlear Implants. *Hear. Res.* **2014**, *316*, 82–93.
- (9) Song, B. B.; Sha, S. H.; Schacht, J. Iron Chelators Protect from Aminoglycoside-Induced Cochleo- and Vestibulo-Toxicity. *Free Radic. Biol. Med.* **1998**, *25* (2), 189–195.

- (10) Green, C. J.; Knight, J.; Precious, S.; Simpkin, S. Ketamine Alone and Combined with Diazepam or Xylazine in Laboratory Animals: A 10 Year Experience. *Lab. Anim.* **1981**, *15* (2), 163–170.
- (11) Kurdi, M. S.; Theerth, K. A.; Deva, R. S. Ketamine: Current Applications in Anesthesia, Pain, and Critical Care. *Anesth. Essays Res.* **2014**, *8* (3), 283–290.
- (12) Sleight, J.; Harvey, M.; Voss, L.; Denny, B. Ketamine – More Mechanisms of Action than Just NMDA Blockade. *Trends Anaesth. Crit. Care* **2014**, *4* (2), 76–81.
- (13) D'Alleinne, C. P.; Mann, D. D. Evaluation of Ketamine/Xylazine Anesthesia in the Guinea Pig: Toxicological Parameters. *Vet. Hum. Toxicol.* **1982**, *24* (6), 410–412.
- (14) Radde, G. R.; Hinson, A.; Crenshaw, D.; Toth, L. A. Evaluation of Anaesthetic Regimens in Guineapigs. *Lab. Anim.* **1996**, *30* (3), 220–227.
- (15) Flecknell, P. A. Chapter 6 - Anaesthesia of Common Laboratory Species: Special Considerations. In *Laboratory Animal Anaesthesia (Third Edition)*; Academic Press: San Diego, **2009**, 181–241.
- (16) Skoe, E.; Kraus, N. Auditory Brainstem Response to Complex Sounds: A Tutorial. *Ear Hear.* **2010**, *31* (3), 302–324.
- (17) Mason, J. A.; Herrmann, K. R. Universal Infant Hearing Screening by Automated Auditory Brainstem Response Measurement. *Pediatrics* **1998**, *101* (2), 221–228.
- (18) Takeyama, N.; Kiyono, H.; Yuki, Y. Plant-Based Vaccines for Animals and Humans: Recent Advances in Technology and Clinical Trials. *Ther. Adv. Vaccines* **2015**, *3* (5–6), 139–154.
- (19) Guan, Z.; Guo, B.; Huo, Y.; Guan, Z.; Dai, J.; Wei, Y. Recent Advances and Safety Issues of Transgenic Plant-Derived Vaccines. *Appl. Microbiol. Biotechnol.* **2013**, *97* (7), 2817–2840.

## Chapter 6: Experimental

### 6.1 General Materials and Methods

Laboratory grade solvents and chemicals were purchased from VWR, Sigma Aldrich, and Alfa Aesar and used as received. Water was distilled and deionized to 18.2 MΩ using a Barnstead Diamond RO Reverse Osmosis machine. Centrifugation for all syntheses was carried out using a Sorvall RT machine at a speed of 4000 rpm at 23°C for 5 minutes. Electronic absorption spectra were obtained on a Varian Cary 50 Bio spectrophotometer in a 2 mL quartz cuvette between 200 – 800 nm. Flow cytometry was completed on a Becton Dickinson LSRII Cell Analyzer. Fluorescence spectra were obtained on a Agilent Cary Eclipse Fluorescence Spectrophotometer. Xeragenx supplied the human intrinsic factor, which was expressed in *Arabidopsis thaliana*. TCII was from R&D Systems. Ex-4 K12-azido were purchased from C.S. Bio Lab (Cambridge, MA). Cyanocobalamin (B12), 2-iodoxybenzoic acid (IBX), 2-hydroxypyridine (HYP), dimethyl sulfoxide (DMSO), 1-amino-3-butyne, 1,1'-carbonyldi(1,2,4-triazole), trimethylamine (TEA), carbodiimide, hydroxybenzotriazole (HOBT), dimethyl formamide (DMF), copper(I) iodine (CuI), 1,1'-carbonyl-di-(1,2,4)-triazole (CDT), ZrCl<sub>4</sub>, *n*-methyl-2-pyrrolidone (NMP), Diisopropylamine (DIPA), mesyl chloride (MsCl), hexamethylphosphoramide (HMPA), sodium azide (NaN<sub>3</sub>), desferoxamine mesylate (DFO), fmoc-propargylglycine (FPG), and piperidine and were purchased from Sigma Aldrich. Sulfo-cyanine5-NHS-ester and cyanine5-alkyne were purchased from Lumiprobe. *p*-SCN-Bn-NOTA was purchased from Macrocyclics. Black costar plates with a clear bottom were purchased from Thermo Fisher Scientific. <sup>1</sup>H NMR was performed on a 400 MHz or 500MHz Bruker spectrometer with the residual solvent peak as an internal standard. All mass spectra were performed on a Bruker autoflex III smartbeam matrix-assisted laser desorption/ionization time of flight mass spectrometer (MALDI) or a Shimadzu

LCMS-8040. Quantification was completed by mass or through a Shimadzu BioSpec-Nano spectrophotometer. RP-HPLC was performed using either an Agilent 1200 system or a Shimadzu Prominence with an Agilent Eclipse C18 XBD analytical column (5  $\mu\text{m}$  x 4.6mm x 150 mm).

### 6.1.1 HPLC Method

Used for HPLC analysis unless otherwise stipulated. Solvent A: 0.1% TFA water.

Time (min)	%B (MeCN)
0	1
15	70
30	70

### 6.1.2 Synthesis of B12 Mesylate (B12-MsCl)

Synthesis was performed as previously reported.<sup>1</sup> In brief, cyanocobalamin (68 mg, 0.050 mmol) was dissolved in NMP (0.5 mL). A solution of MSCl (25 mg, 0.21824 mmol) in NMP (135  $\mu\text{L}$ ) and DIPEA (135  $\mu\text{L}$ ) were added in separately, at the same time, in three intervals 1 h apart. After addition of the third portion, the reaction was stirred for one hour at room temperature. The reaction mixture was then poured into water (50 mL) and washed three times with  $\text{CH}_2\text{Cl}_2$ . The aqueous phase was extracted using a phenol solution (phenol (10 g)/  $\text{CH}_2\text{Cl}_2$  (10 mL)) The organic layer was washed three times with water then diluted to 100 mL and back extracted with water three times. The aqueous layer was combined and solvent was removed under reduced pressure. The residue was dissolved in minimal amount of methanol, precipitated out with cold diethyl ether, centrifuged and dried to a red powder. Crude was purified through RP

chromatography, as previously reported. The product was collected as a red powder (44.2 mg, 65% yield, based on B12 starting material). Calculated  $m/z$  1433.0; found: 1433.

### 6.1.3 Synthesis and Purification of B12-Azide (B12-N<sub>3</sub>)

Synthesis was performed as previously reported.<sup>1</sup> B12-MSCl (15 mg, 0.0106mmol) was dissolved in HMPA (3 mL) and heated to 40°C. NaN<sub>3</sub> (6.3 mg, 0.0975mmol) was added and the reaction mixture was stirred overnight. The reaction mixture was then poured into water (50 mL) and washed 3 times with CH<sub>2</sub>Cl<sub>2</sub>. The aqueous phase was extracted using a phenol solution (phenol (10 g)/ CH<sub>2</sub>Cl<sub>2</sub> (10 mL)) The organic layer was washed 3 times with water then diluted to 100 mL and back extracted with water 3 times. The aqueous layer was combined and solvent was removed under reduced pressure. The residue was dissolved in minimal amount of methanol, precipitated out with cold diethyl ether, centrifuged and dried to as red powder. Crude was purified through RP chromatography as previously reported. The product dried down to a red powder (7.9 mg, 52% yield, based on B12 starting material). Calculated  $m/z$ : 1380.0; found: 1380.

### 6.1.4 Synthesis and Purification of B12-Azide-Linker (B12-azide-linker)

B12 (50 mg, 0.036 mg) was added to 2 mL anhydrous DMSO under Argon atmosphere and was heated to 40°C. After B12 was dissolved, 1,1'-carbonyl-di-(1,2,4)-triazole (CDT) (30 mg, 0.184 mmol) was added to the solution and was allowed to stir for 2 h.<sup>2</sup> The reaction was monitored using HPLC and after 90% or more conversion 1-amin-6-azidohexane was added (200  $\mu$ L, 0.184 mmol) and the reaction was allowed to stir for another 90 min. The reaction was precipitated

with diethyl ether, centrifuged and dried to a red powder. Purified on a reverse silica column with a 5-15% acetonitrile in 0.1% TFA water. Yield: 86%. Purity and yield was determined by RP-HPLC.

#### 6.1.5 Synthesis and purification of B12-azide-linker with Fmoc-propargylglycine (B12-FPG)

B12-FPG was synthesized through Huisgen/Sharpless 'Click' Chemistry.<sup>3,4</sup> CuI (4.1 mg, 0.0216 mmol) was dissolved in DMF and H<sub>2</sub>O (4:1) (v/v) then tris[(1-benzyl-1*H*-1,2,3-triazole-4-yl)methyl]amine (TBTA) (21.8 mg, 0.043 mmol) and was allowed to stir for 30 min at room temperature. B12-azide-linker (30 mg, 0.0196mmol) and fmoc-propargylglycine (FPG) (16.5 mg, 0.0492 mmol) were added sequentially. The reaction was allowed to stir for 24 h at room temperature. The reaction was precipitated out with diethyl ether and was purified on a reverse phase silica column with 10-25% acetonitrile in 0.1% TFA water. Yield 95%, based on B12 starting material. Calculated *m/z* to be 1858.95; found: 1860.0 [M]<sup>+</sup>. <sup>1</sup>H NMR: (7.76, d, 3H), (7.68, s, 1H), (7.60, t, 2H), (7.36, d, 2H), (7.29, d, 2H), (7.19, s, 1H), (7.13, s, 1H), (6.56, s, 1H), (6.19, s, 1H), (6.01, s, 1H).

#### 6.1.6 Deprotection of B12-FPG (B12-PG)

B12-FPG was fully dissolved in DMF and piperidine was added to make the solution a 30% piperidine mixture. The solution was then allowed to stir or was shaken for 15-20 min, precipitated with diethyl ether, centrifuged and dried in vacuo to a red powder. HPLC and NMR confirmed >95% purity. Yield: 100%, based on B12 starting material. Calculated *m/z*: 1636;

found: 1637.0 [M+1]. <sup>1</sup>H NMR: (7.73, s, 1H), (7.16, s, 1H), (6.99, s, 1H), (6.40, s, 1H), (6.20, s, 1H), (5.97, s, 1H).

#### 6.1.7 Synthesis of B12-ethylenediamine (B12-en)

B12-en was made as previously described.<sup>5</sup> B12 (50 mg, 0.036 mmol) was added to anhydrous DMSO under Argon atmosphere and was heated to 40°C. After B12 was dissolved, 1,1'-carbonyl-di-(1,2,4)-triazole (CDT) (30 mg, 0.184 mmol) was added to the solution and was allowed to stir for 2 h. The reaction was monitored using HPLC and after 90% or more conversion, ethylenediamine was added (21.4 mg, 0.184 mmol) and the reaction was allowed to stir for another 90 min. The reaction was precipitated with diethyl ether. This reaction was not purified and was used as is. Yield: 90%, based on B12 starting material. Calculated *m/z*: 1441.48; found: 1442.0 [M]<sup>+</sup>.

#### 6.1.8 Synthesis of B12-ethylenediamine-NOTA (B12-NOTA)

B12-en (20 mg, 0.014 mmol) was dissolved in 100 mM carbonate buffer at pH 10.5 and *p*-SCN-Bn-NOTA (7.7 mg, 0.014 mmol) was added and was allowed to stir at room temperature for 24 h. The reaction was precipitated with diethyl ether, centrifuged and dried to a red powder. The reaction was first purified through RP silica using 10-35% acetonitrile in 0.1% TFA water and was purified again through HPLC. Calculated *m/z* to be 1891.22; found: 1893.0 [M+H]<sup>+</sup>. <sup>1</sup>H NMR: (5.93, s), (6.21, s, 1H), (6.39, s, 1H), (6.98, s, 1H), (7.10, s, 2H), (7.22, s, 2H)

### 6.1.9 Synthesis of Tris[(1-benzyl-1*H*-1,2,3-triazole-4-yl)methyl]amine (TBTA)

Synthesis was performed as previously reported.<sup>6</sup> Copper(II) acetate monohydrate (11.5 mg, 0.058 mmol) was dissolved in 10 mL of MeCN resulting in a bright blue mixture. Tripropargylamine (0.192 g, 1.47 mmol) and benzyl azide (2.5 mmol) were dissolved in 5 mL of MeCN then added to the copper solution. Sodium ascorbate (11.50 mg, 0.058 mmol) was dissolved in 1 mL water and added to the reaction mixture resulting in a clear solution. The reaction mixture was allowed to stir at room temperature for 30 min then was heated to 45°C for 5 h. A second portion of benzyl azide (2.5 mmol) was added and allowed to stir for an additional 24 h. The reaction mixture dried in vacuo and the product was redissolved in dichloromethane (25 mL). Concentrated NH<sub>4</sub>OH (10 mL) was added to the solution and allowed to stir until all was dissolved. The aqueous layer was extracted with dichloromethane (3 x 25 mL) and the combined organic layers were washed with NH<sub>4</sub>OH and brine (1:1 (v/v) (3 x 10 mL) then dried over MgSO<sub>4</sub> and finally filtered. The resulting solution was dried in vacuo then redissolved in dichloromethane (20 mL) and vigorously stirred while diethyl ether (35 mL) was added gradually to the solution resulting in a white precipitate. The solution was filtered and washed with diethyl ether allowing for a collection of white powder. Calculated *m/z* to be 530.6; found: 533.0 [M+H]<sup>+1</sup>

### 6.1.10 Synthesis of 1, 6-diazidohexane

Synthesis was performed as previously reported.<sup>7</sup> In brief, 1,6-dibromohexane (0.0048 mol, 1 eq.) was added to a 9:1 (v/v) solution of DMF/H<sub>2</sub>O. NaN<sub>3</sub> (0.014 mol, 3 eq.) was added and stirred 24 h at 80°C. The reaction mixture was cooled to room temperature and was extracted 4x



with 20 mL diethyl ether. The organic layers were combined and dried over  $\text{MgSO}_4$ , filtered, and concentrated under reduce pressure to obtain a clear liquid. Yield: 90%, based on 1,6-dibromohexane.  $^1\text{H NMR}$ : (3.20, t, 1H), (1.54, m, 1H), (1.33, m, 1H).

#### 6.1.11 Synthesis of 1-amine-6-azidohexane

Synthesis was preformed as previously reported.<sup>7</sup> In brief, a 1:1 (v/v) mixture of ethyl acetate and ether (40 mL) were added to 32 mL of 2M HCl and was allowed to vigorously stir in an ice water bath for 20 min. 3.0 g (0.018 mol) of 1,6-diazidohexane was added to the solution and after 10 min 4.43g  $\text{Ph}_3\text{P}$  (0.0169mol, 0.95 eq) was added in small portions over an hour. The reaction was then removed from the ice bath and allowed to stir at room temperature for 24 h. 20 mL of water was added and the organic layer was discarded. The aqueous layer was extracted with 4x 20 mL of diethyl ether then neutralized with 3M NaOH. The aqueous layer was re-extracted with 4x 20 mL dichloromethane. The organic layer was collected and dried over  $\text{MgSO}_4$ , filtered, and concentrated under reduce pressure to yield a light yellow liquid. Yield: 50%, based on 1,6-diazidohexane starting material.  $^1\text{H NMR}$ : (3.46, t, 1H), (2.63, t,1H), (1.69, m, 2H), (1.42, m, 2H), (1.39, m, 2H)

#### 6.1.12 Synthesis of B12-desferoxamine (B12-DFO)

B12 (50 mg, 0.036 mg) was added to anhydrous DMSO under Argon atmosphere and was heated to 40°C. 1,1'-carbonyl-di-(1,2,4)-triazole (CDT) (30 mg, 0.184 mmol) was added to the solution and was allowed to stir for 2 h.<sup>2</sup> The reaction was monitored using HPLC and after 90% or more conversion, deferoxamine mesylate was added (41.75 mg, 0.023 mmol) and the reaction was

allowed to stir for another 2 h. The reaction was precipitated with methanol/diethyl ether. This reaction was purified through HPLC. Yield: 20%, based on B12 starting material.  $m/z$  to be 1942; found: 972  $[M+2H]^{+2}$  and 648  $[M+3H]^{+3}$ .  $^1H$  NMR: (5.98, s, 1H), (6.21, s, 1H), (6.42, s, 1H), (7.01, s, 1H), (7.17, m, 1H).

#### 6.1.13 B12-Exendin-4-Cyanine-5 (B12-Ex4-Cy5) synthesis

B12-Ex4 was synthesized as previously described.<sup>8</sup> B12-Ex4 (0.5 mg, 0.0001mmol) was dissolved in PBS buffer pH 7.6 (450  $\mu$ L) and then Sulfo-cyanine5-NHS-ester (1 mg, 0.001mmol) was added (in 50  $\mu$ L DMSO). The resulting solution was allowed to mix for 2h at room temperature, protected from light, and then purified through RP-HPLC on a Shimadzu Prominence HPLC using a C18 column (Eclipse XDB-C18 5  $\mu$ m, 4.6 x 150 mm). Solvents: A: 0.1% TFA water and B: Acetonitrile. Method: B%: 1-70% over 15 min.  $t_R$ : 12.1 min. Yield: 98%, based on B12-Ex4 starting material. LC-MS analysis showed the indication of B12-Ex4-Cy5 with 1 and 2 Cy5 molecules with an expected  $m/z$  of 6284 (M1; B12-Ex4+Cy5) or 6923 (M2; B12-Ex4+2xCy5). Excitation and emission profile of 648 and 670 nm, respectively

#### 6.1.14 B12-Cyanine5 (B12-Cy5) synthesis

B12-Cy5 was synthesized through Huisgen/Sharpless 'Click' Chemistry.<sup>3,4</sup> Cu(I) (1 mg, 0.005 mmol) and TBTA (3.5 mg, 0.006 mmol) were dissolved in 0.5 mL DMF/H<sub>2</sub>O (4:1 v/v). Once color change occurred, the previously synthesized B12-Azide (3 mg, 0.002 mmol) (32) and cyanine5 alkyne (0.5 mg, 0.0007mmol) (Lumiprobe) was dissolved in the solution and allowed to stir at room temperature overnight protected from light. This was purified through RP-HPLC

on a Shimadzu Prominence HPLC using a C18 column (Eclipse XDB-C18 5  $\mu$ m, 4.6 x 150 mm). Solvents: A: 0.1% TFA water and B: Acetonitrile. Method: B%: 20-72% over 18 min.  $t_R$ : 4.7 min. Yield: 94%, based on B12 starting material. LC-MS showed 688  $[M+3H]^{+3}$ , 1031  $[M+2H]^{+2}$  with the expected  $m/z$  of 2059. Emission and excitation of 645 and 682 nm, respectively.

#### 6.1.15 B12-carboxylic acid (B12-CA) Synthesis

B12-CA was synthesized as previously described.<sup>9</sup> B12 (100.00 mg, 0.0737mmol) was fully dissolved in DMSO. IBX (53.70mg, 0.191mmol) and HYP (35.10 mg, 0.369mmol) were added. The reaction was stirred at 60°C for 2 h. It was purified through anion exchange. The product was dried to a red powder (12 mg, 12% yield). Calculated  $m/z$  to be 1344.0; found: 1345.8.

#### 6.1.16 Synthesis of B12-aminobutyne (B12-AB)

B12-AB was synthesized as previously described.<sup>8</sup> B12-CA (10 mg, 0.00729 mmol), EDC (14 mg, 0.0731 mmol), and HOBt (19.7 mg, 0.1462 mmol) were mixed in 5 mL anhydrous DMSO for 30 min under argon. To this activated mixture, 1-amino-3-butyne (5.99  $\mu$ L, 0.0731 mmol) was added, and the reaction mixture was stirred for 16 h at rt. The crude reaction was purified via RP-HPLC using a gradient of 10% MeCN, 90% H<sub>2</sub>O/0.1% TFA, increased to 27% MeCN over 17 min, with a flow rate of 1.0 mL/min and UV detection at 360 nm;  $R_t$ = 12.1 min. Yield was 79-80%, based on B12 starting material. LC-MS expected  $m/z$  1421, found  $m/z$  711 $[M]^{+2}$ . <sup>1</sup>H NMR (400 MHz, D<sub>2</sub>O): 7.21 (s, 1H), 7.002 (s, 1H), 6.92 (s, 2H), 5.99 (s, 1H).

#### 6.1.17 Synthesis of B12-Exendin-4 (B12-Ex4)

B12-Ex4 was synthesized as previously described.<sup>8</sup> Cu(I) (1 mg, 0.005 mmol) and TBTA (3.5 mg, 0.006 mmol) were dissolved in 0.5 mL DMF/H<sub>2</sub>O (4:1 v/v). Once color change occurred, the previously synthesized B12-AB (3 mg, 0.002 mmol) (32) and azido-exendin-4 (1 mg, 0.0002 mmol) was dissolved in the solution and allowed to stir at room temperature overnight and then purified through RP-HPLC, solvents: A: 0.1% TFA water and B: Acetonitrile. Method: B%: 1-70% over 15 min. R<sub>t</sub>: 12.1 min. Yield: 98%, based on B12 starting material. Expected m/z 5658, observed m/z 1415[M]<sup>+4</sup>.

#### 6.2 General Radio-Chemistry Materials and Methods

All animal handling and manipulations were conducted in accordance with the guidelines set by WSU Animal Care and Use Committee (IACUC) and Research Animal Resource Center. Breast cancer cells (MDA-MB-453) were obtained from the American Type Culture Collection (ATCC). Charcoal stripped Fetal bovine serum (FBS) and Dulbecco's modified eagles medium (DMEM) were purchased from Sigma and KD medicals, respectively. Penicillin-streptomycin solution with 10,000 units penicillin and 10 mg/mL streptomycin in 0.9% NaCl was obtained from Corning. MALDI imaging was completed on a MALDI-TOF (Bruker Ultraflex). Analysis of the radiotracer was done using instant thin layer chromatography (iTLC, Eckert & Ziegler Mini Scan), respectively. An EDTA (50 mM) mobile phase was used for instant thin layer chromatography (iTLC). PET imaging was done using a  $\mu$ PET scanner (Concord).

### 6.2.1 Binding of radio-B12 to IF

A 1:0.8 ratio was used for IF:compound. The radiolabeled compound (unpurified) was mixed with IF for 30 min at RT then purified through a size exclusion spin filter (30 kDa) volume was adjusted with saline solution.

### 6.2.2 Intrinsic Factor and $^{99m}\text{Tc}$ -B12 Binding Study

10  $\mu\text{L}$  intrinsic factor (20  $\mu\text{M}$ ) and 10  $\mu\text{L}$  B12-PG (20  $\mu\text{M}$ ) were mixed at room temperature and allowed to react for up to 3 h. At each time point 20  $\mu\text{L}$  was taken out of the reaction mixture and was ran down a size exclusion column on the HPLC (Zorbax GF-250, 4  $\mu\text{m}$ , 4.6 x 250 mm) with a 20 mM sodium phosphate and 300 mM NaCl elution buffer (pH 7).

### 6.2.3 Radiolabeling of B12-PG with $^{99m}\text{Tc}(\text{I})$ ( $^{99m}\text{Tc}$ -B12)

B12-PG ( $1.9 \times 10^{-4}$  M) was reacted with  $^{99m}\text{Tc}(\text{I})$  (1 eq) at  $40^\circ\text{C}$  for 30 min at pH 7. Reaction was monitored and purified through RP-HPLC (gamma detection). Yield: 99%, based on HPLC.

### 6.2.4 Radiolabeled $^{99m}\text{Tc}$ -B12 Stability/Challenge Study

$^{99m}\text{Tc}$ -B12 was re-synthesized as mentioned previously, purified and lyophilized down. It was reformulated in a solution of either: saline, saline with histidine, and saline with cysteine at either  $10^{-5}$  M or  $2 \times 10^{-3}$  M and monitored at time points through RP-HPLC.

### 6.2.5 Radiolabeling of B12-NOTA

5 mCi of  $^{64}\text{Cu}$  to 25  $\mu\text{g}$  of compound in ammonium acetate buffer pH 5.5 in 200  $\mu\text{L}$  and allowed to sit at RT for 30 mins. SA was determined by iTLC on reverse phase silica plates using 50 mM EDTA in ammonium acetate buffer.

### 6.2.6 Mouse TCII and human gastric IF Binding to Zr-B12

Mouse TCII or human gastric IF binding of cold  $^{91}\text{Zr}$ -B12 was confirmed by radiometric chase assay using  $^{57}\text{Co}$ -labeled B12 and compared to free B12 as cyano-cobalamin.<sup>10</sup> Significant mouse TCII binding of  $^{91}\text{Zr}$ -B12 (6.8 nM) was maintained in comparison from unmodified B12 (0.12 nM).

### 6.2.7 $^{89}\text{Zr}$ -radiochemistry with B12-DFO

Optimum conditions for radio labeling of B12-DFO were tested by titrating with  $^{89}\text{Zr}$  and analyzing the incubated solution using iTLC.<sup>11</sup> Optimum labeling activity was found to be  $250 \pm 50$  mCi/ $\mu\text{mol}$ . Approximately 1 mCi (37 MBq) of  $^{89}\text{Zr}(\text{C}_2\text{O}_4)_2$  (3D imaging, AZ) was diluted with 0.9% saline and the pH was adjusted to 7–7.5 by adding 1 M  $\text{Na}_2\text{CO}_3$ . A solution of B12-DFO (0.004  $\mu\text{mol}$ , 10.8  $\mu\text{g}$ ) was added to the pH adjusted  $^{89}\text{Zr}$  solution and incubated for 20 min at ambient temperature. Radio labeling efficiency of >97% was determined by iTLC.

### 6.2.8 Synthesis of Zr-B12

B12-DFO (0.25 mg) was dissolved in Na<sub>2</sub>CO<sub>3</sub> solution (0.5 mL) with ZrCl<sub>4</sub> (1 eq.) for 30 min. Binding was confirmed through HPLC.

### 6.2.9 In vitro stability of <sup>89</sup>Zr-B12 and IF-<sup>89</sup>Zr-B12

Stability of <sup>89</sup>Zr-B12 was tested by incubating the tracer (200 μCi, 100 μl) in saline (0.9 % NaCl) and 50% (1:1 serum/saline) human serum (Sigma) at 37 °C and fractions (50 μCi) were analyzed for free <sup>89</sup>Zr at 4, 24, and 48 h intervals using iTLC (Eckert & Ziegler Mini Scan). Samples incubated in serum were filtered using molecular weight cutoff (MWCO 30 KDa, Amicon) filter prior to the analysis.

### 6.2.10 Cell lines and small animal xenografts

For imaging and in vivo uptake experiments, female nude mice (Envigo) were kept under B12 deficient diet (Teklad B12 free custom diet, Envigo) for three weeks. Cells were subcutaneously implanted on the shoulder with MDA-MB-453 breast cancer cells ( $5 \times 10^6$  cells/mouse) after two weeks of B12 free diet. Cells were injected in media/matrigel (Corning LLC) 1:1 mixture of 200 μl after anesthetizing the mice with 1-2% Isoflurine (Baxter). The tumor volume until was calculated using the formula  $\text{Length} \times \text{width}^2 \times \frac{1}{2}$ . Mice with tumors 100-200 mm<sup>3</sup> were used for imaging experiments.

### 6.2.11 PET imaging experiments

$^{89}\text{Zr}$ -B12 was intravenously administered (5.4–6.8 MBq/mouse, 0.8–1 nmol) in sterile saline in mice bearing MDA-MB-453 xenografts. PET imaging was done using a  $\mu\text{PET}$  scanner (Concord) at 4, 24, and 48 h post injection time points. The mice were fully anesthetized using 1–2% Isoflurine during imaging time period (10 or 15 min. scans). Images were reconstructed using filtered back projection algorithm. ASIPro VMTM software package (Concord) was used to draw volume of interest and calculate %ID/g values. Competitive inhibition experiment was done by co-injecting ~200-fold excess of the cold tracer (200 nmol).

### 6.2.12 Ex-vivo distribution and competitive saturation

The tissue distribution of  $^{89}\text{Zr}$ -B12 was studied by administering 10–25  $\mu\text{Ci}$  (0.04–0.1 nmol) of the tracer on the lateral tail vein of the rodent. For the competitive saturation assay, ~20 nmol/mouse of cold B12 was co-injected with  $^{89}\text{Zr}$ -B12. Euthanasia was performed with  $\text{CO}_2$  asphyxiation was performed at 4, 24, and 48 h post injection.

### 6.2.13 Immunohistochemistry of MDA-MB-453 cells and Tumors

Excised tumors were embedded in OCT (optimum cutting temperature) media and were sliced to 10  $\mu\text{m}$  thin slices using a cryomicrotome at  $-30\text{ }^\circ\text{C}$  and placed on a super frost glass slide (Fisher) and stored at  $-80\text{ }^\circ\text{C}$ , until radioactivity was completely decayed (3 weeks). The fixed tissue sections with precooled acetone ( $-20\text{ }^\circ\text{C}$ ) by immersing the sections for 10 min. Sections were washed twice with 1x PBS (100 mL, 5 min each wash) and were then incubated in 0.3%



H<sub>2</sub>O<sub>2</sub> for 10 min followed by washing step with 1x PBS twice. Sections were then incubated with 100 µL of FBS in PBS (10%) in a humidified chamber at ambient temperature for 1h. Excess FBS was rinsed out and added 1: 100 diluted anti-rabbit polyclonal primary antibody (Abcam, MA) and incubated overnight at 4 °C in a humidified chamber. Sections were washed twice with 1x PBS and added 100 µl of 1:1000 diluted anti-goat polyclonal secondary antibody (Abcam, MA) that was conjugated to Alexa Flour 488 (AF488). Sections were incubated another 30 min with the secondary in the humidified chamber prior to adding drop of anti-fade solution mix with DAPI. Slides were covered with a glass slide and kept at 4°C covered in foil until imaged using Fluorescence microscope (Nikon E800) with 2x power for whole tumor images and 40x for individual areas.

### 6.3 General Cell Methods and Materials

All *in vitro* cell studies were performed in a Labconco Purifier I laminar flow hood disinfected with 70 % ethanol and sterilized with UV light. Fetal bovine serum (FBS) was purchased from VWR. Penicillin-streptomycin solution with 10,000 units penicillin and 10 mg/mL streptomycin in 0.9% NaCl was obtained from Thermo Fisher. DMEM with high glucose, F12-K media was purchased from VWR. Hybri-Care 45-x media was purchased from ATCC. Epidermal growth factor (EGF) was purchased from Sigma. 0.05 % Trypsin with 0.53 mM EDTA was supplied by Thermo Fisher. The J774A.1, CHO-K1, FH-74 Int. cell lines were purchased from ATCC. HEPG2 cell line was purchased from ATCC. HEK-293 (GLP-1R) cells were made previously in the Holz lab.<sup>8</sup> BN16 cells were a gift from Dr. Mette Madsen, University of Aarhus, Demark.

J774A.1 and BN16 were cultured as adherent monolayers in DMEM supplemented with 10 % FBS and 1 % pen/strep. CHO-K1 were cultured as adherent monolayers in F12-K supplemented with 10 % FBS and 1 % pen/strep. Fh-74 Int. cells were cultured as adherent monolayers in Hybri-Care 43-x supplemented with 10 % FBS, 1 % pen/strep and 30 ng/mL of EGF. HEK-GLP-1R were cultured as adherent monolayers in DMEM supplemented with 10 % FBS and 1 % pen/strep and 0.1% geneticin. Cells were incubated at 37 °C with 5 % CO<sub>2</sub>.

In vitro plate assays were completed using a Molecular Devices FlexStation III running SoftMaxPro software. A dose response curve was generated by plotting the log of the concentration (M) versus the absorbance using Prism GraphPad 6. Each point for each concentration was at least completed in triplicate.

### 6.3.1 IF Binding to B12-Cy5

B12-Cy5 was bound by IF (0.85 nm to 0.1 nm, respectively) by mixing in HBSS at 4 °C overnight.

### 6.3.2 Flow Cytometry Analysis Using B12-Cy5

Cells were plated at 30,000 cells/well on a 6-well plate and allowed to adhere 24-48 h. Cells were washed 3x with HBSS and then incubated with IF-B12-Cy5 or TCII-B12-Cy5 in 1 mL of 100-500 nM for 1-2 h. Cell were either stripped mechanically or with trypsin. Cells were placed in 1 mL of media and analyzed within 30 min. All cells were excited at 640 nm and detected at 660/20 nM.

### 6.3.3 GLP-1 assay for Cy5-B12-Ex4, Cbi-Ex4 and HC-Cbi-Ex4

Agonism at the GLP-1 receptor was monitored using HEK-293 cells stably transfected with the GLP-1 receptor. Cells were plated on a rat-tail-collagen-coated 96-well plate at 60,000 cell/well and allowed to adhere. The cells were infected with an adenovirus to express the H188 FRET reporter using a 25 MOI for 16-20 h in 75  $\mu$ L of DMEM-1% FBS. After the virus incubation the cells were placed in 200  $\mu$ L standard extracellular matrix with glucose and 0.1% BSA. Conjugates were added to each well at 5x the required concentration. Agonism was determined through an increase in 485/553 nm FRET ratio that indicates cAMP level increase through cAMP binding to an EPAC (exchange protein directly activated by cAMP).<sup>12</sup>

### 6.3.4 Immunohistochemical procedures for the mouse brain

Adult male Sprague Dawley rats were purchased from Charles River. Animals were singly housed in hanging wire mesh cages under a 12h:12h light/dark cycle in a temperature- and humidity-controlled environment. Standard rodent chow (Purina 5001) and tap water were available *ad libitum*. Procedures were approved by the Institutional Care and Use Committee of the University of Pennsylvania, a copy of which was filed with Syracuse University. Rats (275-300g; n=4 per group) were given IP injection of fluorophore-labeled Ex-4 [Flex; 5ug/kg; 0.0001nM; AnaSpec<sup>13</sup>], Cy5-B12-Ex4 (5ug/kg; 0.03nM) Cy5-B12 (5ug/kg) or Cy5-B12-Ex4 delivered at an equimolar dose to Flex (0.0001nM). Three hours after injection, rats were transcardially perfused using 0.1M PBS followed by 4% paraformaldehyde (PFA). The brains were collected and maintained overnight in 4% PFA. Subsequently, the brains were transferred

to 20% sucrose in PBS for 24h. Brains were cut into 30  $\mu\text{m}$  coronal section on a cryostat (Leica) and stored in cryoprotectant until processing for immunohistochemistry.

Free-floating hindbrain sections were collected at the level of the area postrema (from bregma, AP -13.0 to -14.8 mm) and hypothalamus (from bregma, AP 0.0 to -3.5 mm). Briefly, sections were washed in 50% EtOH and subsequently incubated for 20 minutes in 1% sodium borohydride. After blocking of endogenous peroxidase, sections were incubated in immunoblocking buffer (5% normal donkey serum and 0.2% Triton-X in PBS) for 1h. Primary antibodies were applied as a cocktail that included mouse anti-NeuN (1:1000, Millipore) and rabbit anti-GFAP (1:2000, DAKO). After overnight incubation at 4° C, the sections were washed in PBS and incubated for 2h with fluorescent secondary antibodies, also applied as a cocktail: Alexa Fluor 594 donkey anti-mouse and donkey anti-rabbit Alexa Fluor 647 or donkey anti-rabbit Alexa Fluor 488 (1:500 for all antibodies; Jackson ImmunoResearch). Then, sections were subsequently rinsed in PBS, mounted, and coverslipped with DAPI mounting medium.

### 6.3.5 Confocal imaging of mouse brain slices

Sections were visualized with a Leica SP5 X confocal microscope using the 20x dry- and 63x oil-immersion objectives and the 405, 488, 633 and 594 laser lines. Each laser channel was separately scanned using a multitrack PMT configuration to avoid cross-talk between fluorescent dyes or any cross-reactivity between secondary antibodies. To evaluate double-labeling, z-stack sectioning was performed at 0.5-1  $\mu\text{m}$  intervals using 20x dry or 63x oil-immersion objectives. Images were acquired using the Zeiss LSM software, cropped and optimized in Fiji (Image J version 2.0.0).

### 6.3.6 Western Blot Conditions for Cubilin and Megalin

SDS-page gels (6%) were run at 125 v, and 45 amps. Transfer occurred on a BioRad Trans-Blot Turbo Transfer System on a PVDF membrane. Membrane was blocked in PBST with milk overnight at 4°C. Primary antibody was incubated for 24 h at 4°C in PBST with milk then washed 6x 5 min. Secondary antibody was incubated (1:2000) in PBST for 1 h and washed 6x 5 min. Membrane was then viewed by chemiluminescence X-ray exposure. Cubilin primary antibody (Santa Cruz) was incubated at 1:100 dilution. Megalin primary antibody (a gift from Dr. Mette Madsen) was incubated at 5 µg/mL.

### 6.3.7 Western Blot Conditions for HC and TCII in Shrew Blood

SDS-page gel (12%) was run at 125 volts and 45 amps. Transfer occurred on an iBlot system on a nitrocellulose membrane. Membrane was blocked in PBST with milk for 1 h. Primary antibody was incubated overnight at 4°C in PBST with milk then washed 6x 5 min. Secondary antibody was incubated (1:2000) in PBST for 1 h and washed 6x 5 min. Membrane was then viewed by chemiluminescence X-ray exposure. HC primary (Abcam) was incubated at 2 µg/mL and TCII (Santa Cruz) was incubated at a 1:100 dilution.

## 6.4 General Guinea Pig Materials and Methods

All animal handling and manipulations were conducted in accordance with the guidelines set by Syracuse University Animal Care and Use Committee (IACUC) and Research Animal

Resource Center. Ketaset from Henry Schein (Syracuse, NY). Xylazine and Kanamycin sulfate ( $\geq 98\%$ ) was from Sigma. Atipamezole was purchased from Sigma ( $\geq 98\%$ ). Pigmented male guinea pigs initially weighing 200-300 g (Elm Hill Labs, Chelmsford, MA) were maintained on a Lab Diets Certified Guinea Pig Diet 5026 and given free access to water. Animals were allowed 3-4 days of acclimation before studies begun.

#### 6.4.1 Kanamycin and IF Injections

Two separate studies were completed: First, 4 guinea pigs were selected and given kanamycin sulfate (250 mg/kg/day) for 23 days in sterile saline solution via IP. Second, 4 guinea pigs were selected and given kanamycin sulfate (250 mg/kg/day) with a pre-injection of holo-IF (6.25  $\mu\text{g}$ , 15 min before kanamycin) and a post-injection of IF (6.25  $\mu\text{g}$ , 30 min after kanamycin) all injections in sterile saline and IP. Guinea pigs were weighed each day for appropriate dosing.

#### 6.4.3 Anesthesia Protocol for Pigmented Guinea Pigs

A combination anesthetic cocktail of ketamine/xylazine (55 mg/kg and 5 mg/kg via IP, respectively) was injected. After sufficient sedation was observed (about 10-15 min) the ABR's were performed. During this time guinea pig blood flow and breathing rates were monitored. After ABR's were completed atipamezole (1 mg/kg via IM) was administered and guinea pigs were monitored continuously until full recovery. After administration of the anesthesia, and until recovered, guinea pigs were placed on heated pads to maintain body temperature.

#### 6.4.4 Auditory Brainstem Response Hearing Tests

Auditory Brainstem Responses (ABRs) were recorded using the Biologic AEP system to determine auditory thresholds. Thresholds were obtained for each animal preceding administration of treatment, during treatment, and for up to 6 weeks p.i. Animals were anesthetized prior to ABR recordings by IP injections of ketaset (50mg/kg) and xylazine (5 mg/kg). ABRs were generated to a click, 6 kHz and 8 kHz tonebursts, of rarefaction polarity, at a rate of 27.7 per second. Filter settings were set to 100 Hz-3000 Hz with a gain of 100,000. Roughly 350 sweeps were collected for each waveform; less sweeps were obtained in cases of clearly identifiable waveforms. A one channel vertical montage was set up using disposable, subdermal needle electrodes placed SC; inverting M1 and M2 (posterior to pinna), non-inverting CZ, and common on the rump. Waveforms were obtained at 10 dB intervals until no ABR was present or until -10 dBnHL. Thresholds at each frequency were defined as the lowest intensity to yield a reproducible deflection in the evoked response trace and verified at least twice. Threshold shifts were calculated for individual animals by comparison to their pre-treatment thresholds.

#### 6.4.5 Guinea Pig IF Antibody ELISA Kit

A commercial ELISA kit was used (Tecan) to screen blood serum from guinea pigs with small modifications. The recognizing antibody was changed to IgG guinea pig HRP (Santa Cruz), used at a 1:5000 dilution; everything else was performed at manufacture protocol.

## 6.5 References

- (1) Chromiński, M.; Gryko, D. “Clickable” Vitamin B12 Derivative. *Chem. – Eur. J.* **2013**, *19* (16), 5141–5148.
- (2) Synthesis and Biological Activity of Ribose-5'-Carbamate Derivatives of Vitamin B12. *Bioconjug. Chem.* **1999**, *10*, 1131–1136.
- (3) Huisgen, R. 1,3-Dipolar Cycloadditions. Past and Future. *Angew. Chem. Int. Ed. Engl.* **1963**, *2* (10), 565–598.
- (4) Kolb, H. C.; Finn, M. G.; Sharpless, K. B. Click Chemistry: Diverse Chemical Function from a Few Good Reactions. *Angew. Chem. Int. Ed.* **2001**, *40* (11), 2004–2021.
- (5) Ikotun, O. F.; Marquez, B. V.; Fazen, C. H.; Kahkoska, A. R.; Doyle, R. P.; Lapi, S. E. Investigation of a Vitamin B12 Conjugate as a PET Imaging Probe. *ChemMedChem* **2014**, *9* (6), 1244–1251.
- (6) Hein, J. E.; Krasnova, L. B.; Iwasaki, M.; Fokin, V. V. Cu-Catalyzed Azide-Alkyne Cycloaddition: Preparation of Tris((1-Benzyl-1H-1,2,3-Triazolyl)methyl)amine. In *Organic Syntheses*; John Wiley & Sons, Inc., 2003.
- (7) Coutrot, F.; Busseron, E. Controlling the Chair Conformation of a Mannopyranose in a Large-Amplitude [2]Rotaxane Molecular Machine. *Chem. - Eur. J.* **2009**, *15* (21), 5186–5190.
- (8) Bonaccorso, R. L.; Chepurny, O. G.; Becker-Pauly, C.; Holz, G. G.; Doyle, R. P. Enhanced Peptide Stability Against Protease Digestion Induced by Intrinsic Factor Binding of a Vitamin B12 Conjugate of Exendin-4. *Mol. Pharm.* **2015**, *12* (9), 3502–3506.
- (9) Clardy-James, S.; Bernstein, J.; Kerwood, D.; Doyle, R. Site-Selective Oxidation of Vitamin B12 Using 2-Iodoxybenzoic Acid. *Synlett* **2012**, *23* (16), 2363–2366.
- (10) Stupperich, E.; Nexø, E. Effect of the Cobalt-N Coordination on the Cobamide Recognition by the Human Vitamin B12 Binding Proteins Intrinsic Factor, Transcobalamin and Haptocorrin. *Eur. J. Biochem.* **1991**, *199* (2), 299–303.
- (11) Perk, L. R.; Vosjan, M. J. W. D.; Visser, G. W. M.; Budde, M.; Jurek, P.; Kiefer, G. E.; Dongen, G. A. M. S. van. P-Isothiocyanatobenzyl-Desferrioxamine: A New Bifunctional Chelate for Facile Radiolabeling of Monoclonal Antibodies with Zirconium-89 for Immuno-PET Imaging. *Eur. J. Nucl. Med. Mol. Imaging* **2010**, *37* (2), 250–259.



- (12) Klarenbeek, J.; Goedhart, J.; van Batenburg, A.; Groenewald, D.; Jalink, K. Fourth-Generation Epac-Based FRET Sensors for cAMP Feature Exceptional Brightness, Photostability and Dynamic Range: Characterization of Dedicated Sensors for FLIM, for Ratiometry and with High Affinity. *PLoS ONE* **2015**, *10* (4).
- (13) Hayes, M. R.; De Jonghe, B. C.; Kanoski, S. E. Role of the Glucagon-Like-Peptide-1 Receptor in the Control of Energy Balance. *Physiol. Behav.* **2010**, *100* (5), 503–510.

## Chapter 7: Current and Future Work

### 7.1 Using Systemically Administered IF-B12 to Detect Cubilin Positive Tumors

As discussed in Chapter 3, in vivo intravenous injection of  $^{89}\text{Zr}$ -IF shows a clear shift from kidney to liver uptake (for more detail see Chapter 3, Section 3.4). This established control, showing limited uptake in tissues, now allows for the investigation  $^{89}\text{Zr}$ -IF as a way to detect a CUBN positive tumor. To explore rIF as a probe to detect CUBN positive tumors a new cell line, BN16 cells, will be used as a tumor model. BN16 cells are the gold standard for in vitro CUBN experiments.<sup>1,2</sup> In Chapter 4, BN16 cells demonstrate a clear increase in uptake when IF-B12-Cy5 is administered at low doses compared to the controls (see Chapter 4, Section 4.2.1). However, BN16's have yet to be xenographed into animal models.

Initially BN16 cells will be investigated as a valid tumor xenograph by injected cells under the skin of nude athymic female mice. Once tumor growth has been established rIF will be injected as previously described in Chapter 3 with imaging and biodistribution completed. This will establish rIF as an imaging tool to detect metastasized kidney cancer.

### 7.2 Using Haptocorrin Binding Substrates to Increase Peptide Half-life

HC is a B12 transport protein found both in the GI track and the blood serum in humans (for more detail refer to Chapter 1, Section 1.1.4.1). HC role in the blood serum is unknown as there is no known receptor that recognizes and internalizes it.<sup>3,4</sup> This lack of receptor recognition leads to HC half-life to be ~9 days in humans as opposed to TCII being within minutes (as it is recognized by the CD320 receptor expressed on proliferating cells).<sup>3,5,6</sup> Also HC binds to “incomplete” B12 analogs, namely B12 analogs lacking the dimethylbenzimidazole group

located on the f-side chain (refer to Figure in Chapter 1), a unique trait of HC compared to that of TCII and IF.<sup>5,7</sup>

Short half-life is a crucial challenge for therapeutic peptides. Peptides as therapeutics offer increased specificity, potency and reduce side effects compared to synthesized small molecule chemical drugs.<sup>8</sup> However, peptides have a susceptibility to be digested by enzymes and cause antigenicity.<sup>8,9</sup> To combat this peptides can be changed by chemical modification or exchanging labile amino acids to increase its half-life and therefore creating a better pharmacokinetic profile.<sup>8,10,11</sup>

The hypothesis for this work is that a cobinamide (Cbi) - peptide conjugate when injected into the blood would be bound by HC and would retain HC's long half-life and therefore the peptide would have better pharmacokinetic profile. The rationale for this project is that 1) HC will bind Cbi and remain in the blood for ~ 9 days and 2) Doyle *et al.* have shown that B12 transport proteins offer peptide protection from degradation.<sup>3,5,12</sup> The peptide of interest for this project is Ex4 (for more detail refer to Chapter 1, Section 1.5.2) as Ex4's and B12-Ex4 pharmacokinetic profile have been previously explored.<sup>12,13,14</sup>

### 7.2.1 Design, synthesis and characterization of Cobinamide Peptide Conjugates

The synthesis of Cbi-alkyne was completed in collaboration with Dr. Dorota Gryko's lab at the Polish Academy for Sciences in Warsaw, Poland.



The author visiting the Institute of Organic Chemistry at the Polish Academy of Sciences, Warsaw, Poland, to study B12 chemistry for one month, in Prof. Dorota Gryko's group.

Cobinamide-exendin-4 (Cbi-Ex4) was synthesized by conjugating off of the secondary alcohol on the f-side chain located on Cbi. The alcohol was activated with CDT at 40 C for 1 h in triethylamine then aminobutyne was added and the reaction was allowed to stir for another two hours resulting in the synthesis resulting in Cbi-alkyne with a yield of ~80% (Figure 1). Cbi-alkyne was purified through on an RP-column and is shown in Figure 2. Two peaks are indicative of two isomers with a hydroxo-group located on the alpha and beta positions ( $\alpha$ -cyano- $\beta$ -aqua- and  $\alpha$ -aqua- $\beta$ -cyano-) causing this effect. LC-MS shows the expected m/z [M-H<sub>2</sub>O]: 1110 (Figure 2).

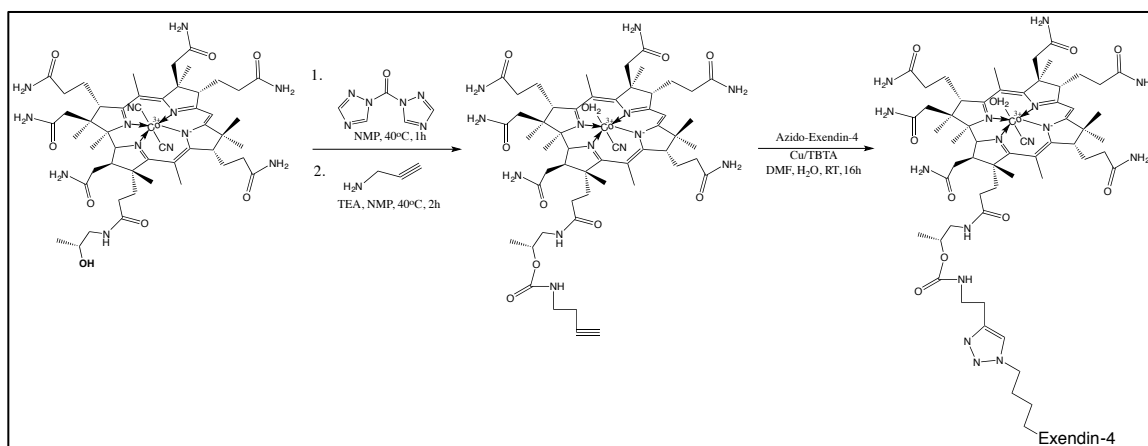


**Figure 1.** Synthetic scheme for Cbi-Ex4. Dicyano-Cbi was functionalized with a terminal alkyne through CDT activation of the secondary alcohol with subsequent addition of aminobutyne in a one-pot reaction. Once purified the Cbi-alkyne and azido-Ex4 were linked using CuAAC chemistry. Final yield of 95%, based on B12-Ex4 starting material.

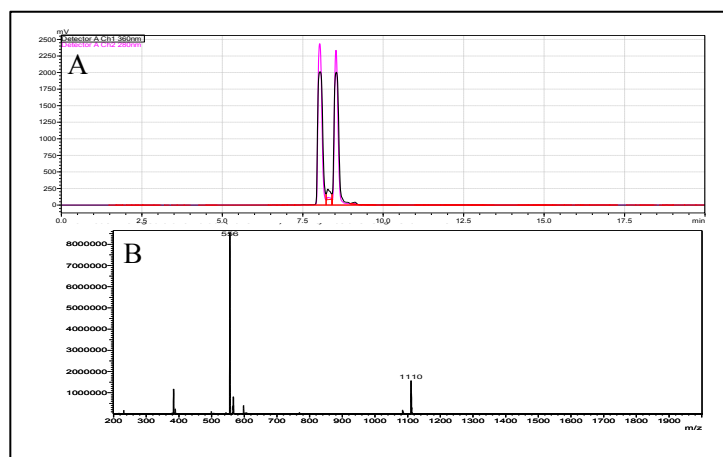


**Figure 2.** Characterization of Cbi-alkyne. A) RP-HPLC of Cbi-alkyne using an Eclipse XDB-C18 column. 0.1% TFA/H<sub>2</sub>O with MeCN gradient of 1 – 70% MeCN over 15 min,  $t_r$  = 8.0 and 8.4 min. Analysis shows compound is 97% pure. B) LC-MS: Shimadzu LCMS-8040, ESMS Expected  $m/z$  = 1129, observed  $m/z$  = 556  $[M-H_2O+2H]^{+2}$ , 1110  $[M-H_2O]^+$ .

The alkyne moiety on the Cbi primes it for the use of Huisgen/Sharpless CuAAC ‘Click’ chemistry with azido-Ex4 with Cu(I)/TBTA with a yield of ~95% (Figure 1).<sup>15,16</sup> Cbi-Ex4 was purified to  $\geq 96\%$  as shown in Figure 3. LC-MS analysis showed the expected  $m/z = 5354$ , observed  $m/z = 1338$   $[M+4H]^{+4}$ ,  $1071$   $[M+5H]^{+5}$ ,  $893$   $[M+6H]^{+6}$ .

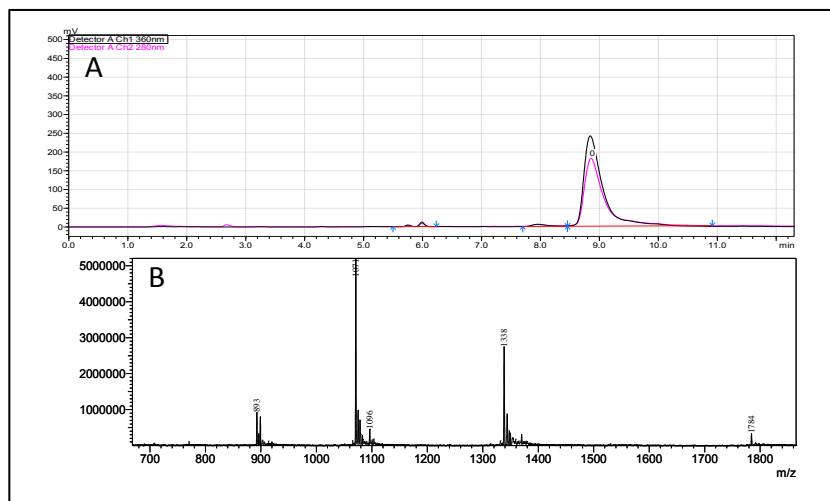


**Figure 3.** A) RP-HPLC of Cbi-Ex4 using an Eclipse XDB-C18 column. 0.1% TFA/H<sub>2</sub>O with MeCN gradient of 1 – 70% MeCN over 15 min,  $t_r = 8.9$  min. Analysis shows compound is 96% pure. B) LC-MS: Shimadzu LCMS-8040, ESMS Expected  $m/z = 5354$ , observed  $m/z = 1784$   $[M+3H]^{+3}$ ,  $1338$   $[M+4H]^{+4}$ ,  $1071$   $[M+5H]^{+5}$ ,  $893$   $[M+6H]^{+6}$ . No detection of free exendin-4 was seen.

### 7.2.2 Agonism of Cbi-Ex4 at the GLP-1 receptor

To use HC as a platform to increase peptide half-life it is imperative that we retain function of the peptide of interest. Cbi-Ex4 agonism at the Ex4 receptor, GLP-1, was explored using the FRET reporter H188 in stably transfected HEK-GLP-1 cells (as described in Chapter 1,

section 1.5.3).<sup>17</sup> Cbi-Ex4 showed dose response and pM function at the GLP-1 receptor (Figure 4 and 5). Cbi-Ex4 EC<sub>50</sub> was determined to be 120 pM (Figure 5).

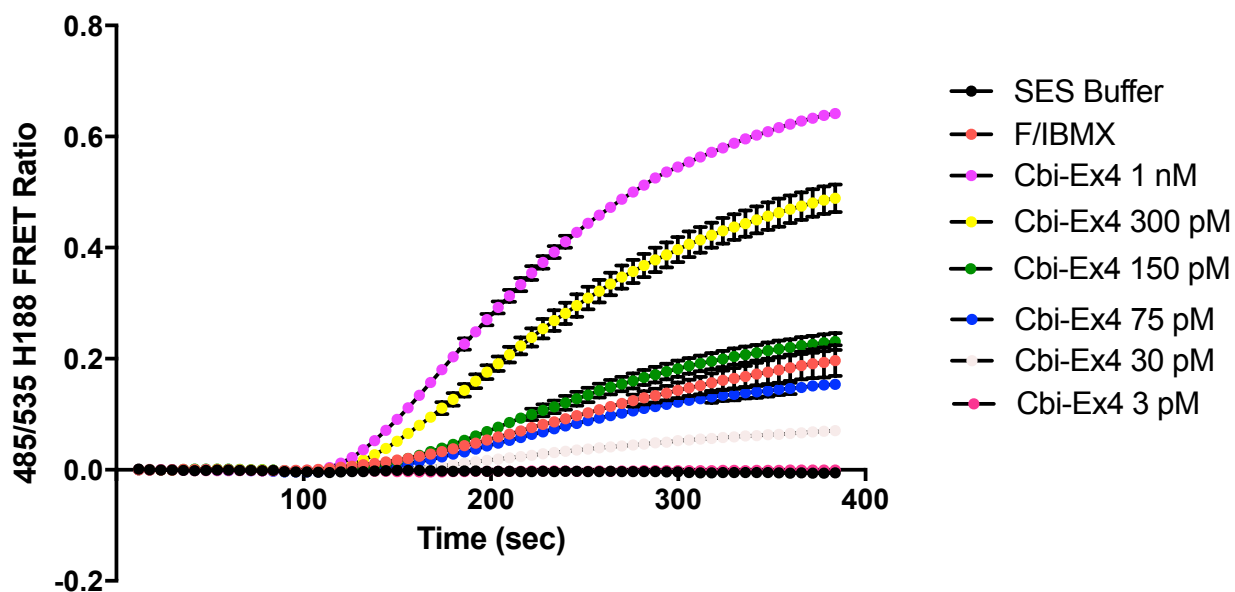


**Figure 4.** Dose response of cAMP binding to the H188 reporter in real time after administration of Cbi-Ex4 ranging from 1 nM – 3 pM. SES: standard extracellular solution with 0.01% BSA and 0.1 mM glucose. F/IBMX: forskolin and (3-isobutyl-1-methylxanthine) (IBMX) as a positive control.

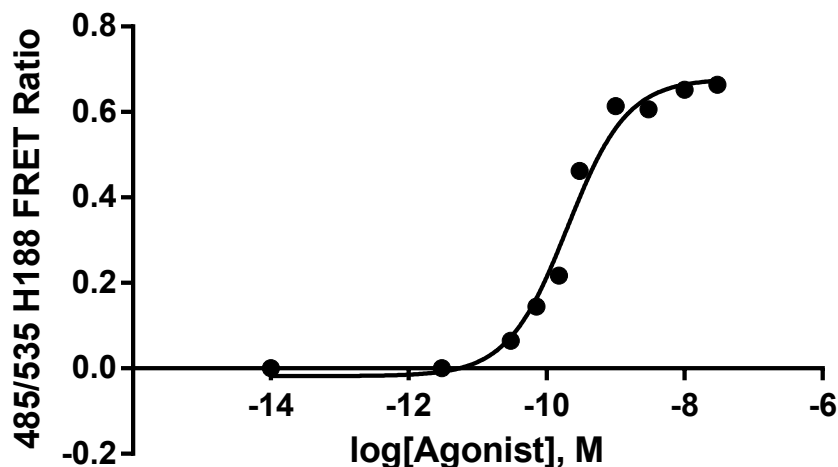


**Figure 5.** Cbi-Ex4 agonism at the GLP-1 receptor using the FRET H188 reporter in stability transfected HEK-GLP-1 cells. EC<sub>50</sub> of Cbi-Ex4 was determined to be 120 pM.

The EC<sub>50</sub> of 120 pM shows a slight loss in function as compared to Ex-4 which has been determined to be 33 pM.<sup>1218</sup> This decrease was expected as previous work from Doyle *et al.* showed that conjugation of Ex4 to B12 decreased to 68-405 pM (not all data published).<sup>12</sup> This could be due to the Cbi interacting with the peptide, causing hydrogen bonds with critical amino acids resulting in a decrease in flexibility and therefore receptor recognition and agonism as seen previously in cobalamin based peptides.<sup>19</sup> The removal of the rigid dimethylbenzylimidazole group found in B12 and not in Cbi would bring the peptide closer to the corrin ring, allowing for these hydrogen bonds to form and decrease in agonism to be observed.

### 7.2.3 Agonism of HC-Cbi-Ex4 at the GLP-1 receptor

Once Cbi-Ex4 activity at the GLP-1 receptor was determined, investigating agonism once bound by HC was warranted. Once injected Cbi-peptide will be bound by HC in the blood serum allowing for the increased half-life but its essential for the peptide to retain function at its



receptor once bound. HC was bound to Cbi-Ex4 overnight at 4°C in SES with 0.01% BSA at a 1.2:1 ratio (HC:Cbi-Ex4) to ensure there was no unbound Cbi-Ex4. HC-Cbi-Ex4 agonism at the GLP-1 receptor was determined using the FRET reporter H188 in stably transfected HEK-GLP-1 cells (as described in Chapter 4, Section 4.4.3). HC-Cbi-Ex4 showed a dose response as shown in Figure 6.

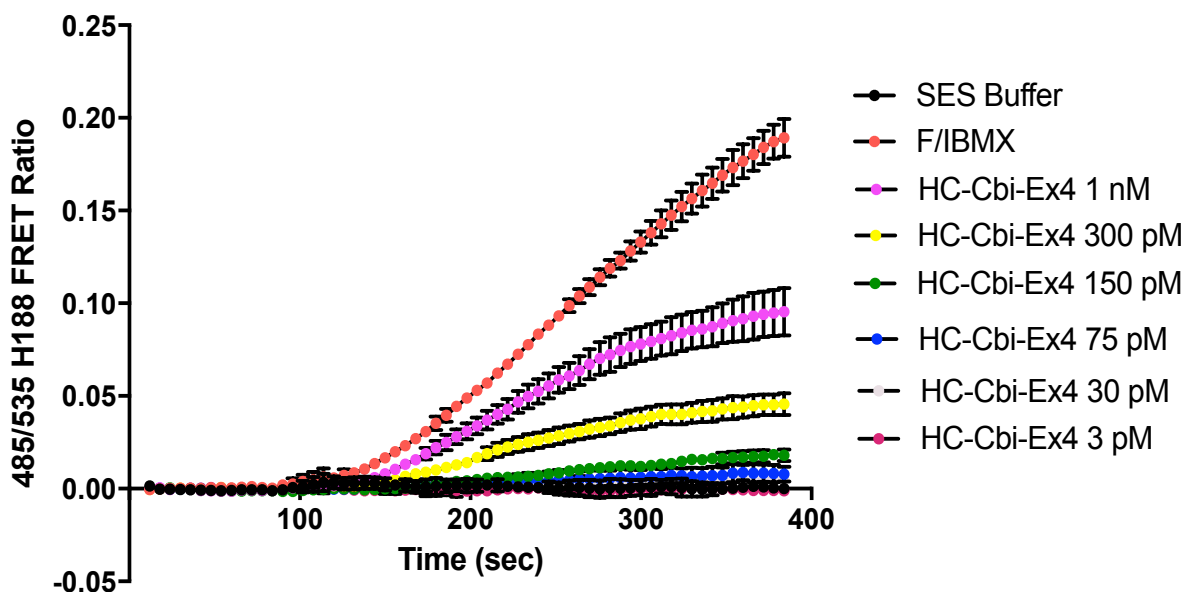


**Figure 6.** Dose response of cAMP binding to the H188 reporter in real time after administration of HC-Cbi-Ex4 ranging from 1 nM – 3 pM. SES: standard extracellular solution with 0.01% BSA and 0.1 mM glucose. F/IBMX: forskolin and IBMX as a positive control.

Comparing the dose response from Figure 4 to Figure 6, which has the same range in administration of the compounds, shows a significant decrease in response once Cbi-Ex4 is bound by HC. The  $EC_{50}$  of HC-Cbi-Ex4 was determined to be 3 nM, presented in Figure 7.

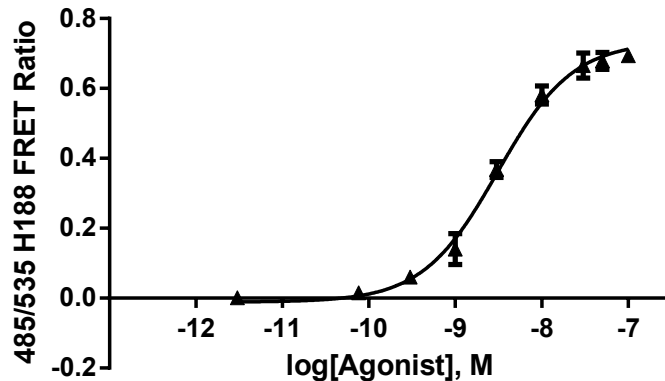


**Figure 7.** HC-Cbi-Ex4 agonism at the GLP-1 receptor using the FRET H188 reporter in stability transfected HEK-GLP-1 cells.  $EC_{50}$  of HC-Cbi-Ex4 was determined to be 3 nM. Full sigmoidal curve could not be obtained due to assay limits.

This decrease in function of Cbi-Ex4 once bound to HC (in comparison to Cbi-Ex4 alone) was an anticipated as this trend has been seen before in Bonaccorso *et al.* where they observed a decrease in agonism when IF bound to B12-Ex4 (68 pM vs 120 pM with B12-Ex4 and IF-B12Ex4, respectively).<sup>12</sup> However, this significant decrease in function, a 25 fold decrease, was not expected. This decrease is likely contributed to by the length of the “linker” between Cbi and Ex4. When HC binds Cbi conjugates it has the characteristic association to the central Co(III) and the corrin ring, surrounding it such as two hands would surround a baseball.<sup>Citation</sup> As shown in the structure of Cbi vs B12 (Figure 1 and Chapter 1, Section 1.1.2, respectively) the loss of the dibenzylmethylimidazole group from B12 “shortens” the conjugate and thus once bound by a transport protein, namely HC, this brings Ex4 to a closer proximity to HC. This closer proximity would allow for more intermolecular interactions between the two proteins (Ex4 and IF) creating a disruption in the receptor recognition of Ex4 and accounting for

decreased EC<sub>50</sub>. In the future the Cbi-Ex4 linker length warrants investigation into its effects of agonism at the GLP-1 receptor for Cbi-Ex4 and HC-Cbi-Ex4.

## 7.2.4 Future in vivo Work Using HC-Cbi-Ex4 as a Platform Technology to Increase Peptide Half-life

### 7.2.4.1 Tree Shrews as in vivo Models for HC-Cbi-Ex4

When considering in vivo experiments using HC to increase half-life an essential component of those models would be to have the two distinct transport proteins TCII and HC in their blood. The traditional models used for in vivo experiments (i.e. rats and mice) have been shown to have a hybrid transport protein to act as both TCII and HC, having characteristics of both proteins.<sup>20</sup> This hybrid TCII is able to bind incomplete analogs of B12 (such as Cbi), as does HC and also deliver bound conjugates to proliferating cells such as TCII.<sup>20</sup> This creates a half-life of about 1 h for this hybrid and therefore could not be used.<sup>3,20</sup> Select animal models have been shown to have both proteins such as rabbit, pig, and bovine.<sup>21,22</sup>

In continuation of the studies at UPenn with Dr. Hayes (as discussed in Chapter 4, Section 4.4) a mammalian model with a known neurological network is also desired for this project. The animal model to meet these criteria is the Tree Shrew, an animal classified in the Primate order.<sup>23</sup>

### 7.2.4.2 Analysis of Asian Shrew Blood for HC and TCII

While the Asian Tree Shrew genome has not been fully sequenced, BLAST has confirmed the genes for TCII and HC are present. Western Blot analysis was used to confirm that HC and TCII are present within Shrew blood. As shown in Figure 8 analysis shows hits for

HC and TCII using their respective primary antibody without cross reactivity to each other. The molecular weight for the observed bands is at ~50 kDa which is expected for HC and TCII protein. These results support the BLAST search in that the Asian Tree Shrew has both HC and TCII in their blood and therefore will be used in future in vivo experiments at UPenn using Cbi-Ex4 and Cbi-Cy5.

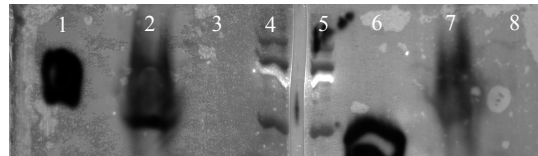


**Figure 8.** Western Blot of Asian Tree Shrew Blood. HC primary antibody (lanes 1-4) and TCII primary antibody (lanes 5-8). 1: recombinant human HC, 2: shrew serum, 3: recombinant pig TCII, 4 and 5: BioRad Kaleidoscope Protein Markers (10-250 kDa), 6: recombinant pig TCII, 7: shrew serum, 8: recombinant human HC.

### 7.3 Mitigating Hearing Loss in Pigmented Guinea Pigs from Aminoglycoside Toxicity

As discussed in Chapter 5 base-line earing in pigmented guinea pigs using ABR's have been established. However, numerous attempts to cause hearing damage have not been unsuccessful. In May 2017, a grant from the Kirsh Foundation was granted to investigate the role of CUBN in the uptake of AGA's. The following is the research plan to be executed in Fall 2017.

The primary goal of the project are to 1) develop a cell based assay to explore the role of the receptor CUBN in AGA induced hearing damage, and 2) to conduct studies in vivo in a guinea pig model to investigate whether AGA induced hearing damage can be reduced/eliminated by IF.

IF based interference with select AGA toxicity to best choose the antibiotic for in vivo studies. Such studies will allow us to best optimize the antibiotic to target, and the exact form of

IF to use in such targeting, in the in vivo studies as described below.

### 7.3.1 In vitro Validation of IF Interference with AGA Toxicity

Fluorescent analogs of the AGA antibiotics gentamicin, neomycin, and tobramycin will be synthesized and characterized.<sup>24,25,26</sup> We will screen for internalization of each fluorescent AGA in a CUBN positive cell line, namely BN16 cells, with CHO cells as negative control.<sup>2</sup> Uptake using confocal imaging and flow cytometry including the use of siRNA for CUBN knock-down to confirm, and quantify, the role of CUBN in their internalization. Inhibitory concentrations (IC) of each AGA antibiotics will be established initially in BN16 cells and then doses at 0.5, 1x and 2x the IC<sub>50</sub> will be used for each AGA antibiotic to be screened. Once toxicity level and role of CUBN have been confirmed, studies that challenge this uptake through administration (pre- and/or co-) of hIF will be conducted at various concentrations in relation to the AGA. IF-B12-Cy5 will be used in these studies to allow the tracking of both components (IF and AGA's) of the design. IC<sub>50</sub> values will be measured again in the presence of hIF.

### 7.3.2 In Vivo Mitigation of Aminoglycoside Toxicity Using IF

As discussed in Chapter 5 the small animal model suitable for AGA hearing loss studies are pigmented guinea pigs (for more detail see Chapter 5, Section 5.2.1). This study will utilize the AGA kanamycin, an AGA known to cause hearing loss in humans and guinea pigs.<sup>27</sup> While extensive conditions and dose regimens have been explored in guinea pigs, the use of a test range of 250-400 mg/kg of kanamycin administered SC once a day for 23 days, a schedule known to produce ~ 40 dB hearing loss.<sup>27</sup> This regimen will be validated in a cohort (n = 4) by measuring

hearing loss beginning on day 14 and then at one-week intervals for 3 weeks. The hearing range measured will be between 4,000-18,000 Hz and will be conducted with ABR's with the animals under anesthesia. Once completed and affirmed, a cohort of guinea pigs (n = 4) will be administered AGA via SC as described above with a co-injection of IF by IP. 5-10 min after kanamycin injection with a trailing dose of hIF given at 2 hour post initial administration as this is the Cmax of most AGA administered via SC injection.<sup>28</sup> As before, pre-dose hearing will be measured by ABR's, with post-dose hearing ABR's measurements beginning on the 14<sup>th</sup> day and continuing weekly for 3 months. hIF will be tested at two different concentrations to establish a dose-response, namely the established ration concentrations determined for blocking AGA uptake with IF as described above and 5x that concentration. All cohorts will be pre- and co-administered mannan with IF (30 min pre-administration) to inhibit possible glycoprotein receptor (mannose receptor, see Chapter 3, Section 3.6.4) mediated uptake of the hIF protein by the liver (as determined in Chapter 3, Section 3.4.2).

#### 7.4 References

- (1) Burmeister, R.; Bøe, I.-M.; Nykjaer, A.; Jacobsen, C.; Moestrup, S. K.; Verroust, P.; Christensen, E. I.; Lund, J.; Willnow, T. E. A Two-Receptor Pathway for Catabolism of Clara Cell Secretory Protein in the Kidney. *J. Biol. Chem.* **2001**, 276 (16), 13295–13301.
- (2) Le Panse, S.; Verroust, P.; Christensen, E. Internalization and Recycling of Glycoprotein 280 in Epithelial Cells of Yolk Sac. *Eur. J. Cell Biol.* **1997**, 72 (3), 257–267.
- (3) Burger, R. L.; Schneider, R. J.; Mehlman, C. S.; Allen, R. H. Human Plasma R-Type Vitamin B12-Binding Proteins. II. The Role of Transcobalamin I, Transcobalamin III, and the Normal Granulocyte Vitamin B12-Binding Protein in the Plasma Transport of Vitamin B12. *J. Biol. Chem.* **1975**, 250 (19), 7707–7713.

- (4) Nielsen, M. J.; Rasmussen, M. R.; Andersen, C. B. F.; Nexø, E.; Moestrup, S. K. Vitamin B12 Transport from Food to the Body's Cells—a Sophisticated, Multistep Pathway. *Nat. Rev. Gastroenterol. Hepatol.* **2012**, *9* (6), 345–354.
- (5) Waibel, R.; Treichler, H.; Schaefer, N. G.; Staveren, D. R. van; Mundwiler, S.; Kunze, S.; Küenzi, M.; Alberto, R.; Nüesch, J.; Knuth, A.; et al. New Derivatives of Vitamin B12 Show Preferential Targeting of Tumors. *Cancer Res.* **2008**, *68* (8), 2904–2911.
- (6) Sah, B.-R.; Schibli, R.; Waibel, R.; Boehmer, L. von; Bläuenstein, P.; Nexø, E.; Johayem, A.; Fischer, E.; Müller, E.; Soyka, J. D.; et al. Tumor Imaging in Patients with Advanced Tumors Using a New <sup>99m</sup>Tc-Radiolabeled Vitamin B12 Derivative. *J. Nucl. Med.* **2014**, *55* (1), 43–49.
- (7) Gherasim, C.; Lofgren, M.; Banerjee, R. Navigating the B12 Road: Assimilation, Delivery, and Disorders of Cobalamin. *J. Biol. Chem.* **2013**, *288* (19), 13186–13193.
- (8) Bruno, B. J.; Miller, G. D.; Lim, C. S. Basics and Recent Advances in Peptide and Protein Drug Delivery. *Ther. Deliv.* **2013**, *4* (11), 1443–1467.
- (9) Uhlig, T.; Kyprianou, T.; Martinelli, F. G.; Oppici, C. A.; Heiligers, D.; Hills, D.; Calvo, X. R.; Verhaert, P. The Emergence of Peptides in the Pharmaceutical Business: From Exploration to Exploitation. *EuPA Open Proteomics* **2014**, *4*, 58–69.
- (10) Sai, W.; Tian, H.; Yang, K.; Tang, D.; Bao, J.; Ge, Y.; Song, X.; Zhang, Y.; Luo, C.; Gao, X.; et al. Systematic Design of Trypsin Cleavage Site Mutated Exendin4-Cysteine 1, an Orally Bioavailable Glucagon-Like Peptide-1 Receptor Agonist. *Int. J. Mol. Sci.* **2017**, *18* (3).
- (11) Bulaj, L. Z. and G. Converting Peptides into Drug Leads by Lipidation <http://www.eurekaselect.com/96279/article> (accessed Jun 11, 2017).
- (12) Bonaccorso, R. L.; Chepurny, O. G.; Becker-Pauly, C.; Holz, G. G.; Doyle, R. P. Enhanced Peptide Stability Against Protease Digestion Induced by Intrinsic Factor Binding of a Vitamin B12 Conjugate of Exendin-4. *Mol. Pharm.* **2015**, *12* (9), 3502–3506.
- (13) Gao, W.; Jusko, W. J. Target-Mediated Pharmacokinetic and Pharmacodynamic Model of Exendin-4 in Rats, Monkeys, and Humans. *Drug Metab. Dispos.* **2012**, *40* (5), 990–997.
- (14) Gao, W.; Jusko, W. J. Pharmacokinetic and Pharmacodynamic Modeling of Exendin-4 in Type 2 Diabetic Goto-Kakizaki Rats. *J. Pharmacol. Exp. Ther.* **2011**, *336* (3), 881–890.

- (15) Huisgen, R. 1,3-Dipolar Cycloadditions. Past and Future. *Angew. Chem. Int. Ed. Engl.* **1963**, *2* (10), 565–598.
- (16) Kolb, H. C.; Finn, M. G.; Sharpless, K. B. Click Chemistry: Diverse Chemical Function from a Few Good Reactions. *Angew. Chem. Int. Ed.* **2001**, *40* (11), 2004–2021.
- (17) Klarenbeek, J.; Goedhart, J.; van Batenburg, A.; Groenewald, D.; Jalink, K. Fourth-Generation Epac-Based FRET Sensors for cAMP Feature Exceptional Brightness, Photostability and Dynamic Range: Characterization of Dedicated Sensors for FLIM, for Ratiometry and with High Affinity. *PLoS ONE* **2015**, *10* (4).
- (18) Thorens, B.; Porret, A.; Bühler, L.; Deng, S.-P.; Morel, P.; Widmann, C. Cloning and Functional Expression of the Human Islet GLP-1 Receptor: Demonstration That Exendin-4 Is an Agonist and Exendin-(9–39) an Antagonist of the Receptor. *Diabetes* **1993**, *42* (11), 1678–1682.
- (19) Henry, K. E.; Kerwood, D. J.; Allis, D. G.; Workinger, J. L.; Bonaccorso, R. L.; Holz, G. G.; Roth, C. L.; Zubieta, J.; Doyle, R. P. Solution Structure and Constrained Molecular Dynamics Study of Vitamin B12 Conjugates of the Anorectic Peptide PYY(3–36). *ChemMedChem* **2016**, *11* (9), 1015–1021.
- (20) Hygum, K.; Lildballe, D. L.; Greibe, E. H.; Morkbak, A. L.; Poulsen, S. S.; Sorensen, B. S.; Petersen, T. E.; Nexø, E. Mouse Transcobalamin Has Features Resembling Both Human Transcobalamin and Haptocorrin. *PLOS ONE* **2011**, *6* (5), e20638.
- (21) Nexø, E.; Olesen, H. Purification and Characterization of Rabbit Haptocorrin. *Biochim. Biophys. Acta BBA - Protein Struct.* **1981**, *667* (2), 370–376.
- (22) Polak, D. M.; Elliot, J. M.; Haluska, M. Vitamin B12 Binding Proteins in Bovine Serum. *J. Dairy Sci.* **1979**, *62* (5), 697–701.
- (23) Fan, Y.; Huang, Z.-Y.; Cao, C.-C.; Chen, C.-S.; Chen, Y.-X.; Fan, D.-D.; He, J.; Hou, H.-L.; Hu, L.; Hu, X.-T.; et al. Genome of the Chinese Tree Shrew. *Nat. Commun.* **2013**, *4*, ncomms2416.
- (24) Arbuzova, A.; Martushova, K.; Hangyás-Mihályiné, G.; Morris, A. J.; Ozaki, S.; Prestwich, G. D.; McLaughlin, S. Fluorescently Labeled Neomycin as a Probe of Phosphatidylinositol-4,5-Bisphosphate in Membranes. *Biochim. Biophys. Acta BBA - Biomembr.* **2000**, *1464* (1), 35–48.



- (25) Escobedo, J. O.; Chu, Y.-H.; Wang, Q.; Steyger, P. S.; Strongin, R. M. Live Cell Imaging of a Fluorescent Gentamicin Conjugate. *Nat. Prod. Commun.* **2012**, *7* (3), 317–320.
- (26) Jolley, M. E.; Stroupe, S. D.; Wang, C. H.; Panas, H. N.; Keegan, C. L.; Schmidt, R. L.; Schwenger, K. S. Fluorescence Polarization Immunoassay. I. Monitoring Aminoglycoside Antibiotics in Serum and Plasma. *Clin. Chem.* **1981**, *27* (7), 1190–1197.
- (27) Campbell, K. C. M.; Martin, S. M.; Meech, R. P.; Hargrove, T. L.; Verhulst, S. J.; Fox, D. J. D-Methionine (D-Met) Significantly Reduces Kanamycin-Induced Ototoxicity in Pigmented Guinea Pigs. *Int. J. Audiol.* **2016**, *55* (5), 273–278.
- (28) Chung, M.; Parravicini, L.; Assael, B. M.; Cavanna, G.; Radwanski, E.; Symchowicz, S. Comparative Pharmacokinetics of Aminoglycoside Antibiotics in Guinea Pigs. *Antimicrob. Agents Chemother.* **1982**, *22* (6), 1017–1021.

## **Appendix A: Publications**

Kelly E. Henry, Deborah J. Kerwood, Damian G. Allis, **Jayme L. Workinger**, Ron L.

Bonaccorso, George G. Holtz, Christian L. Roth, Jon Zubieta, and Robert P. Doyle. Solution Structure and Constrained Molecular Dynamics Study of Vitamin B<sub>12</sub> Conjugates of the Anorectic Peptide PYY(3-36). *ChemMedChem*. **2016**, 1015-1021.

**Jayme L. Workinger** and Robert P. Doyle. The Role of Vitamin B<sub>12</sub> in Drug Discovery. In *Vitamin B<sub>12</sub>: Advances and Insights*. Science Publishers, Boca Raton, FL. **2017**, 338-364. ISBN: 9781498706995.

**Jayme L. Workinger**, Akhila N. Wedagedara, Ebba Nexo Robert P. Doyle, Nerissa T. Viola-Villegas. <sup>89</sup>Zr-Cobalamin PET Tracer: Synthesis, Cellular Uptake, and Use for Tumor Imaging. *ACS Omega* **2017**, 2 (10), 6314–6320.

Elizabeth G. Mietlicki-Baase, Claudia G. Liberini, **Jayme L. Workinger**, Ron L. Bonaccorso, David J. Reiner, Kieran Koch-Laskowski, Lauren E. McGrath, Bart C. De Jonghe, George G. Holz, Christian L. Roth, Robert P. Doyle, Matthew R. Hayes. A Vitamin B<sub>12</sub> conjugate of Exendin-4 Produces Hypoglycemia Without Associated Hypophagia or Nausea in Male Rats. *Submitted to Diabetes, Obesity, and Metabolism*.

## **Appendix B: Curriculum Vitae**

# Solution Structure and Constrained Molecular Dynamics Study of Vitamin B<sub>12</sub> Conjugates of the Anorectic Peptide PYY(3–36)

Kelly E. Henry,<sup>[a]</sup> Deborah J. Kerwood,<sup>[a]</sup> Damian G. Allis,<sup>[a]</sup> Jayme L. Workinger,<sup>[a]</sup> Ron L. Bonaccorso,<sup>[a]</sup> George G. Holz,<sup>[b]</sup> Christian L. Roth,<sup>[c]</sup> Jon Zubieta,<sup>[a]</sup> and Robert P. Doyle<sup>\*[a, b]</sup>

Vitamin B<sub>12</sub>–peptide conjugates have considerable therapeutic potential through improved pharmacokinetic and/or pharmacodynamic properties imparted on the peptide upon covalent attachment to vitamin B<sub>12</sub> (B<sub>12</sub>). There remains a lack of structural studies investigating the effects of B<sub>12</sub> conjugation on peptide secondary structure. Determining the solution structure of a B<sub>12</sub>–peptide conjugate or conjugates and measuring functions of the conjugate(s) at the target peptide receptor may offer considerable insight concerning the future design of fully optimized conjugates. This methodology is especially useful in tandem with constrained molecular dynamics (MD)

studies, such that predictions may be made about conjugates not yet synthesized. Focusing on two B<sub>12</sub> conjugates of the anorectic peptide PYY(3–36), one of which was previously demonstrated to have improved food intake reduction compared with PYY(3–36), we performed NMR structural analyses and used the information to conduct MD simulations. The study provides rare structural insight into vitamin B<sub>12</sub> conjugates and validates the fact that B<sub>12</sub> can be conjugated to a peptide without markedly affecting peptide secondary structure.

## Introduction

Peptide YY (PYY), a member of the pancreatic polypeptide family,<sup>[1–8]</sup> was first isolated from porcine intestinal tissue extracts in 1980<sup>[9]</sup> and was later shown to be a critical enteroendocrine hormone involved in appetite regulation.<sup>[10–12]</sup> PYY has two main circulating forms: PYY(1–36) and a truncated form, PYY(3–36).<sup>[13]</sup> PYY(1–36) is released in concert with caloric intake or exercise and is cleaved by dipeptidyl peptidase IV (DPP-IV)<sup>[14]</sup> in the gut to produce PYY(3–36). PYY(1–36) has an appetite-stimulating effect through activation of the orexigenic Y1 receptor (Y1-R) located in the intestines, blood vessels, and brain.<sup>[15]</sup> The two-amino-acid N-terminal (Tyr-Pro) truncation to PYY(3–36) results in an approximate 100-fold decrease in activity at the Y1-R,<sup>[5, 16]</sup> and generates an agonist of the anorexigen-

ic Y2 receptor (Y2-R) located in the intestines (vagal afferent sensory neuron signaling)<sup>[17, 18]</sup> and brain,<sup>[19, 20]</sup> which exerts a G-protein-coupled receptor (GPCR) G<sub>i</sub>-mediated anorectic effect.

We recently reported a B<sub>12</sub>–PYY(3–36) conjugate that demonstrated similar activity to native PYY(3–36) at the Y2-R in vitro, but improved function over PYY(3–36) upon subcutaneous (s.c.) administration in vivo in a lean rat model (conjugate **3** as described herein below).<sup>[21]</sup> In earlier work, we focused on conjugating to B<sub>12</sub> through the ribose hydroxy group, as it is well established in the field that this is an optimal site for such conjugation, as it does not hinder recognition of B<sub>12</sub> by its carrier proteins.<sup>[22–25]</sup> Likewise, we focused on an N-terminal region of PYY(3–36) for conjugation (specifically the K<sub>4</sub> residue), because again it has been well documented that modifications at (or indeed complete loss of) this area do not significantly affect Y2-R agonism.<sup>[26–28]</sup> These assumptions bore out, as the EC<sub>50</sub> values at the Y2-R obtained for the conjugate produced (and noted as conjugate **3** herein) were similar to that of unconjugated PYY(3–36) used for comparison. These were established using a Fura-2 assay that monitors intracellular Ca<sup>2+</sup> mobilization under conditions in which the Y2-R signals through a promiscuous G<sub>q</sub> GTP binding protein.<sup>[21]</sup> Questions that remained from this work, however, were what affect, if any, does B<sub>12</sub> conjugation actually have on the PYY(3–36) secondary structure and whether MD simulations could be used to better understand, and possibly predict, any structural modifications observed. To investigate these questions, two conjugates located at the same coupling sites (ribose on B<sub>12</sub> and K<sub>4</sub> on PYY(3–36)

[a] Dr. K. E. Henry, Dr. D. J. Kerwood, Dr. D. G. Allis, J. L. Workinger, R. L. Bonaccorso, Prof. J. Zubieta, Prof. R. P. Doyle  
Department of Chemistry, Center for Science and Technology  
Syracuse University, 111 College Place, Syracuse, NY 13244 (USA)  
E-mail: rpdoyle@syr.edu

[b] Prof. G. G. Holz, Prof. R. P. Doyle  
Department of Medicine and Pharmacology  
Institute for Human Performance, SUNY Upstate Medical University  
750 East Adams Street, Syracuse, NY 13210 (USA)

[c] Prof. C. L. Roth  
Department of Pediatrics, University of Washington, Division of Endocrinology and Diabetes, Seattle Children's Research Institute, Center for Integrative Brain Research, 1900 Ninth Avenue, Seattle, WA 98101 (USA)

Supporting information and the ORCID identification number(s) for the author(s) of this article can be found under <http://dx.doi.org/10.1002/cmdc.201600073>.

but with a slightly varying spacer length (one methylene unit difference) were assayed for agonism of the Y2-R using a new fluorescence resonance energy transfer (FRET)-based assay that faithfully reports the normal signal transduction process by which the Y2-R signals through  $G_i$  proteins to lower levels of intracellular cyclic adenosine monophosphate (cAMP).<sup>[29]</sup> NMR structures were solved for these conjugates, and their in-solution NMR structures were compared with those previously reported by Keire et al.<sup>[30]</sup> and Nygaard et al.<sup>[7]</sup> Subsequent unconstrained and NMR constrained MD simulations were then also performed.

## Results and Discussion

### In vitro evaluation of conjugates 3 and 4

All assays were performed *at least* in triplicate. Conjugates 3 and 4 were tested for their abilities to lower cAMP levels. Figure 1 shows the dose–response relationships for 3 and 4 relative to  $K_4$ PYY, showing both conjugates are less active than  $K_4$ PYY and that 4 is more active than 3. Both conjugates are, however, within one-half log order of  $K_4$ PYY.

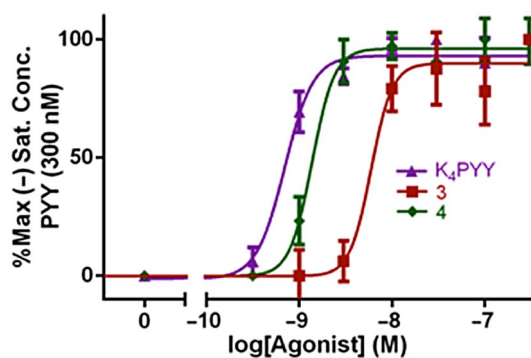


**Figure 1.** Dose–response curves monitored as percent inhibition of Ex-4 action at AKAR3 by  $K_4$ PYY and conjugates 3 and 4 at the Y2-R.  $EC_{50}$  values:  $K_4$ PYY:  $1 \pm 0.2$  nM, 3:  $6 \pm 2$  nM, 4:  $2 \pm 0.2$  nM.  $EC_{50}$  values are the average  $\pm$  SEM.

This difference in  $EC_{50}$  values in comparing conjugates with  $K_4$ PYY was initially presumed to be a compromise between steric hindrance and/or unfavorable flexibility resulting in modifications/interactions that negatively affect the peptide structure–activity profile. At this point we decided to pursue NMR and molecular dynamics (MD) studies to further explore these in vitro observations.

### NMR analysis of 3 and 4

Proton chemical shifts for 3 were assigned by analyzing TOCSY, DQF-COSY, and 2D NOE spectra at 25 °C. The experiments were also performed at 20 and 30 °C, at which slight shifts of some proton signals resolved overlapping peaks. The NMR spectra of 3 have some similarity to those of PYY(3–36), such as line broadening of many signals,<sup>[7]</sup> indicating increased dynamics,

and a decrease in the chemical shift range of the backbone amide protons relative to full-length PYY. All backbone amide protons were assigned with the exception of Leu24, which could not be definitely determined due to overlap. Figure S17 (Supporting Information) shows the proton chemical shift difference between 3 and PYY(3–36). There are chemical shift differences for residue Lys4, which is not surprising, as this is the attachment site for  $B_{12}$ . Figure 2 shows an overlay of 3 after

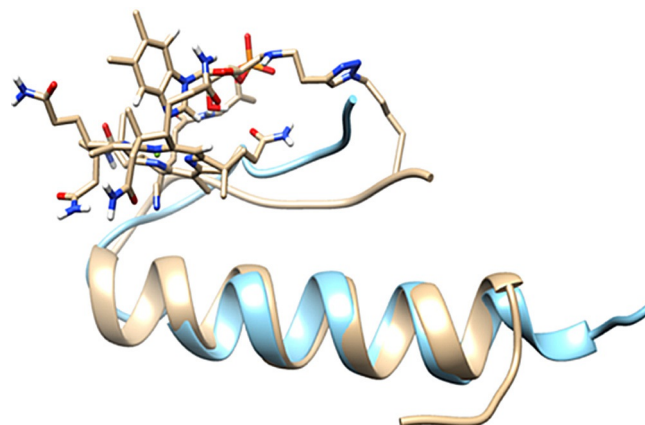


**Figure 2.** Overlay of PYY(3–36) (blue) versus 3 (tan). The structure of PYY(3–36) was obtained from the RCSB Protein Data Bank ([www.pdb.org](http://www.pdb.org)); PDB ID: 2DF0. The program Chimera (UCSF; [www.cgl.ucsf.edu/chimera/](http://www.cgl.ucsf.edu/chimera/))<sup>[31]</sup> was used to display the image.

MD calculations and PYY(3–36). The first chemical shift difference to consider is that for the methyl and  $\alpha$  protons of Ala7. In PYY(3–36), the methyl group of residue Ala7 is pointing toward the  $\alpha$  helix, whereas in conjugate 3 the methyl group is oriented away from the  $\alpha$  helix. A 2D NOE cross-peak between the Ala7 methyl group and the ring protons of Tyr20 was observed in PYY(3–36),<sup>[7]</sup> but in 3 only a very weak cross-peak was observed in the longest mixing time 2D NOE experiment. This difference in orientation would also put the Ala7  $\alpha$  proton in distinct environments. The backbone amide protons have different chemical shifts for the  $\beta$  turn residues and residues in the N-terminal side of the  $\alpha$  helix, specifically residues Gly9, Ala12, Ser13, Glu15, Leu17, and Arg19. This can be explained by the unraveling of the  $\alpha$  helix and increased dynamics at the N-terminal side in the PYY(3–36) structure. Conjugate 3 maintains an  $\alpha$ -helical structure similar to that of full-length PYY, and the residue with the largest chemical shift difference for the amide proton, Leu17, has a chemical shift value closer to that of the full-length peptide: PYY Leu17 NH 8.40 ppm,<sup>[7]</sup> 3 Leu17 NH 8.36 ppm, PYY(3–36) 7.95 ppm.<sup>[7]</sup> Nygaard et al. suggest that the Pro2–Tyr27 interaction is important for the stability of the PP fold, and that loss of this interaction in PYY(3–36) creates both conformational and dynamic changes in the structure, especially around the turn region.<sup>[7]</sup> Close inspection of 3 indicates possible hydrogen bonds from Glu6 to Tyr27 and Ser23, which may stabilize the PP fold in the conjugate.<sup>[7]</sup>

To elaborate on the structural studies, we decided to also investigate the solution structure of **4** to allow a direct comparison with **3**. Based on the NMR spectra, the conjugate structures appear very similar with only minor differences in the proton chemical shift assignments (Supporting Information Figure S18) and greater than 95% similarity in the 2D NOE spectra (Supporting Information Figure S19).

The major difference observed between **3** and **4** is the proton chemical shift change at B7 and B2 on the dimethylbenzimidazole (DMB) ligand (see Supporting Information Figure S12 for B<sub>12</sub> atom numbering scheme). The C20 methyl protons are closer to the B4 and B2 protons in **4** based on the presence of a weak cross-peak between the C20 methyl protons and B2, which is only seen in the longest mixing time 2D NOE spectra of **3**, and a cross-peak between the methyl protons and B4, which is stronger for **4**. Weak cross-peaks are observed in **4** between a propionamide proton of the *g* side chain of B<sub>12</sub> (Supporting Information Figure S12) and the H $\alpha$  of D11 as well as the methyl protons of A12. The  $\alpha$  helix motif as a whole is critical for association and subsequent agonism.<sup>[26]</sup> This is consistent with reported Y2-R interactions, as the C-terminal pentapeptide region is well established as the critical region, or “address”, of the main interactions with Y2-R, while the  $\alpha$  helix is considered the “message”, indicating that both areas are critical in Y2-R agonism.<sup>[26]</sup>

#### NMR constrained MD studies of **3** and **4**

Molecular dynamics simulations of **3** and **4** were performed both with and without the NMR constraints defined for **3** to consider differences in behavior and potential alternative structures in the simulations. The observed structural changes

across the simulations identified intra-PYY(3–36) interactions that might, through their stabilization in the isolated conjugate, promote the decreased activity of **3** relative to **4**. The unconstrained MD simulation data then provide an additional set of structures for considering accessible geometries beyond the restrained set. The average structures from representative MD time ranges for **3** and **4** are shown in Figures 3 (front/side view) and 4 (top view). Apparent from these views, and the full simulations in general, are the persistence of 1) much of the  $\alpha$  helical structure and 2) localization of the B<sub>12</sub> fragment itself to the unstructured region approaching the loop into the  $\alpha$  helix (in the images, this loop is at the base of all structures, including residues Glu10, Asp11, and Ala12). Across all of the simulations, several hydrogen bonding motifs are found to persist at the onset of the simulations and over the time evolution of the structure dynamics that serve to effectively anchor the B<sub>12</sub> at this loop region. Those which specifically anchor the B<sub>12</sub> to this region in all simulations are shown in Figure 5, visualizing the two most persistent motifs for these structures: a pair of hydrogen bonds from a single B<sub>12</sub> amide side chain to Pro8 and Glu16 (left, Motif 1) and an amide side chain to Pro8 hydrogen bond and coordination of a hydroxy group H atom on Ser13 to the B<sub>12</sub> cyano nitrogen atom (right, Motif 2). The structural basis for preservation of the loop region itself across all simulations is evident in Figure 6, which shows that (left) Glu16 is engaged in several persistent hydrogen bonding interactions with Gly9, Glu10, and Asp11, whereas at the far end of the loop (right), Glu6 is in close proximity to hydrogen bond acceptors on Tyr27 and Ser23. The NMR distance lists, ranges, and time-averaged MD structures for **3** and **4** are provided in the Supporting Information.

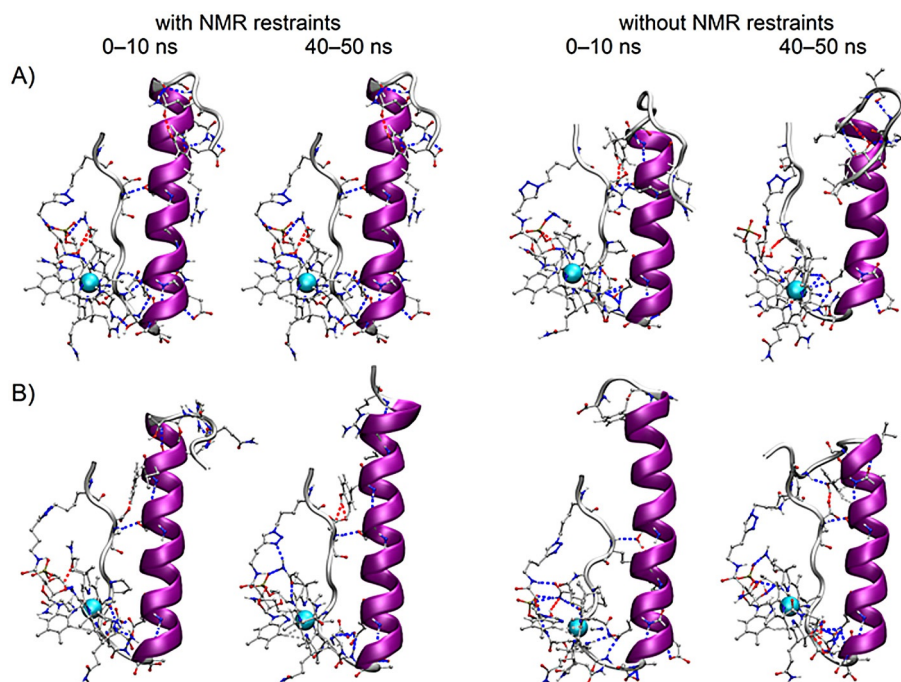


**Figure 3.** Side-on views (aligned along the  $\alpha$  helix) of RMSD average structures (across 10 ns sampling increments) for restrained (left) and unrestrained (right) MD simulations of A) **3** and B) **4**.

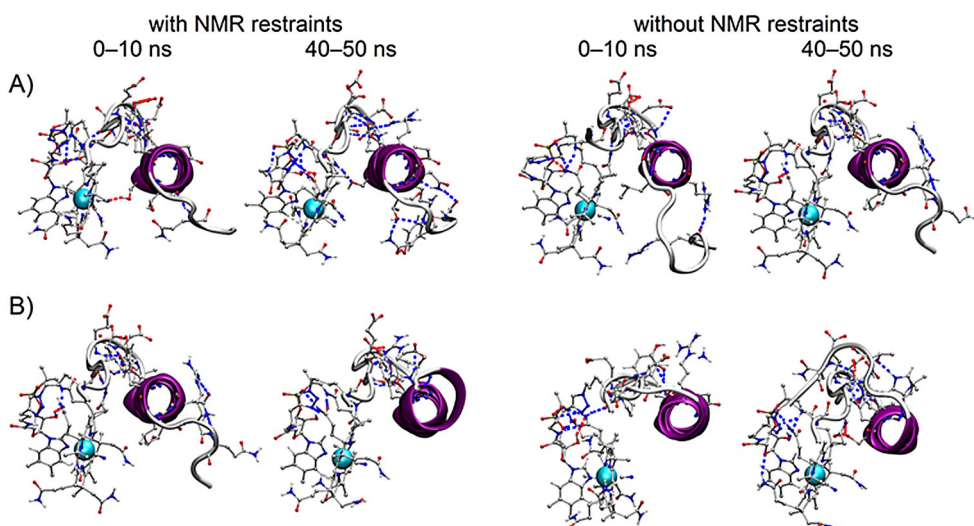


**Figure 4.** Top-down views (aligned along the  $\alpha$  helix) of RMSD average structures (across 10 ns sampling increments) for restrained (left) and unrestrained (right) MD simulations of A) **3** and B) **4**.

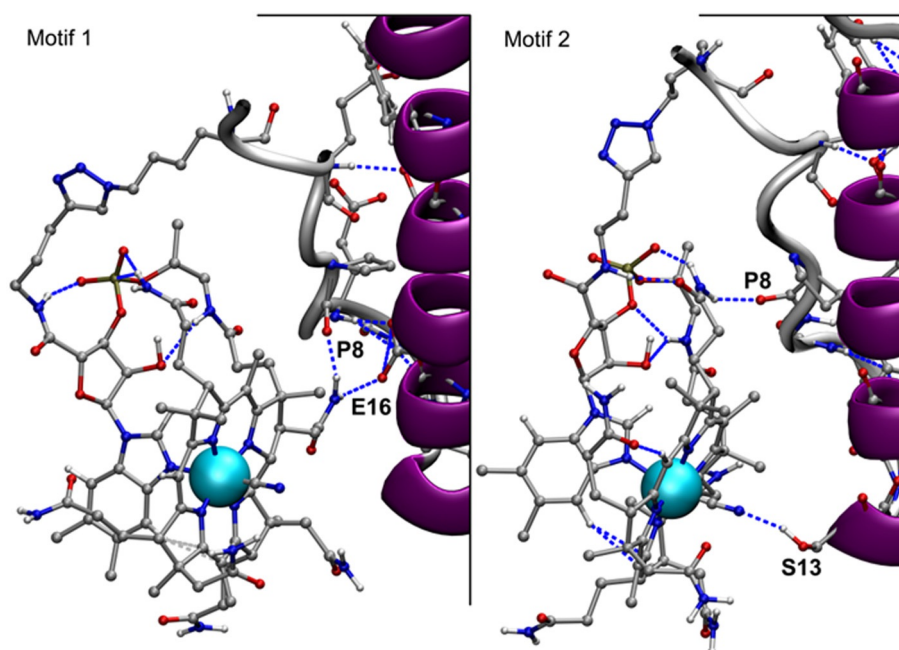


**Figure 5.** Two persistent hydrogen bonding interaction motifs between the  $B_{12}$  and PYY(3–36) unstructured region (residues 3–10) across all simulations.

The differences between structures **3** and **4**, both with and without NMR constraints, are largely localized to the C-terminal side of the  $\alpha$  helix and occur to varying degrees in all of the simulations. With the  $B_{12}$  largely predicted to be confined to the PYY(3–36) loop due to several strong hydrogen bonding interactions, and with the well-known attenuation of PYY(3–36) activity with modifications to or removal of the C-terminal region, the most logical explanation for any change in behavior to come from these single conjugate simulations is some structural change at the C-terminal region of PYY(3–36). This may occur from  $B_{12}$  binding-induced conformational changes at the PYY N terminus, causing changes in activity, meaning

any observed interactions between the  $B_{12}$  binding-constrained N terminus and concomitantly proximal C-terminal regions are of great interest. Despite the small change in tether length for these two cases, RMSD analyses and average structure generation produced two distinct structures that, for each case, revealed binding interactions deemed consistent with the trends in activity.

MD simulations of **3** and **4** highlight hydrogen bonding interactions that may govern the differences observed in Y2-R agonism and subsequent calcium mobilization and inhibitory cAMP effects. PYY(3–36) does not tolerate any interaction at the C terminus with respect to Y2-R stimulation.<sup>[32]</sup> If the

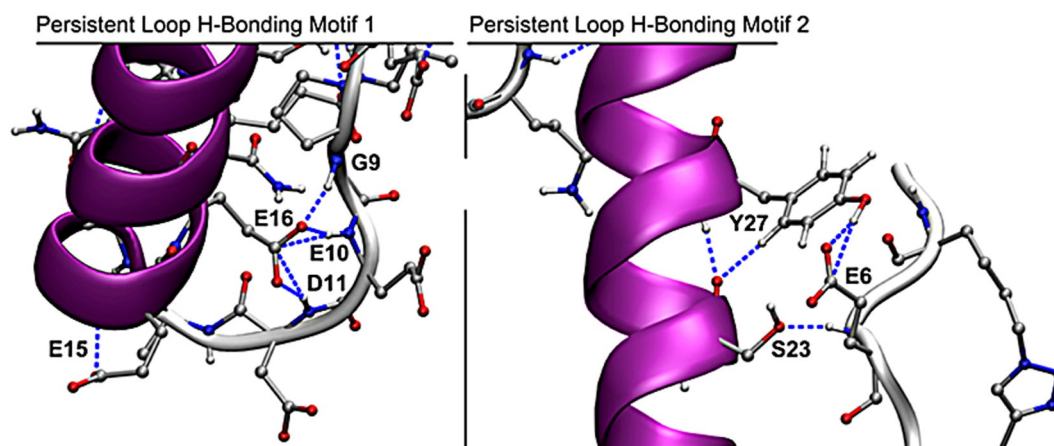


**Figure 6.** Two persistent hydrogen bonding motifs that define the PYY(3–36) loop region (left) and stabilizing interactions between the unstructured N-terminal region and the  $\alpha$  helix.

answer to the decreased activity of **3** lies solely on some response internal to the conjugate, one might argue from the MD simulations that the shortened tether length enhances the stiffness of the unstructured region (residues 3–9) by decreasing its conformational flexibility upon hydrogen bonding between the  $B_{12}$  and the near-loop region. This result would provide a less flexible N-terminal region and a more persistent hydrogen bonding pocket for the C-terminal region with which to interact. By the loss of flexibility, necessary at the C-terminal region for biological activity, reduced activity would be predicted (and is observed). Kaiser et al. recently reported data showing that unwinding of C-terminal residues of neuropeptide Y (NPY) is critical for Y2 receptor binding and activation.<sup>[32]</sup> Solution NMR experiments showed that the ligand is tethered to the second extracellular loop by hydrophobic contacts and revealed NPY to undergo remarkable structural changes within the C terminus. The C-terminal pentapeptide plays a role in extensive and susceptible interactions in NPY; a network that is also relevant for PYY(3–36) in regards to Y2-R agonism. Changes in the C-terminal amino acids can easily disturb receptor binding or switch receptor selectivity for both NPY and PYY(3–36) as observed in numerous earlier structure-activity studies.<sup>[33]</sup> The ultimate conclusion from Kaiser et al. directly relates to our work, as the binding mode of NPY [and in our case,  $B_{12}$  conjugates of PYY(3–36)] might have more general implications for peptide binding GPCR systems.

The MD simulations from this study do indicate that if the origin of the decreased activity of **3** is entirely due to factors internal to the  $B_{12}$ -PYY(3–36) conjugate itself, then constraint of the C-terminal region by hydrogen bonding interactions with the N-terminal region could explain it—and that this kind of internal mechanism may have its origin in the reduction of tether length.

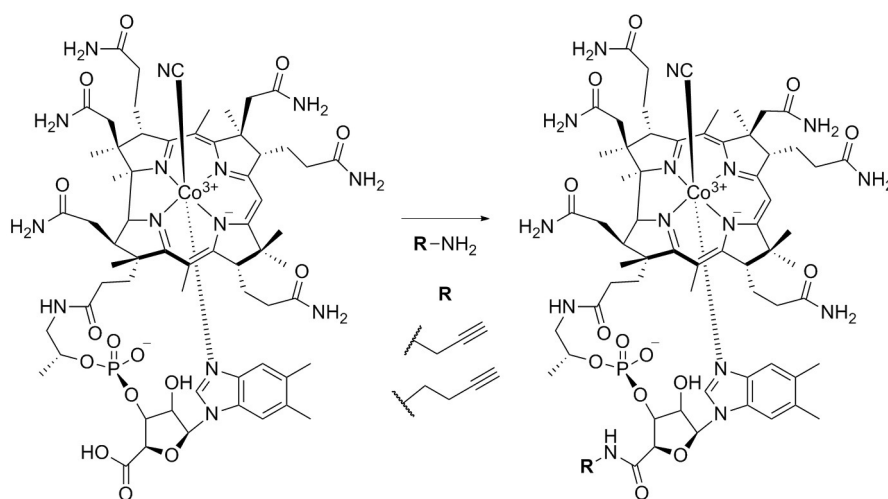
## Conclusions

$B_{12}$ -PYY(3–36) conjugates **3** and **4** with various methylene spacer lengths between the  $B_{12}$  and PYY(3–36) show similar

Y2-R agonism to that of PYY(3–36). Both intra- and intermolecular interactions between  $B_{12}$  and the peptide and small changes in the secondary structure of the peptide brought on by conjugation were observed. Based on the information collected from the NMR constrained MD studies, it would have been possible to offer a detailed assessment of the potential function of both conjugates. These observations suggest that MD could be used a priori to guide conjugate rational design and minimize the number of conjugates that would need to be screened—information of considerable benefit in development terms. Conjugates and modifications of  $B_{12}$  have garnered much interest in recent years for their clinical and medicinal applicability.<sup>[34]</sup> Based on the studies described herein, an ideal  $B_{12}$ -peptide conjugate would be one with an appropriate linker length to allow optimal function of both the peptide and  $B_{12}$ , which could be predicted by MD via inter- and intramolecular interactions that are known to be useful and/or harmful to the overall function of each component.

## Experimental Section

**Synthesis of alkyne precursors (1 and 2) and conjugates (3 and 4):** Two  $B_{12}$ -alkyne precursors were prepared by activation of a  $B_{12}$ -carboxylic acid ( $B_{12}$ -CA) derivative<sup>[35]</sup> with 1-ethyl-3-(3-dimethylaminopropyl)carbodiimide (EDC) and hydroxybenzotriazole (HOBt) in anhydrous DMSO under argon (Scheme 1). Full characterization of the alkyne precursor **1** and **2**, including RP-HPLC, MALDI-ToF MS, and NMR can be found in the Supporting Information (Figure S1–11, Table S1). For conjugate synthesis, click chemistry<sup>[36]</sup> was implemented using a copper iodide (CuI) and tris[(1-benzyl-1*H*-1,2,3-triazol-4-yl)methyl]amine (TBTA) method, adapted from Gryko et al.<sup>[37,38]</sup> Copper(I)-catalyzed alkyne-azide cycloaddition (CuAAC) synthesis of conjugates **3** and **4** via the alkyne precursors **1** and **2** and a  $K_4$ -azido PYY(3–36) ( $K_4$ PYY) is described in Scheme 2 (spacer length  $n=2, 3$  for precursors **1** and **2**).  $K_4$ PYY was initially tested against PYY(3–36) amide (Sigma–Aldrich), and there was no observed difference in Y2-R agonism. Subsequently,  $K_4$ PYY was used as the control for all assays. Characterization of the  $B_{12}$ -PYY(3–36) conjugates **3** and **4**, including HPLC and MALDI-ToF MS, can be found in the Supporting Information (Figure S13–16).



**Scheme 1.** Synthesis of B<sub>12</sub>-alkyne precursors **1** and **2**. *Reagents and conditions:* EDC, HOBT, anhydrous DMSO; reactions carried out under argon for 16 h at RT.

**In vitro assay of 3 and 4 at the Y2 receptor coupled to G<sub>i</sub>:** Conjugates **3** and **4** were tested for their abilities to lower levels of cAMP in an in vitro assay using HEK293 cell monolayers (Figure 7).<sup>[29]</sup> These cells were engineered so that they stably express the human GLP-1 receptor (GLP-1R), while also transiently expressing the human Y2-R. Furthermore, these cells were virally transduced with the genetically encoded FRET reporter AKAR3, which is used to monitor cAMP-dependent protein kinase (PKA) activation intracellularly. This assay is unique in that it allows FRET-based detection of the ability of PYY(3–36) to counteract the action of a GLP-1R agonist (Exendin-4; Ex-4) to raise levels of cAMP. When the cells are first treated with Ex-4 (33  $\mu$ M; injection 1) so that levels of cAMP are elevated, AKAR3 exhibits increased FRET, measured as a decrease in the 485/535 nm emission ratio (Figure 7). This change of FRET occurs after an approximate lag time of 50 s. If PYY(3–36) is then applied at the 180 s time point (injection 2), a functional antagonism of the action of Ex-4 is measured so that the change of FRET is decreased. Note that no

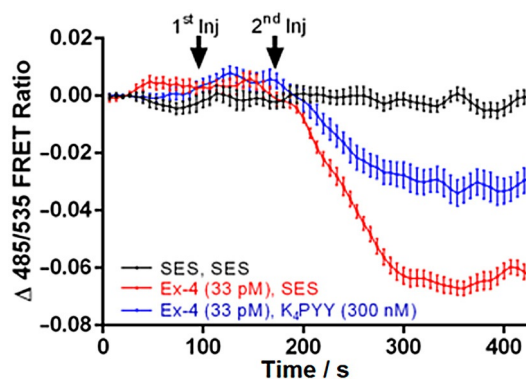
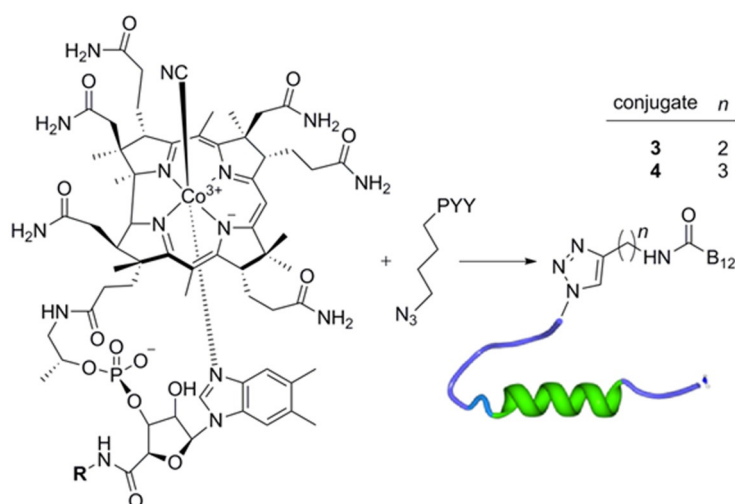


**Figure 7.**  $\Delta$ 485/535 FRET ratio through the course of a run. The first injection occurs at 100 s followed by a second injection at 180 s.



**Scheme 2.** Copper(I) alkyne-azide cycloaddition synthesis of B<sub>12</sub>-PYY(3–36) conjugates **3** and **4** via alkyne precursors **1** and **2** with two- or three-methylene-unit spacer between the 5'-amide on B<sub>12</sub> and the triazole linkage to K<sub>4</sub>PYY. *Reagents and conditions:* Cu<sup>I</sup>, TBTA; reactions were carried out for 16 h at RT. PYY(3–36) adapted from PDB ID: 2DF0.

change of FRET is measured in response to the administration of a negative control standard extracellular saline (SES; Figure 7). By varying the concentration of added conjugate, it is possible to determine dose–response relationships, and to also determine EC<sub>50</sub> values describing inhibitory actions of PYY(3–36) conjugates versus 33  $\mu$ M Ex-4 in this assay. Figure 7 illustrates these responses to the first injection of either Ex-4 or SES, and the second injection of K<sub>4</sub>PYY or SES. To normalize these raw data for subsequent dose–response analysis, “end-point” values of FRET were measured during the last 10 sample intervals (Figure 7). As illustrated in Figure 1, the dose-dependent inhibitory actions of PYY(3–36) conjugates are then quantified relative to a value of 100% that corresponds to the maximal inhibitory effect measured when testing 300 nM PYY(3–36) in this assay.

**NMR studies of 3 and 4:** NMR studies were executed initially to observe any structural differences between the conjugates and free peptide in solution. Because in vivo studies had previously established in vivo function for **3**, extensive structural studies were first performed with **3** and a direct comparison made to published PYY(3–36).<sup>[17]</sup> Full NMR studies of **4** were then completed to serve as



a comparison with **3**. Full descriptions of methods and conditions are provided in the Supporting Information.

**MD studies of 3 and 4:** To complement the NMR studies, MD simulations of **3** and **4** were completed in attempts to explain the minor differences of Y2-R agonism between the two conjugates. These MD studies took the form of 50 ns simulations to probe the potential variation in simulation geometries and time-averaged structures that arise from different tether lengths. MD simulations were performed using the GROMACS (ver. 5.0.4)<sup>[39]</sup> software package. The NMR distance lists, ranges, and tabulated distances from the time-averaged MD structure for **3** are provided in the Supporting Information.

## Acknowledgements

This research was supported by the National Institute of Diabetes and Digestive and Kidney Diseases of the US National Institutes of Health (NIH) under award number R15K097675-01A1. The content is solely the responsibility of the authors and does not necessarily represent the official views of the US NIH. The authors thank the Syracuse University HTC Campus Grid, supported by US National Science Foundation (NSF) award ACI-1341006, for computational resource use.

**Keywords:** GPCR · molecular dynamics · NMR spectroscopy · PYY(3–36) · vitamin B<sub>12</sub>

- [1] C. Martins, L. M. Morgan, S. R. Bloom, M. D. Robertson, *J. Endocrinol.* **2007**, *193*, 251–258.
- [2] E. Ekblad, F. Sundler, *Peptides* **2002**, *23*, 251–261.
- [3] E. Karra, R. L. Batterham, *Mol. Cell. Endocrinol.* **2010**, *316*, 120–128.
- [4] D. Larhammar, *Regul. Pept.* **1996**, *62*, 1–11.
- [5] C. Cabrele, A. G. Beck-Sickinger, *J. Pept. Sci.* **2000**, *6*, 97–122.
- [6] A. G. Blomqvist, C. Söderberg, I. Lundell, R. J. Milner, D. Larhammar, *Proc. Natl. Acad. Sci. USA* **1992**, *89*, 2350–2354.
- [7] R. Nygaard, S. Nielbo, T. W. Schwartz, F. W. Poulsen, *Biochemistry* **2006**, *45*, 8350–8357.
- [8] B. Bjoernholm, F. S. Joergensen, T. W. Schwartz, *Biochemistry* **1993**, *32*, 2954–2959.
- [9] K. Tatamoto, V. Mutt, *Nature* **1980**, *285*, 417–418.
- [10] T. H. Moran, U. Smedh, K. P. Kinzig, K. A. Scott, S. Knipp, E. E. Ladenheim, *Am. J. Physiol. Regul. Integr. Comp. Physiol.* **2005**, *288*, R384–R388.
- [11] L. Degen, S. Oesch, M. Casanova, S. Graf, S. Ketterer, J. Drewe, C. Beglinger, *Gastroenterology* **2005**, *129*, 1430–1436.
- [12] R. L. Batterham, H. Heffron, S. Kapoor, J. E. Chivers, K. Chandarana, H. Herzog, C. W. Le Roux, E. L. Thomas, J. D. Bell, D. J. Withers, *Cell Metab.* **2006**, *4*, 223–233.
- [13] D. Grandt, M. Schimiczeka, Ch. Beglinger, P. Layera, H. Goebella, V. E. Eysselein, J. R. Reeve, Jr., *Regul. Pept.* **1994**, *51*, 151–159.
- [14] R. Mentlein, P. Dahms, D. Grandt, R. Krüger, *Regul. Pept.* **1993**, *49*, 133–144.
- [15] L. A. Selbie, K. Darby, C. Schmitz-Peiffer, C. L. Browne, H. Herzog, J. Shine, T. J. Biden, *J. Biol. Chem.* **1995**, *270*, 11789–11796.
- [16] P. Sjödin, S. K. Holmberg, H. Åkerberg, M. M. Berglund, N. Mohell, D. Larhammar, *Biochem. J.* **2006**, *393*, 161–169.
- [17] C. R. Abbott, M. Monteiro, C. J. Small, A. Sajedi, K. L. Smith, J. R. Parkinson, M. A. Ghatei, S. R. Bloom, *Brain Res.* **2005**, *1044*, 127–131.
- [18] S. Koda, Y. Date, N. Murakami, T. Shimbara, T. Hanada, K. Toshinai, A. Nijima, M. Furuya, N. Inomata, K. Osuye, M. Nakazato, *Endocrinology* **2005**, *146*, 2369–2375.
- [19] J. E. Blevins, P. K. Chelikani, A. C. Haver, R. D. Reidelberger, *Peptides* **2008**, *29*, 112–119.
- [20] N. M. Neary, C. J. Small, M. R. Druce, A. J. Park, S. M. Ellis, N. M. Semjounous, C. L. Dakin, K. Filipsson, F. Wang, A. S. Kent, G. S. Frost, M. A. Ghatei, S. R. Bloom, *Endocrinology* **2005**, *146*, 5120–5127.
- [21] K. E. Henry, C. T. Efers, R. M. Burke, O. G. Chepurny, G. G. Holz, J. E. Blevins, C. L. Roth, R. P. Doyle, *Endocrinology* **2015**, *156*, 1739–1749.
- [22] J. F. McEwan, H. S. Veitch, G. J. Russell-Jones, *Bioconjugate Chem.* **1999**, *10*, 1131–1136.
- [23] A. K. Petrus, A. R. Vortherms, T. J. Fairchild, R. P. Doyle, *ChemMedChem* **2007**, *2*, 1717–1721.
- [24] C. H. Fazzen, D. Valentin, T. J. Fairchild, R. P. Doyle, *J. Med. Chem.* **2011**, *54*, 8707–8711.
- [25] S. Clardy-James, O. G. Chepurny, C. A. Leech, G. G. Holz, R. P. Doyle, *ChemMedChem* **2013**, *8*, 582–586.
- [26] S. L. Pedersen, B. Holst, N. Vrang, K. J. Jensen, *J. Pept. Sci.* **2009**, *15*, 753–759.
- [27] S. L. Pedersen, P. G. Sasikumar, S. Chelur, B. Holst, A. Artmann, K. J. Jensen, N. Vrang, *J. Pept. Sci.* **2010**, *16*, 664–673.
- [28] S. L. Pedersen, C. Steentoft, N. Vrang, K. J. Jensen, *ChemBioChem* **2010**, *11*, 366–374.
- [29] G. G. Holz, C. A. Leech, M. W. Roe, O. G. Chepurny in *Cyclic Nucleotide Signaling* (Ed.: Xiaodong Cheng), Taylor and Francis Group, CRC Press, Boca Raton, **2015**, 35–60.
- [30] D. A. Keire, M. Kobayashi, T. E. Solomon, J. R. Reeve, *Biochemistry* **2000**, *39*, 9935–9942.
- [31] E. F. G. Pettersen, T. D. Goddard, C. C. Huang, G. S. Couch, D. M. Greenblatt, E. C. Meng, T. E. Ferrin, *J. Comput. Chem.* **2004**, *25*, 1605–1612.
- [32] A. Kaiser, P. Müller, T. Zellmann, H. A. Scheidt, L. Thomas, M. Bosse, R. Meier, J. Meiler, D. Huster, A. G. Beck-Sickinger, P. Schmidt, *Angew. Chem. Int. Ed.* **2015**, *54*, 7446–7449; *Angew. Chem.* **2015**, *127*, 7554–7558.
- [33] X. Pedragosa Badia, J. Stichel, A. G. Beck-Sickinger, *Front. Endocrinol.* **2013**, *4*, 5.
- [34] F. Zelder, *Chem. Commun.* **2015**, *51*, 14004–14017.
- [35] S. Clardy-James, J. Bernstein, D. Kerwood, R. P. Doyle, *Synlett* **2012**, *23*, 2363–2366.
- [36] H. C. Kolb, M. G. Finn, K. B. Sharpless, *Angew. Chem. Int. Ed.* **2001**, *40*, 2004–2021; *Angew. Chem.* **2001**, *113*, 2056–2075.
- [37] M. Chromiński, D. Gryko, *Chemistry* **2013**, *19*, 5141–5148.
- [38] K. ó Proinsias, M. Giedyk, D. Gryko, *Chem. Soc. Rev.* **2013**, *42*, 6605–6619.
- [39] B. Hess, C. Kutzner, D. van der Spoel, E. Lindahl, *J. Chem. Theory Comput.* **2008**, *4*, 435–447.

Received: February 2, 2016

Published online on March 30, 2016

# 14

## Vitamin B12 and Drug Development

*Jayme L Workinger and Robert P Doyle*

---

---

### **1. Background and Scope on Utilizing the Vitamin B12 Dietary Pathway for Drug Development**

#### **1.1 Vitamin B12 and its dietary uptake**

The consumption of vitamin B12 (B12), also known as cobalamin (Cbl), is essential for humans. B12 is produced naturally by select bacteria (and likely certain archaea) (Doxey et al. 2015) and organisms must acquire the vitamin through their diet (about 2.5 µg per day for humans) (Martens et al. 2002; Nielsen et al. 2012). There are two primary biologically active forms of B12: methylcobalamin and adenosylcobalamin. Methionine synthase uses methylcobalamin to produce the amino acid methionine from homocysteine, and methylmalonyl-CoA mutase uses adenosylcobalamin as a cofactor to produce succinyl CoA (Nielsen et al. 2012; Kräutler 2005). Mammals have developed a complex dietary uptake pathway for B12 involving a series of transport proteins and specific receptors across various tissues and organs (vide infra) (Nielsen et al. 2012; Gherasim et al. 2013). It is the understanding and exploitation of this uptake pathway that offers considerable scope for drug development.

B12 is a water-soluble vitamin with a highly complex structure, comprising a midplanar corrin ring composed of four pyrrole rings linked to a central cobalt (III) atom (Hodgkin et al. 1955). The corrin ring is similar to the more commonly known porphyrin structure, but with key differences in terms of degree of saturation, symmetry and planarity (see Figure 1).

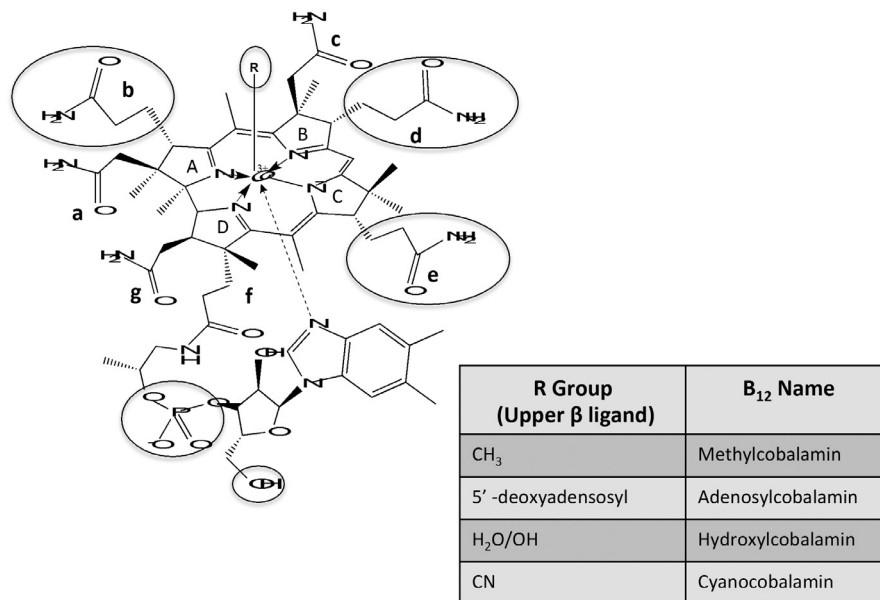


**Figure 1.** Structure of vitamin B12. R is –methyl or –adenosyl in active cofactors. In center is the corrin ring, which has a greater number of sp<sup>3</sup> carbons than a porphyrin rendering it less planar and less conjugated, and with one less carbon (19 rather than 20) due to the lack of a methylene spacer unit between the ‘C’ and ‘D’ rings as is found in a porphyrin. Listed are the common variable R groups found on B12. H<sub>2</sub>O/OH are the same group but is dependent on pH (OH at alkaline pH and H<sub>2</sub>O at neutral and acidic). Also highlighted are the major modifiable sites on B12 for conjugation to small molecules or peptides/proteins, whereby binding by the dietary uptake proteins can be minimally affected or selected for, based on drug development requirements.

Several functional groups are synthetically available for modification on B12 (see Figure 1). Only select modification sites, however, maintain the recognition needed to utilize the full B12 uptake pathway (see Figures 1 and 2). Modifications can, however, be made to target specific proteins while reducing affinity for others, a fact recently exploited to target haptocorrin-positive tumors (Waibel et al. 2008). An in-depth discussion of modification sites for either complete, or targeted pathway access, can be found in Section 1.2.

Transport and delivery of B12 through the gastrointestinal tract is dependent on three primary carrier proteins: haptocorrin (HC;  $K_d = 0.01$  pM), intrinsic factor (IF;  $K_d = 1$  pM), and transcobalamin II (TCII;  $K_d = 0.005$  pM), each responsible for carrying a single B12 molecule (Fedosov et al. 2002). B12 is initially released from food by the action of peptic enzymes and the acidic environment of the gastrointestinal system and bound by HC (also known as R-binder or transcobalamin I (TCI)) (Nielsen et al. 2012). HC is a glycoprotein with an apparent molecular mass of between 60–70 kDa and is secreted by the salivary glands (Furger et al. 2013). HC has a high affinity for B12 under acidic conditions ( $pH < 3$ ), allowing it to protect B12 (Holo-HC) from acid

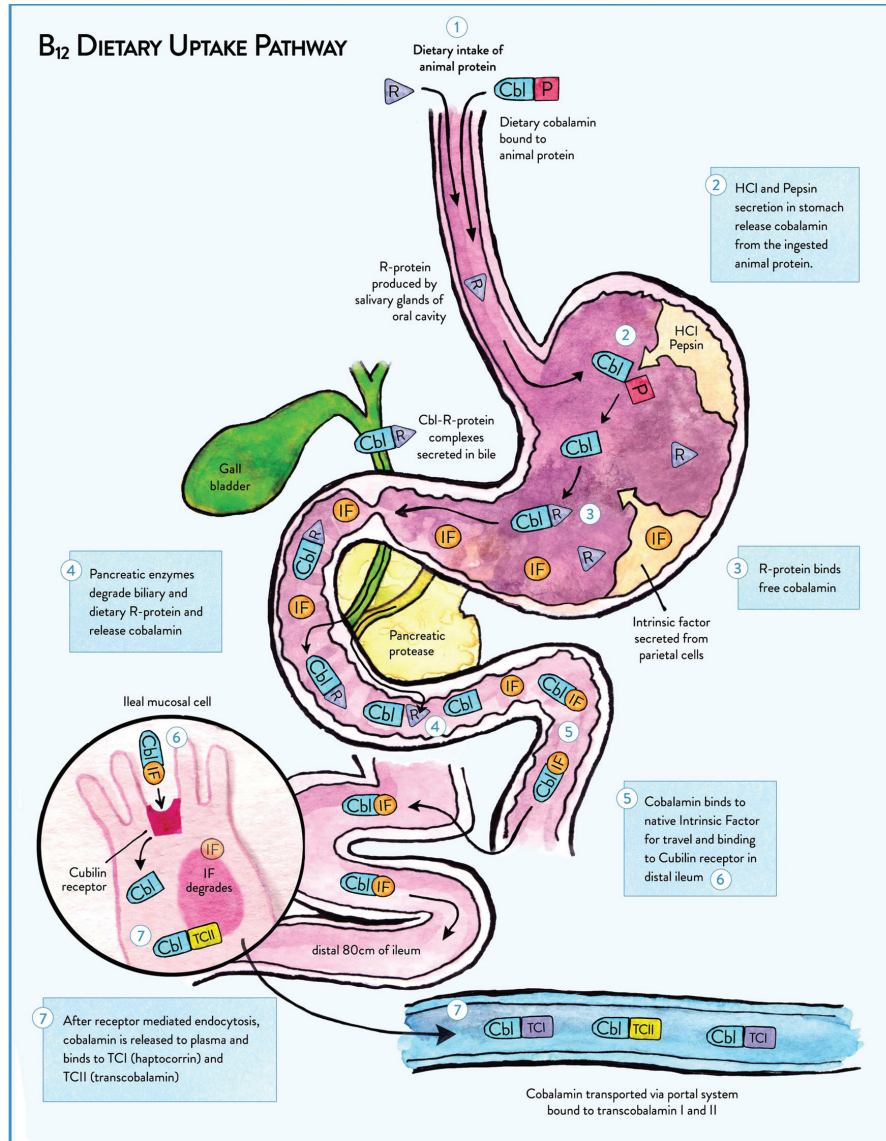


**Figure 2.** Dietary uptake pathway for B<sub>12</sub> in humans. Abbreviations used: R-protein/TCI: Haptocorrin (HC); IF: Intrinsic factor; TCII: Transcobalamin II; Cbl: cobalamin/B<sub>12</sub>. Image produced and used with permission of Xeragenx LLC (St. Louis, MO, USA).

hydrolysis. Holo-HC travels from the stomach to the duodenum, where the increase in pH (> 5) decreases the affinity of HC for B<sub>12</sub> and, combined with pancreatic digestion of HC, causes B<sub>12</sub> release, whereupon it is bound by gastric intrinsic factor (Glass 1963).

IF is a ~50 kDa glycosylated protein that is secreted from the gastric mucosa (Mathews et al. 2007). Once B12 is bound to IF, it facilitates transport to the ileum and passage across intestinal enterocytes. This occurs by receptor-mediated endocytosis via an IF-B12 receptor cubilin (CUB) (Christensen et al. 2013). CUB transports holo-IF in concert with a transmembrane protein amnionless (AM), creating a CUBAM receptor for holo-IF (Fyfe et al. 2004). Following internalization, IF is degraded by lysosomal proteases, such as cathepsin L, and B12 is released into the blood stream, either as free B12 or pre-bound to transcobalamin II (TCII) (Nielsen et al. 2012; Beedholm-Ebsen et al. 2010). There is some controversy in this area as to whether both methods occur or one dominates over the other, and indeed whether there is a third mechanism at play also. Cells that require B12 express the holo-TCII receptor, CD320. Upon internalization, TCII is degraded and B12 is transported from the lysosome for cellular use (Kräutler 2005). Kidney cells also express the megalin receptor, which in part reabsorbs filtered holo-TCII from urine (Moestrup et al. 1996).

Knowledge of the binding between B12 and its various transport proteins is critical if the system is to be successfully exploited from bench-top to bedside. In the last 10 years there has been a huge advance in our critical understanding of protein structure as it relates to the B12 uptake pathway, with the publication of HC, IF, TCII, and cubilin-IF-B12 structures (Furger et al. 2013; Mathews et al. 2007; Wuerges et al. 2006; Andersen et al. 2010). The first solution structure of a B12 conjugate, that of B12 coupled to the anorectic peptide PYY<sub>3-36'</sub> was also recently reported (using NMR methodology) (Henry et al. 2016).

Researchers have a better understanding now of how B12 interacts with its transport proteins, and how these transport proteins interact with their receptors. The implications this can have on drug delivery and sites of potential conjugation can then be better predicted, detailed, rationalized and hence optimized. These endeavors need fundamental knowledge of properties and behavior of B12 in biological systems but also require new or improved synthetic routes to introduce the exact desired modification into the vitamin necessary for specific exploitation.

### **1.2 Modifying B12: the crossing of synthetic and end-goal considerations**

There are multiple sites for chemical modification on the B12 molecule, depending on whether retention of recognition by all transport proteins, or the selective recognition of a subset is required. Therefore, it is critical to consider solvent-accessible surfaces of B12 transport proteins and how such proteins physically bind B12. For IF, this exposure is ~13% (~163 Å<sup>2</sup>), with TCII at ~6.5% (~80 Å<sup>2</sup>) and HC, having the least accessible area at 3.2% (~40 Å<sup>2</sup>) (Figure 3) (Wuerges et al. 2007). These exposures allow for a wide range of modification at select sites on B12 conjugates while retaining (A)

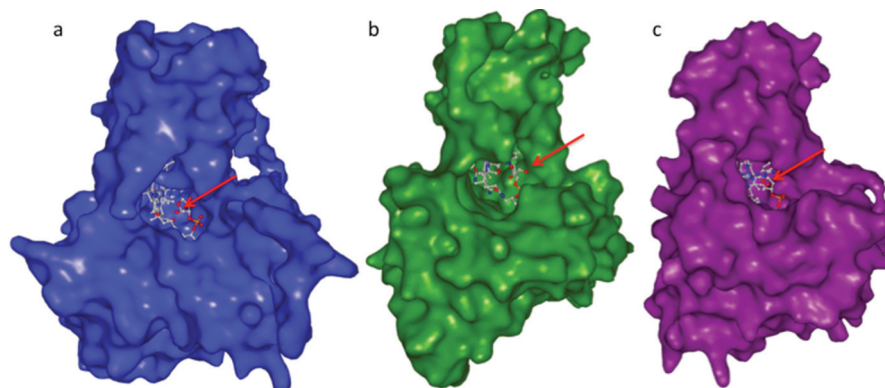


**Figure 3.** Crystal Structures of the Three Transport Proteins Bound to B12. The ribose 5'OH is solvent accessible in all three transport proteins as shown by the arrows. (a) TCII, (b) IF, (c) HC. The structure of TCII, IF, and HC was obtained from [www.pdb.org](http://www.pdb.org); (PDB code 2BB5, 2PMV, 4KK1 respectively). The program Protein Workshop Version 3 was used to display the image.

general pathway acceptance or (B) for selecting specific parts thereof (both (A) and (B) are discussed separately below in Section 1.2).

B12 and the molecule of interest ('drug') can be: (1) coupled directly together; (2) held apart by "spacer" units to give distance between B12 and the molecule; or (3) have the desired drug contained within the carrier, unconjugated, but with the carrier covalently bound to B12. Several functional groups are available for modification on B12, including propionamides, acetamides, hydroxyl groups, the cobalt(III) ion and the phosphate moiety (Proinsias et al. 2013). However, the sites for modification capable of maintaining the recognition of all three transport proteins is limited due to the manner in which B12 is bound by each protein.

All three transport proteins (HC, IF and TCII) bind to B12 with high affinities, but the specificity varies. IF shows the highest specificity for B12, followed closely by TCII, with HC have a broad substrate base including B12 analogs such as cobinamides (Fedosov et al. 2002; Fedosov et al. 2007). It is thought because of the affinity of HC for many inactive B12 analogs that it acts as a scavenger, removing such from the blood and partially digested B12 from the intestine, preventing bacterial access (thus suggesting a role for B12 in bacteriostasis). Viewed synthetically, this implies of course that B12 can be readily modified and retain recognition by HC, whereas IF and TCII offer significantly less range for modification.

### 1.2.1 *General pathway acceptance*

Conjugation of molecules to B12 resulting in the recognition of HC, IF, and TCII have been successful with five major sites to date: (1) the peripheral

corrin ring e-propionamide (Alsenz et al. 2000); (2) the peripheral corrin ring b-propionamide (Waibel et al. 2008); (3) the 5'-hydroxyl group of the ribose ring on the dimethylbenzimidazole 'tail' (Petrus et al. 2007); (4) the 2'-hydroxyl group of the ribose ring (Wang et al. 2007); and (5) the cobalt cation (Tran et al. 2016).

The crystal structure of holo-TCII provides a rationale for why these positions are favored for modification. The phosphate moiety, 2' hydroxyl group, and a, c, d, and g-propionamides have various hydrogen bonds between multiple TCII residues and the solvent molecules indicating any modifications would disrupt that bonding and stability of the TCII-B12 complex (Wuerges et al. 2006). In addition, TCII does not completely encompass B12 and leaves a 1.4 nm solvent-accessible pocket of B12. This pocket shows the phosphate and the ribose moieties protruding and both have been exploited in conjugate design whereby TCII and IF binding has been maintained (Figure 3).

The 2'-hydroxyl group has been modified through activation by diglycolic anhydride but this has not been extensively used in the B12 conjugation field, given the ease of 5'-OH coupling (Wang et al. 2007). Conjugation to the b- and e-propionamides have been a popular choice for chemists for conjugation (Alsenz et al. 2000; Waibel et al. 2008). Such a route requires acid hydrolysis of the amides, typically using 1 N HCl (Pathare et al. 1996). This synthetic route creates multiple mono-acids at the b, d and e-positions, which makes access to targeted specific acids low yielding ( $\leq 15\%$ ) and complex to purify (Pathare et al. 1996). A recent result exploiting this approach however, is that of Schubiger et al., who showed that, based on the tether length off of the b-acid side chain, selectively towards specific transport proteins (IF over TCII, for example) could be achieved (see Section 2.5) (Waibel et al. 2008).

The most common site for modification has, however, become the 5' hydroxyl group, for three main reasons: (1) molecules conjugated here still allow binding retention of the transport proteins (Bonaccorso et al. 2015; McEwan et al. 1999; Fowler et al. 2013); and (2) conjugation to this site is highly facile and selective (Clardy-James et al. 2012; Chromiński and Gryko 2013); and (3) a wide range of modifications have been developed for this site, expanding scope for substrate conjugation (Clardy-James et al. 2012; Wierzba et al. 2016; Chromiński and Gryko 2013; McEwan et al. 1999). The "classic" activation with 1,1'-carbonyldiimidazole or 1,1'-carbonyldi(1,2,4-triazole) with an addition of a primary amine, producing a carbamate linked conjugation, allows for a wide range of molecules to be used (McEwan et al. 1999). Doyle et al. directly modified this position, using 2-iodoxybenzoic acid and 2-hydroxypyridine, to create a carboxylic acid at this position, which could then be readily used to produce amide linked conjugates (Clardy-James et al. 2012; Bonaccorso et al. 2015; Henry et al. 2016; Henry et al. 2015). Later, Gryko et al. developed a "clickable" B12 conjugate, replacing the 5'hydroxyl with an azide, which allows for a high yielding Huisgen-Sharpless copper-azide-alkyl reaction, creating a stable triazole linker with alkyne containing molecules (Chromiński

and Gryko 2013). Most recently, Gryko et al. also developed a reactive pyridyl disulfide group at this site with moderate yield (~60%) (Wierzba et al. 2016). A reactive thiol group creates the possibility of direct disulfide bonds to proteins and molecules, opening up a new area for conjugation that readily exploits redox for the first time.

Another increasingly popular site for modification is the cobalt atom. Transport proteins accommodate significant change at the cobalt  $\beta$ -ligand site, a feature exploited in the biochemistry of B12 (Kräutler 2005). Comparing the binding constants of different biological axial ligands such as methyl, hydroxyl, 5'-adenosylcobalamin, and cyano-cobalamin show no significant difference (Fedosov et al. 2002). In synthetic approaches the Co(III) is typically reduced to Co(I) and then reacted with electrophiles, similar to the biological enzymatic process by methionine synthases (Ruetz et al. 2013; Kräutler 2005). Modifications at the cobalt ion have been limited by the fact that most products are extremely light sensitive (Ruetz et al. 2013; Ruiz-Sánchez et al. 2007). However, in 2013, two groups published light stable phenylethynylcobalamin in two separate syntheses: (1) radical reduction chemistry (Ruetz et al. 2013) and (2) reduction free synthesis (Chromiński et al. 2013). These syntheses allowed for a wide tolerance to functional groups, allowing for more complex ligands on this site to be conjugated or subsequently reacted forward. Another way of modifying the cobalt ion is by metalating the cyano axial group. Fluorophores, radionuclides, cisplatin, vanadate, chlorambucil, and colchicine have been attached to this site (see Table 1).

In 2016, Gryko et al. published moderate-to-high yielding (~40–80%) modifications to the phosphate moiety, the first complete investigation of this group to also include binding studies (Proinsias et al. 2016). The phosphate modification showed preferential binding to IF based on the length of the linker attached to the phosphate. Interestingly, these conjugates are acid, heat, and UV light sensitive possibly allowing for a future new class of cleavable B12 conjugates for drug delivery.

A more recent approach in B12 modifications is creating a dual functionalization of the (a) cobalt ion and (b) 5' hydroxyl group. These conjugates are used for detection and delivery by designing a detectable component with a drug on the same molecule. The detectable component, such as a radionuclide or fluorophore, is conjugated to the 5' hydroxyl group and a drug is either added directly to the cobalt atom or attached via a linker (Tran et al. 2016; Shell et al. 2014). In 2014, Lawrence et al. used this idea to target erythrocytes with the 5'-hydroxyl moiety and delivered a cleavable drug via the cobalt linker (see Section 2.4) (Smith et al. 2014).

While understanding the maintenance of transport protein binding and modified B12 conjugate design and synthesis has made significant strides, it is important to note that little is known about the effects a modified holo-protein complex had on recognition and binding to its receptor. In 2010, Andersen et al. published the crystal structure of cubilin<sub>(5-8)</sub>-IF-B12 (Andersen et al. 2010). This structure provides an outline of how the holo-IF interacts with cubilin,



Table 1. Vitamin B12-Small Molecule Conjugates.

Molecule	Conjugation Site	Linker	Application	Ref
b-nido-carborane	b-acid	diaminobutane	Antitumor therapy	(Hogenkamp et al. 2000)
d-nido-carborane	d-acid	diaminobutane	Antitumor therapy	
Bis-nido-carborane	b- and d-acid	diaminobutane	Antitumor therapy	(Bauer et al. 2002)
NO	cobalt atom	direct	Antitumor therapy	(McGreavy et al. 2003)
SulfoCy5	Ribose 5'-OH	1,6-diaminohexane	Imaging	
Colchicine	Cobalt atom	4-chlorobutyricacid chloride	Delivery	
[Re(OH <sub>2</sub> )(CO) <sub>3</sub> ]	Ribose 5'-OH*	Octadecylamine	Delivery	(Smith et al. 2014)
	Cyano ligand	Imidazolecarboxylic acid	Linker for biomolecules	(Kunze et al. 2004)
	Cyano ligand	2,4-dipicolinic acid	Linker for biomolecules	
	Cyano ligand	Serine	Linker for biomolecules	
	Cyano ligand	N,N-dimethylglycine	Linker for biomolecules	
Cisplatin	Cobalt atom	Cyano ligand	Oral anticancer	(Mundwiler et al. 2005)
Cisplatin-2'deoxyguanosine	Cobalt atom	Cyano ligand	Proof of principle	
Cisplatin-methylguaniosine	Cobalt atom	Cyano ligand	Proof of principle	
[trans-PtCl(NH <sub>3</sub> ) <sub>2</sub> ]	Cobalt atom	Cyano ligand	Delivery	(Ruiz-Sánchez et al. 2007)
[trans-PtCl <sub>2</sub> (NH <sub>3</sub> ) <sub>2</sub> ]	Cobalt atom	Cyano ligand	Delivery	
[Cis-PtCl <sub>2</sub> (NH <sub>3</sub> ) <sub>2</sub> ]	Cobalt atom	Cyano ligand	Delivery	
PtCl <sub>3</sub>	Cobalt atom	Cyano ligand	Delivery	
VO <sub>2</sub> (OH/H)	Cobalt atom	3-hydroxy-2-methyl-1-propyl-1H-pyridin-4-one	Diabetes treatment	(Mukherjee et al. 2008)
VO <sub>2</sub>	Cobalt atom		Diabetes treatment	
Khodamine 6G	Ribose 5'-OH	Trans-1,4-diaminocyclohexane	Imaging	(Lee and Grissom 2009)
Gd <sup>3+</sup>	Ribose 5'-OH	Anhydride of DTPA	Imaging	(Siega et al. 2009)
		Anhydride of TTHA	Imaging	
Rhodamine isothiocyanate	NA	HPMA	Imaging	(Russell-Jones et al. 2011)
Re(CO) <sub>3</sub> - 1,1 -bisthiazole	Ribose 5'-OH	1,4- diaminobutane	Imaging	(Vortherms et al. 2011)
[(trans-Pt(NH <sub>3</sub> ) <sub>2</sub> )-(Cyt)] <sup>+2</sup>	Cobalt atom	Cyano ligand	Delivery, IC <sub>50</sub> of 230 nM*	(Tran et al. 2013)

Table 1. contid....

Table 1. *contd.*

Molecule	Conjugation Site	Linker	Application	Ref
$[\{\text{trans-Pt}(\text{NH}_3)_2\}\text{-}\{\text{DTIC}\}]^{+2}$	Cobalt atom	Cyano ligand	Delivery	
$[\{\text{trans-Pt}(\text{NH}_3)_2\}\text{-}\{\text{Ana}\}]^{+2}$	Cobalt atom	Cyano ligand	Delivery	
Bodipy650	Cobalt atom	3-aminopropyl	Delivery	(Shell et al. 2014)
cAMP	Cobalt atom	3-aminopropyl	Delivery	
Doxorubicin	Cobalt atom	3-aminopropyl	Delivery <sup>†</sup>	
Methotrexate	Cobalt atom	3-aminopropyl	Delivery	(Smith et al. 2014)
Dexamethasone	Ribose 5'-OH <sup>*</sup>	Octadecylamine	Delivery	
	Cobalt atom	3-aminopropyl	Delivery	
$[\{\text{Re}\}\text{-}\{\text{cis-PtCl}(\text{NH}_3)_2\}]^+$	Ribose 5'-OH <sup>*</sup>	Octadecylamine	Delivery	
	Cobalt and 5'-OH	Cobalt and Ribose-5'-OH	Delivery	(Tran et al. 2016)

NA: Not available; DTPA: diethylenetriamine- $N,N,N',N'',N'''$ -pentaacetic acid; DCC:  $N,N'$ -dicyclohexylcarbodiimide; TTHA: Triethylenetetramine- $N,N,N',N'',N''',N''''$ -hexacetic acid; HPMA: Lysine-modified-hydroxypropyl-methacrylamide; Cyt: cytarabine; DTIC: dacarbazine; Ana: anastrozole. <sup>\*</sup>compared to  $IC_{50}$  of B12- $[\text{trans-PtCl}(\text{NH}_3)_2]$  of 8  $\mu\text{M}$ . <sup>\*</sup>A two functional B12 conjugate. <sup>†</sup>Showed similar cell death as the control doxorubicin. Imaging defined as fluorescence/confocal microscopy.

allowing researchers a new tool to determine the implications of modification on receptor binding (a study not yet conducted to our knowledge).

### 1.2.2 Targeting specific transport proteins

A B12 conjugate injected in the systemic circulation can be bound by HC or TCII. Initially, it was hypothesized that cancer therapy/imaging using a B12 based delivery mechanism would work based on a projected increase in the TCII receptor, CD320, in a variety of cancer types such as breast, ovarian, thyroid, uterine, testis, and brain cancer (Mundwiler et al. 2005; Collins and Hogenkamp 1997). This overexpression of CD320 would provide sufficient uptake of a tracer bound to endogenous TCII vs uptake in healthy tissue. Such studies, however, suffered from high background (Section 2.5).

The use of HC binding was not investigated until 2008, when Schubiger et al. made a series of B12 conjugates that would selectively bind HC (and IF), but not TCII (Waibel et al. 2008). The hypothesis here was that, given the presence of TCII and HC in serum, and assigning the high background to TCII mediated cell entry, targeting only HC would offer improved results. Membrane associated HC, expressed *de novo*, in certain cancer cell lines offered a possible route to selectivity, absent from the approach to CD320 uptake (Carmel 1975). In 2014, a select conjugate,  $^{99m}\text{Tc}$ -PAMA-cobalamin capable of selectively binding HC in blood serum, used in the detection of breast, colon, lung, and pharyngeal cancers in human patients, showed greater tumor

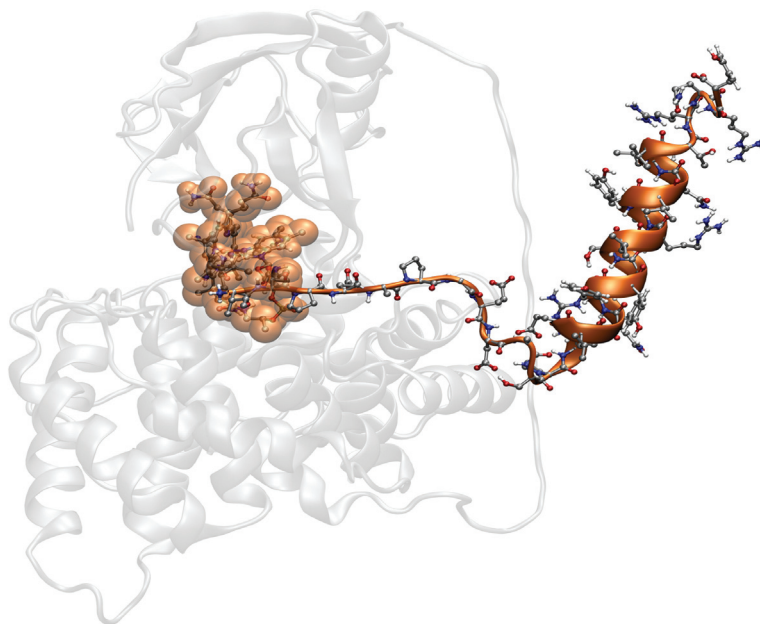


**Figure 4.** IF-B12-PYY<sub>3-36</sub>. Highlighted is the B12-PYY<sub>3-36</sub> (gold) and IF (gray).

uptake and reduced TCII-based background (see Figure 4) (Sah et al. 2014). This publication is highly significant for B12 drug development, especially since it was performed in a human patient.

### 1.2.3 Structural investigations of B12 conjugates

As mentioned above there are three ways in which B12 and a molecule can be connected (elaborated upon in Section 1.2). Connecting through a “linker” to create length is favored in conjugates mainly for ease of synthesis (a result of favored modification techniques). In considering modification a few questions arise; (a) are all linker lengths created equal, and (b) do you need a certain “space” to better allow binding to transport proteins as well as allow the peptide to function properly?

In 2016, Doyle et al. published a structural study, using NMR and molecular dynamics, to predict agonism at the peptide receptor for a B12-peptide (Henry et al. 2016). They used two B12-peptides (both based on B12 conjugates of the anorectic Y2-receptor agonist Peptide YY (PYY<sub>3-36</sub>)) with a difference of one methylene unit length and assessed the B12-peptide’s agonism at its receptor as well as performed constrained molecular dynamics (MD) with each. The data (collected by NMR and used to constrain MD) showed that the conjugate with a longer tether had more hydrogen bonding to B12 and predicted lower agonism at the Y2-R target receptor, a result confirmed by *in vitro* cell assay (Henry et al. 2016). Such work offers the possibility of using constrained MD to predict function a priori and minimize the need to synthesize extensive libraries of compounds for screening. This data also showed for the first time in a solution structure, that a B12-peptide/protein can be made without prominently affecting the peptides secondary structure (and hence function).

## 2. Recent Highlights in B12 Drug Development

There are several excellent reviews in this area that the reader is referred to here (Zelder 2015; Clardy et al. 2011). What is noted below are recent specific highlights and general overview considerations that endeavor to ask where the field is going and what the big hurdles/goals are in the field of B12 drug development.

### 2.1 Oral delivery

Few peptide/protein-based drugs have the ability to survive the gastrointestinal tract and/or cross the intestinal wall to make it to the systemic circulation. The B12 pathway has naturally developed a complex mechanism for this uptake. Researchers can “hijack” this pathway to deliver B12-drugs in an oral manner. Early research in B12-peptide/protein oral drug delivery was conducted by Russell-Jones and co-workers in the 1990’s focusing on B12 conjugates of

Table 2. Vitamin B12-Peptide Bioconjugates.

Peptides	Conjugation Site	Linker	Application	Ref
BS Albumin	Phosphate	Phosphate-amine	NA	(Hippe et al. 1971)
YG-globulin	Phosphate	Phosphate-amine	NA	
HS-albumin	e-acid	GABA	Antibody response	(Ahrenstedt and Thorell 1979)
IFN-con	Ribose 5'-OH	Glutaryl	24 – 28% activity*	(Habberfield et al. 1996)
G-CSF	e-acid	Disulfide	61-66% activity <sup>†</sup>	(Russell-Jones, Westwood, and Habberfield 1995)
		Amide	29-85% activity <sup>‡</sup>	
EPO	e-acid	Hydrazine	ND-100% activity <sup>†</sup>	
		Amide	ND-34% activity <sup>†</sup>	
ANTIDE-1	e-acid	Hydrazide	17-22% activity <sup>‡</sup>	
		EGS	ND	(Russell-Jones et al. 1995)
		Amide	30% IF recognition	
		disulfide	65% IF recognition	
		Hindered thiol	54% IF recognition	
		thioester	81% IF recognition	
		Transglutamase cleavable tetrapeptide	60% IF recognition	
ANTIDE-3	e-acid	EGS	ND	
		Amide	ND	
		disulfide	ND	
		Hindered thiol	37% IF recognition	
		thioester	65% IF recognition	
		Transglutamase cleavable tetrapeptide	48% IF recognition	
LHRH	e-acid	Amide	45% absorbed	(Alsensz et al. 2000)
DP3	e-acid	Amide	23% absorbed	
		Hexyl	42% absorbed	
Insulin	Ribose 5'-OH	Amide	26% drop is glucose	(Petrus et al. 2007)
PYY <sup>(3-36)</sup>	Ribose 5'-OH	Amide	Oral delivery, 200 times higher plasma levels <sup>††</sup>	(Fazen et al. 2011)

Table 2. contd....

Table 2. *contd.*

Peptides	Conjugation Site	Linker	Application	Ref
Exendin-4	Ribose 5'-OH	l-amino-3-butyne	11% decrease in food intake <sup>g</sup>	(Henry et al. 2015)
<b>Encapsulated insulin delivery</b>	Ribose 5'-OH	l-amino-3-butyne	4 fold increase in stability <sup>y</sup>	(Bonaccorso et al. 2015)
B <sub>12</sub> coated-dextran nanoparticles	Ribose 5'-OH	Amide	70 – 75% drop in plasma glucose	(Chalasanmi et al. 2007)
B <sub>12</sub> -phthaloyl chitosan carboxymethyl nanoparticles	Ribose 5'OH	dihydrazine	35% drug release	(Fowler et al. 2013)
B <sub>12</sub> -trimethyl chitosan nanoparticles	Ribose 5'-OH	dihydrazine	29% drug release	
B <sub>12</sub> -chitosan layered CaPO <sub>4</sub> nanoparticles	Ribose 5'-OH	Amide	12 fold increase in effective duration <sup>Δ</sup>	(Verma et al. 2016)

\*compared with native IFN-con. <sup>T</sup>compared with unconjugated G-CSF and EPO. <sup>g</sup> compared to native PYY levels are meal ingestion. <sup>h</sup>compared to unconjugated PYY<sub>(3-36)}</sub>. <sup>y</sup>when bound to IF vs unbound to IF. <sup>Δ</sup> compared to injected insulin. ND = not determined. BS, HS: Bovine and human serum; IFN-con: Consensus interferon; G-CSF: Granulocyte colony stimulating factor; EPO: Erythropoietin; ANTIDE: N-Ac-D-Nal(2)D, D-Phe (pCl), D-Phe (3), Ser, Lys (Nic), D-Lys(Nic), Leu, Lys(IPr), Pro, D-Ala-NH<sub>2</sub>; LHRH: Luteinizing hormone-releasing hormone; DP3: Octapeptide (Glu-Ala-Ser-Ala-Ser-Tyr-Ser-Ala); GABA: γ amino butyric acid; EGS: Ethylene glycol bis(succinimidyl succinate).

granulocyte colony stimulating factor, erythropoietin, luteinizing hormone-releasing hormone, ANTIDE-1, and ANTIDE-3 (see Table 2) (Russell-Jones et al. 1995; Russell-Jones, Westwood and Habberfield 1995). Since then other groups have shown B12-molecules being transported via the B12 pathway across intestine cell lines *in vitro* and *in vivo* (Petrus et al. 2009; Dix et al. 1990; Verma et al. 2016). More recent highlights include that of a B12-PYY<sub>3-36</sub> conjugate, which, when administered orally achieved clinically relevant levels of PYY<sub>3-36</sub> in blood of a rat model (~200 pg/mL after 1 h) (see Table 2 and Figure 4) (Fazen et al. 2011). This conjugate was not, however, shown to have any functional effect. In 2016, Mishra et al. showed a B12-chitosan layered nanoparticle that encapsulated insulin had a 10-fold increase in effective insulin duration *in vivo* when administered orally, achieving a maximum drop in glucose of ~40% (Verma et al. 2016).

Although data suggests drugs can be delivered orally through this pathway there are some questions left unanswered such as; (a) would oral administration be feasible because of the limit of uptake due to the expression of CUB, (b) amount of drug that gets into the blood serum and (2) would pre-binding of B12-drug to IF allow more efficient uptake? It is known that there is a limited pool of CUB expressed in the terminal ileum, which limits IF-mediated absorption to around 1.5 µg per meal (1 nmole/dose) (Schjonsby and Andersen 1974). Survival of enterocyte passage by a peptide bound to B12 is also unknown, as is whether such a conjugate would arrive in serum bound or unbound to TCII (with implications for subsequent function) (see Section 3).

## 2.2 Subcutaneous delivery

As mentioned above a “hijacking” of the B12 pathway can be exploited for oral delivery. However, this “hijacking” is not limited to the use of oral administration. In 2015, Doyle et al. published on a subcutaneously administered B12-PYY<sub>3-36</sub> (Henry et al. 2015). Peptide YY<sub>3-36</sub> (PYY<sub>3-36</sub>) is an endogenous appetite suppressing peptide that is an agonist for the NPY2 receptor in the intestines and arcuate nucleus of the hypothalamus. Food intake (FI) was significantly reduced over a five-day course for B12-PYY<sub>3-36</sub> (24%) compared to PYY<sub>3-36</sub> (13%). In addition, reduction of FI was more consistent after each dose through the course of a rat feeding cycle for B12-PYY<sub>3-36</sub> (26%, 29%, 27%) compared with PYY<sub>3-36</sub> treatment (3%, 21%, 16%)<sup>ref</sup>. These findings demonstrate significant pharmacodynamic (PD) improvement upon simple conjugation of B12 to PYY<sub>3-36</sub> for subcutaneous delivery. Of interest also was the fact that, when looking at the pharmacokinetic (PK) parameters of the B12 conjugate compared to free PYY<sub>3-36</sub>, it is clear there is minimal improvement in terms of serum half-life, clearance, volume of distribution. Of note, in PK terms, was the observed increased C<sub>max</sub> for B12-PYY<sub>3-36</sub> compared to PYY<sub>3-36</sub>, but at the same T<sub>1/2</sub> (suggesting B12 conjugation did not increase subcutaneous uptake rate, but did improve amount that was passaged).

### **2.3 Peptide and protein protection**

One of the major open questions in the field has been whether binding a peptide/protein to B12, with or without subsequent B12 binding protein interaction, could offer any protection against proteolysis. In 2015, Doyle et al. attempted to address this focusing on the stability (as defined by retention of peptide/protein agonist receptor function) of a B12 conjugate of the glucose controlling (GLP-1 receptor agonist) incretin exendin-4 (Ex-4) (Bonaccorso et al. 2015). Either as the straight B12-conjugate, or bound by IF, function at the GLP1-R relative to undigested controls was investigated using proteases from both the gastrointestinal tract (trypsin and chymotrypsin) and kidney (meprin  $\beta$ ). The addition of IF produced up to a four-fold increase in function compared to Ex-4 alone, when digested by trypsin, and no statistical decrease in function when challenged by meprin  $\beta$  (Bonaccorso et al. 2015). These results offer a significant opportunity for exploitation. Increase in gastric stability, even on a small percentage scale, could provide a route to achieving the desired effect orally. This work also suggests the possibility of utilizing an IF-B12-drug complex in serum, thus expanding use of IF beyond oral administration. If the fact that IF is not found in serum produces antigenicity, it is likely that switching IF for HC would achieve similar improvements in protease protection, and mitigate the antigenicity (thus, suggesting here using the pathway for PK improvements).

### **2.4 Photo-cleavable conjugates**

In 2014, Lawrence et al. published a series of B12-fluorophores that were modified on the cobalt atom. This series was designed, and proven, to be selectively photocleavable at different wavelengths, tissue-penetrating light (600–900 nm), in a mixture (Shell et al. 2014). The photocleavable-B12 system was then used as a platform to selectively deliver drugs. Initially, B12-cAMP and B12-doxorubicin (B12-Dox) activity was shown *in vitro*. B12-Dox showed cell viability equal to that of the control doxorubicin and B12-cAMP showed a light only induced cell morphology change typical of cAMP-dependent protein kinase activity (Shell et al. 2014).

A follow up paper, also published in 2014 by Lawrence et al., used the photocleavable-B12 platform to deliver three anti-inflammatories: methotrexate, colchicine, and dexamethasone (see Table 2) (Smith et al. 2014). They used the 5'-hydroxyl group to target erythrocytes by using a C<sub>18</sub> hydrophobic linker and functionalized the cobalt atom with each drug. After loading the erythrocyte with the B12-drug and a modified fluorophore (added as a separate molecule) they were able to photocleave the drug into the surrounding media and observe cell morphology changes (Smith et al. 2014). This approach then was able to selectively deliver drugs to targeted cell lines.



## 2.5 Imaging

Table 3 lists the B12-imaging agents reported to date. As mentioned above in Section 1.2.2, historically, imaging using B12 targeted the CD320 receptor, based on the premise that overexpression of CD320 on rapidly proliferating tumor cells would provide necessary tumor to background ratio's (Collins and Hogenkamp 1997; Mundwiler et al. 2005). However, this technique proved highly limited due to observed high background uptake across tissues. In 2014, Burger et al. published a human *in vivo* study using a  $^{99m}\text{Tc}$  probe, based on a B12-conjugate modified at the b-acid with a 4-carbon linker (B12-PAMA) in patients with five types of cancer: lung, colon, hypopharyngeal, prostate, and breast (Sah et al. 2014). The conjugate was shown initially to be selectivity bound by HC, but not to be bound by TCII (Waibel et al. 2008). Initial results showed uptake in select cancers but with moderate background (see Figure 5). After pre-dosing with excess B12, background was further reduced with an average uptake of ~4.5% was observed (Sah et al. 2014).

In 2014, Ikotun et al. published a B12-PET imaging probe based on a B12-NOTA conjugate with  $^{64}\text{Cu}$  (Ikotun et al. 2014). Small animals tumor studies were conducted with four cancer cell lines: pancreatic, ovarian, colorectal, and murine melanoma. However, as was observed with  $^{99m}\text{Tc}$  studies, the same high background trend was seen. The tumor % ID/g achieved was ~4%.

## 2.6 Anti-vitamins

For a full comprehensive review of anti-vitamins, we refer you to two recent reviews by Zelder and Kräutler (Kräutler 2015; Zelder et al. 2015).

B12 based anti-vitamins are a new class of B12 conjugates. Anti-vitamins are defined as molecules that counteract biological action of vitamins. B12 based conjugates interfere with B12's ability during the enzymatic process by preventing the redox potential of the cobalt atom. There are two types of antivitamins: ones they prevent B12 from (a) forming into methylcobalamin and adenosylcobalamin (Ruetz et al. 2013), and (b) converting into a base "off" form (Zhou and Zelder 2010). These conjugates are designed to "lock" the cobalt atom and therefore remove its capability to act as a B12 vitamin.

Zelder et al. has focused on modifying the dimethylbenzimidazole (DMB) group within B12 (see Figure 1) (Zhou et al. 2012). By altering DMB's linker to resemble peptides, creating a rigid backbone, the B12 is locked into a "base on" form. These conjugates have been shown *in vitro* to inhibit L. Delbruekii growth in a concentration dependent manner (Zhou et al. 2012). Kräutler et al. have modified the R axial group, shifting the cobalt redox potential more negative and therefore making reduction very difficult (Ruetz et al. 2013). The inert 'aryl-cobalamins' thus produced have been shown to bind to transport proteins but are not functional in B12 dependent enzymes (Mutti et al. 2013).

Table 3. Vitamin B<sub>12</sub> Used in Radio Imaging.

Molecule	Conjugation Site	Linker	Use	Ref
<sup>99m</sup> Tc-DTPA	b-acid	1,4diaminobutane	Radio Imaging	(Collins and Hogenkamp 1997)
<sup>111</sup> In-DTPA	b-acid	1,4diaminobutane	Radio Imaging	(Kunze et al. 2004)
[ <sup>99m</sup> TcO <sub>4</sub> ] <sup>-</sup>	cyano ligand	Imidazolecarboxylic acid	Radiodiagnosis	
		Picolinic acid	Radiodiagnosis	
		2,4-dipicolinic acid	Radiodiagnosis	
		Serine	Radiodiagnosis	
		N,N'-dimethylglycine	Radiodiagnosis	
<sup>131</sup> I	Cobalt atom	Cisplatin	Radio Imaging	(Ruiz-Sánchez et al. 2007)
[ <sup>99m</sup> Tc(CO) <sub>3</sub> (OH <sub>2</sub> ) <sub>3</sub> ]	b-acid	Propyl-PAMA-OEt	Radio Imaging	(Waibel et al. 2008)
		Ethyl-PAMA-OEt	Radio Imaging	
		Butyl-PAMA-OEt	Radio Imaging	(Sah et al. 2014)
		Pentyl-PAMA-OEt	Radio Imaging	
		Hexyl-PAMA-OEt	Radio Imaging	
<sup>64</sup> Cu-SCN-Bn-NOTA	Ribose 5'-OH	Ethylenediamine	Radio Imaging	(Ikotun et al. 2014)

DTPA: diethylenetriamine-N,N',N'', N'''- pentaacetic acid; PAMA: [pyridine-2-ylmethyl-aminol]-acetic acid; SCN-Bn-NOTA: isothiocyanatobenzyl-1,4,7- triazacyclononane-N,N',N''-triacetic acid. \* Conjugate was selected for human studies targeting tumors.

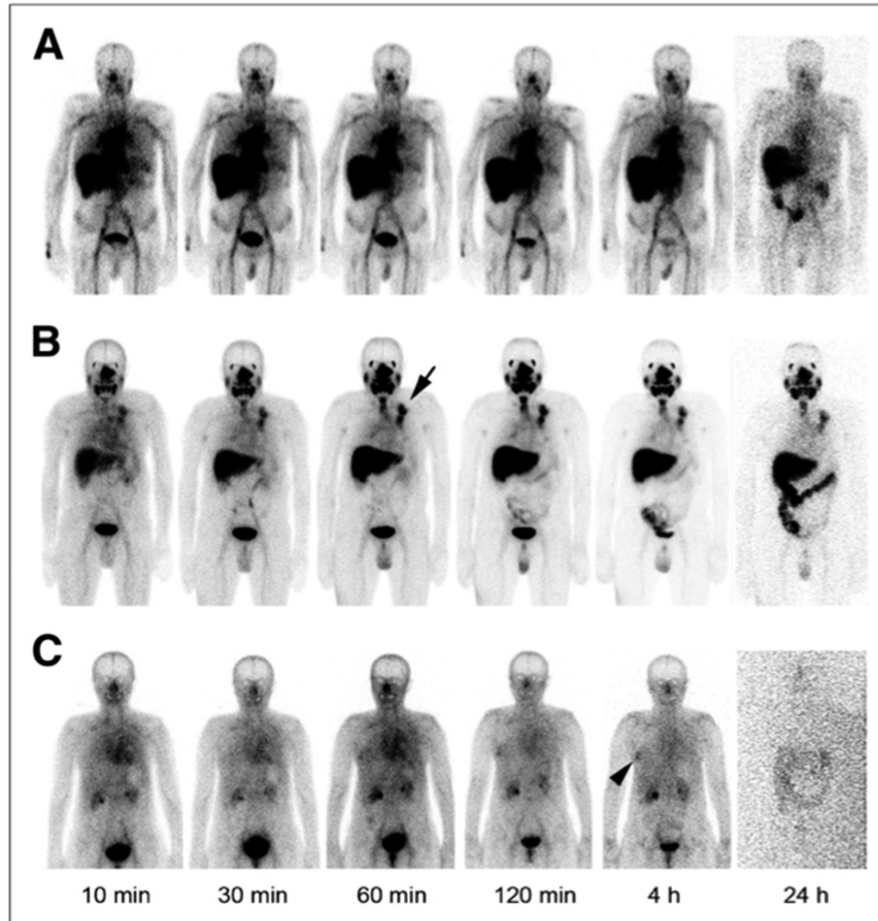


**Figure 5.** SPECT-CT Scans Targeting Haptocorrin in Human Patients. Partial-body scans after distribution of  $^{99m}\text{Tc}$ -PAMA-cobalamin at 10, 30, 60, 120, 240 min, and 24 h. (A) Without Cbl pre-dose has high blood-pool uptake over 24 h and no tracer accumulation in the tumor (hypopharynx), (B) After 20-mg Cbl pre-dose has reduced blood-pool activity and high uptake in bronchial carcinoma (arrow) stable over 24 h, (C) After 1,000-mg Cbl pre-dose has reduced liver uptake and only faint uptake in metastatic right axillary lymph node (arrowhead). This research was originally published in the *Journal of Nuclear Medicine* by I. A. Burger et al. 2014; 55: 43–49. © by the Society of Nuclear Medicine and Molecular Imaging, Inc.

B12 anti-vitamins could be used to attempt to effectively starve cancer cells of B12. The overall effect on the patient would most likely be concomitant pernicious anemia. Looked at another way, these antivitamins could also be used in animal models, to study the effects of B12 deficiency in a variety of diseases.

### **2.7 Considerations for murine models of B12 conjugates in *In vivo* studies**

Upon careful consideration of structural design and *in vitro* target validation, the next obvious step is to move into animal models, and in particular that of rodent models. What needs to be made clear here is the fact that there are several major concerns about using murine models for extrapolation to humans.

The first major issue in the use of murine models lies in the fact that, humans, as described in Section 1.1, have two B12 binding proteins in serum, namely TCII and HC (Nielsen et al. 2012). As demonstrated in a 2011 paper by Nexø et al., mouse TCII has a single serum protein with features of both TCII and HC (Hygum et al. 2011). This work can be extrapolated to rats and other common small animal models such as guinea pigs by BLAST analysis. Developing systems to prevent TCII binding (to lower background uptake in imaging studies or to prevent loss of function upon serum delivery in oral studies, for example) by modifying the B12 structure (as discussed in Section 1.2.2 and 2.5) are significantly hampered then, since the broader specificity of binding inherent in the murine TCII prevents the desired effect from being manifest. In such situations, it is likely that models, such as the rabbit (documented to contain both the serum TCII and HC proteins as in humans) would be a more appropriate choice (Nexø and Olesen 1981). Cow (Polak et al. 1979), monkey, pig, and dog (Hygum et al. 2011) have also been documented to contain each of the two serum proteins, although these are not typically first pass *in vivo* screen models.

Another issue with the choice of murine models is the variation in unsaturated TCII concentrations both within model (depending on diet) and then (in terms of nmol/L) between the mouse (> 20 nmol/L), rat (2 nmol/L) and human (0.6–1.5 nmol/L). The concern here has to be with knowing the concentration of unsaturated TCII in the actual model as measured on the specific diet that model is being provided. Factoring this information into the concentration range difference inherent across the species noted, the fact that the murine models have a single serum TCII protein with HC-type properties and understanding that typically 80% of total bound B12 in human serum is bound to HC, not TCII, all must be considered when looking to use a murine model in *in vivo* B12 conjugate drug development studies (Nielsen et al. 2012).

When considering model choice for oral studies, the B12 uptake capacity must also be noted. In humans the uptake capacity is in the range of 1 nmoles per dose (Schjonsby and Andersen 1974), whereas in rats, for example, it is in

the order of 10 pmoles per dose (Nexø et al. 1985). Combining such an uptake capacity with the increased serum TCII levels noted above, makes extrapolating anything observed (or not observed) from murine model to human relevance exceedingly difficult.

### 3. Open Questions and Possible Directions

The use of B12 supplementation in the treatment of B12 deficiencies or in tandem with other drugs to treat or mitigate disease is well documented. A recent review of clinical trials data through the US National Institutes of Health ([www.clinicaltrials.gov](http://www.clinicaltrials.gov); accessed April 7th 2016; search term: vitamin B12) reveals 79 open studies (of 346 total studies), all of which are focusing on B12 supplementation in the methyl-, hydroxo-, or cyano-B12 forms primarily, and all aiming to investigate such for improved uptake responses in the elderly, in children, those with feeding issues, etc., or looking at whether such can lower homocysteine levels in vegetarians, or positively effect neurological development, etc. While there has been considerable progress and developments made in exploring and pushing pharmaceutical development based on exploiting the B12 dietary pathway and its various components through use of B12 conjugation (or in general terms, covalent attachment to B12 or B12 analogs such as cobinamides), there remains no FDA approved drug based on such a system, or indeed any open trials noted under the criteria above).

Several questions that remain to be addressed then are:

1. Whether a drug (particularly a nucleic acid or peptide/protein), can be successfully and reproducibly delivered orally upon conjugation to B12 and produce a clinically relevant response, especially beyond the rodent model. Empirical studies of function upon oral dosing would answer this directly but interesting side questions that remain are (a) whether a bound nucleic acid or peptide/protein, can survive the lysosome upon cubilin mediated uptake, and (b) if the conjugate arrives in the blood pre-bound to TCII or not (or both).

Question 1a is important because partial destruction upon enterocyte passage would undermine, or change, PK function, but also may provide false positive data for successful delivery of certain levels of drug, if part of the surviving B12-peptide conjugate for example, retained the target epitope (e.g., using ELISA). Validating, *in vitro*, IF protection against lysosomal degradation would be a missing link between the gastrointestinal track and blood for a B12-conjugate.

Question 1b a is critical when one considers that, if/when bound to TCII, there is a strong likelihood that the delivered pharmaceutical will be rapidly endocytosed into proliferating cells. This rapid clearance and non-specific targeting would be expected to have a detrimental effect on

drug function where it is necessary to target receptors on a particular organ, for example. Establishing the surety of conjugate arrival in the blood, but loss of function due to TCII binding, would then warrant an investigation of oral uptake using B12 modified to maintain IF recognition but not that by TCII. Even if it is shown that the primary mechanism of B12 delivery into blood is bound to TCII, it is clear from the work of Nexo et al. that at least 50% of the B12 dose enters the blood when TCII is removed (Beedholm-Ebsen et al. 2010). This reduced uptake would then need to be factored into uptake capacity calculations.

2. Whether the B12 pathway can be used to (a) increase or decrease drug delivery across the blood-brain barrier (BBB), and (b) whether upon BBB passage, it can change localization within the brain. These questions are of interest because, in general, it is difficult to passage drugs to the brain and any effect on such can be a positive. In some cases, removing brain uptake, while maintaining general systemic effects, is warranted. A B12-peptide conjugate that maintained glucoregulatory control via the pancreas while removing CNS activation that triggers food intake reduction (and under-wanted malaise/nausea) would be of interest for example. Along a similar line, modifying localization within specific brain architectures by, for example, targeting a B12-peptide to the paraventricular neurons and keeping them from the arcuate nucleus would make for a platform technology with, probably inherent and definable, characteristics that could be applied to a particular drug subset.
3. Whether the pathway can be used to develop a new pharmacokinetic (PK) platform technology along the lines of targeting serum albumin to improve serum half-life *in vivo*. A recent patent (R. P. Doyle; Syracuse University, 62/323,013)), describes HC targeting substrates such as dicyano-cobinamide peptide conjugates to achieve this half-life improvement. With a half-life in blood of ~9 hours and no known receptors in healthy cells when fully glycosylated, HC is an exciting avenue for PK improvement. The unsaturated binding concentration for HC in serum is 0.3 nmol/L (compared to ~1 nmol/L for TCII in humans with 80% of B12 and B12 analogs bound up by HC and the remaining 20% by TCII) so, while B12 itself would be expected to be bound up by both HC and TCII, some of the administered drug would be lost to TCII if such were used (Sheppard et al. 1984). Exploiting this area of the dietary pathway remains mostly unexplored, although it worth noting again here that Alberto et al. did attempt to target *de novo* expressed membrane associated HC in cancer cells for imaging (Waibel et al. 2008; Sah et al. 2014).
4. Whether prolonged administration of a B12-drug would have detrimental effects on healthy B12 dependent physiology. Nexo et al. produced a study over 27 days in mice administered high doses of dicyano-cobinamide (4.25 nmol/h) by osmotic pump and followed B12 bio-markers such

as the plasma levels of cysteine, total homocysteine, methionine and methylmalonic acid (Lilballe et al. 2012). This study showed no significant changes in plasma levels for the markers in question over the time-period under study. The production of so-called 'antivitamin B12' will allow further elaboration of this area, as would the incorporation of the B12-conjugate under investigation into a B12 dependent assay to gauge if such B12 remained functional (or to what degree it remained functional, at least).

The future of the field lies in expanding and exploiting on the successes of the past several years. What is evident from the work to date is that there is considerable potential in the use of B12 and/or its transport proteins, be it for delivery, targeting, improved PK/PD, etc. The full potential of the B12 dietary uptake pathway has not been realized and the authors believe that with such realization, will come clinical development.

### Acknowledgments

This research was supported by the National Institute of Diabetes and Digestive and Kidney Diseases of the US National Institutes of Health under award number R15K097675-01A1. This work was also supported by Xeragenx LLC (St. Louis, MO, USA). The content is solely the responsibility of the authors and does not necessarily represent the official views of the US NIH or Xeragenx LLC.

**Keywords:** Vitamin B12, drug delivery, dietary pathway, targeting, synthesis, modification, cubilin, CD320, blood-brain barrier, imaging, cancer, pharmacokinetics, pharmacodynamics, oral uptake

### Abbreviations

HoloTC	:	holotranscobalamin
HC	:	haptocorrin
TCII	:	transcobalamin
holoHC	:	holohaptocorrin
IF	:	intrinsic factor
B12/Cbl/ cobalamin	:	vitamin B12
CUB	:	cubilin
AMN	:	amnioless
CUBAM	:	cubilin/amnioless receptor
BBB	:	blood brain barrier
NMR	:	nuclear magnetic resonance
PYY	:	peptide YY
FI	:	food intake

PD	:	pharmacodynamics
PK	:	pharmacokinetics
C <sub>max</sub>	:	maximum serum concentration
T <sub>1/2</sub>	:	half-life
Ex4	:	exendin-4
<sup>99m</sup> Tc	:	<sup>99m</sup> -technetium
PAMA	:	pyridine-2-ylmethyl-amino]-acetic acid
NOTA	:	1,4,7- triazacyclononane-N,N',N''-triacetic acid
PET	:	positron emission tomography
SPEC-CT	:	single-photon emission computed tomography
<sup>64</sup> Cu	:	64-copper
DMB	:	dimethylbenzimidazole.

## Bibliography

- Ahrenstedt S Stefan and Jan I Thorell. 1979. The production of antibodies to vitamin B12. *Clinica Chimica Acta*. 95(3): 419–423.
- Alsensz J, Russell-Jones GJ, Westwood S, Levet-Trafit B and de Smidt PC. 2000. Oral absorption of peptides through the cobalamin (vitamin B12) pathway in the rat intestine. *Pharmaceutical Research*. 17(7): 825–832.
- Andersen Christian Brix Folsted, Mette Madsen, Tina Storm, Søren K Moestrup and Gregers R Andersen. 2010. Structural basis for receptor recognition of vitamin-B12–intrinsic factor complexes. *Nature*. 464(7287): 445–448.
- Bagnato Joshua D, Alanna L Eilers, Robert A Horton and Charles B Grissom. 2004. Synthesis and characterization of a cobalamin-colchicine conjugate as a novel tumor-targeted cytotoxin. *The Journal of Organic Chemistry*. 69(26): 8987–8996.
- Bauer Joseph A, Bei H Morrison, Ronald W Grane et al. 2002. Effects of interferon beta on transcobalamin II-receptor expression and antitumor activity of nitrosylcobalamin. *Journal of the National Cancer Institute*. 94(13): 1010–1019.
- Beedholm-Ebsen Rasmus, Koen van de Wetering, Tore Hardlei et al. 2010. Identification of multidrug resistance protein 1 (MRP1/ABCC1) as a molecular gate for cellular export of cobalamin. *Blood*. 115(8): 1632–1639.
- Bonaccorso Ron L, Oleg G Chepurny, Christoph Becker-Pauly, George G Holz and Robert P Doyle. 2015. Enhanced peptide stability against protease digestion induced by intrinsic factor binding of a vitamin B12 conjugate of exendin-4. *Molecular Pharmaceutics*. 12(9): 3502–3506.
- Carmel Ralph. 1975. Extreme elevation of serum transcobalamin I in patients with metastatic cancer. *New England Journal of Medicine*. 292(6): 282–284.
- Chalasanani Kishore B, Gregory J Russell-Jones, Akhlesh K Jain, Prakash V Diwan and Sanjay K Jain. 2007. Effective oral delivery of insulin in animal models using vitamin B12-coated dextran nanoparticles. *Journal of Controlled Release*. 122(2): 141–150.
- Christensen Erik I, Rikke Nielsen and Henrik Birn. 2013. From bowel to kidneys: The role of cubilin in physiology and disease. *Nephrology Dialysis Transplantation*. 28(2): 274–281.
- Chromiński Mikołaj and Dorota Gryko. 2013. “Clickable” vitamin B12 derivative. *Chemistry—A European Journal*. 19(16): 5141–5148.
- Chromiński Mikołaj, Agnieszka Lewalska and Dorota Gryko. 2013. Reduction-free synthesis of stable acetylides cobalamins. *Chemical Communications*. 49(97): 11406–11408.
- Clardy-James Susan, Jaime Bernstein, Deborah Kerwood and Robert Doyle. 2012. Site-selective oxidation of vitamin B12 using 2-iodoxybenzoic acid. *Synlett*. 23(16): 2363–2366.
- Clardy Susan M, Damian G Allis, Timothy J Fairchild and Robert P Doyle. 2011. Vitamin B12 in drug delivery: Breaking through the barriers to a B12 bioconjugate pharmaceutical. *Expert Opinion on Drug Delivery*. 8(1): 127–140.



- Collins Douglas A, Harry PC Hogenkamp and Mark W Gebhard. 1999. Tumor imaging via indium 111-labeled DTPA-adenosylcobalamin. *Mayo Clinic Proceedings*. 74(7): 687–691.
- Collins Douglas A and Hogenkamp H.P.C. 1997. Transcobalamin II receptor imaging via radiolabeled diethylene-triaminepentaacetate cobalamin analogs. *Journal of Nuclear Medicine*. 38(5): 717–723.
- Dix CJ, Hassan IF, Obray HY, Shah R and Wilson G. 1990. The transport of vitamin B12 through polarized monolayers of Caco-2 cells. *Gastroenterology* 98(5 PART 1). Scopus. 1272–1279.
- Doxey Andrew C, Daniel A Kurtz, Michael DJ Lynch, Laura A Sauder and Josh D Neufeld. 2015. Aquatic metagenomes implicate thaumarchaeota in global cobalamin production. *The ISME Journal*. 9(2): 461–471.
- Fazen Christopher H, Debbie Valentin, Timothy J Fairchild and Robert P Doyle. 2011. Oral delivery of the appetite suppressing peptide hPYY(3–36) through the vitamin B12 uptake pathway. *Journal of Medicinal Chemistry*. 54(24): 8707–8711.
- Fedosov Sergey N, Lars Berglund, Natalya U Fedosova, Ebba Nexø and Torben E Petersen. 2002. Comparative analysis of cobalamin binding kinetics and ligand protection for intrinsic factor, transcobalamin, and haptocorrin. *Journal of Biological Chemistry*. 277(12): 9989–9996.
- Fedosov Sergey N, Natalya U Fedosova, Bernhard Kräutler, Ebba Nexø and Torben E Petersen. 2007. Mechanisms of discrimination between cobalamins and their natural analogues during their binding to the specific B12-transporting proteins. *Biochemistry*. 46(21): 6446–6458.
- Fowler Robyn, Driton Vllasaliu, Franco H Falcone et al. 2013. Uptake and transport of B12-conjugated nanoparticles in airway epithelium. *Journal of Controlled Release*. 172(1): 374–381.
- Furger Evelyne, Dominik C Frei, Roger Schibli, Eliane Fischer and Andrea E Prota. 2013. Structural basis for Universal corrinoid recognition by the cobalamin transport protein haptocorrin. *Journal of Biological Chemistry*. 288(35): 25466–25476.
- Fyfe John C, Mette Madsen, Peter Højrup et al. 2004. The functional cobalamin (vitamin B12)–intrinsic factor receptor is a novel complex of Cubilin and Amnionless. *Blood*. 103(5): 1573–1579.
- Gherasim Carmen, Michael Lofgren and Ruma Banerjee. 2013. Navigating the B12 road: Assimilation, delivery, and disorders of cobalamin. *Journal of Biological Chemistry*. 288(19): 13186–13193.
- Glass GBJ. 1963. Gastric intrinsic factor and its function in the metabolism of vitamin B12. *Physiological Reviews* 43. CAB Direct. 2: 529–849.
- Haberfeld Alan David, Olaf Boris Kinstler and Colin Geoffrey Pitt. 1996. Conjugates of vitamin b12 and proteins. <http://www.google.com/patents/WO1996004016A1>, accessed April 17, 2016.
- Henry Kelly E, Clinton T Elfers, Rachael M Burke et al. 2015. Vitamin B12 conjugation of peptide-YY3–36 decreases food intake compared to native peptide-YY3–36 upon subcutaneous administration in male rats. *Endocrinology*. 156(5): 1739–1749.
- Henry Kelly E, Deborah J Kerwood, Damian G Allis et al. 2016. Solution structure and constrained molecular dynamics study of Vitamin B12 conjugates of the anorectic peptide PYY(3–36). *Chem Med Chem*. DOI: 10.1002/cmdc.201600073.
- Hippe Erik, Edgar Haber and Henrik Olesen. 1971. Nature of vitamin B12 binding. *Biochimica et Biophysica Acta (BBA)—Protein Structure*. 243(1): 75–82.
- Hodgkin Dorothy Crowfoot, Jenny Pickworth, John H Robertson et al. 1955. Structure of vitamin B12 : The crystal structure of the hexacarboxylic acid derived from B12 and the molecular structure of the vitamin. *Nature*. 176(4477): 325–328.
- Hogenkamp HP, Collins DA, Live D, Benson LM and Naylor S. 2000. Synthesis and characterization of Nido-Carborane-Cobalamin conjugates. *Nuclear Medicine and Biology*. 27(1): 89–92.
- Hygum Katrine, Dorte L Lildballe, Eva H Greibe et al. 2011. Mouse Transcobalamin Has Features Resembling Both Human Transcobalamin and Haptocorrin. *PLOS ONE*. 6(5): e20638.
- Ikotun Oluwatayo F, Bernadette V Marquez, Christopher H Fazen et al. 2014. Investigation of a vitamin B12 conjugate as a PET imaging probe. *Chem Med Chem*. 9(6): 1244–1251.
- Kräutler B. 2005. Vitamin B12: Chemistry and biochemistry. *Biochemical Society Transactions*. 33(4): 806–810.
- Kräutler B. 2015. Antivitamins B12—A structure- and reactivity-based concept. *Chemistry—A European Journal*. 21(32): 11280–11287.

- Kunze Susanne, Fabio Zobi, Philipp Kurz, Bernhard Spingler and Roger Alberto. 2004. Vitamin B12 as a Ligand for Technetium and Rhenium Complexes. *Angewandte Chemie (International Ed. in English)*. 43(38): 5025–5029.
- Lee Manfai and Charles B Grissom. 2009. Design, synthesis, and characterization of fluorescent cobalamin analogues with high quantum efficiencies. *Organic Letters*. 11(12): 2499–2502.
- Lildballe Dorte L, Elena Mutti, Henrik Birn and Ebba Nexø. 2012. Maximal load of the vitamin B12 transport system: A study on mice treated for four weeks with high-dose vitamin B12 or cobinamide. *PLOS ONE*. 7(10): e46657.
- Martens J-H, Barg H, Warren M and Jahn D. 2002. Microbial production of vitamin B12. *Applied Microbiology and Biotechnology*. 58(3): 275–285.
- Mathews FS, Gordon MM, Chen Z et al. 2007. Crystal structure of human intrinsic factor: Cobalamin complex at 2.6-Å resolution. *Proceedings of the National Academy of Sciences*. 104(44): 17311–17316.
- McEwan JF, Veitch HS and Russell-Jones GJ. 1999. Synthesis and biological activity of ribose-5'-carbamate derivatives of vitamin B12. *Bioconjugate Chemistry*. 10(6): 1131–1136.
- McGreevy James M, Michelle J Cannon and Charles B Grissom. 2003. Minimally invasive lymphatic mapping using fluorescently labeled vitamin B12. *The Journal of Surgical Research*. 111(1): 38–44.
- Moestrup SK, Birn H, Fischer PB et al. 1996. Megalin-mediated endocytosis of transcobalamin-vitamin-B12 complexes suggests a role of the receptor in vitamin-B12 homeostasis. *Proceedings of the National Academy of Sciences*. 93(16): 8612–8617.
- Mukherjee Riya, Edward G Donnay, Michal A Radomski et al. 2008. Vanadium-vitamin B12 bioconjugates as potential therapeutics for treating diabetes. *Chemical Communications (Cambridge, England)*. (32): 3783–3785.
- Mundwiler Stefan, Bernhard Spingler, Philipp Kurz, Susanne Kunze and Roger Alberto. 2005. Cyanide-bridged vitamin B12-cisplatin conjugates. *Chemistry (Weinheim an Der Bergstrasse, Germany)*. 11(14): 4089–4095.
- Mundwiler Stefan, Robert Waibel, Bernhard Spingler, Susanne Kunze and Roger Alberto. 2005. Picolylamine-methylphosphonic acid esters as tridentate ligands for the labeling of alcohols with the  $\text{Fac-[M(CO)}_3\text{]}^+$  core ( $\text{M}=\text{}^{99\text{m}}\text{Tc}$ ,  $\text{Re}$ ): Synthesis and biodistribution of model compounds and of a  $^{99\text{m}}\text{Tc}$ -labeled cobinamide. *Nuclear Medicine and Biology*. 32(5): 473–484.
- Mutti Elena, Markus Ruetz, Henrik Birn, Bernhard Kräutler and Ebba Nexø. 2013. 4-Ethylphenyl-cobalamin impairs tissue uptake of vitamin B 12 and causes vitamin B 12 deficiency in mice. *PLOS ONE*. 8(9): e75312.
- Nexø Ebba and Jørgen Andersen. 1977. Unsaturated and cobalamin saturated transcobalamin I and II in normal human plasma. *Scandinavian Journal of Clinical and Laboratory Investigation*. 37(8): 723–728.
- Nexø Ebba and Henrik Olesen. 1981. Purification and characterization of rabbit haptocorrin. *Biochimica et Biophysica Acta (BBA)—Protein Structure*. 667(2): 370–376.
- Nexø Ebba, Mads Hansen, Steen Seier Poulsen and Peter Skov Olsen. 1985. Characterization and immunohistochemical localization of rat salivary cobalamin-binding protein and comparison with human salivary haptocorrin. *Biochimica et Biophysica Acta (BBA)—General Subjects*. 838(2): 264–269.
- Nielsen Marianne J, Mie R Rasmussen, Christian BF Andersen, Ebba Nexø and Søren K Moestrup. 2012. Vitamin B12 transport from food to the body's cells—a sophisticated, multistep pathway. *Nature Reviews Gastroenterology and Hepatology*. 9(6): 345–354.
- Pathare Pradip M, D Scott Wilbur, Shannon Heusser et al. 1996. Synthesis of cobalamin–Botin conjugates that vary in the position of cobalamin coupling. Evaluation of cobalamin derivative binding to transcobalamin II. *Bioconjugate Chemistry*. 7(2): 217–232.
- Petrus Amanda K, Timothy J Fairchild and Robert P Doyle. 2009. Traveling the vitamin B12 pathway: Oral delivery of protein and peptide drugs. *Angewandte Chemie International Edition*. 48(6): 1022–1028.
- Petrus Amanda K, Anthony R Vortherms, Timothy J Fairchild and Robert P Doyle. 2007. Vitamin B12 as a carrier for the oral delivery of insulin. *Chem Med Chem*. 2(12): 1717–1721.

- Polak DM, Elliot JM and Haluska M. 1979. Vitamin B12 binding proteins in bovine serum. *Journal of Dairy Science*. 62(5): 697–701.
- Proinsias Keith ó, Maciej Giedyk and Dorota Gryko. 2013. Vitamin B12: Chemical modifications. *Chemical Society Reviews*. 42(16): 6605–6619.
- Proinsias Keith ó, Michal Ociepa, Katarzyna Pluta, Mikolaj Chrominski, Ebba Nexo and Dorota Gryko. 2016. Vitamin B12 phosphate conjugation and its effect on binding to the human B12 binding proteins intrinsic factor and haptocorrin. *Chemistry—A European Journal*. IN PRESS.
- Ruetz Markus, Carmen Gherasim, Karl Gruber et al. 2013. Access to organometallic arylcobaltcorrins through radical synthesis: 4-Ethylphenylcobalamin, a potential “Antivitamin B12.” *Angewandte Chemie International Edition*. 52(9): 2606–2610.
- Ruetz Markus, Robert Salchner, Klaus Wurst, Sergey Fedosov and Bernhard Kräutler. 2013. Phenylethynylcobalamin: A light-stable and thermolysis-resistant organometallic vitamin B12 derivative prepared by radical synthesis. *Angewandte Chemie International Edition*. 52(43): 11406–11409.
- Ruiz-Sánchez Pilar, Stefan Mundwiler, Alfredo Medina-Molner, Bernhard Spingler and Roger Alberto. 2007. Iodination of Cisplatin adduct of vitamin B12 [B12]-CN-{cis-PtCl(NH<sub>3</sub>)<sub>2</sub>}<sup>+</sup>. *Journal of Organometallic Chemistry* 692(6). Third International Symposium on Bioorganometallic Chemistry (ISBOMC'06) Third International Symposium on Bioorganometallic Chemistry. 1358–1362.
- Ruiz-Sánchez Pilar, Stefan Mundwiler, Bernhard Spingler et al. 2007. Syntheses and characterization of vitamin B12–Pt(II) conjugates and their Adenosylation in an enzymatic assay. *JBIC Journal of Biological Inorganic Chemistry*. 13(3): 335–347.
- Russell-Jones GJ, Westwood SW and Habberfield AD. 1995. Vitamin B12 mediated oral delivery systems for granulocyte-colony stimulating factor and erythropoietin. *Bioconjugate Chemistry*. 6(4): 459–465.
- Russell-Jones Gregory, Kirsten McTavish and John McEwan. 2011. Preliminary studies on the selective accumulation of vitamin-targeted polymers within tumors. *Journal of Drug Targeting*. 19(2): 133–139.
- Russell-Jones G, Westwood S, Farnworth P, Findlay J and Burger H. 1995. Synthesis of LHRH antagonists suitable for oral administration via the vitamin B12 uptake system. *Bioconjugate Chemistry*. 6(1): 34–42.
- Sah Bert-Ram, Roger Schibli, Robert Waibel et al. 2014. Tumor imaging in patients with advanced tumors using a new <sup>99m</sup>Tc-radiolabeled vitamin B12 derivative. *Journal of Nuclear Medicine*. 55(1): 43–49.
- Schjonsby H and Andersen KJ. 1974. The intestinal absorption of vitamin B12. *Scan J Gastro Suppl*. 29: 7–11.
- Seetharam Bellur and David H Alpers. 1994. Cobalamin binding proteins and their receptors. In *Vitamin Receptors. Intercellular and Intracellular Communication*. Cambridge University Press. dx.doi.org/10.1017/CBO9780511525391.006.
- Shell Thomas A, Jennifer R Shell, Zachary L Rodgers and David S Lawrence. 2014. Tunable visible and near-IR photoactivation of light-responsive compounds by using fluorophores as light-capturing antennas. *Angewandte Chemie International Edition*. 53(3): 875–878.
- Sheppard K, Bradbury DA, Davies JM and Ryrie DR. 1984. Cobalamin and folate binding proteins in human tumour tissue. *Journal of Clinical Pathology*. 37(12): 1336–1338.
- Siega Patrizia, Jochen Wuerges, Francesca Arena et al. 2009. Release of toxic Gd<sup>3+</sup> ions to tumour cells by vitamin B12 bioconjugates. *Chemistry (Weinheim an Der Bergstrasse, Germany)*. 15(32): 7980–7989.
- Smith Weston J, Nathan P Oien, Robert M Hughes et al. 2014. Cell-mediated assembly of phototherapeutics. *Angewandte Chemie International Edition*. 53(41): 10945–10948.
- Takahashi-Iñiguez Tóshiko, Enrique García-Hernandez, Roberto Arreguín-Espinosa and María Elena Flores. 2012. Role of vitamin B12 on methylmalonyl-CoA mutase activity. *Journal of Zhejiang University. Science. B*. 13(6): 423–437.
- Tran Mai Thanh Quynh, Evelyne Furger and Roger Alberto. 2013. Two-step activation prodrugs: Transplatin mediated binding of chemotherapeutic agents to vitamin B12. *Organic & Biomolecular Chemistry*. 11(19): 3247–3254.

- Tran Mai Thanh Quynh, Stefan Stürup, Ian Henry Lambert et al. 2016. Cellular uptake of metallated cobalamins. *Metallomics*. 8(3): 298–304.
- Verma Ashwini, Shweta Sharma, Pramod Kumar Gupta et al. 2016. Vitamin B12 functionalized layer by layer calcium phosphate nanoparticles: A mucoadhesive and pH responsive carrier for improved oral delivery of insulin. *Acta Biomaterialia*. 31: 288–300.
- Vortherms Anthony R, Anna R Kahkoska, Amy E Rabideau et al. 2011. A water soluble vitamin B12-Re(I) fluorescent conjugate for cell uptake screens: Use in the confirmation of Cubilin in the lung cancer line A549. *Chemical Communications*. 47(35): 9792–9794.
- Waibel Robert, Hansjörg Treichler, Niklaus G Schaefer et al. 2008. New derivatives of vitamin B12 show preferential targeting of tumors. *Cancer Research*. 68(8): 2904–2911.
- Wang Xiaoyang, Lianhu Wei and Lakshmi P Kotra. 2007. Cyanocobalamin (vitamin B12) conjugates with enhanced solubility. *Bioorganic & Medicinal Chemistry*. 15(4): 1780–1787.
- Wierzba Aleksandra, Monika Wojciechowska, Joanna Trylska and Dorota Gryko. 2016. Vitamin B12 suitably tailored for disulfide-based conjugation. *Bioconjugate Chemistry*. 27(1): 189–197.
- Wuerges, Jochen, Gianpiero Garau, Silvano Geremia et al. 2006. Structural basis for mammalian vitamin B12 transport by transcobalamin. *Proceedings of the National Academy of Sciences of the United States of America*. 103(12): 4386–4391.
- Wuerges Jochen, Silvano Geremia, Sergey N Fedosov and Lucio Randaccio. 2007. Vitamin B12 transport proteins: Crystallographic analysis of  $\beta$ -axial ligand substitutions in cobalamin bound to transcobalamin. *IUBMB Life*. 59(11): 722–729.
- Zelder Felix. 2015. Recent trends in the development of vitamin B12 derivatives for medicinal applications. *Chemical Communications*. 51(74): 14004–14017.
- Zelder Felix, Marjorie Sonnay and Lucas Prieto. 2015. Antivitamins for medicinal applications. *Chem Bio Chem*. 16(9): 1264–1278.
- Zhou Kai, René M Oetterli, Helmut Brandl et al. 2012. Chemistry and bioactivity of an artificial adenosylpeptide B12 cofactor. *Chem Bio Chem*. 13(14): 2052–2055.
- Zhou Kai and Felix Zelder. 2010. Vitamin B12 mimics having a peptide backbone and tuneable coordination and redox properties. *Angewandte Chemie International Edition*. 49(30): 5178–5180.

# <sup>89</sup>Zr-Cobalamin PET Tracer: Synthesis, Cellular Uptake, and Use for Tumor Imaging

Akhila N. W. Kuda-Wedagedara,<sup>†,‡</sup> Jayme L. Workinger,<sup>‡,‡</sup> Ebba Nexø,<sup>||</sup> Robert P. Doyle,<sup>\*,‡,§,§</sup> and Nerissa Viola-Villegas<sup>\*,†</sup>

<sup>†</sup>Department of Oncology, Karmanos Cancer Institute, Wayne State University, Detroit, Michigan 48202, United States

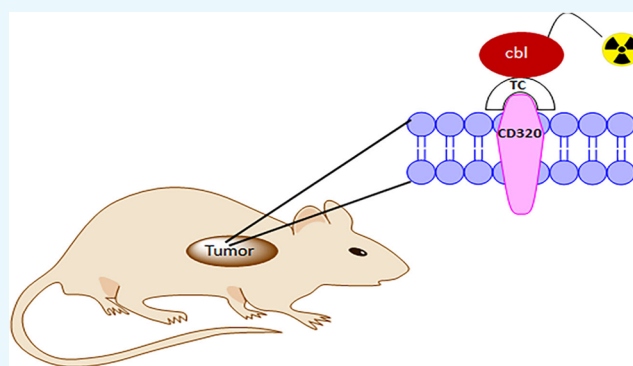
<sup>‡</sup>Department of Chemistry, Syracuse University, 111 College Place, Syracuse, New York 13102, United States

<sup>§</sup>Department of Medicine, State University of New York Upstate Medical University, Syracuse, New York 13102, United States

<sup>||</sup>Department of Clinical Biochemistry and Institute of Clinical Medicine, Aarhus University Hospital, Aarhus 8000, Denmark

## S Supporting Information

**ABSTRACT:** Vitamin B<sub>12</sub>, or cobalamin (Cbl), is an essential nutrient. Acquisition, transport, and cellular internalization of Cbl are dependent on specific binding proteins and associated receptors. The circulating transport protein transcobalamin (TC) promotes cellular uptake via binding to specific receptors such as CD320, a receptor upregulated in several cancer cell lines. In this study, we report the successful synthesis of <sup>89</sup>Zirconium-labeled Cbl that was derivatized with desferrioxamine (<sup>89</sup>Zr-Cbl). We document the purity of the tracer and its binding to TC compared with that of unmodified cyano-Cbl (CN-Cbl). In vitro studies employing the CD320 receptor-positive breast cancer cell line MDA-MB-453 showed a 6- to 10-fold greater uptake of <sup>89</sup>Zr-Cbl when compared with the uptake in the presence of 200-fold excess of CN-Cbl at 37 °C. We used nude mice with MDA-MB-453 tumors to study the feasibility of employing the tracer to visualize CD320 positive tumors. In vivo positron emission tomography images displayed a clear visualization of the tumor with 1.42 ± 0.48 %ID/g uptake (*n* = 3) at 4 h after injection (p.i.) with the tracer retained at 48 h p.i. Ex vivo biodistribution studies using <sup>89</sup>Zr-Cbl exhibited the highest uptake in kidney and liver at 48 h p.i. Results document the feasibility of synthesizing a Cbl-based tracer suitable for both in vivo and ex vivo studies of Cbl trafficking and with the potential to visualize tumors expressing TC receptors, such as CD320.



## INTRODUCTION

Vitamin B<sub>12</sub> (cobalamin, Cbl) is a critical nutrient that is physiologically required to maintain cell growth and differentiation.<sup>1–4</sup> Cbl is involved in the biosynthesis of nucleic acids, lipids, and proteins, and its deficiency leads to a reduction in functional methionine synthase and metabolism of methylmalonic acid in humans, leading to megaloblastic anemia and/or various neurological disorders.<sup>1–4</sup>

Cbl gains entry into cells upon binding to transport proteins and subsequent receptor mediated transport. Cbl in blood is bound to the transport protein transcobalamin (TC) (holo-TC), which, in turn, is recognized by specific receptors such as CD320.<sup>1–4</sup> Upregulation of CD320 receptors has been reported in several malignancies including breast, prostate, thyroid, cervical, colorectal, and stomach cancers.<sup>5</sup> The important role of Cbl in cellular proliferation and the upregulation of CD320 in tumor cells has made Cbl uptake an attractive candidate for tumor imaging, mainly using single-photon emission computed tomography with <sup>99m</sup>Techetium- or <sup>111</sup>Indium-labeled Cbl.<sup>6–13</sup> One Cbl-positron emission

tomography (PET) imaging agent, labeled with <sup>64</sup>Cu (*t*<sub>1/2</sub> ~ 12.7 h), has also been reported.<sup>14</sup>

Herein, the utility of Cbl as a vector was explored for delivering the PET radionuclide <sup>89</sup>Zr (*t*<sub>1/2</sub> ~ 3.27 days). We hypothesized that <sup>89</sup>Zr would (1) retain the sensitivity of PET imaging and (2) provide a longer visualization window by providing a greater signal-to-noise ratio compared with prior tracers reported, allowing for an improved tumor targeting and imaging. Following radiosynthesis, we evaluated the in vitro uptake and in vivo pharmacokinetics of the CD320-positive MDA-MB-453 breast cancer in athymic nude mice.

## RESULTS

**Synthesis of Cbl-Desferrioxamine (Cbl-DFO).** Cbl-desferrioxamine (Cbl-DFO) was synthesized by forming a carbamate linkage between the 5'-hydroxyl of deoxyribose moiety in Cbl and the amine group of DFO (Scheme 1, Figure

Received: August 14, 2017

Accepted: September 18, 2017

Published: October 2, 2017

Scheme 1. Synthesis and Radiolabeling of Cbl-DFO

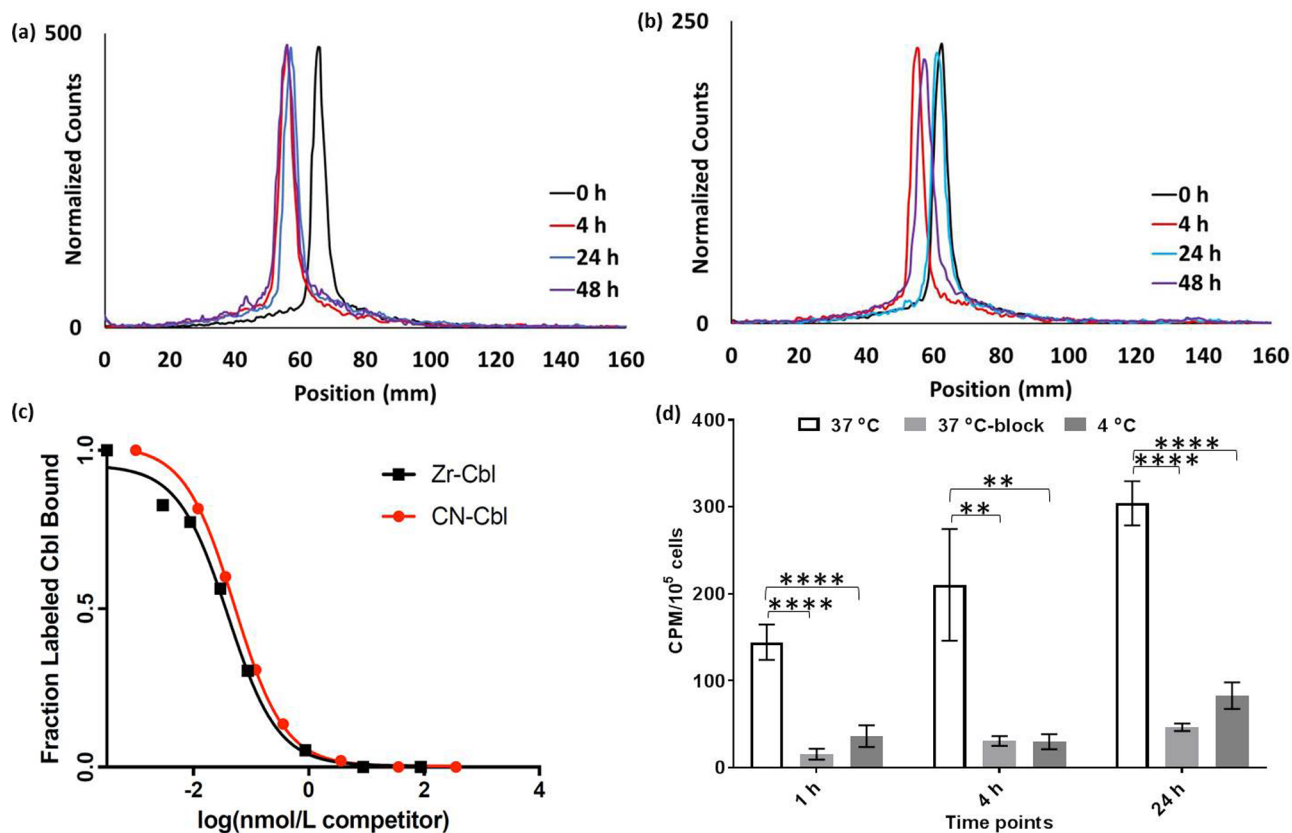
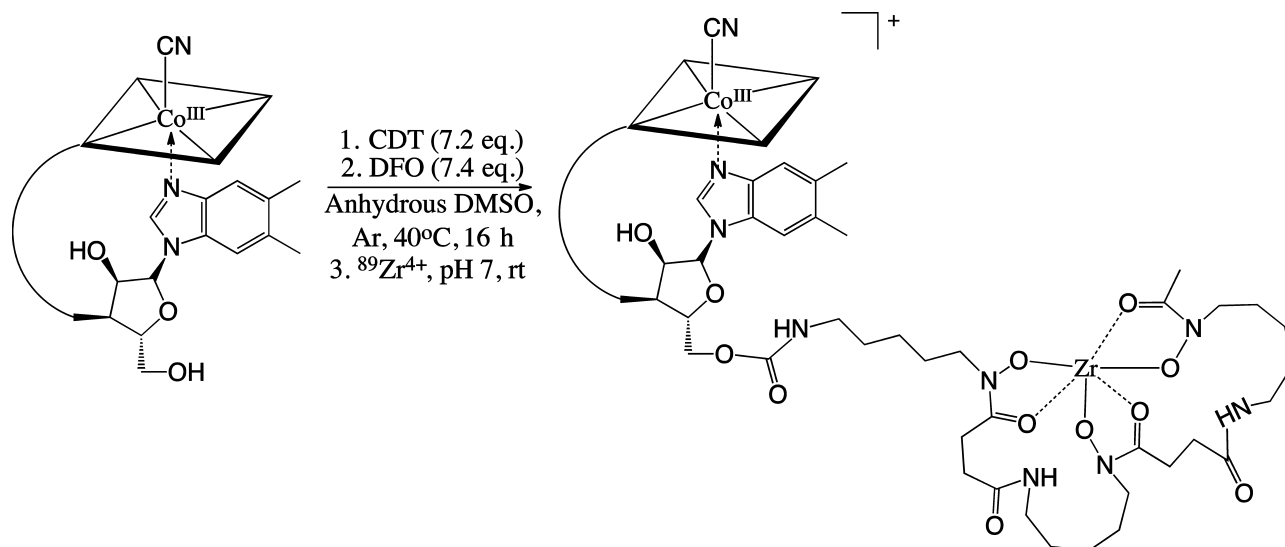


**Figure 1.** In vitro stability of  $^{89}\text{Zr}$ -Cbl (a) in saline at 37 °C, (b) in human serum at 37 °C, (c) TC binding of  $^{91}\text{Zr}$ -Cbl and CN-Cbl, expressed as the fraction bound compared to binding without added competitor and (d) internalization of  $^{89}\text{Zr}$ -Cbl (0.1  $\mu\text{Ci}$ , 3.7 KBq, 0.4 pmol/well) with MDA-MB-453 cells at 1, 4, 24 h time points incubated at 4 and 37 °C. A competition assay was also performed at each time point using unlabeled Cbl (Cbl 40 pmol/well co-incubated with 0.1  $\mu\text{Ci}$ , 0.4 pmol/well of  $^{89}\text{Zr}$ -Cbl). The fraction of  $^{89}\text{Zr}$ -Cbl internalized in MDA-MB-453 cells is expressed as cpm/ $10^5$ . \*\*\*\* and \*\* indicate  $p \leq 0.0001$  and  $p \leq 0.01$ , respectively. Data are shown as mean and standard deviation,  $n \geq 3$ .

S1).<sup>15</sup> Cbl was activated using 1,1'-carbonyl-di-(1,2,4-triazole) (CDT), followed by the addition of DFO, which links through the primary amine. Purification and characterization confirmed that the conjugate was of  $\geq 97\%$  purity (Figures S2–S4). The yield of Cbl-DFO was  $40 \pm 5\%$  based on the Cbl content in the starting material. Calculated mass ( $m/z$ ): 1942 [M]; observed: 972 [M + 2H] $^{2+}$  and 648 [M + 3H] $^{3+}$ .

**Radiolabeling of Cbl with  $^{89}\text{Zr}$ .** Cbl-DFO was labeled with  $^{89}\text{Zr}$  ( $^{89}\text{Zr}$ -Cbl) using a previously established protocol (Scheme 1).<sup>16</sup> A radiolabeling efficiency of  $\sim 97\%$  was determined by instant thin-layer chromatography (iTLC, Figure S5a). The specific activity of the tracer was determined by titrating  $^{89}\text{Zr}^{4+}$  and Cbl at different mole ratios with an

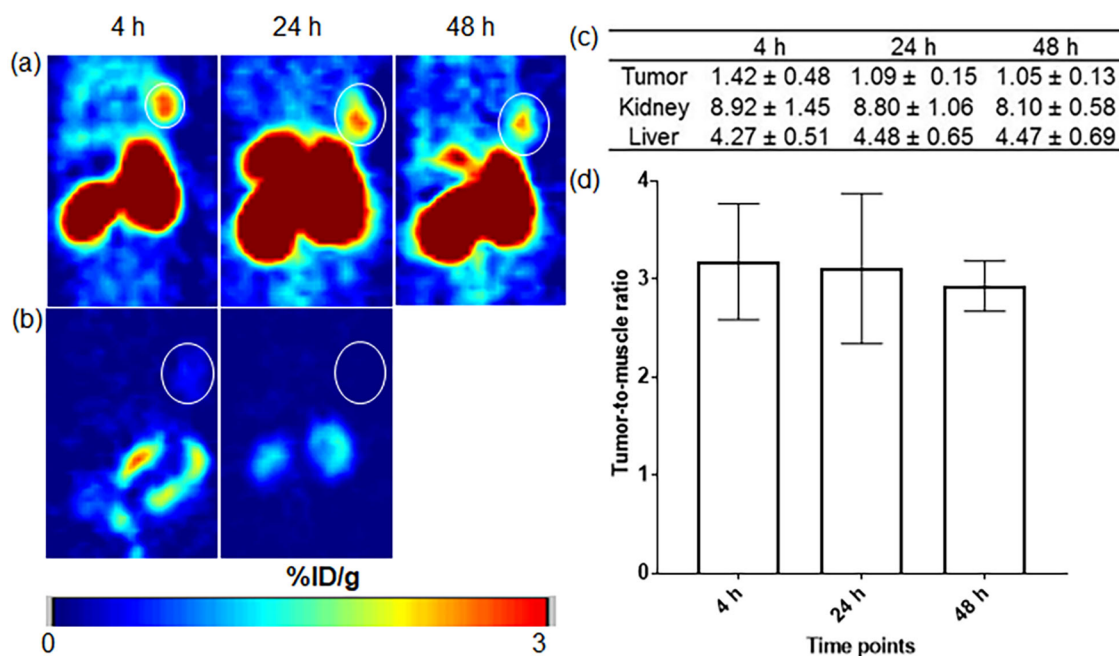


**Figure 2.** PET images of representative mice bearing (a) MDA-MB-453 tumors imaged with  $^{89}\text{Zr}$ -Cbl ( $\sim 1$  nmol/mouse, 9 MBq) at 4, 24, and 48 h p.i. time points, (b) MDA-MB-453 tumors imaged with  $^{89}\text{Zr}$ -Cbl ( $\sim 1$  nmol/mouse, 9 MBq), co-injected with 200-fold excess of unradio-labeled Cbl at 4 and 24 h p.i., (c) %ID/g values for selected organs in MDA-MD-453 tumor-bearing mice, and (d) tumor-to-muscle ratios at all imaging time points. The tumor location is indicated by a white circle.

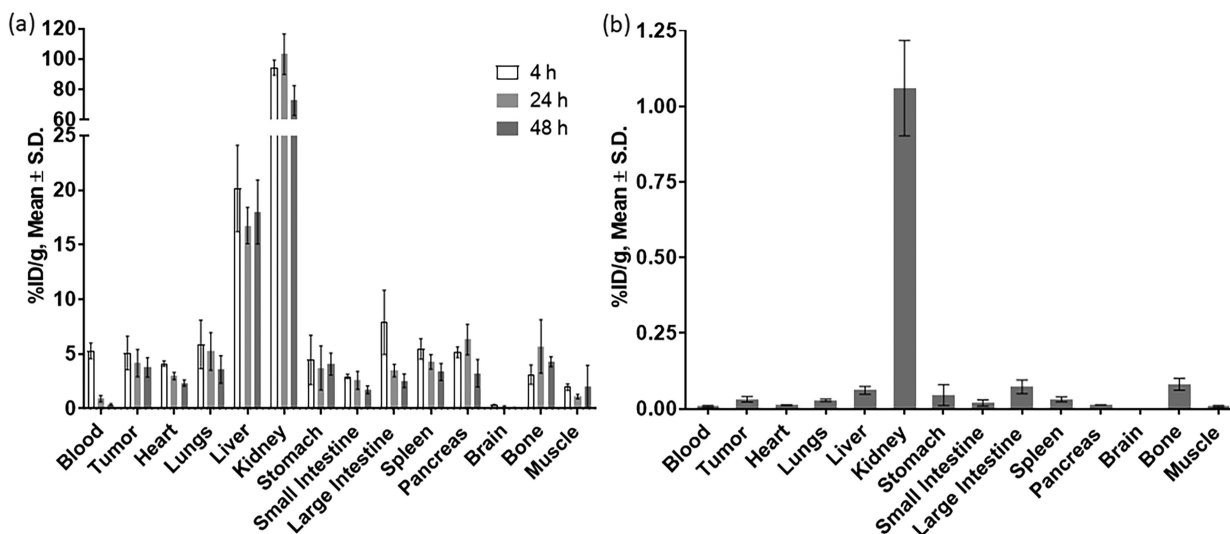


**Figure 3.** Ex vivo tissue distribution of (a)  $^{89}\text{Zr}$ -Cbl in mice ( $n = 4$ ) bearing MDA-MB-453 tumors at 4, 24, and 48 h p.i. and (b) a blocking study with 200-fold unmodified Cbl co-injected with  $^{89}\text{Zr}$ -Cbl ( $n = 4$ ) and tissue collection 48 h p.i. Data are displayed as mean  $\pm$  standard deviation, with  $^{89}\text{Zr}$  decay accounted for in the analyses.

achieved optimum specific activity of  $250 \pm 20$  mCi/ $\mu\text{mol}$  (mean  $\pm$  standard deviation,  $n = 3$ ).

**In Vitro Stability of  $^{89}\text{Zr}$ -Cbl.** Stability of the tracer was analyzed by incubating  $^{89}\text{Zr}$ -Cbl in saline and in human serum at  $37^\circ\text{C}$ . Bound versus unbound radio metal was analyzed at 0, 4, 24, and 48 h after incubation using iTLC (Figure 1a,b). The intact tracer was located closer to the origin (40–80 mm), whereas unbound tracer was found at 100–140 mm. After 48 h of incubation, free  $^{89}\text{Zr}$  was  $<1\%$  in both saline and serum.

**TC Binding Studies.** Mouse TC binding of  $^{91}\text{Zr}$ -Cbl was studied by radiometric chase assay using  $^{57}\text{Co}$ -labeled Cbl employing a previously described design.<sup>17</sup>  $^{91}\text{Zr}$ -Cbl was synthesized similar to  $^{89}\text{Zr}$ -Cbl, but with  $^{91}\text{ZrCl}_4$ . Mouse TC

binding of  $^{91}\text{Zr}$ -Cbl displaced  $^{57}\text{Co}$ -labelled Cbl in a manner comparable to that of CN-Cbl (Figure 1c), indicating that the modification of Zr-Cbl did not compromise binding to TC. The same results were obtained for binding to human intrinsic factor (data not shown).

**In Vitro Uptake.** An internalization assay was performed to test the uptake of  $^{89}\text{Zr}$ -Cbl on CD320 receptor cell line MDA-MB-453 at 4 and  $37^\circ\text{C}$  (Figure 1d). The internalized fractions of  $^{89}\text{Zr}$ -Cbl were expressed as counts per minute (cpm) normalized to  $10^5$  cells (cpm/ $10^5$  cells). Internalization of  $^{89}\text{Zr}$ -Cbl was higher at  $37^\circ\text{C}$  versus  $4^\circ\text{C}$  at all time points with  $144 \pm 20$  versus  $36 \pm 12$  cpm/ $10^5$  cells at 1 h ( $p < 0.0001$ ),  $210 \pm 64$  versus  $30 \pm 9$  cpm/ $10^5$  cells at 4 h ( $p = 0.01$ ), and  $304 \pm 25$

versus  $83 \pm 15$  cpm/ $10^5$  cells at 24 h ( $p < 0.0001$ ). Competitive assays using excess Cbl at 37 °C displayed lower binding at all time points ( $p < 0.01$ ). All of the data are reported as mean  $\pm$  standard deviation of four independent measurements.

**PET Imaging.** PET imaging was performed after the administration of  $\sim 1$  nmol/mouse (200–250  $\mu$ Ci, 7.4–9.3 MBq) of  $^{89}\text{Zr}$ -Cbl to nude mice bearing a CD320 positive MDA-MB-453 tumor ( $n = 3$ ). The image showed visualization of the tumor with tracer uptake of  $1.42 \pm 0.48$  %ID/g at 4 h p.i. with retention observed up to 48 h p.i. (Figure 2a). Cohorts ( $n = 3$ ) that were co-injected with 200-fold excess unlabeled Cbl (Figure 2b) showed significantly less uptake in the tumors ( $0.20 \pm 0.05$  %ID/g) at 24 h p.i. ( $p \leq 0.001$ ). Other tissues that displayed high tracer uptake were the kidney and liver with  $8.92 \pm 1.45$ ,  $8.80 \pm 1.06$ , and  $8.10 \pm 0.58$  %ID/g for kidney and  $4.27 \pm 0.51$ ,  $4.48 \pm 0.65$ , and  $4.47 \pm 0.69$  %ID/g for liver at 4, 24, and 48 h p.i., respectively (Figure 2c). Tumor-to-muscle ratio ( $\sim 3:1$ ) did not change significantly over 48 h p.i., indicating that the maximum tumor-to-background ratio was achieved at 4 h p.i. (Figure 2d). All percent injected dose per gram of tissue (%ID/g) values are reported as mean  $\pm$  standard deviation.

**Ex Vivo Tissue Analysis.** Biodistribution data obtained from tumor-bearing mice injected 0.1 nmol (25 microcuries, 0.9 MBq) of  $^{89}\text{Zr}$ -Cbl showed  $5.11 \pm 1.33$ ,  $4.16 \pm 1.09$ , and  $3.78 \pm 0.77$  %ID/g (mean  $\pm$  standard deviation,  $n = 4$ ) tumor uptake in MDA-MB-453 tumors at 4, 24, and 48 h p.i., respectively (Figure 3a, Table S1). The kidneys showed the highest uptake of the tracer with  $94.42 \pm 4.27$ ,  $103.33 \pm 11.50$ , and  $72.74 \pm 8.41$  %ID/g and the liver showed the second highest uptake with  $20.15 \pm 3.42$ ,  $16.75 \pm 1.44$ , and  $17.99 \pm 2.54$  %ID/g at 4, 24, and 48 h p.i., respectively. Administration of a 200-fold excess of unmodified Cbl (as CN-Cbl) together with the tracer ( $n = 4$  mice) resulted in an approximately 100-fold decrease ( $0.04 \pm 0.01$  %ID/g) in tracer uptake in tumors at 48 h and also a decreased uptake in the kidney ( $1.39 \pm 0.18$  %ID/g) and the liver ( $0.08 \pm 0.01$  %ID/g). These results are consistent with a Cbl-specific uptake of  $^{89}\text{Zr}$ -Cbl (Figure 3b, Table S1) and all of the %ID/g values were reported as mean  $\pm$  standard deviation.

## DISCUSSION

In this proof-of-concept study, we report the successful production of a Cbl-derived  $^{89}\text{Zr}$  tracer suitable for use in PET studies. Studies on nude mice bearing a human breast cancer cell tumor allow us to demonstrate the use of the tracer for PET visualization of the tumor.

In agreement with previous data,<sup>17,18</sup> we found that  $^{91}\text{Zr}$ -Cbl bound to mouse TC in a manner comparable to that of CN-Cbl (Figure 1c). Next, an in vitro assay was performed in the breast cancer cell line MDA-MB-453 to demonstrate a specific uptake of  $^{89}\text{Zr}$ -Cbl.<sup>19</sup> We demonstrated a greater than 4-fold uptake of  $^{89}\text{Zr}$ -Cbl at 37 °C versus 4 °C; blocking with 200-fold excess unlabeled Cbl had a similar reduced uptake (Figure 1d). These results support the idea that the targeting properties of  $^{89}\text{Zr}$ -Cbl in MDA-MB-453 cells rely on a Cbl-dependent internalization mechanism, likely through the CD320 receptor.

In vivo imaging with  $^{89}\text{Zr}$ -Cbl showed an uptake in MDA-MB-453 tumors with  $1.42 \pm 0.48$  of %ID/g, whereas ex vivo tissue distribution studies showed a tumor uptake of  $5.11 \pm 1.33$  %ID/g at 4 h p.i. (Figures 2 and 3). Notable uptake was also observed in the liver and kidneys with  $4.27 \pm 0.51$  and  $8.92 \pm 1.45$  %ID/g at 4 h p.i., respectively (Figure 2c). An in vivo

block using 200-fold excess of unradiolabeled Cbl showed a significantly reduced uptake ( $p < 0.001$ ) of the tracer, indicating that the in vivo tumor initialization is Cbl dependent, supported in the in vitro internalization assay. Muscle-to-tumor ratio showed that the maximum tumor-to-background ratio was achieved at 4 h p.i.

To compare the uptake values with those described in the literature, the biodistribution data will be used for a more accurate comparative analysis for the rest of the discussion. Tumor uptake persisted throughout the 4–48 h imaging period without a significant change ( $5.11 \pm 1.33$  at 4 h vs  $3.78 \pm 0.77$  at 48 h,  $p > 0.1$ ), whereas blood clearance was evident between 4 and 24 h with approximately  $\sim 80\%$  decrease ( $5.28 \pm 0.62$  at 4 h vs  $0.92 \pm 0.25$  %ID/g at 24 h) in the circulating  $^{89}\text{Zr}$ -Cbl; the final blood activity was observed to be  $0.39 \pm 0.06$  %ID/g at 48 h p.i.

The tumor uptake achieved in our model is comparable to that of the other Cbl-based tracers reported thus far.<sup>6–14</sup> Ikotun et al. investigated the tumor uptake of  $^{64}\text{Cu}$ -labeled Cbl in pancreatic, ovarian, murine melanoma, and colorectal tumor models, with the highest %ID/g being  $4.84 \pm 0.32$  at 6 h p.i. in the colorectal tumor models.<sup>14</sup> In the melanoma model, the tumor uptake was highest ( $3.43 \pm 0.87$  %ID/g) at 1 h, which decreased to  $2.64 \pm 0.10$  %ID/g after 24 h, whereas  $^{89}\text{Zr}$ -Cbl had a higher accumulation and did not show a significant decrease in tumor accumulation over 4–48 h,  $p > 0.1$ .

One of the limitations of our  $^{89}\text{Zr}$ -Cbl tracer is the observed kidney uptake ( $94.42 \pm 4.27$  %ID/g at 4 h), a problem across all of the Cbl tracers to date. Renal processing is the most prominent route for Cbl accumulation/storage and/or reabsorption and is driven by megalin, a known TC-Cbl receptor expressed in kidney proximal tubuli.<sup>20,21</sup> In addition, this is the first positively charged PET tracer reported, the effect of which is unknown. An overall positive charge on the Cbl (as  $^{89}\text{Zr}$ -Cbl conjugate), or indeed simply the result of modification of the  $\beta$ -axial position, may affect the Cbl cellular processing across tissues, as has been shown previously for two forms with varying  $\alpha$ -ligands (OH-Cbl and CN-Cbl) Cbl species, and warrants further investigation.<sup>12,22–24</sup>

$^{89}\text{Zr}$ -Cbl shows feasibility as a PET tracer to identify MDA-MB-453 tumors in vivo. The longer window for PET imaging allowed for reduced uptake in the kidneys, a problem to date in Cbl radiotracers, while still maintaining a moderate tumor uptake over 48 h p.i. This tracer is promising since, to our knowledge, tumor uptake is the highest reported to date for a B12 based PET probe.

## CONCLUSIONS

We have successfully developed and evaluated the first  $^{89}\text{Zr}$ -labeled Cbl tracer as a viable tool for visualizing TC-mediated Cbl uptake into a CD320 positive tumor.  $^{89}\text{Zr}$ -Cbl displayed retained tumor uptake up to 48 h p.i., allowing for a longer imaging window. Our data paves the road for future studies to understand the kinetics of Cbl transport and to study the use as a tool for visualizing tumors capable of accumulating Cbl.

## EXPERIMENTAL METHODS

**General.** Reagents listed below were purchased and used without further manipulations: dimethyl sulfoxide (DMSO, 99%, Sigma), vitamin B<sub>12</sub> (Cbl,  $\geq 98\%$ , Sigma), 1,1'-carbonyl-di-(1,2,4-triazole) (CDT,  $\geq 90\%$ , Fluka), and acetonitrile (MeCN, 99.8%, Pharmaco-Aaper). Compounds were confirmed to be



>96% pure by high-performance liquid chromatography (HPLC), proton nuclear magnetic resonance ( $^1\text{H}$  NMR), and/or inductively coupled plasma.

Proton nuclear magnetic resonance ( $^1\text{H}$  NMR) was performed using 400 MHz Bruker spectrometer with the residual solvent peak as an internal standard. Electrospray ionization (ESI) mass spectrometry analyses were carried out on a Shimadzu LCMS-8100. Breast cancer cells (MDA-MB-453) were obtained from the American Type Culture Collection. Charcoal stripped fetal bovine serum (FBS) and Dulbecco's modified Eagle's medium (DMEM) were purchased from Sigma and KD medicals, respectively. Penicillin–streptomycin solution with 10 000 units of penicillin and 10 mg/mL streptomycin in 0.9% NaCl was obtained from Corning.

Analysis of the radiotracer was performed using instant thin-layer chromatography (iTLC, Eckert & Ziegler Mini Scan) with an ethylenediaminetetraacetic acid (EDTA) (50 mM) mobile phase.

**Synthesis of Cbl-DFO.** Cbl-DFO was synthesized through the activation of the 5'-ribose-hydroxyl group with CDT. CDT (34 mg, 0.261 mmol, 7.2 equiv) was added with cyano-Cbl (50 mg, 0.0368 mmol, 1 equiv) in anhydrous DMSO (3 mL) at 40 °C for 2 h. DFO (208 mg, 0.313 mmol, 7.4 equiv) was added to the reaction mixture and mixed overnight. Purification of Cbl-DFO was done using reversed-phase (RP)-HPLC (Agilent 1200) with a C18 column (Agilent Eclipse XDB-C18 5  $\mu\text{m}$ , 4.6 mm  $\times$  150 mm) at a flow rate of 1 mL/min. Detection was done using a UV–vis detector at 360 nm. RP-HPLC method: (A) 0.1% trifluoroacetic acid water and (B) MeCN as solvents with the following gradient: 1% B to 70% B over 15 min, ( $R_t$  = 9.4 min). Purity was  $\geq 97\%$  via RP-HPLC. Yield: 30–40%.  $^1\text{H}$  NMR analysis of the aromatic region: 7.178 (s, 1H), 7.016 (s, 1H), 6.426 (s, 1H), 6.218 (s, 1H), 5.989 (s, 1H). Liquid chromatography–mass spectrometry (LC–MS) analysis: expected  $m/z$ : 1942; observed: 972 [ $M + 2\text{H}$ ] $^{2+}$  and 648 [ $M + 3\text{H}$ ] $^{3+}$ .

**$^{89}\text{Zr}$ -Radiochemistry.** Optimum conditions for radiolabeling of Cbl-DFO were tested by titrating with  $^{89}\text{Zr}$  and analyzing the incubated solution using iTLC. Optimum labeling activity was found to be  $250 \pm 20$  mCi/ $\mu\text{mol}$  ( $9250 \pm 740$  MBq/micromole). Approximately 1 mCi (37 MBq) of  $^{89}\text{Zr}(\text{C}_2\text{O}_4)_2$  (3D Imaging, LLC) was diluted with 0.9% saline and the pH was adjusted to 7–7.5 by adding 1 M  $\text{Na}_2\text{CO}_3$ . A solution of Cbl-DFO (0.004  $\mu\text{mol}$ , 10.8  $\mu\text{g}$ ) was added to the pH-adjusted  $^{89}\text{Zr}$  solution and incubated for 20 min at ambient temperature (Scheme 1). Radiolabeling efficiency of  $>97\%$  was determined by iTLC using silica iTLC strips and EDTA mobile phase (Figure S5a). The identity of the tracer was characterized via matrix-assisted laser desorption ionization mass spectrometry (MALDI-MS) analysis using Cbl-DFO labeled with cold  $\text{Zr}^{4+}$  as standard. Expected: 2030.2 [ $M^+$ ]; observed: 2005.2 [ $M^+ - \text{CN}^- + \text{H}^+$ ] $^+$  (Figure S5b).

**In Vitro Stability of  $^{89}\text{Zr}$ -Cbl.** Stability of  $^{89}\text{Zr}$ -Cbl was tested by incubating the tracer (200  $\mu\text{Ci}$ , 7.4 MBq, 100  $\mu\text{L}$ ) in saline (0.9% NaCl) and 50% (1:1 serum/saline) human serum (Sigma) at 37 °C, and the solutions were analyzed at 0, 4, 24, and 48 h intervals using iTLC (Eckert & Ziegler Mini Scan).

**Mouse TC Binding to  $^{91}\text{Zr}$ -Cbl.** Nonradioactive  $^{91}\text{Zr}$ -Cbl was synthesized for TC binding studies by reacting Cbl-DFO with  $^{91}\text{ZrCl}_4$  as described above. The conjugate was characterized by ESI-MS (data not shown). Mouse TC binding of  $^{91}\text{Zr}$ -Cbl was confirmed by radiometric chase assay using

$^{57}\text{Co}$ -labeled Cbl and compared with free Cbl (cyanocobalamin) employing a previously described protocol.<sup>17</sup> Mouse TC was derived as previously described.<sup>25</sup>

**In Vitro Uptake.** Modified internalization assay was performed. MDA-MB-453 cells were cultured in Cbl-free media (DMEM with 10% charcoal stripped FBS) and plated in six-well plates. Each well contained 200 000 cells plated and incubated overnight. To each well,  $^{89}\text{Zr}$ -Cbl (0.1  $\mu\text{Ci}$ , 3.7 KBq, 0.4 pmol of Cbl per well) was added. For the blocking experiment, unmodified Cbl was added (40 pmol per well). Plates were incubated for 1, 4, and 24 h intervals at either 37 or 4 °C. At the end of each time point, wells were serially washed with phosphate-buffered saline (1 $\times$ ), acid (1 mM acetic acid and 1 mM glycine), and base (1 M NaOH, 1 mL, 5 min). Each wash was collected and measured for bound activity using a  $\gamma$  counter (Perking Elmer 2480 WIZARD). Control wells were trypsinized and counted using a cell counter (Contessa II). Internalized activity was normalized to  $10^5$  cells.

**Cell Lines and Small Animal Xenografts.** All of the animal handling and manipulations were conducted in accordance with the guidelines set by WSU Animal Care and Use Committee (IACUC). For imaging and in vivo uptake experiments, female nude mice (Envigo) were kept under Cbl-deficient diet (Teklad Cbl-free custom diet, Envigo) for 3 weeks. Cells were subcutaneously implanted on the shoulder with MDA-MB-453 cancer cells ( $5 \times 10^6$  cells/mouse) after 2 weeks of Cbl-free diet. Cells were injected in 1:1 media/matrigel (Corning LLC) at a volume of 200  $\mu\text{L}$ . The tumor volume until was calculated using the formula length  $\times$  width $^2 \times 0.52$ . Mice with tumors of 100–200  $\text{mm}^3$  dimensions were used for imaging experiments.

**PET Imaging Experiment.**  $^{89}\text{Zr}$ -Cbl was intravenously administered (200–250  $\mu\text{Ci}$ /mouse, 7.4–9.3 MBq, 0.8–1 nmol) in sterile saline in mice bearing MDA-MB-453 xenografts. PET imaging was done using a  $\mu\text{PET}$  scanner (Concord) at 4, 24, and 48 h p.i. time points, while the mice were anesthetized with 1–2% isoflurane. Images were reconstructed using filtered back projection algorithm. ASIPRO VMTM software version 6.3.3.0 (Concord) was used to analyze the images to acquire volumes-of-interest expressed as percent injected dose per gram of tissue (%ID/g). Competitive inhibition was done by co-injecting  $\sim 200$ -fold excess of unmodified Cbl (200 nmol) with the radiotracer.

**Ex Vivo Distribution and Competitive Saturation.** The tissue distribution of  $^{89}\text{Zr}$ -Cbl was studied by administering 10–25  $\mu\text{Ci}$  (0.37–0.93 MBq, 0.04–0.1 nmol) of the tracer on the lateral tail vein of the rodent. For the competitive saturation assay,  $\sim 20$  nmol/mouse of cold CN-Cbl was co-injected with  $^{89}\text{Zr}$ -Cbl. Euthanasia was performed via  $\text{CO}_2$  asphyxiation at 4, 24, and 48 h p.i.

## ■ ASSOCIATED CONTENT

### 📄 Supporting Information

The Supporting Information is available free of charge on the ACS Publications website at DOI: 10.1021/acsomega.7b01180.

Synthesis of Cbl-DFO, LC–MS characterization of Cbl-DFO, RP-HPLC characterization of Cbl-DFO,  $^1\text{H}$  NMR characterization of Cbl-DFO, characterization of  $^{89}\text{Zr}$ -Cbl, %ID/g values from ex vivo analysis (PDF)

## AUTHOR INFORMATION

### Corresponding Authors

\*E-mail: rpdoyle@syr.edu (R.P.D.).

\*E-mail: villegan@karmanos.org (N.V.-V.).

### ORCID

Robert P. Doyle: 0000-0001-6786-5656

### Author Contributions

<sup>1</sup>A.N.W.K.-W. and J.L.W. contributed equally to this work.

### Author Contributions

R.P.D. and N.V.-V. conceived of the project and oversaw and designed the experiments. A.N.W.K.-W. performed the stability testing, radiolabeling, in vitro, in vivo, and ex vivo radio experiments. J.L.W. synthesized and characterized Cbl-DFO, performed radiolabeling, and conducted in vivo radio experiments. E.N. performed TC binding assays. All of the authors analyzed the data, and the manuscript was written through contributions of all of the authors. All of the authors have given approval to the final version of the manuscript.

### Notes

The authors declare the following competing financial interest(s): R.P.D. sits on the scientific advisory board of Xeragenx LLC.

## ACKNOWLEDGMENTS

R.P.D. and N.V.-V. would like to thank Xeragenx LLC (St. Louis, MO) for funding, in part, of this research. Research reported in this publication was also supported in part by the National Institute of Diabetes, Digestive and Kidney Disorder and the National Institute of Health to RPD under award number R15DK097675. The content is solely the responsibility of the authors and does not necessarily represent the official views of the National Institutes of Health. All of the in vivo imaging was conducted using resources managed by KCI Microscopy, Imaging, and Cytometry Resources core (P30CA022453).

## ABBREVIATIONS

Cbl, vitamin B<sub>12</sub> (cyanocobalamin); DFO, desferrioxamine; TC, transcobalamin; CD320, holo-transcobalamin receptor; <sup>89</sup>Zr, 89-Zirconium isotope; PET, positron emission tomography; FBS, fetal bovine serum; iTLC, instant thin-layer chromatography; MALDI-MSI, matrix-assisted laser desorption ionization mass spectrometry imaging; %ID/g, percent injected dose per gram; DMEM, Dulbecco's modified Eagle's medium

## REFERENCES

- (1) Nielsen, M. J.; Rasmussen, M. R.; Andersen, C. B. F.; Nexø, E.; Moestrup, S. K. Vitamin B<sub>12</sub> transport from food to the body's cells—a sophisticated, multistep pathway. *Nat. Rev. Gastroenterol. Hepatol.* **2012**, *9*, 345–354.
- (2) Green, R.; Allen, L. H.; Børke-Monsen, A.-L.; Brito, A.; Guéant, J.-L.; Miller, J. W.; Molloy, A. M.; Nexø, E.; Stabler, S.; Toh, B.-H.; Ueland, P. M.; Yajnik, C. Vitamin B<sub>12</sub> deficiency. *Nat. Rev. Dis. Primers* **2017**, *3*, No. 17040.
- (3) Gherasim, C.; Lofgren, M.; Banerjee, R. Navigating the B<sub>12</sub> Road: Assimilation, Delivery, and Disorders of Cobalamin. *J. Biol. Chem.* **2013**, *288*, 13186–13193.
- (4) Quadros, E. V.; Sequeira, J. M. Cellular Uptake of Cobalamin: Transcobalamin and the TCb1R/CD320 Receptor. *Biochimie* **2013**, *95*, 1008–1018.
- (5) Sysel, A. M.; Valli, V. E.; Nagle, R. B.; Bauer, J. A. Immunohistochemical Quantification of the Vitamin B<sub>12</sub> Transport

Protein (TCII), Cell Surface Receptor (TCII-R) and Ki-67 in Human Tumor Xenografts. *Anticancer Res.* **2013**, *33*, 4203–4212.

(6) Zelder, F.; Alberto, R. *The Porphyrin Handbook*; Elsevier Science: San Diego, 2012; Vol. 25, pp 83–130.

(7) Collins, D. A.; Hogenkamp, H. P. C.; Gebhard, M. W. Tumor Imaging Via Indium 111–Labeled DTPA–Adenosylcobalamin. *Mayo Clin. Proc.* **1999**, *74*, 687–691.

(8) Ruiz-Sánchez, P.; Mundwiler, S.; Medina-Molner, A.; Spingler, B.; Alberto, R. Iodination of Cisplatin Adduct of Vitamin B<sub>12</sub> [B<sub>12</sub>]-CN- $\{cis-PtCl(NH_3)_2\}^+$ . *J. Organomet. Chem.* **2007**, *692*, 1358–1362.

(9) Kunze, S.; Zobi, F.; Kurz, P.; Spingler, B.; Alberto, R. Vitamin B<sub>12</sub> as a Ligand for Technetium and Rhenium Complexes. *Angew. Chem., Int. Ed Engl.* **2004**, *43*, 5025–5029.

(10) Sah, B. R.; Schibli, R.; Waibel, R.; von Boehmer, L.; Blauenstein, P.; Nexø, E.; Johayem, A.; Fischer, E.; Müller, E.; Soyka, J. D.; et al. Tumor Imaging in Patients with Advanced Tumors Using a New <sup>99m</sup>Tc-Radiolabeled Vitamin B<sub>12</sub> Derivative. *J. Nucl. Med.* **2014**, *55*, 43–49.

(11) Baldoni, D.; Waibel, R.; Blauenstein, P.; Galli, F.; Iodice, V.; Signore, A.; Schibli, R.; Trampuz, A. Evaluation of a Novel Tc-<sup>99m</sup> Labeled Vitamin B<sub>12</sub> Derivative for Targeting *Escherichia coli* and *Staphylococcus aureus* In Vitro and in an Experimental Foreign-Body Infection Model. *Mol. Imaging Biol.* **2015**, *17*, 829–837.

(12) Zelder, F. Recent Trends in the Development of Vitamin B<sub>12</sub> derivatives for medicinal applications. *Chem. Commun.* **2015**, *51*, 14004–14017.

(13) Waibel, R.; Treichler, H.; Schaefer, N. G.; van Staveren, D. R.; Mundwiler, S.; Kunze, S.; Küenzi, M.; Alberto, R.; Nüesch, J.; Knuth, A.; et al. New Derivatives of Vitamin B<sub>12</sub> Show Preferential Targeting of Tumors. *Cancer Res.* **2008**, *68*, 2904–2911.

(14) Ikotun, O. F.; Marquez, B. V.; Fazen, C. H.; Kahkoska, A. R.; Doyle, R. P.; Lapi, S. E. Investigation of a Vitamin B<sub>12</sub> Conjugate as a PET Imaging Probe. *ChemMedChem* **2014**, *9*, 1244–1251.

(15) McEwan, J. F.; Veitch, H. S.; Russell-Jones, G. J. Synthesis and Biological Activity of Ribose-5'-Carbamate Derivatives of Vitamin B<sub>12</sub>. *Bioconjugate Chem.* **1999**, *10*, 1131–1136.

(16) Perk, L. R.; Vosjan, M. J. W. D.; Visser, G. W. M.; Budde, M.; Jurek, P.; Kiefer, G. E.; van Dongen, G. A. M. S. *p*-Isothiocyanato-benzyl-desferrioxamine: a new bifunctional chelate for facile radiolabeling of monoclonal antibodies with zirconium-89 for immuno-PET imaging. *Eur. J. Nucl. Med. Mol. Imaging* **2010**, *37*, 250–259.

(17) Stupperich, E.; Nexø, E. Effect of the cobalt-N coordination on the cobamide recognition by the human vitamin B<sub>12</sub> binding proteins intrinsic factor, transcobalamin and haptocorrin. *Eur. J. Biochem.* **1991**, *199*, 299–303.

(18) Bonaccorso, R. L.; Chepurny, O. G.; Becker-Paully, C.; Holz, G. G.; Doyle, R. P. Enhanced Peptide Stability Against Protease Digestion Induced by Intrinsic Factor Binding of a Vitamin B<sub>12</sub> Conjugate of Exendin-4. *Mol. Pharm.* **2015**, *12*, 3502–3506.

(19) Mutti, E.; Ruetz, M.; Birn, H.; Kräutler, B.; Nexø, E. 4-Ethylphenyl-Cobalamin Impairs Tissue Uptake of Vitamin B<sub>12</sub> and Causes Vitamin B<sub>12</sub> Deficiency in Mice. *PLoS One* **2013**, *8*, No. e75312.

(20) Christensen, E. I.; Birn, H. Megalin and Cubilin: Multifunctional Endocytic Receptors. *Nat. Rev. Mol. Cell Biol.* **2002**, *3*, 256–268.

(21) Christensen, E. I.; Willnow, T. E. Essential Role of Megalin in Renal Proximal Tubule for Vitamin Homeostasis. *J. Am. Soc. Nephrol.* **1999**, *10*, 2224–2236.

(22) Akizawa, H.; Arano, Y.; Mifune, M.; Iwado, A.; Saito, Y.; Mukai, T.; Uehara, T.; Ono, M.; Fujioka, Y.; Ogawa, K.; Kiso, Y.; Saji, H. Effect of molecular charges on renal uptake of <sup>111</sup>In-DTPA-conjugated peptides. *Nucl. Med. Biol.* **2001**, *28*, 761–768.

(23) Ferdani, R.; Stigers, D. J.; Fiamengo, A. L.; Wei, L.; Li, B. T. Y.; Golen, J. A.; Rheingold, A. L.; Weisman, G. R.; Wong, E. H.; Anderson, C. J. Synthesis, Cu(II) complexation, <sup>64</sup>Cu-labeling and biological evaluation of cross-bridged cyclam chelators with phosphonate pendent arms. *Dalton Trans.* **2012**, *41*, 1938–1950.

(24) Kornerup, L. S.; Fedosov, S. N.; Juul, C. B.; Greibe, E.; Heegaard, C. W.; Nexø, E. Tissue Distribution of Oral Vitamin B<sub>12</sub> Is

Influenced by B12 Status and B12 Form: An Experimental Study in Rats. *Eur. J. Nutr.* **2017**, 1–11.

(25) Hygum, K.; Lildballe, D. L.; Greibe, E. H.; Morkbak, A. L.; Poulsen, S. S.; Sorensen, B. S.; Petersen, T. E.; Nexø, E. Mouse transcobalamin has features resembling both human transcobalamin and haptocorrin. *PLoS One* **2011**, 6, No. e20638.

**A Vitamin B12 Conjugate of Exendin-4 Improves Glucose Tolerance Without Associated  
Nausea or Hypophagia in Rodents**

**Elizabeth G. Mietlicki-Baase<sup>1</sup>, Claudia G. Liberini<sup>1</sup>, Jayme L. Workinger<sup>2</sup>, Ron L.  
Bonaccorso<sup>2</sup>, Tito Borner<sup>3</sup>, David J. Reiner<sup>1</sup>, Kieran Koch-Laskowski<sup>1</sup>, Lauren E.  
McGrath<sup>1</sup>, Rinzin Lhamo<sup>1</sup>, Lauren M. Stein<sup>1</sup>, Bart C. De Jonghe<sup>3</sup>, George G. Holz<sup>4</sup>,  
Christian L. Roth<sup>5</sup>, Robert P. Doyle<sup>2,4\*#</sup>, Matthew R. Hayes<sup>1,3\*#</sup>**

<sup>1</sup>Department of Psychiatry, Perelman School of Medicine, University of Pennsylvania, Philadelphia, PA 19104; <sup>2</sup>Department of Chemistry, Syracuse University, Syracuse, NY 13244; <sup>3</sup>Department of Biobehavioral Health Sciences, School of Nursing, University of Pennsylvania, Philadelphia, PA 19104; <sup>4</sup>Department of Medicine, State University of New York, Upstate Medical University, Syracuse, New York 13210; <sup>5</sup>Center for Integrative Brain Research, Seattle Children's Research Institute, Division of Endocrinology, Department of Pediatrics, University of Washington, Seattle, WA

\* These authors contributed equally

# Address correspondence to:

Dr. Matthew R. Hayes, University of Pennsylvania, 125 South 31<sup>st</sup> St., Philadelphia, PA 19104,  
215-573-6070, [hayesmr@mail.med.upenn.edu](mailto:hayesmr@mail.med.upenn.edu)

Dr. Robert P. Doyle, Syracuse University, 111 College Place, Syracuse, NY 13244, 315-443-  
3584, [rpdoyle@syr.edu](mailto:rpdoyle@syr.edu)

**Running Title:** B12-conjugated Exendin-4 improves glycemia

**Abstract Word Count:** 245

**Main Text Word Count:** 3,486

**Number of References:** 45

**Number of Figures:** 5

## **Abstract**

*Aims:* While pharmacological glucagon-like peptide-1 receptor (GLP-1R) agonists are FDA-approved for treating type 2 diabetes mellitus (T2DM) and obesity, major side effects are nausea/malaise and hypophagia. We recently developed a conjugate of vitamin B12 bound to the GLP-1R agonist exendin-4 (Ex4), which displays enhanced proteolytic stability and retention of GLP-1R agonism. Here, we evaluate whether the conjugate (B12-Ex4) can improve glucose tolerance without producing anorexia and malaise.

*Materials and Methods:* We evaluated the effects of systemic B12-Ex4 and unconjugated Ex4 on food intake and body weight change, oral glucose tolerance, and nausea/malaise in male rats, and effects on intraperitoneal glucose tolerance in mice. To evaluate whether differences in the profile of effects of B12-Ex4 versus unconjugated Ex4 are due to altered CNS penetrance, rats received systemic injections of fluorescein-Ex4 (Flex), Cy5-B12 or Cy5-B12-Ex4 and brain penetrance was evaluated using confocal microscopy. Uptake of systemically administered Cy5-B12-Ex4 in insulin-containing pancreatic beta cells was also examined.

*Results:* B12-Ex4 conjugate improves glucose tolerance, but does not elicit the malaise and anorexia produced by unconjugated Ex4. While Flex robustly penetrates into the brain (dorsal vagal complex, paraventricular hypothalamus), Cy5-B12 and Cy5-B12-Ex4 fluorescence were not observed centrally, supporting a lack of CNS penetrance in line with the observed reduction in CNS-associated Ex4 side effects. Cy5-B12-Ex4 colocalizes with insulin in the pancreas, suggesting direct pancreatic action as a potential mechanism underlying the hypoglycemic effects of B12-Ex4.

*Conclusions:* These novel findings highlight the potential clinical utility of B12-Ex4 conjugates as possible future T2DM therapeutics with reduced incidence of adverse effects.

## Introduction

Multiple incretin-based therapeutics are approved for the treatment of type 2 diabetes mellitus (T2DM) due to their ability to elicit pancreatic insulin secretion and reduce blood glucose levels. These pharmacotherapies include compounds designed to increase endogenous concentrations of the incretin hormone glucagon-like peptide-1 (GLP-1) by inhibiting the endopeptidase DPP-IV, as well as synthetic peptide-based GLP-1 receptor (GLP-1R) agonists resistant to DPP-IV degradation<sup>1</sup>. In addition to being the more potent class of GLP-1-based therapeutics for reducing glycemia, GLP-1R agonists significantly reduce food intake and body weight in both humans and animal models<sup>1-3</sup>. This anorectic effect is attractive when considering the utilization of GLP-1R agonists as an on- or off-label treatment option for obesity, and indeed, the GLP-1R agonist liraglutide is FDA-approved for the treatment of obesity<sup>4</sup>. However, a sizeable percentage of individuals with T2DM do not have obesity or overweight<sup>5-7</sup> and may want to avoid weight loss. Furthermore, it is important to note that the hypophagic effects of all GLP-1R agonists on the market are accompanied by pronounced incidence of nausea, vomiting, and malaise<sup>3,8,9</sup>. In fact, ~20-50% of T2DM patients prescribed GLP-1-based medication experience nausea and/or vomiting, leading to discontinuation of drug treatment in ~6-10% and reduced dose tolerance in another ~15%<sup>10-14</sup>. These adverse effects are surprisingly under-investigated, as they limit the widespread use, efficacy, and potential ubiquitous utility of GLP-1R agonists (e.g. liraglutide, exenatide) for the treatment of metabolic disease.

A wealth of literature provides convincing evidence that a significant portion of the increase in glucose-stimulated insulin secretion following exogenous GLP-1R ligand administration is mediated by direct activation of GLP-1R expressed on pancreatic  $\beta$ -cells [see <sup>1-</sup>

<sup>3,15</sup> for review], mimicking the paracrine effects of pancreatic-derived GLP-1 that may not occur with endogenous L-cell-derived GLP-1<sup>16-18</sup>. Importantly, activation of GLP-1R expressed on vagal afferent fibers and/or in discrete nuclei in the central nervous system (CNS) also contributes to exogenous GLP-1R agonist-mediated improvements in glycemic control<sup>1-3,15,19-21</sup>. Interestingly, these dual sites of action (i.e. vagal and direct CNS activation) also mediate the intake- and body weight-suppressive effects of exogenous systemic GLP-1R agonist administration<sup>21-23</sup>. Both liraglutide and exenatide can penetrate into the CNS and activate central GLP-1R-expressing nuclei leading to hypophagia and weight loss<sup>22,24</sup>. Remarkably, however, GLP-1R agonist-induced illness behaviors (e.g. nausea, conditioned taste avoidance, hypophagia, emesis) are mediated by GLP-1Rs expressed within the CNS and not by vagal afferent GLP-1Rs when these compounds are delivered systemically<sup>8</sup>. Although other T2DM medications (e.g., DPP-IV inhibitors) may improve glycemic control with minimal effects on energy balance<sup>25,26</sup>, long-lasting GLP-1R agonists provide several advantages such as improved glycemic control and less frequent administration<sup>27-29</sup>. Thus, from a therapeutic standpoint, designing a novel GLP-1R agonist that is resistant to DPP-IV degradation, does not penetrate readily into the CNS, but retains enhanced pharmacokinetic and pharmacodynamics action on pancreatic  $\beta$ -cells would theoretically provide an improved pharmacological tool for glycemic control in T2DM patients without eliciting unwanted hypophagia and nausea.

Recently, we demonstrated that covalent conjugation of the GLP-1R agonist exendin-4 (Ex4) to vitamin B12 (Cyanocobalamin; B12) between the vitamin 5'-OH group and the K12 position of Ex4 retains picomolar agonism of the GLP-1R, either as the free conjugate (B12-Ex4) or bound to Intrinsic Factor (IF), a B12 transport protein critical for B12 absorption in humans<sup>30</sup>.

This work also confirmed that IF bound B12-Ex4 with low nanomolar affinity (as occurs with cyanocobalamin)<sup>30</sup>.

Interestingly, while Ex4 readily penetrates the CNS<sup>22,31</sup>, little is known about the penetrance of B12 in the brain. Uptake of B12 into the brain is putatively a receptor-mediated process with megalin (a receptor capable of TCII-B12 uptake in the kidney, for example) being expressed in the choroid plexus<sup>32,33</sup>. Additional evidence points to the importance of the CD320 receptor, as genetic ablation in mice results in severe cobalamin deficiency in the mouse brain<sup>34,35</sup>, as well as the transmembrane protein amnionless, natural mutations of which result in Imerslund-Gräsbeck syndrome and congenital cobalamin malabsorption<sup>36</sup>. Collectively, this information points to a receptor-mediated process of B12 blood-brain barrier penetrance, but little is known of where B12 is transported in the brain, and to what extent<sup>37</sup>, relative to total concentrations. It is evident that CNS uptake is considerably lower compared to other organs, especially the liver and kidney<sup>38,39</sup>. To this end, we hypothesized that a B12-Ex4 conjugate retains the incretin profile of a GLP-1R agonist to improve glucose tolerance but prevents development of nausea/malaise by reduced CNS penetration of the agonist.

The rat is a unique animal model for pre-clinical testing of the B12-Ex4 conjugate. Rats, unlike humans and mice, demonstrate an unexpected hyperglycemic response to systemic Ex4 delivery. This hyperglycemic effect is unique to the Ex4 molecule (among approved GLP-1R agonists) in the rat and is due in part to CNS-mediated sympathetic activation<sup>40</sup>. Further, rats show well-documented hypophagic effects to GLP-1R ligands mediated partly by accompanying acute effects on nausea/malaise, similar to humans, but not to mice<sup>8,9</sup>. Rats were therefore used as the primary model to evaluate the effects of B12-Ex4 on glycemic control, energy balance, and nausea/malaise, and these effects were compared with the response profile after peripheral



administration of unconjugated Ex4. Given that Ex4 produces hypoglycemic effects in mice<sup>41,42</sup>, similar to the effect observed in humans, blood glucose levels in mice were assessed in a glucose tolerance test after B12-Ex4 or Ex4. The data presented here provide evidence for a second-generation class of “cobalaminylated” GLP-1R agonists for the treatment of T2DM, with a pronounced profile of effects that include glucoregulation without anorexia or body weight loss, and most importantly an absence of nausea/malaise.

## **Materials and Methods**

*Animals.* Adult male Sprague Dawley rats (Charles River) were singly housed in hanging wire mesh cages. Four-month old C57BL/6J mice (Jackson Laboratory) were singly housed in plastic cages. All animals were housed under a 12h:12h light/dark cycle in a temperature- and humidity-controlled environment. Standard rodent chow (Purina 5001) and tap water were available *ad libitum* except where noted. Procedures were approved by the Institutional Care and Use Committee of the University of Pennsylvania.

*Compounds.* B12-conjugated exendin-4 (B12-Ex4) was produced, characterized and screened for agonism at the GLP-1R as previously described<sup>30</sup>. One addition to the characterization was the measure of TCII binding of B12-Ex4 (Figure 1D) , which was conducted at the Department of Clinical Medicine- Clinical Biochemistry, University of Aarhus, Denmark as described<sup>43</sup>. B12-Ex4, Ex4 (Bachem), and lithium chloride (LiCl; Sigma Aldrich) were dissolved in sterile 0.9% NaCl for peripheral injections. Injections were separated by at least 48h. For most *in vivo* experiments, injections were administered using a within-subjects, Latin square design. The

exception was the conditioned taste avoidance (CTA) study, which used a between-subjects design.

*Effects of B12-Ex4 on energy balance.* Shortly before the onset of the dark phase, rats (n=12) were given subcutaneous (SC) injection of B12-Ex4 (1, 5, or 20 $\mu$ g/kg) or vehicle (1ml/kg sterile saline). Chow intake was measured at 1, 3, 6, and 24h post-injection. Food spillage was accounted for in all intake measurements. Body weight was also measured at 0 and 24h.

*Effects of B12-Ex4 on glycemic control during an oral glucose tolerance test (OGTT).* Rats (n=12) were deprived of food overnight before testing. On the morning of testing, just after the onset of the dark phase, water was also removed from the cage. A small drop of blood was collected from the tail tip and analyzed for blood glucose (BG) level using a standard glucometer (AccuCheck). Immediately after this baseline BG reading (t=-30min), each rat received SC injection of B12-Ex4 (5 or 20 $\mu$ g/kg) or vehicle (1ml/kg sterile saline); doses of drug were selected based on the results of the feeding study. Thirty minutes later (t=0min), BG was measured and each rat received an oral gavage of glucose (2g/kg). Subsequent BG readings were taken at 20, 40, 60, and 120min after glucose gavage. After the final BG reading, food and water were returned.

*Effects of systemic Ex4 on glycemic control and energy balance.* The effects of unconjugated Ex4 were evaluated in an OGTT, using methods similar to those described above, with two major differences: SC injections were Ex4 (5 or 20 $\mu$ g/kg) or vehicle (1ml/kg sterile saline), and food intake and body weight change after the completion of the OGTT were monitored. Pre-

weighed food was returned to the rats after the OGTT, and chow intake was measured for ~21.5h (e.g., until 24h after the SC injections). Spillage was accounted for in food intake measurements. Body weight was recorded at 0 and 24h. For the OGTT, n=10 rats were tested; food and body weight data were collected from n=9 due to a technical error in food intake measurement.

*Effects of B12-Ex4 on expression of a conditioned taste avoidance (CTA).* Rats (n=8-10 per drug) were evaluated for expression of a CTA to a flavor paired with B12-Ex4 (5 $\mu$ g/kg, IP). Ex4 (5 $\mu$ g/kg, IP) and LiCl (0.15M) were used as positive controls. A two-bottle test was used so each rat had access to a flavor that had been paired previously with vehicle (1 ml/kg saline, IP) and a flavor that had been paired previously with drug (B12-Ex4, Ex4, or LiCl). See Supplemental Methods for more details.

*Effect of B12-Ex4 on glycemic control in mice during an intraperitoneal glucose tolerance test (IPGTT).* The experimental procedure for IPGTT in mice was similar to that used for OGTT in rats. Briefly, mice (n=13; 8 females, 5 males) were food and water deprived for 4h before and during the IPGTT. Testing was completed mid-light phase. Blood was collected from the tail tip and analyzed for BG. Immediately after this baseline reading (t=-30min), each mouse received IP injection of Ex4 (5 $\mu$ g/kg), B12-Ex4 (same equimolar dose to Ex4), or saline (10 $\mu$ l/g). Thirty minutes later (t=0min), BG was measured and each mouse received an IP injection of glucose (2g/kg). Subsequent BG readings were taken at 20, 40, 60, and 120min after glucose injection. After the final BG reading, food and water were returned. Area under the curve (AUC) was calculated from 0-120 min (e.g., beginning at the time of glucose administration).

*B12-Exendin-4-Cyanine-5 (Cy5-B12-Ex4) synthesis.* B12-Ex4 was synthesized as previously described<sup>30</sup>. B12-Ex4 (0.5mg, 0.0001mmol) was dissolved in PBS buffer pH 7.6 (450 $\mu$ L) and sulfo-cyanine5-NHS-ester (1mg, 0.001mmol) (Lumiprobe) was added (in 50 $\mu$ L DMSO). The resulting solution was allowed to mix for 2h at room temperature, protected from light, and then purified through RP-HPLC on a Shimadzu Prominence HPLC using a C18 column (Eclipse XDB-C18 5 $\mu$ m, 4.6 x 150mm). Solvents: A: 0.1% TFA water and B: Acetonitrile. Method: B%: 1-70% over 15min.  $t_R$ : 12.1min. Yield: 98%. Emission and excitation were 648 and 670nm, respectively using a Varian Cary UV Spectrophotometer and Agilent Cary Eclipse Fluorescence Spectrophotometer, solvent H<sub>2</sub>O/MeCN. LC-MS analysis (Shimadzu LCMS-8040, Method: 0.1% formic acid and 35% methanol water at 0.2mL/min, DL temp: 150°C, heat block temp: 400°C.): expected m/z: 6923 [B12-Ex4-(Cy5)<sub>2</sub>], observed: 1383 [M+5H]<sup>+5</sup>, 1728 [M+4H]<sup>+4</sup>. See Figure 1 for more information.

*B12-Cyanine-5 (Cy5-B12) synthesis.* Cy5-B12 was synthesized through Huisgen/Sharpless 'Click' Chemistry<sup>44,45</sup>. Cu(I) (1mg, 0.005mmol) and Tris[(1-benzyl-1H-1,2,3-triazol-4-yl)methyl]amine (3.5mg, 0.006mmol) were dissolved in 0.5mL DMF/H<sub>2</sub>O (4:1 v/v). Once color change occurred, the previously synthesized B12-Azide (3mg, 0.002mmol)<sup>46</sup> and Cyanine-5 alkyne (0.5mg, 0.0007mmol) (Lumiprobe) was dissolved in the solution and allowed to stir at room temperature overnight protected from light. This was purified through RP-HPLC on a Shimadzu Prominence HPLC using a C18 column (Eclipse XDB-C18 5  $\mu$ m, 4.6 x 150mm). Solvents: A: 0.1% TFA water and B: Acetonitrile. Method: B%: 20-72% over 18min.  $t_R$ : 4.7min. Yield: 94%. LC-MS analysis (Shimadzu LCMS-8040, Method: 0.1% Formic acid and 35% methanol water at 0.2mL/min, DL temp: 150°C, heat block temp: 400°C.): expected m/z: 2059

observed: 1031  $[M+2H]^{+2}$ , 1042  $[M+Na+2H]^{+2}$ , and 1050  $[M+K+2H]^{+2}$ . Emission and excitation were 645 and 682nm, respectively using a Varian Cary UV Spectrophotometer and Agilent Cary Eclipse Fluorescence Spectrophotometer, solvent H<sub>2</sub>O. See Figure 1 for more information.

*GLP-1 assay for Cy5-B12-Ex4.* Agonism at the GLP-1 receptor was monitored using HEK-293 cells stably transfected with the GLP-1 receptor cultured in DMEM with 10% FBS, 1% pen/strep, and 250 $\mu$ g/mL genetecin/g-418. Cells were plated on a rat-tail-collagen-coated 96-well plate at 60,000 cell/well and allowed to adhere overnight. The cells were infected with an adenovirus to express the H188 FRET reporter using a 25 MOI for 16-20h in 75 $\mu$ L of DMEM-1% FBS. After viral incubation, the cells were placed in 200 $\mu$ L standard extracellular matrix with glucose and 0.1% BSA. Conjugates were added to each well at 5x the required concentration. Agonism was determined through an increase in 485/553nm FRET ratio indicative of an increase in cAMP level through cAMP binding to an EPAC (exchange protein directly activated by cAMP)<sup>47</sup>.

*Immunohistochemical procedures and confocal imaging.* Rats (n=4/group) were given IP injection of fluorophore-labeled Ex-4 (Flex; 5 $\mu$ g/kg; 0.0001nM; AnaSpec<sup>48</sup>), Cy5-B12-Ex4 (5 $\mu$ g/kg; 0.03nM), Cy5-B12 (5 $\mu$ g/kg), or Cy5-B12-Ex4 delivered at an equimolar dose to Flex (0.0001nM). Rats were transcardially perfused 3h after injection, using 0.1M PBS followed by 4% paraformaldehyde (PFA). Brains were collected and sections from the area postrema and hypothalamus were processed via immunohistochemistry for NeuN and GFAP, mounted, and coverslipped with DAPI mounting medium. Sections were visualized via confocal microscopy. See Supplemental Methods for more detail.

To evaluate the penetrance of B12-Ex4 in the pancreas, rats (n=3) were given IP injection of Cy5-B12-Ex4 (5µg/kg) and transcardially perfused 3h later with 4% paraformaldehyde in PBS. Pancreases were collected and sagittally sectioned, processed via immunohistochemistry for insulin, and coverslipped with DAPI mounting medium. Sections were visualized with confocal microscopy and three-dimensional rotational animations were rendered from the collected z-stack images using Imaris 8.1.2 (Bitplane). See Supplemental Methods for more information.

*Statistical analyses.* See Supplemental Methods.

## **Results**

*B12-Ex4 has potent beneficial effects on glycemic control, but minimal impact on feeding and body weight in rats.*

Ex4 and other GLP-1R agonists reduce blood glucose levels, and are used clinically to treat T2DM<sup>49</sup>. In addition, the food intake- and body weight-suppressive effects of GLP-1R agonists have highlighted the utility of these pharmacotherapies for the treatment of obesity<sup>50</sup>. To evaluate whether the metabolic effects of B12-Ex4 are similar to those of other GLP-1R agonists such as unconjugated Ex4, the effects of SC injection of B12-Ex4 on energy balance and glycemic control were evaluated. To confirm TCII binding of B12 in its Ex4 conjugated form (i.e. B12-Ex4), a radio chase assay using <sup>57</sup>Co-labelled B12 was conducted<sup>43</sup> and confirmed low nanomolar binding (~ 75nM) was maintained (Figure 1D).

First, to test whether B12-Ex4 has similar intake- and body weight-suppressive effects as Ex4, rats were given SC injection of B12-Ex4 (0, 1, 5, or 20µg/kg in 1ml/kg sterile saline), and

subsequent food intake (1, 3, 6, 24h) and body weight gain were measured. The highest dose of B12-Ex4, 20 $\mu$ g/kg, significantly suppressed food intake at 3h and 6h post-injection (Figure 2A; drug x time interaction,  $F_{9,99}=3.69$ ,  $p<0.001$ ; 0 $\mu$ g/kg versus 20 $\mu$ g/kg,  $p<0.05$  at 3h and 6h). No other significant effects on food intake were observed at other times or by other doses of drug (all other  $p>0.05$ ). There was also no significant effect of B12-Ex4 on 24h body weight change (Figure 2B;  $F_{3,33}=0.50$ ,  $p=0.69$ ), which is consistent with the fact that cumulative 24h energy intake was similar among the treatment conditions.

Next, the glycemic effects of B12-Ex4 (5 or 20 $\mu$ g/kg) or vehicle (1ml/kg sterile saline, SC) were evaluated via OGTT. B12-Ex4 significantly reduced blood glucose levels in the OGTT (Figure 2C; main effect of drug,  $F_{2,22}=4.01$ ,  $p<0.04$ ; drug x time interaction,  $F_{10,110}=17.29$ ,  $p<0.000001$ ). Posthoc analyses showed that both doses of B12-Ex4 significantly suppressed BG at 20 and 40min after glucose gavage (versus vehicle, all  $p<0.05$ ). A dose-responsive effect is also suggested by the finding that 20 $\mu$ g/kg B12-Ex4 had more potent BG-suppressive effects than 5 $\mu$ g/kg at 20min after glucose gavage ( $p<0.05$ ). Interestingly, BG levels were increased by both doses of B12-Ex4 at 60min and by the higher dose at 120min (all  $p<0.05$ ). Importantly, injection of B12-Ex4 had no effect on blood glucose levels on its own ( $t=0$ , all  $p>0.05$ ).

#### *Systemic injection of Ex4 produces hyperglycemia, hypophagia, and weight loss.*

The rat is a particularly interesting model to test the effects of an Ex4-based drug on glycemic and energy balance control, because rats exhibit a hyperglycemic response to acute peripheral administration of Ex4 due to sympathetic activation<sup>40</sup>, but also show pronounced reductions in feeding and body weight gain<sup>51-53</sup>. To evaluate the effects of SC administration of unconjugated Ex4 on these measures, and to be able to more directly compare the effects of B12-

Ex4 to those of Ex4, an OGTT was administered to rats after SC injection of Ex4 (5 or 20 $\mu$ g/kg) or vehicle (1ml/kg), and subsequent chow intake and body weight were monitored after the OGTT. Similar to previous findings<sup>40</sup>, systemic Ex4 produced a pronounced hyperglycemic response in the rats (Figure 3A, main effect of drug,  $F_{2,18}=8.84$ ,  $p<0.01$ ; drug x time interaction,  $F_{10,90}=11.89$ ,  $p<0.000001$ ). Injection of either dose of Ex4 increased BG on its own (e.g., before administration of glucose; at  $t=0$ min, vehicle versus 5 or 20 $\mu$ g/kg,  $p<0.05$ ). BG levels remained significantly elevated in Ex4-treated rats at 40, 60, and 120min after the glucose gavage (vehicle versus 5 or 20 $\mu$ g/kg, all  $p<0.05$ ).

When food was returned after the last BG reading, Ex4-treated rats ate significantly less than did vehicle-treated controls in the subsequent 21.5h (Figure 3B,  $F_{2,16}=43.74$ ,  $p<0.000001$ ; vehicle versus 5 or 20 $\mu$ g/kg,  $p<0.05$ ) and gained less body weight (Figure 3C,  $F_{2,16}=8.31$ ,  $p<0.01$ ; vehicle versus 20 $\mu$ g/kg,  $p<0.05$ ). These results demonstrate the unique constellation of effects produced by peripheral Ex4 administration in the rat, and more importantly, highlight the distinct differences between Ex4 and B12-Ex4 for glycemic and energy balance control.

*Ex4 elicits expression of a robust CTA that is not observed with B12-Ex4.*

GLP-1R agonists such as Ex4 have undesired side effects including nausea/malaise<sup>8,49</sup>. To evaluate whether B12-Ex4 produces nausea/malaise, rats were evaluated for expression of a conditioned taste avoidance (CTA) to B12-Ex4 (5 $\mu$ g/kg, IP). Additional groups of rats were evaluated in this experiment for CTA to Ex4 (5 $\mu$ g/kg, IP) or to LiCl (0.15M, IP), which is well known to produce nausea and CTA in rodents<sup>8,54,55</sup>. As shown in Figure 3D, acceptance of the drug-paired flavor was significantly higher in the B12-Ex4-treated group compared to either LiCl



or Ex4 ( $F_{2,24}=5.29$ ,  $p<0.01$ ; B12-Ex4 versus LiCl or Ex4,  $p<0.05$ ; LiCl versus Ex4,  $p>0.05$ ), suggesting that B12-Ex4 does not produce the same nausea/malaise as Ex4.

*The glycemic effects of B12-Ex4 in mice are comparable to those of Ex4.*

To confirm the ability of B12-Ex4 to improve glycemic control in species that do not exhibit Ex4-induced stress-mediated hyperglycemic responses, the glycemic effects of equimolar doses of B12-Ex4 and Ex4 were tested via IPGTT in mice. In contrast to rats, and more in line with human data, Ex4 administration strongly attenuated the increase in blood glucose levels after IP glucose administration. Similarly, B12-Ex4 reduced blood glucose levels in the IPGTT (Figure 4A; main effect of drug,  $F_{2,24}=41.04$ ,  $p<0.0001$ ; drug x time interaction,  $F_{10,120}=13.29$ ,  $p<0.0001$ ). Posthoc analyses showed that both compounds significantly suppressed BG at 20, 40, 60, and 120min after glucose injection (all  $p<0.05$ ). Interestingly, injection of B12-Ex4 or Ex4 also reduced BG levels prior to IP glucose injection ( $t=0$ , all  $p<0.05$ ). Although Ex4 had a more potent effect on BG at 20min compared to B12-Ex4 ( $p<0.05$ ), area under the curve analyses revealed that both compounds had similar hypoglycemic effects post-glucose load compared to saline (Figure 4B; NEED STATS HERE).

*Unlike Ex4, B12-Ex4 does not readily penetrate into the CNS.*

Previous work shows that Ex4 crosses the blood-brain barrier to exert effects on energy balance and illness/malaise<sup>22,31,48</sup>. As B12-Ex4 treatment produces the glycemic benefits associated with Ex4 without producing the centrally-mediated effects of hypophagia and nausea, this suggests that B12-Ex4 may be excluded from the CNS. To evaluate this possibility, rats were treated systemically with a fluorescent-tagged version of B12-Ex4 (Cy5-B12-Ex4), and

penetration into the brain was evaluated using confocal microscopy. The results were compared with CNS penetration of a fluorescent-tagged version of Ex4 (Flex), which has been shown to penetrate into the CNS<sup>48</sup>, and fluorescent-tagged B12 (Cy5-B12). The presence of each of these fluorescent compounds was evaluated in the dorsal vagal complex (DVC; Figure 5) and paraventricular nucleus of the hypothalamus (PVN; Figure 6), due to the known importance of these areas in mediating the feeding effects of GLP-1R activation<sup>56,57</sup> and the hyperglycemic response observed in rats after systemic Ex4<sup>40</sup>. Consistent with previous data<sup>48</sup>, Flex was observed in both sites. In contrast, Cy5-B12 and Cy5-B12-Ex4 were not detected in either nucleus, suggesting that exogenously-injected B12 does not readily penetrate into these regions of the CNS, and hence that conjugation of B12 to Ex4 greatly reduces or prevents Ex4 from entering the same areas.

*B12-Ex4 is colocalized on insulin-producing pancreatic beta cells.*

The finding that peripherally administered B12-Ex4 is not detected in the DVC or PVN suggests that the glycemic effects of the compound are likely mediated via peripheral actions. The pancreas is a prime candidate for a peripheral site of action for B12-Ex4. GLP-1R agonists can act directly on pancreatic beta cells to stimulate insulin release, thereby improving blood glucose levels<sup>58-60</sup>. To assess whether B12-Ex4 is taken up by insulin-producing pancreatic beta cells, rats were given systemic injection of Cy5-B12-Ex4 (5µg/kg) and colocalization with insulin was analyzed in the pancreas with confocal microscopy. Results show robust colocalization of Cy5-B12-Ex4 with insulin in pancreatic sections (Figure 7; Supplemental Materials, Videos 1 and 2), supporting the hypothesis that B12-Ex4 acts at the pancreas to improve glycemic control.

## Discussion

GLP-1-based pharmacotherapies for T2DM have been revolutionary in providing largely safe and efficacious means to reduce chronic hyperglycemia [see <sup>1,3,15</sup> for review]. However, due to side effects of current GLP-1-based compounds including anorexia, nausea, and vomiting, nearly one in four T2DM patients are not able to benefit from the full pharmaceutical advantages of these pharmacotherapies<sup>10-14</sup>. There is clearly a critical need to develop a new generation of GLP-1 pharmacotherapies that provide hypoglycemic benefit without eliciting detrimental side effects. Although the hypophagic effects of GLP-1R agonists are often attractive to clinicians and overweight/obese T2DM patients, much of the same CNS circuitry underlying GLP-1R ligand-mediated anorexia is also partially responsible for mediating nausea/malaise<sup>8</sup>. Moreover, weight loss may be undesirable for some T2DM patients, such as individuals with a normal BMI. As the hypophagia and illness-like effects of existing GLP-1R agonists require CNS penetrance and direct central action<sup>8,21-23</sup>, we sought to create a GLP-1R agonist conjugate that minimizes anorexia and nausea by reducing CNS penetrance, but that retains potent pharmacodynamics and pharmacokinetic profile on peripheral GLP-1R populations to exert glycemic benefits. This report shows for the first time the ability of B12-Ex4 [see <sup>30</sup> for previous biochemical GLP-1R agonism analyses] to improve glucose tolerance in rodents without producing hypophagia, body weight loss, or CTA. Immunohistochemical data suggest that this unique profile involves a direct effect of B12-Ex4 on pancreatic beta cells coupled with a virtual absence of CNS penetrance of the compound.

The rat provides a unique model for the proof-of-concept testing needed for the preclinical evaluation of B12-Ex4. Rats show an unexpected hyperglycemic response to Ex4, due

in part to a CNS-mediated activation of the sympathetic nervous system<sup>40</sup>. In addition, like humans, rats show a pronounced profile of behavioral effects to systemic Ex4 including reduced food intake and body weight, as well as illness-like behaviors, again due to CNS action<sup>8,22,61</sup>. B12-Ex4 did not produce the same suppression of food intake, reduction in body weight, and induction of CTA as did Ex4 in rats. The effect of B12-Ex4 on glycemic control was also evaluated in mice, a species in which Ex4 produces a hypoglycemic response similar to that observed in humans. In mice, B12-Ex4 elicited a hypoglycemic response similar to that of unconjugated Ex4 in an IPGTT. Collectively, these data provide an ideal preclinical set of outcomes to support the therapeutic potential of this conjugate as a future antidiabetic drug for humans.

The *in vivo* behavioral data were supported by our immunohistochemical analyses showing a virtual absence of B12-Ex4 CNS penetrance in the DVC and PVN, two areas of the brain showing unconjugated Ex4 penetrance and believed to mediate in part the hyperglycemic, hypophagic, body weight suppressive, and malaise-producing effects of Ex4 in rats. Future studies are warranted to identify the mechanisms responsible for the minimal CNS uptake of B12 and the molecular mechanisms by which B12 conjugation reduces CNS Ex4 access. It will also be important to address whether higher doses of B12-Ex4 are able to penetrate the CNS. The 5 $\mu$ g/kg dose of Cy5-B12-Ex4 used for this study was selected because 5 $\mu$ g/kg B12-Ex4 had no effect on feeding or body weight in rats, but produced hypoglycemia in the OGTT, suggesting that a lower dose of B12-Ex4 elicits an optimal profile of glycemic and energy balance effects. In contrast, a higher dose of B12-Ex4 (20 $\mu$ g/kg) reduced blood glucose but also caused a small but significant transient suppression of feeding, suggesting that higher doses may have a slightly

different pattern of effects. Nevertheless, these results clearly underscore the lack of CNS penetrance but retention of glycemic benefits by lower doses of B12-Ex4.

As B12-Ex4 is not extensively penetrating into the CNS, pancreatic GLP-1R represents the likely cellular substrate mediating the hypoglycemic effects of B12-Ex4. Further analyses supported this hypothesis, as immunohistochemical data showed colocalization of Cy5-B12-Ex4 with insulin in the pancreas. This suggests that B12-Ex4 may exert its glycemic effects via a direct action at pancreatic beta cells, while CNS-mediated effects of GLP-1R activation such as anorexia, nausea, and malaise are minimal or absent due to lack of penetrance of B12-Ex4 into the brain.

The current data provide novel mechanistic evidence that B12 conjugation to a GLP-1R agonist can be used as a means to retain the hypoglycemic properties of GLP-1R agonists but greatly reduce the CNS-mediated anorexia and illness effects observed with all current approved GLP-1-based ligands. These studies are far from the complete set of *in vivo* glycemic analyses needed for B12-Ex4, but certainly justify the need for more comprehensive future analyses. Further investigations are warranted to examine the acute actions of B12-Ex4 in diabetic animal models, as well as to evaluate the metabolic effects of chronic B12-Ex4 administration. It will also be critical to evaluate whether, and to what extent, B12-Ex4 may localize within other CNS nuclei not examined here. Collectively, these data highlight the discovery that B12 conjugation to Ex4 results in a next-generation incretin therapeutic with the clinically desired hypoglycemic effects but not concomitant hypophagia, body weight loss and, most notably, illness-like behaviors, ideal for the future of T2DM treatment in humans. This method of conjugation may also be broadly beneficial to other therapeutics that would benefit from reduced CNS penetrance.

**Acknowledgements:** This research was supported by NIH-DK096139 (MRH), NIH-DK069575 (GGH) and NIH-DK097675 (RPD and CLR). Elizabeth G. Mietlicki-Baase's current affiliation is the Department of Exercise and Nutrition Sciences, School of Public Health and Health Professions, State University of New York at Buffalo, Buffalo, NY 14214. Ron L. Bonaccorso's current affiliation is Lonza (Rochester, NY). A portion of this work was submitted in abstract form for the 2017 meeting of the Society for the Study of Ingestive Behavior.

**Author Contributions:** RPD and MRH conceived of the project. RPD and MRH conceptualized the hypotheses and designed the experiments. JLW, RLB, and RPD designed and synthesized the compounds. EGM-B, CGL, TB, DJR, KK-L, LEM, RL, and LMS conducted experiments and collected data. EGM-B, CGL, TB, DJR, LMS, BCDJ, GGH, RPD, and MRH analyzed data. EGM-B, CGL, TB, BCDJ, RPD, and MRH wrote the manuscript. All authors edited the manuscript. RPD and MRH are guarantors for this work.

**Financial Disclosure:** MRH and EGM-B receive funding from Zealand Pharma that was not used in support of these studies. MRH receives funding from Novo Nordisk that was not used in support of these studies. RPD is a scientific advisory board member and receives funding from Xeragenx LLC (St. Louis, MO, US) that was used in part support of these studies. RPD is a scientific advisory board member of Ichor Therapeutics (Lafayette, NY, US) and Balchem (New Hampton, NY, US) and receives funding from both that was not used in support of these studies. RPD is the named author of a patent pursuant to this work that is owned by Syracuse University.

**Conflict of Interests:** The authors declare no other competing financial interests or conflicts of interest.

## References

1. Hayes MR, Mietlicki-Baase EG, Kanoski SE, De Jonghe BC. Incretins and amylin: neuroendocrine communication between the gut, pancreas, and brain in control of food intake and blood glucose. *Annu Rev Nutr.* 2014;34:237-260.
2. Hayes MR, De Jonghe BC, Kanoski SE. Role of the glucagon-like-peptide-1 receptor in the control of energy balance. *Physiol Behav.* 2010;100(5):503-510.
3. Kanoski SE, Hayes MR, Skibicka KP. GLP-1 and weight loss: unraveling the diverse neural circuitry. *Am J Physiol Regul Integr Comp Physiol.* 2016;310(10):R885-895.
4. Gomez G, Stanford FC. US health policy and prescription drug coverage of FDA-approved medications for the treatment of obesity. *Int J Obes (Lond).* 2017.
5. Hartmann B, Lanzinger S, Bramlage P, et al. Lean diabetes in middle-aged adults: A joint analysis of the German DIVE and DPV registries. *PLoS One.* 2017;12(8):e0183235.
6. George AM, Jacob AG, Fogelfeld L. Lean diabetes mellitus: An emerging entity in the era of obesity. *World J Diabetes.* 2015;6(4):613-620.
7. Coleman NJ, Miernik J, Philipson L, Fogelfeld L. Lean versus obese diabetes mellitus patients in the United States minority population. *J Diabetes Complications.* 2014;28(4):500-505.
8. Kanoski SE, Rupprecht LE, Fortin SM, De Jonghe BC, Hayes MR. The role of nausea in food intake and body weight suppression by peripheral GLP-1 receptor agonists, exendin-4 and liraglutide. *Neuropharmacology.* 2012;62(5-6):1916-1927.
9. De Jonghe BC, Holland RA, Olivos DR, Rupprecht LE, Kanoski SE, Hayes MR. Hindbrain GLP-1 receptor mediation of cisplatin-induced anorexia and nausea. *Physiol Behav.* 2016;153:109-114.
10. Bergenstal RM, Wysham C, Macconell L, et al. Efficacy and safety of exenatide once weekly versus sitagliptin or pioglitazone as an adjunct to metformin for treatment of type 2 diabetes (DURATION-2): a randomised trial. *Lancet.* 2010;376(9739):431-439.
11. Buse JB, Henry RR, Han J, Kim DD, Fineman MS, Baron AD. Effects of exenatide (exendin-4) on glycemic control over 30 weeks in sulfonylurea-treated patients with type 2 diabetes. *Diabetes Care.* 2004;27(11):2628-2635.
12. DeFronzo RA, Ratner RE, Han J, Kim DD, Fineman MS, Baron AD. Effects of exenatide (exendin-4) on glycemic control and weight over 30 weeks in metformin-treated patients with type 2 diabetes. *Diabetes Care.* 2005;28(5):1092-1100.

13. Kendall DM, Riddle MC, Rosenstock J, et al. Effects of exenatide (exendin-4) on glycemic control over 30 weeks in patients with type 2 diabetes treated with metformin and a sulfonyleurea. *Diabetes Care*. 2005;28(5):1083-1091.
14. John LE, Kane MP, Busch RS, Hamilton RA. Expanded Use of Exenatide in the Management of Type 2 Diabetes. *Diabetes Spectrum*. 2007;20:59-63.
15. Drucker DJ. The biology of incretin hormones. *Cell Metab*. 2006;3(3):153-165.
16. Lamont BJ, Li Y, Kwan E, Brown TJ, Gaisano H, Drucker DJ. Pancreatic GLP-1 receptor activation is sufficient for incretin control of glucose metabolism in mice. *J Clin Invest*. 2012;122(1):388-402.
17. Smith EP, An Z, Wagner C, et al. The role of beta cell glucagon-like peptide-1 signaling in glucose regulation and response to diabetes drugs. *Cell Metab*. 2014;19(6):1050-1057.
18. Chambers AP, Sorrell JE, Haller A, et al. The Role of Pancreatic Preproglucagon in Glucose Homeostasis in Mice. *Cell Metab*. 2017;25(4):927-934 e923.
19. Hunter K, Holscher C. Drugs developed to treat diabetes, liraglutide and lixisenatide, cross the blood brain barrier and enhance neurogenesis. *BMC Neurosci*. 2012;13:33.
20. McClean PL, Parthasarathy V, Faivre E, Holscher C. The diabetes drug liraglutide prevents degenerative processes in a mouse model of Alzheimer's disease. *J Neurosci*. 2011;31(17):6587-6594.
21. Secher A, Jelsing J, Baquero AF, et al. The arcuate nucleus mediates GLP-1 receptor agonist liraglutide-dependent weight loss. *J Clin Invest*. 2014;124(10):4473-4488.
22. Kanoski SE, Fortin SM, Arnold M, Grill HJ, Hayes MR. Peripheral and Central GLP-1 Receptor Populations Mediate the Anorectic Effects of Peripherally Administered GLP-1 Receptor Agonists, Liraglutide and Exendin-4. *Endocrinology*. 2011;152(8):3103-3112.
23. Sisley S, Gutierrez-Aguilar R, Scott M, D'Alessio DA, Sandoval DA, Seeley RJ. Neuronal GLP1R mediates liraglutide's anorectic but not glucose-lowering effect. *J Clin Invest*. 2014;124(6):2456-2463.
24. Mietlicki-Baase EG, Ortinski PI, Rupprecht LE, et al. The food intake-suppressive effects of glucagon-like peptide-1 receptor signaling in the ventral tegmental area are mediated by AMPA/kainate receptors. *Am J Physiol Endocrinol Metab*. 2013.
25. Herman GA, Bergman A, Stevens C, et al. Effect of single oral doses of sitagliptin, a dipeptidyl peptidase-4 inhibitor, on incretin and plasma glucose levels after an oral glucose tolerance test in patients with type 2 diabetes. *J Clin Endocrinol Metab*. 2006;91(11):4612-4619.
26. Raz I, Hanefeld M, Xu L, et al. Efficacy and safety of the dipeptidyl peptidase-4 inhibitor sitagliptin as monotherapy in patients with type 2 diabetes mellitus. *Diabetologia*. 2006;49(11):2564-2571.
27. Stolar MW, Grimm M, Chen S. Comparison of extended release GLP-1 receptor agonist therapy versus sitagliptin in the management of type 2 diabetes. *Diabetes Metab Syndr Obes*. 2013;6:435-444.
28. Russell-Jones D, Cuddihy RM, Hanefeld M, et al. Efficacy and safety of exenatide once weekly versus metformin, pioglitazone, and sitagliptin used as monotherapy in drug-naive patients with type 2 diabetes (DURATION-4): a 26-week double-blind study. *Diabetes Care*. 2012;35(2):252-258.



29. Lind M, Matsson PO, Linder R, et al. Clinical Effectiveness of Liraglutide vs Sitagliptin on Glycemic Control and Body Weight in Patients with Type 2 Diabetes: A Retrospective Assessment in Sweden. *Diabetes Ther.* 2016;7(2):321-333.
30. Bonaccorso RL, Chepurny OG, Becker-Paully C, Holz GG, Doyle RP. Enhanced Peptide Stability Against Protease Digestion Induced by Intrinsic Factor Binding of a Vitamin B12 Conjugate of Exendin-4. *Mol Pharm.* 2015;12(9):3502-3506.
31. Kastin AJ, Akerstrom V. Entry of exendin-4 into brain is rapid but may be limited at high doses. *Int J Obes Relat Metab Disord.* 2003;27(3):313-318.
32. Carro E, Spuch C, Trejo JL, Antequera D, Torres-Aleman I. Choroid plexus megalin is involved in neuroprotection by serum insulin-like growth factor I. *J Neurosci.* 2005;25(47):10884-10893.
33. Christensen EI, Birn H. Megalin and cubilin: multifunctional endocytic receptors. *Nat Rev Mol Cell Biol.* 2002;3(4):256-266.
34. Lai SC, Nakayama Y, Sequeira JM, et al. The transcobalamin receptor knockout mouse: a model for vitamin B12 deficiency in the central nervous system. *FASEB J.* 2013;27(6):2468-2475.
35. Fernandez-Roig S, Lai SC, Murphy MM, Fernandez-Ballart J, Quadros EV. Vitamin B12 deficiency in the brain leads to DNA hypomethylation in the TCbIR/CD320 knockout mouse. *Nutr Metab (Lond).* 2012;9:41.
36. Luder AS, Tanner SM, de la Chapelle A, Walter JH. Amnionless (AMN) mutations in Imerslund-Grasbeck syndrome may be associated with disturbed vitamin B12 transport into the CNS. *J Inherit Metab Dis.* 2008;31 Suppl 3:493-496.
37. Worm-Petersen J. Vitamin B12 Haemoglobin and Iron Concentration in Human Brain Tissue. *Acta Neurol Scand.* 1964;40:241-248.
38. Sah BR, Schibli R, Waibel R, et al. Tumor imaging in patients with advanced tumors using a new (99m) Tc-radiolabeled vitamin B12 derivative. *J Nucl Med.* 2014;55(1):43-49.
39. Ikotun OF, Marquez BV, Fazen CH, Kahkoska AR, Doyle RP, Lapi SE. Investigation of a vitamin B12 conjugate as a PET imaging probe. *ChemMedChem.* 2014;9(6):1244-1251.
40. Perez-Tilve D, Gonzalez-Matias L, Aulinger BA, et al. Exendin-4 increases blood glucose levels acutely in rats by activation of the sympathetic nervous system. *Am J Physiol Endocrinol Metab.* 2010;298(5):E1088-1096.
41. Lamont BJ, Drucker DJ. Differential antidiabetic efficacy of incretin agonists versus DPP-4 inhibition in high fat fed mice. *Diabetes.* 2008;57(1):190-198.
42. Young AA, Gedulin BR, Bhavsar S, et al. Glucose-lowering and insulin-sensitizing actions of exendin-4: studies in obese diabetic (ob/ob, db/db) mice, diabetic fatty Zucker rats, and diabetic rhesus monkeys (*Macaca mulatta*). *Diabetes.* 1999;48(5):1026-1034.
43. Stupperich E, Nexø E. Effect of the cobalt-N coordination on the cobamide recognition by the human vitamin B12 binding proteins intrinsic factor, transcobalamin and haptocorrin. *Eur J Biochem.* 1991;199(2):299-303.
44. Huisgen R. 1,3-Dipolar Cycloadditions. Past and Future. *Angewandte Chemie International Edition in English.* 1963;2(10):565-598.
45. Kolb HC, Finn MG, Sharpless KB. Click Chemistry: Diverse Chemical Function from a Few Good Reactions. *Angew Chem Int Ed Engl.* 2001;40(11):2004-2021.

46. Chrominski M, Gryko D. "Clickable" vitamin B12 derivative. *Chemistry*. 2013;19(16):5141-5148.
47. Klarenbeek J, Goedhart J, van Batenburg A, Groenewald D, Jalink K. Fourth-generation epac-based FRET sensors for cAMP feature exceptional brightness, photostability and dynamic range: characterization of dedicated sensors for FLIM, for ratiometry and with high affinity. *PLoS One*. 2015;10(4):e0122513.
48. Reiner DJ, Mietlicki-Baase EG, McGrath LE, et al. Astrocytes Regulate GLP-1 Receptor-Mediated Effects on Energy Balance. *J Neurosci*. 2016;36(12):3531-3540.
49. Garber AJ. Long-acting glucagon-like peptide 1 receptor agonists: a review of their efficacy and tolerability. *Diabetes Care*. 2011;34 Suppl 2:S279-284.
50. Iepsen EW, Torekov SS, Holst JJ. Liraglutide for Type 2 diabetes and obesity: a 2015 update. *Expert Rev Cardiovasc Ther*. 2015;13(7):753-767.
51. Rodriguez de Fonseca F, Navarro M, Alvarez E, et al. Peripheral versus central effects of glucagon-like peptide-1 receptor agonists on satiety and body weight loss in Zucker obese rats. *Metabolism*. 2000;49(6):709-717.
52. Williams DL, Baskin DG, Schwartz MW. Evidence that intestinal glucagon-like peptide-1 plays a physiological role in satiety. *Endocrinology*. 2009;150(4):1680-1687.
53. Hayes MR, Kanoski SE, Alhadeff AL, Grill HJ. Comparative effects of the long-acting GLP-1 receptor ligands, liraglutide and exendin-4, on food intake and body weight suppression in rats. *Obesity (Silver Spring)*. 2011;19(7):1342-1349.
54. Spector AC, Breslin P, Grill HJ. Taste reactivity as a dependent measure of the rapid formation of conditioned taste aversion: a tool for the neural analysis of taste-visceral associations. *Behav Neurosci*. 1988;102(6):942-952.
55. Mietlicki-Baase EG, Reiner DJ, Cone JJ, et al. Amylin modulates the mesolimbic dopamine system to control energy balance. *Neuropsychopharmacology*. 2015;40(2):372-385.
56. McMahan LR, Wellman PJ. PVN infusion of GLP-1-(7-36) amide suppresses feeding but does not induce aversion or alter locomotion in rats. *Am J Physiol*. 1998;274(1 Pt 2):R23-29.
57. Hayes MR, Leichner TM, Zhao S, et al. Intracellular signals mediating the food intake-suppressive effects of hindbrain glucagon-like peptide-1 receptor activation. *Cell Metab*. 2011;13(3):320-330.
58. Drucker DJ, Philippe J, Mojsov S, Chick WL, Habener JF. Glucagon-like peptide I stimulates insulin gene expression and increases cyclic AMP levels in a rat islet cell line. *Proc Natl Acad Sci U S A*. 1987;84(10):3434-3438.
59. Arakawa M, Ebato C, Mita T, et al. Effects of exendin-4 on glucose tolerance, insulin secretion, and beta-cell proliferation depend on treatment dose, treatment duration and meal contents. *Biochem Biophys Res Commun*. 2009;390(3):809-814.
60. Alarcon C, Wicksteed B, Rhodes CJ. Exendin 4 controls insulin production in rat islet beta cells predominantly by potentiation of glucose-stimulated proinsulin biosynthesis at the translational level. *Diabetologia*. 2006;49(12):2920-2929.
61. Shah M, Vella A. Effects of GLP-1 on appetite and weight. *Rev Endocr Metab Disord*. 2014;15(3):181-187.

## Figure Legends

**Figure 1.** (A) Synthetic scheme for Cy5-B12, Cy5 alkyne was “clicked” onto a B12-azide conjugate. (B) RP-HPLC of Cy5-B12 showing purity  $\geq 98\%$  and LC-MS showing  $1031[M+2H]^{+2}$ ,  $1042[M+Na+2H]^{+2}$ , and  $1050 [M+K+2H]^{+2}$ , consistent with the conjugate. (C) Excitation and emission spectra of Cy5-B12 at 645 and 682nm, respectively. (D) Human recombinant TCII binding of B12-Ex4 and cyano-B12 with a  $K_d$  of 0.75 and 0.98nM,

respectively. (E) Synthetic scheme for Cy5-B12-Ex4, Cy5-NHS ester was conjugated to Ex4's lysine 26 and N-terminal. (F) RP-HPLC of Cy5-B12-Ex4 showing purity  $\geq 91\%$  and LC-MS showing  $m/z = 1728 [M+4H]^+$ , consistent with conjugate containing two molecules of Cy5 per B12-Ex-4 component. (G) Excitation and emission spectra of Cy5-B12-Ex4 at 648 and 670 nm, respectively. (H) Cy5-B12-Ex4 agonism at the GLP-1 receptor reported using the FRET reporter H188;  $EC_{50} = 13nM$ .

**Figure 2.** B12-Ex4 potently suppresses blood glucose in an oral glucose tolerance test but has minimal effects on energy balance control. Food intake and body weight change were measured after SC administration of B12-Ex4. Only the highest dose of drug, 20 $\mu$ g/kg, produced any reduction in feeding (A). No changes in 24h body weight gain were observed as a result of B12-Ex4 administration (B). In a separate experiment, SC injection of B12-Ex4 (0  $\mu$ g/kg indicated by white circles, 5 $\mu$ g/kg by lighter blue circles, 20 $\mu$ g/kg by darker blue circles) reduced blood glucose in an oral glucose tolerance test from 20-40min after injection (C). \*, significantly different from vehicle ( $p < 0.05$ ); &, significantly different from 5  $\mu$ g/kg ( $p < 0.05$ ). Key in (A) also applies to (B). Data are mean  $\pm$  SEM.

**Figure 3.** Systemic administration of Ex4 produces a different profile of metabolic effects than B12-Ex4. In contrast to the potent suppression of blood glucose produced by B12-Ex4, SC injection of Ex4 (0 $\mu$ g/kg indicated by white squares, 5 $\mu$ g/kg by lighter red squares, 20 $\mu$ g/kg by darker red squares) produced a robust hyperglycemic response (A). Food intake (B) and body weight gain (C) were suppressed by SC Ex4. To compare the induction of nausea/malaise by Ex4 with that potentially produced by B12-Ex4, rats were tested for expression of a conditioned taste

avoidance (CTA) of a flavor paired with IP injection of B12-Ex4 (5 $\mu$ g/kg), Ex4 (5 $\mu$ g/kg), or LiCl as a positive control (0.15M). The percent acceptance of the drug-paired flavor is shown as a box-and-whiskers plot in (D). Both Ex4 (individual responses represented by black circles, overall group response represented in light gray box) and LiCl (individual responses represented by white circles, overall group response represented in white box) produce avoidance of the drug-paired flavor, as indicated by a reduced acceptance of the flavor. These effects are significantly different from acceptance of the drug-paired flavor in B12-Ex4-treated animals (individual responses represented by white squares, overall group response represented in dark gray box). \*, significantly different from vehicle ( $p < 0.05$ ); &, significantly different from all other groups ( $p < 0.05$ ). Key under (B) and (C) applies to both panels. Data in (A-C) are mean  $\pm$  SEM.

**Figure 4.** Systemic administration of B12-Ex4 or Ex4 suppresses blood glucose in mice. In an intraperitoneal glucose tolerance test, Ex4 (5 $\mu$ g/kg) and B12-Ex4 (dose equimolar to Ex4) suppressed blood glucose levels prior to ( $t=0$ min) and after ( $t=20, 40, 60, 120$ min) IP glucose administration (A) Area under the curve analyses from 0-120min (e.g., post-glucose load) show that B12-Ex4 and Ex4 both reduce AUC compared to saline vehicle (B). [NEED DESCRIPTION OF SIGNIFICANCE SYMBOLS HERE] Data are mean  $\pm$  SEM.

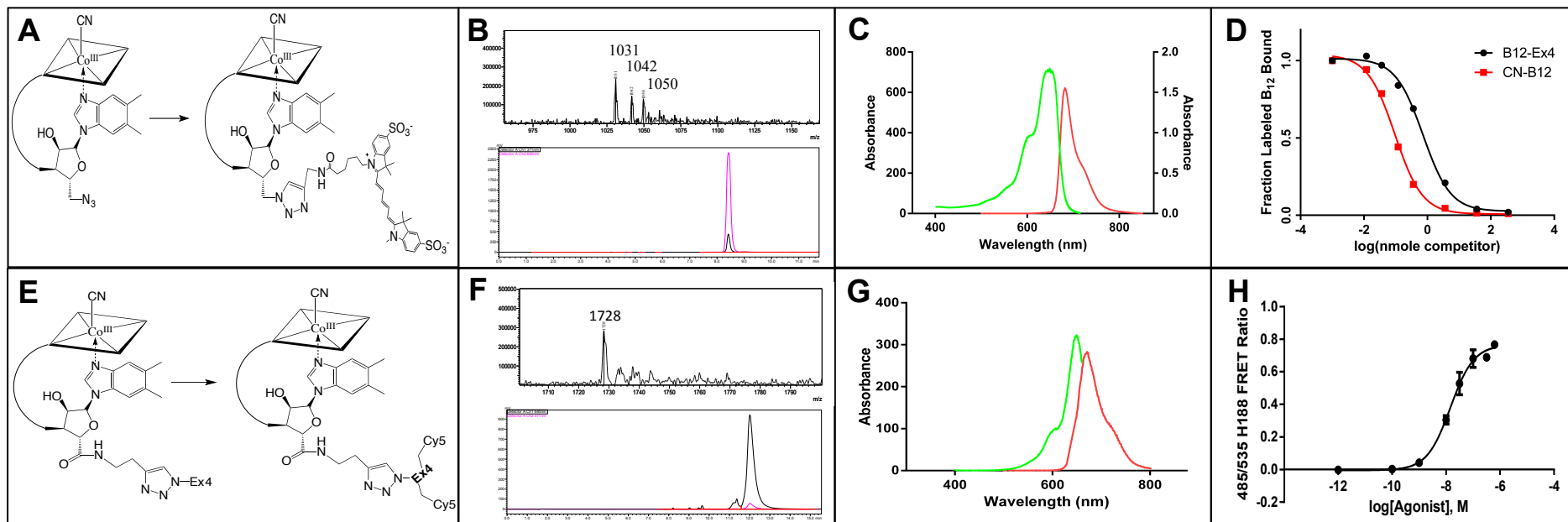
**Figure 5.** Systemically-delivered fluorescently labeled Ex-4 (Flex) highly penetrates within the DVC, whereas Cy5-B12 and Cy5-B12-Ex4 do not. Images were acquired at 10-20x (A,C,E,G) or 63x (with 2-3x optical zoom) (B,D,F,H) magnifications. Brains were processed for immunohistochemistry to label Flex, Equimolar-Flex, Cy5-B12 and Cy5-B12-Ex4 (yellow),

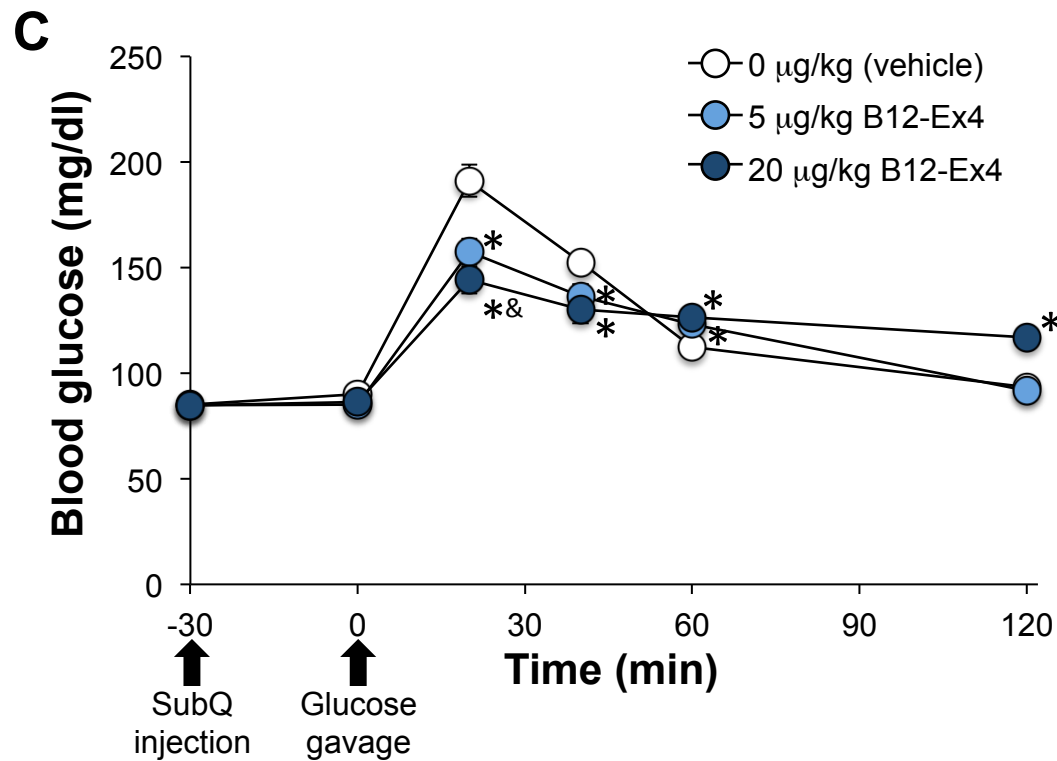
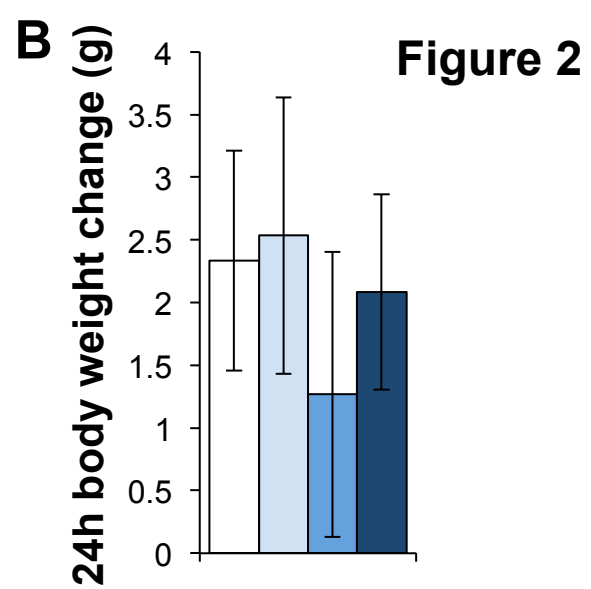
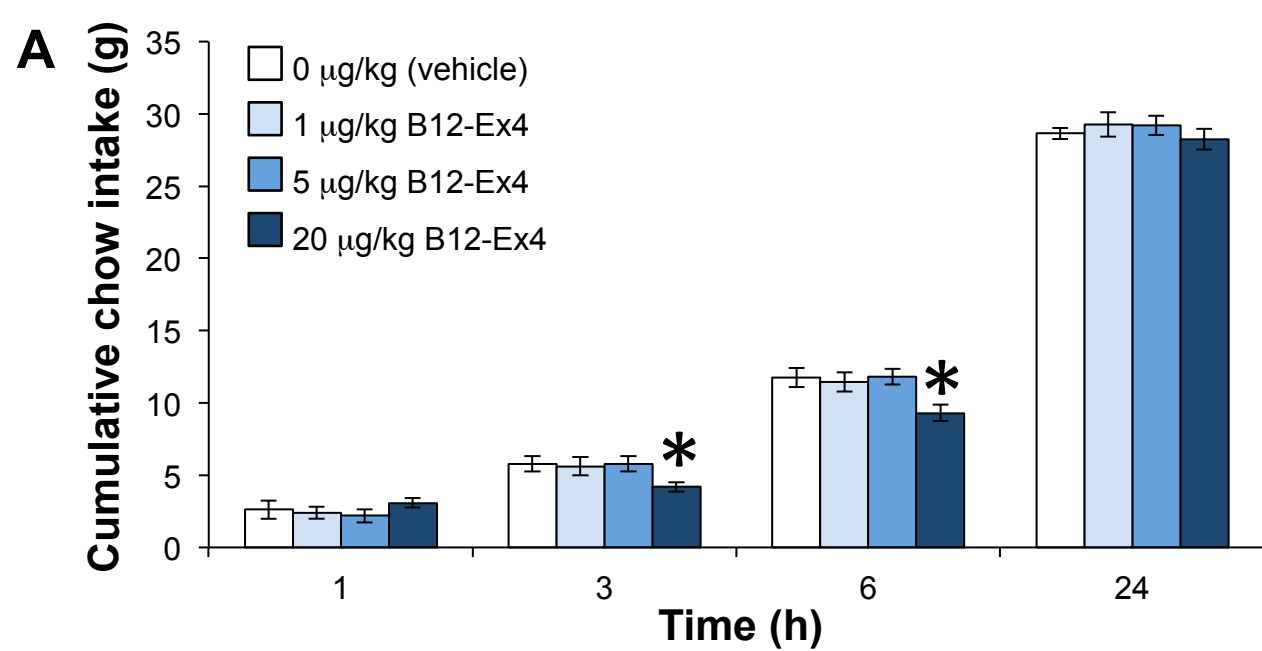
astrocytes (GFAP; green) and neurons (NeuN; red). Sections were counterstained using DAPI (blue) to visualize cell nuclei. (B) Flex and (D) equimolar-Flex immunoreactivity is readily visualized in neurons and astrocytes in the DVC. (F) Cy5-B12 and (H) Cy5-B12-Ex4 are not present either in neurons or in astrocytes within the DVC. AP, area postrema; CC, central canal; DVC, dorsal vagal complex; NTS, nucleus tractus solitarius.

**Figure 6.** Systemically-delivered fluorescently labeled Ex-4 (Flex) highly penetrates within the PVN, whereas Cy5-B12 and Cy5-B12-Ex4 do not. Images were acquired at 10-20x (A,C,E,G) or 63x (with 2-3x optical zoom) (B,D,F,H) magnifications. Brains were processed for immunohistochemistry to label Flex, Equimolar-Flex, Cy5-B12 and Cy5-B12-Ex4 (yellow), astrocytes (GFAP; green) and neurons (NeuN; red). Sections were counterstained using DAPI (blue) to visualize cell nuclei. (B) Flex and (D) equimolar-Flex immunoreactivity is readily visualized in neurons in the PVN. (F) Cy5-B12 and (H) Cy5-B12-Ex4 are not present either in neurons or in astrocytes within the PVN. 3V, third ventricle; PVN paraventricular hypothalamic nucleus.

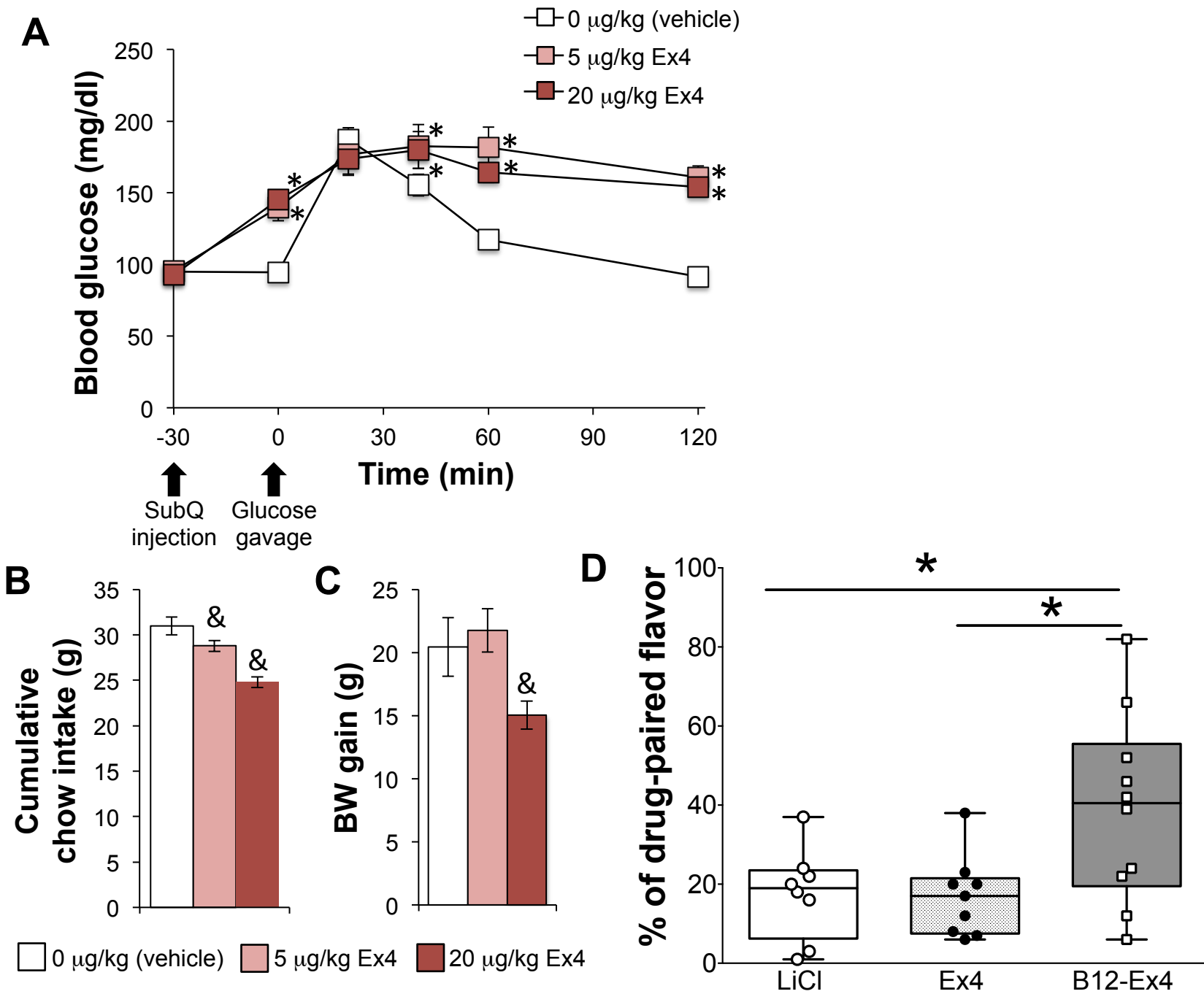
**Figure 7.** Systemically-delivered Cy5-B12-Ex4 is colocalized with insulin in the pancreas. The representative still images from three-dimensional rotational videos (Supplemental Materials) demonstrate that Cy5-B12-Ex4 (yellow) is colocalized with insulin (red) in pancreatic beta cells. Sections were counterstained with DAPI (blue). Videos and corresponding representative images were taken from a z-stack (2 $\mu$ m step size) at 40x (A; Video 1) and from a z-stack (1 $\mu$ m step size) at 40x with 4-5x optical zoom (B; Video 2).

# Figure 1



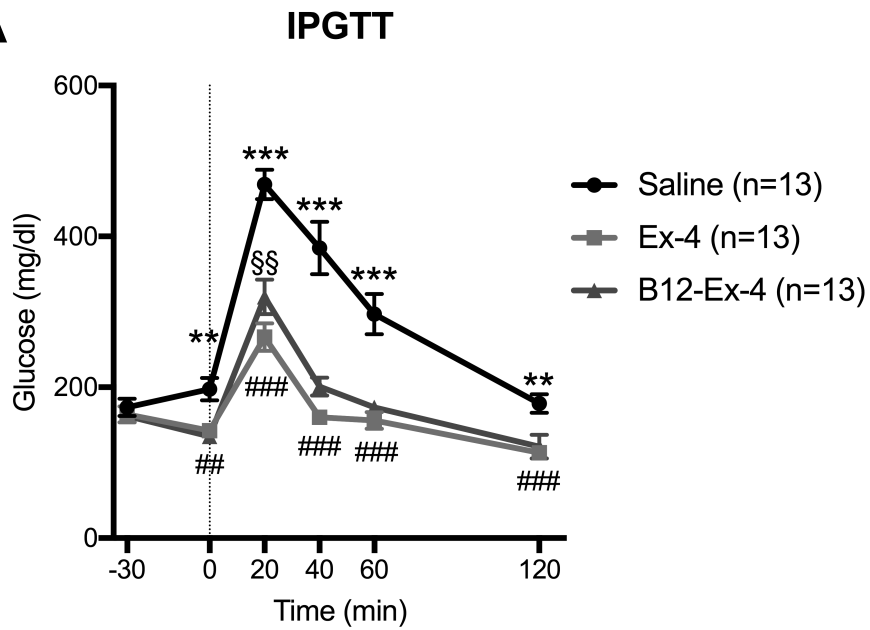




**Figure 3**

**Figure 4**

**A**



**B**

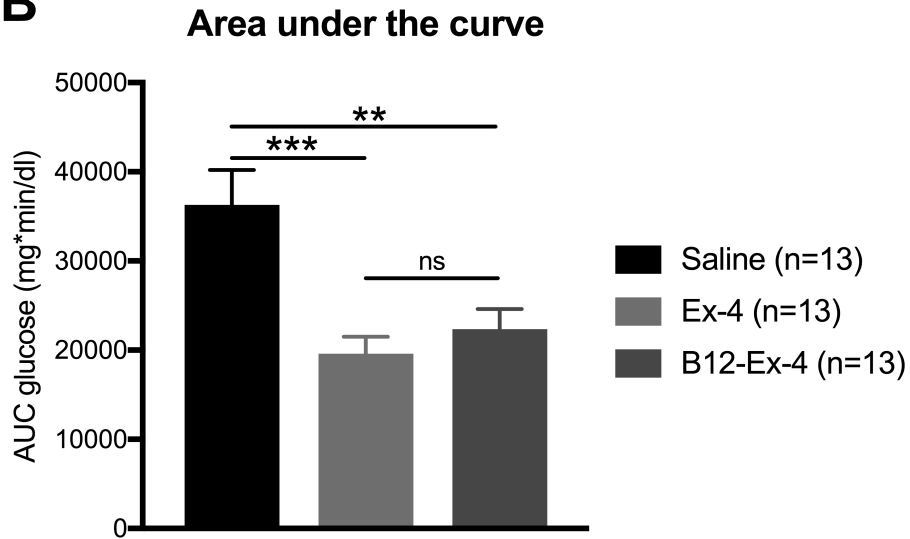


Figure 5

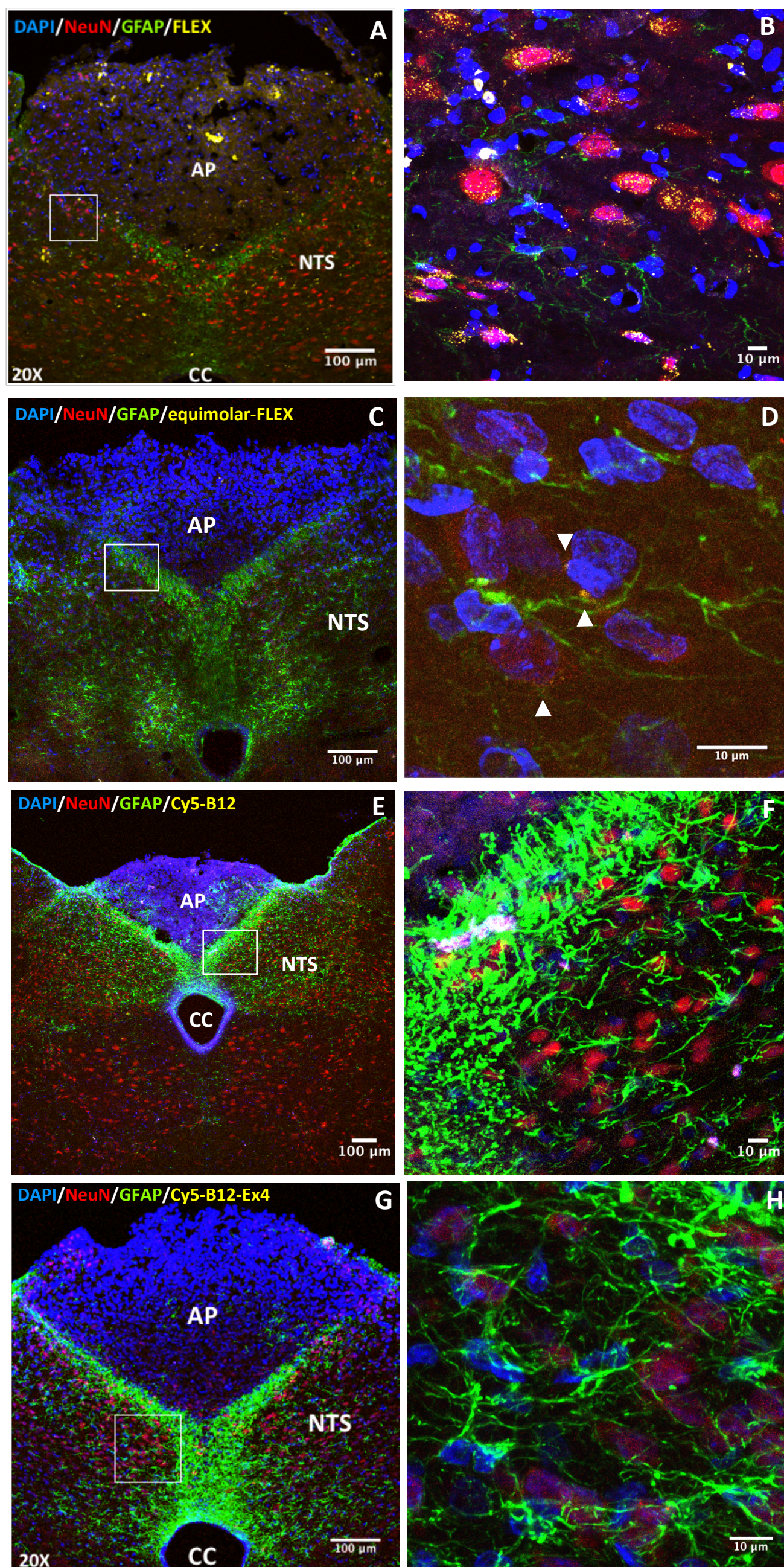


Figure 6

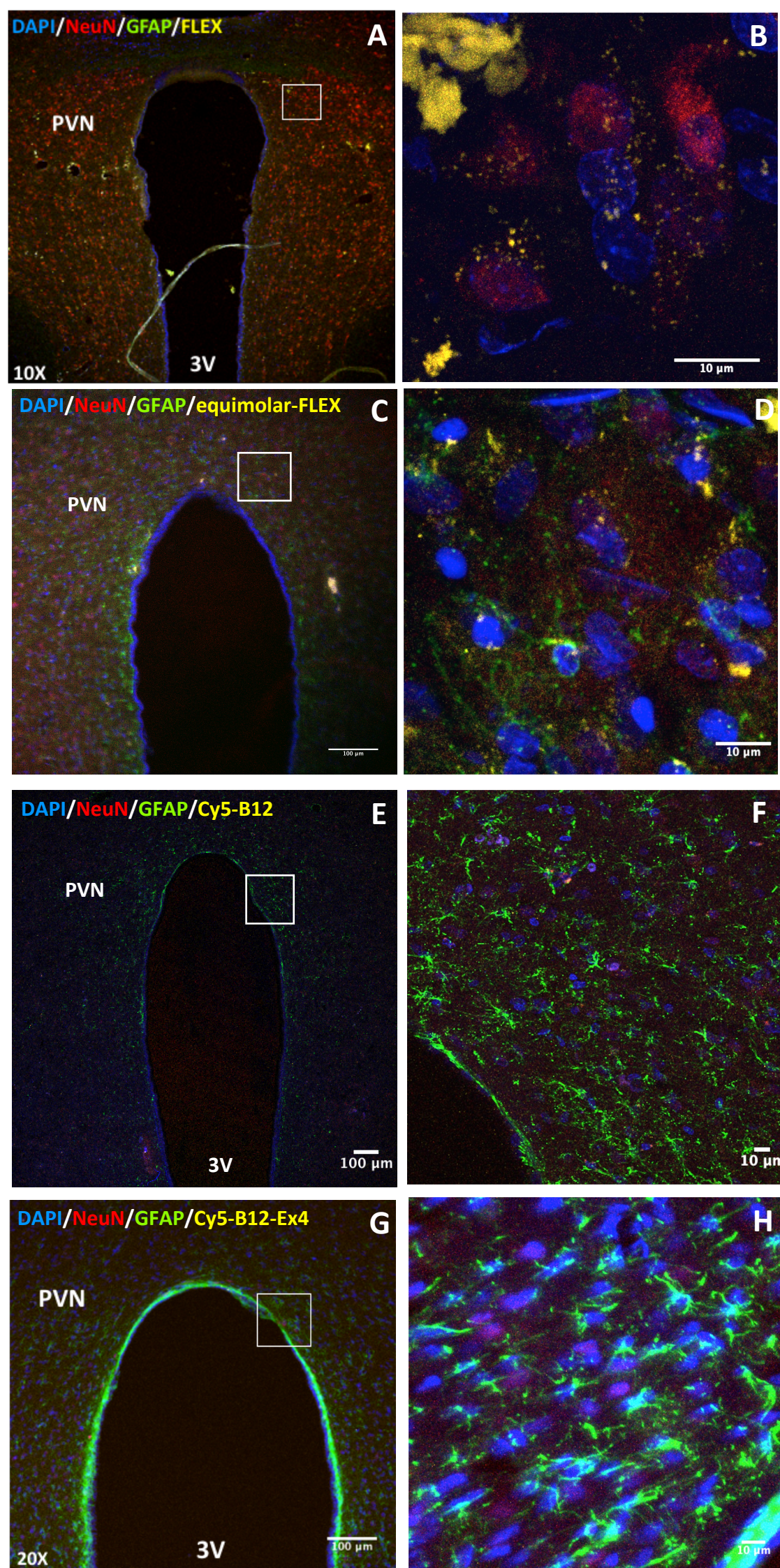
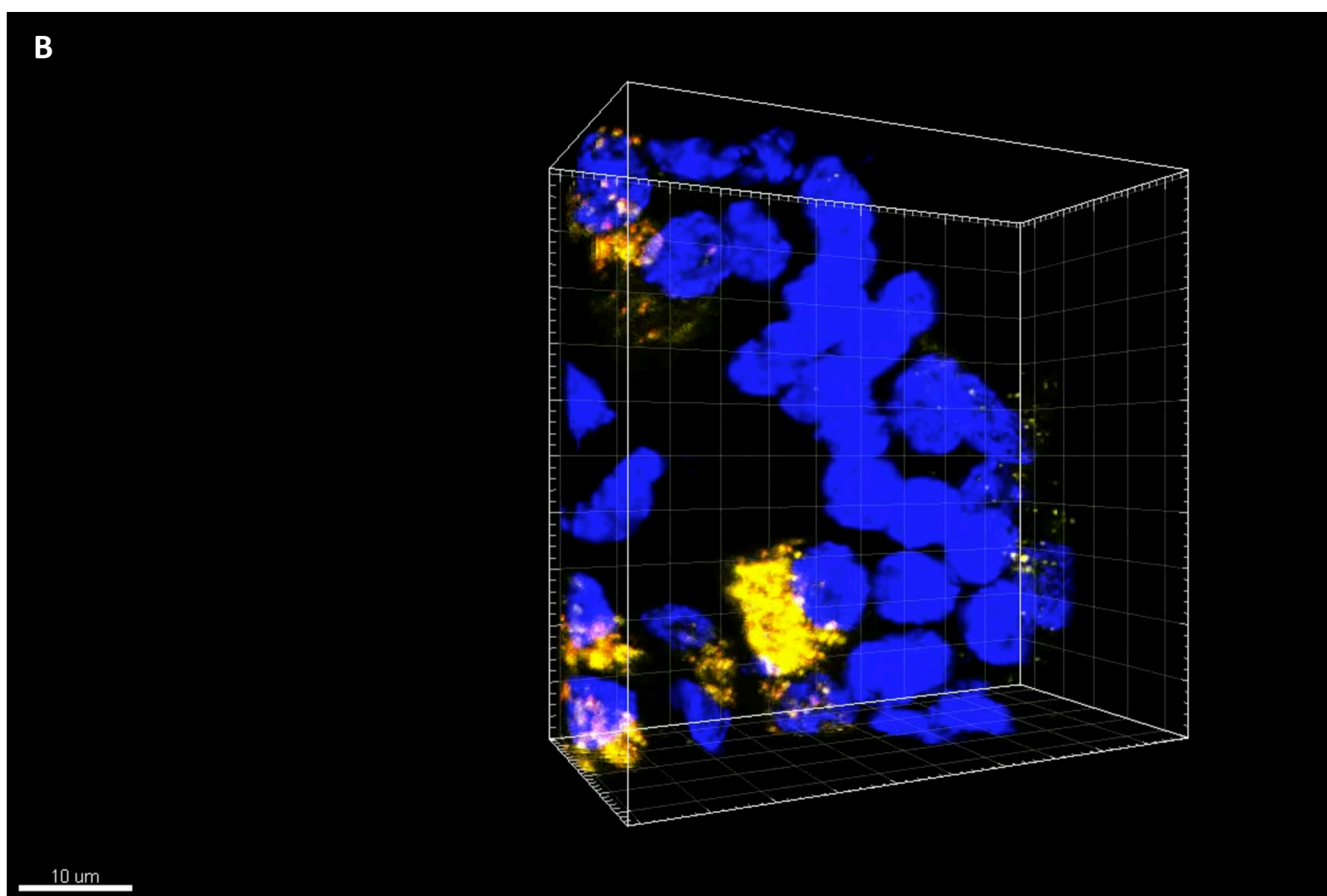
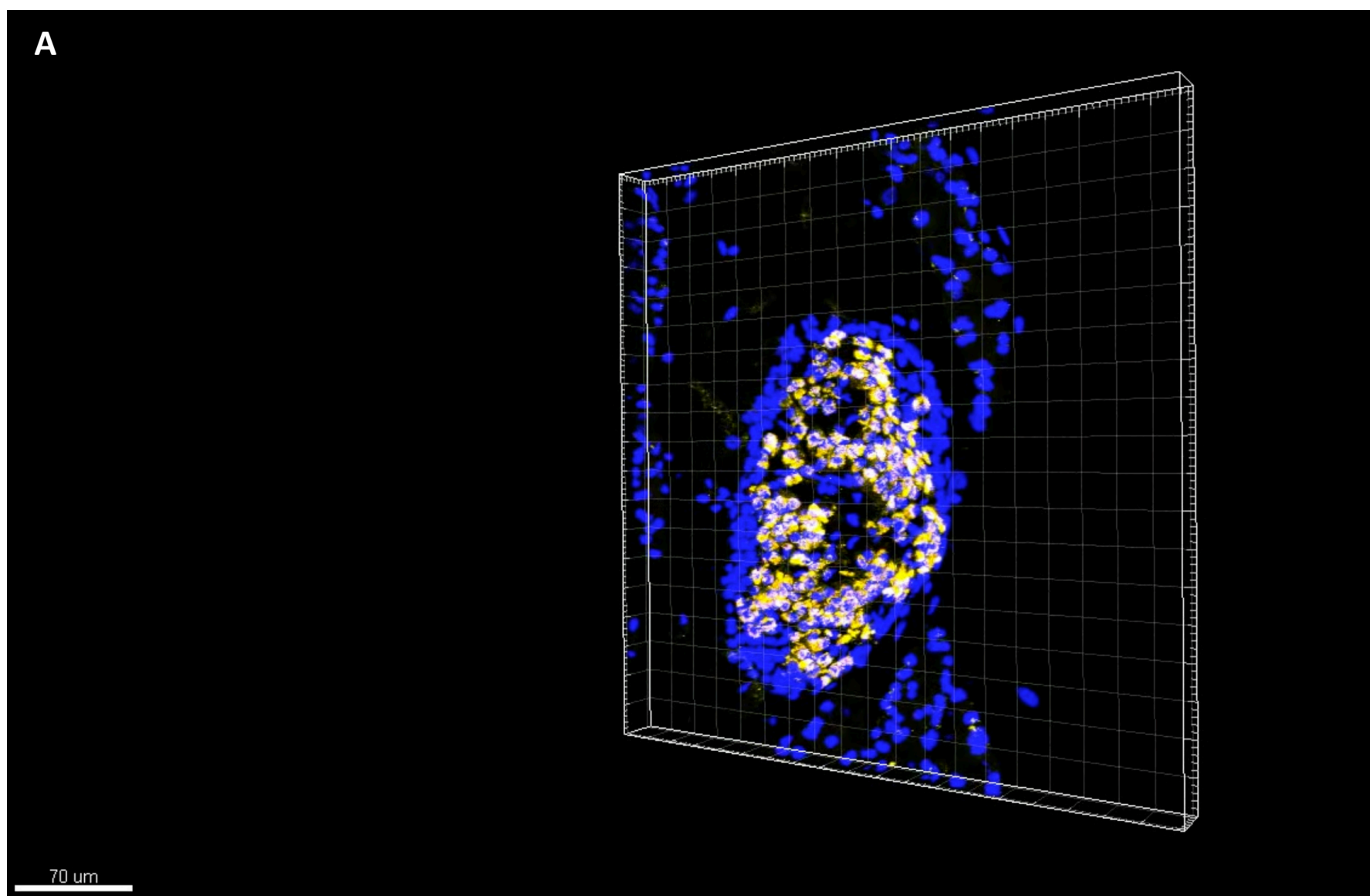


Figure 7



# Jayme Leigh Workinger

Business Address:  
Department of Chemistry  
1-014 Center for Science and Technology  
Syracuse, NY 13244-4100  
(315) 443-5928  
jlworkin@syr.edu

Home Address:  
109 Fordham Road  
Apt. 2C  
Syracuse, NY 13203  
(412) 403-0055

Education     **Muskingum University**     New Concord, OH  
Bachelor of Science, Chemistry, May 2012. Participated in a year long, self developed, senior research program. Thesis: The Use of Fluorescent Pyrimido-pyrimidindole Cytosine Nucleoside Derivatives as Probes to Detect Abasic Sites.

**Syracuse University**     Syracuse, NY  
Doctor of Philosophy Candidate, Department of Chemistry. Research focuses on using vitamin B<sub>12</sub>'s uptake pathway to detect cubilin positive tissue for drug development. (August 2013 – present)

Personal Statement     I have conducted research focusing on exploiting the vitamin B<sub>12</sub> uptake pathway to target select tissues or modify pharmacokinetic properties of therapeutics. My research incorporates organic chemistry, biochemistry, cell biology, and radiochemistry and the analytical techniques typical of those disciplines (see skills). My research aims to design, synthesize, and characterize vitamin B<sub>12</sub> conjugates to specifically target renal cell and hepatocellular carcinoma. The **hypothesis** of my work is that systemically administered gastric intrinsic factor will allow targeting of the cubilin receptor. In order to detect the two carcinomas, I utilize synthetic skills to design and synthesize fluorescent and radio-probes to be used in vitro and in vivo. I've studied at the Polish Academy of Sciences in Warsaw, Poland and the Barbara Ann Karmanos Cancer Institute (KCI) in Detroit, MI. It was in Detroit that I conducted small animal studies with <sup>64</sup>Cu and <sup>89</sup>Zr. I have been invited to speak at the KCI, the ACS Northeastern Regional Meeting in 2015, and the 249<sup>th</sup> ACS National Meeting (03/2015, Denver). My goal upon graduating in 2017 is to further my skills by continuing to work in translational research focusing on the utilization of one carbon metabolism and associated pathways.

Skills     Design, synthesis, and purification of organic and metal chelating conjugates, inert atmospheric synthesis, RP-HPLC analysis and purification, UV-Vis spectrometry, fluorescence, and liquid chromatography mass spectrometry, MALDI-TOF mass spectrometry, <sup>1</sup>H NMR, flow cytometry, fluorescence microscope analysis, western blot analysis, ELISA, mammalian cell culture, BSL 1-2 trained, WSK-8 assays, fluorescent cell assays such as Fura-2 and AKAR3, radiation license, SPEC/CT and PET imaging, biodistribution in small animals, small animal husbandry, CSA Schedule III controlled substance handling and administration.

# Jayme Leigh Workinger

## Research Experience

### **Syracuse University**

Syracuse, NY

Adviser: Robert P. Doyle, Ph.D.

Currently developing a method to detect cubilin positive cells by exploitation of the vitamin B<sub>12</sub> delivery system for ultimate use in the early detection and treatment of metastasized renal carcinoma. Work involves vitamin B<sub>12</sub> conjugate synthesis and characterization, RP-HPLC, column chromatography, NMR spectroscopy, mammalian cell cultures, radiolabeling, flow cytometry, and fluorescence microscopy.

### **Muskingum University**

New Concord, OH

Adviser: Deepamali Perera, Ph.D

Synthesized DNA abasic fluorescent probes to quantify abasic sites within calf DNA. Techniques involved synthesis and characterization of fluorescent nucleoside derivatives. (August 2011 – May 2012)

### **Magee-Womans Research Institute**

Pittsburgh, PA

Adviser: Judy Chang, MD, MPH

Explored provider communication during pregnancy in a clinical setting. Thesis: that women between the ages of eighteen and twenty-five were less likely to be offered help for psychiatric concerns and illnesses than women between the ages of twenty-five and thirty. My role was to recruit and interview patients into the study, then later I quantitatively and qualitatively interpreted the data, looking at statistics and comparing results. (May – August 2010)

## Publications

Kelly E. Henry, Deborah J. Kerwood, Damian G. Allis, **Jayme L. Workinger**, Ron L. Bonaccorso, George G. Holtz, Christian L. Roth, Jon Zubieta, and Robert P. Doyle. Solution Structure and Constrained Molecular Dynamics Study of Vitamin B<sub>12</sub> Conjugates of the Anorectic Peptide PYY(3-36). *ChemMedChem*. **2016**, 1015-1021.

**Jayme L. Workinger** and Robert P. Doyle. The Role of Vitamin B<sub>12</sub> in Drug Discovery. In *Vitamin B<sub>12</sub>: Advances and Insights*. Science Publishers, Boca Raton, FL. **2017**, 338-364. ISBN: 9781498706995.

**Jayme L. Workinger**, Annie Shim, and Robert P. Doyle. Fetal Human Intestinal Cell Line, FH-74 Int., Have Functional Megalin and Cubilin. **2017**. *In preparation for submission to Physiological Reports*.

Ron L. Bonaccorso, Clinton T. Elfers, **Jayme L. Workinger**, George G. Holtz, Matthew Hayes, Christian L. Roth, and Robert P. Doyle. Vitamin B<sub>12</sub> conjugation of Exnedin-4 mitigates central nervous systems associated nausea and food intake reduction in male rats. **2017**. *In revision for Diabetes, Obesity, and Metabolism*.

**Jayme L. Workinger**, Akhila N. Wedagedara, Ebba Nexo Robert P. Doyle, Nerissa T. Viola-Villegas, 89Zr-Cobalamin PET Tracer: Synthesis, Cellular Uptake, and Use for Tumor Imaging. *ACS Omega* **2017**, 2 (10), 6314–6320.

# Jayme Leigh Workinger

**Jayme L. Workinger**, Akhila N. Wedagedara, Nerissa T. Viola, and Robert P. Doyle. Targeting the Cubilin Receptor Through Gastric Intrinsic Factor for Diagnostic Imaging. **2017**. *In preparation for submission to ACS Molecular Pharmaceutics*.

Ron L. Bonaccorso, Clinton T. Elfers, **Jayme L. Workinger**, George G. Holtz, Matthew Hayes, Christian L. Roth, and Robert P. Doyle. EPI: A dual agonist of the GLP-1 and NPY-2 receptors promotes greater food intake reduction than exendin-4 and PYY<sub>3-36</sub> combined. **2017**. *In preparation for submission to Current Pharmacological Design*.

## Presentations

“Investigation of Radiolabeled Holo-Intrinsic Factor in Detection of Cubilin.”  
Institute of Organic Chemistry, Polish Academy of Sciences, 2014.

“Investigating a Vitamin B<sub>12</sub> Conjugate as a PET Imaging Probe” 249<sup>th</sup> ACS National Meeting and Exposition, Denver, CO, 2015

“Investigating a Vitamin B<sub>12</sub> Conjugate as a PET Imaging Probe” ACS Northeast Regional Meeting, Ithaca, NY, 2015 (oral)

“Gastric Intrinsic Factor in the Systemic Targeting of the Cubilin Receptor” Barbara Ann Karmanos Cancer Institute, Department of Oncology, Detroit, MI, 2015

“Targeting The Cubilin Receptor Through Gastric Intrinsic Factor For Diagnostic Imaging” World Molecular Imaging Congress, New York, NY, 2016

“Detecting Renal Cell Carcinoma Utilizing Vitamin B<sub>12</sub>” University of California, San Francisco, San Francisco, CA, 2017 (oral)

## Teaching Experience

### **Syracuse University**

Syracuse, NY

General Chemistry Lecture I. Teaching Assistant.

*August - December 2013 - 2014*

General Chemistry Lecture II. Teaching Assistant.

*January - May 2014 - 2016*

General Chemistry Laboratory. Teaching Assistant.

*January - May 2014 - 2015*

### **Muskingum University**

New Concord, OH

Chemical Laboratory Assistant. Department of Chemistry.

*August 2009 - May 2012*

First Year Student Mentor Program. Teaching Assistant.

*August 2009- December 2011*



# Jayne Leigh Workinger

## Professional Affiliations

WMIC Member	2016 - present
American Chemical Society	2008 - present
Tri Beta Biological Honor Society	2008 - present
Kappa Mu Epsilon Math Honorary	2009 - present